Faculty of Science and Engineering

Department of Chemistry

Chemical Characterisation and Classification of Forensic Trace Evidence

Mark Maric

This thesis is presented for the Degree of

Doctor of Philosophy

of

Curtin University

August 2014

Declaration

To the best of my knowledge and belief, this thesis contains no material previously published by any other person except where due acknowledgement has been made.

This thesis contains no material which has been accepted for the award of any other degree or diploma in any university.

Signature: 

Date: **29/08/2014**

Acknowledgements

No one goes through life being entirely self-sufficient, as we constantly rely on others for help. With that in mind, the completion of this dissertation would not be possible without the assistance of many people. First and foremost, I would like to acknowledge my three supervisors; my principal supervisor Professor Simon Lewis, and my co-supervisors Professor Wilhelm van Bronswijk and Dr Kari Pitts (ChemCentre). It would be an understatement to say that I would not be in the position where I am today, without these three individuals. I am grateful not only for the knowledge they imparted to me, but for the continuous encouragement and support they provided over the years. It would be remiss of me not to also acknowledge Mr Peter Chapman, who I personally consider as an 'unofficial' supervisor. I cannot recall how often he has taken time out of his busy schedule to assist me in my research and for that I am truly appreciative.

I wish to acknowledge the Australian Synchrotron and in particular the members of the Infrared beam-line staff; including Dr Mark Tobin, Dr Ljiljana Puskar, Dr Danielle Martin and Dr Keith Bambery. Their contribution has been extremely valuable, not only for providing technical assistance with the beam-line, but also due to the vast amount of knowledge they provided me with. I must also acknowledge the Australian Synchrotron for providing me with funding to attend a symposium on chemometrics, which was pivotal for my research. I would also like to thank the Asia-Oceania Forum for Synchrotron Radiation Research for providing me with funding to attend the Cheiron School in Hyogo, Japan. Likewise, I credit the Cheiron School organising committee for imparting me with valuable knowledge regarding synchrotron radiation and for providing me with an unbelievable experience.

I would like to recognise Kelvin Parker and the staff of Prestige Sunroofs WA, for continuously providing me with automotive paint samples throughout the duration of my PhD. Needless to say, research focused on automotive paint would have been difficult to undertake without automotive paint samples, and for that I am truly grateful. I must also acknowledge the contribution of Dr Paolo Raiteri for assisting me with advanced spectral processing of my data. His constant willingness to help, sometimes probably to the detriment of his own work, was truly significant.

On a personal note, I must thank the forensic chemistry research group and all of the other friends that I have made in the Chemistry department. Unsurprisingly, they have all contributed in making this experience more fun than I ever imagined it would be. I must also thank my friends outside of University for keeping me grounded and providing me with an escape from my PhD. Finally, and probably most importantly, I wish to thank my parents and my younger brother. Although they struggled to understand my research, their continual support and encouragement has propelled me to reach this point, so for that I am very thankful.

List of Abbreviations

ANOVA	analysis of variance
ASTM	American Society for Testing and Materials
ATR	attenuated total reflectance
DESI	desorption electrospray ionisation
EDS	energy dispersive spectroscopy
EHA	ethylhexylacrylate
FPA	focal plane array
FT	Fourier transform
GC	gas chromatography
HEMA	hydroxyethylmethacrylate
HSV	Holden special vehicles
ICP	inductively coupled plasma
IR	infrared
IRM	infrared microspectroscopy
LA	laser ablation
LDA	linear discriminant analysis
MCT	mercury cadmium telluride
MS	mass spectroscopy
MSP	microspectrophotometry
NAS	National Academy of Sciences
nBMA	n-butylmethacrylate
NIPALS	non-linear iterative partial least squares
OEM	original equipment manufacturer
OMA	octylmethacrylate
PC	principal component
PCA	principal component analysis
PDQ	paint data query
PLM	polarised light microscopy

PMA	pentylmethacrylate
Py	pyrolysis
RGB	red-green-blue
SEM	scanning electron microscopy
SIMCA	soft independent modelling of class analogy
SWGMAT	Scientific Working Group on Materials Analysis
UV	ultraviolet
VDS	vehicle descriptor section
VIN	vehicle identification number
VIS	vehicle identification section
VOC	volatile organic compound
WMI	world manufacturer identifier
XRD	X-ray diffraction spectroscopy
XRF	X-ray fluorescence spectroscopy

Abstract

Automotive paint, in the form of paint chips and/or smears, is one of the most commonly encountered forms of trace evidence located at automotive related incidents. In many scenarios, such as hit-and-run accidents, automotive paint is often the only significant form of physical evidence available to forensic examiners, making its subsequent analysis critical to the investigation. Whilst guidelines have been established for the analysis of paint evidence, these typically rely on subjective interpretations of the analytical results by the forensic examiner, raising serious concerns regarding human error and bias. Consequently, there is an increasing demand for more scientifically rigorous approaches to the interpretation of forensic evidence. Multivariate statistics or chemometrics allows the formation of objective conclusions based upon experimental data, through the use of well characterised statistical protocols. This dissertation presents studies examining the use of a suite of spectroscopic techniques in conjunction with chemometrics, in order to develop analytical and interpretational protocols for automotive paint evidence.

Attenuated total reflectance (ATR) Fourier transform-infrared (FT-IR) spectroscopy was used to analyse original manufacturer clear coats, from a statistically significant population of automotive paint systems. Chemometrics performed on the resultant data revealed a number of groupings in the sample population, which could be correlated to common vehicle descriptors, including vehicle origin, manufacturer, model, assembly plant and year of manufacture. The statistical model developed could enable the procurement of investigative leads from questioned paint sources, when a questioned *vs.* known sample comparison is not possible. Fundamental chemical studies were conducted to investigate the applicability of the subsequent model in a real-life context. High spatial resolution synchrotron source transmission FT-IR spectra of thin automotive paint cross-sections, revealed that inter-layer migration of chemical components can and does occur. In select samples, the cross-linking agent melamine was shown to migrate from the underlying layers into the clear coat. Unless appropriate analytical and sampling protocols are used this could affect the classification of clear coats in the model. ATR FT-IR spectroscopy was

also used to investigate the effect of weathering and the environment on automotive clear coats. Moderate weathering of the automotive clear coats over an 18 month time period did not affect the outcomes from the ATR-based clear coat model.

In instances where IR spectra of clear coats are inconclusive, further information can be obtained from the underlying primer surfacer coating. Principal component analysis conducted on synchrotron FT-IR spectra obtained from the primer surfacer, revealed a number of visually distinct groupings that were indicative of the vehicle manufacturer. This model provides more specific information pertaining to the vehicle manufacturer than the equivalent clear coat model.

FT-Raman spectroscopy was also utilised to chemically interrogate original automotive clear coats. Multivariate statistics performed on the subsequent data revealed a grouping pattern and structure comparable to the ATR-based model. However, the statistical model generated from the Raman data had a higher discriminating capacity than the corresponding IR model. Additionally, a combined statistical approach developed by concatenating FT-IR and FT-Raman data from clear coats, provided increased discrimination between samples over the individual spectroscopic models. The combined statistical approach will enable a larger amount of information to be extracted from questioned paint specimens.

Publications

This thesis dissertation contains work which has been submitted for publication in peer reviewed journal articles.

Maric, M., van Bronswijk, W., Lewis, S.W., and K. Pitts, *Rapid characterisation and classification of automotive clear coats by attenuated total reflectance infrared spectroscopy*. Analytical Methods, 2012. **4**(9): p. 2687-2693.*

Maric, M., van Bronswijk, W., Lewis, S.W., Pitts, K., and D.E. Martin, *Characterisation of chemical component migration in automotive paint by synchrotron infrared imaging*. Forensic Science International, 2013. **228**(1-3): p. 165-169.

Sauzier, G., Maric, M., van Bronswijk, W., and S.W. Lewis, *Preliminary studies into the effect of environmental degradation on the characterisation of automotive clear coats by attenuated total reflectance infrared spectroscopy*. Analytical Methods, 2013. **5**(19): p. 4984-4990.†

Maric, M., van Bronswijk, W., Lewis, S.W., and K. Pitts. *Synchrotron FTIR characterisation of automotive primer surfacer paint coatings for forensic purposes.* Talanta, 2014. **118**: p. 156-161.

* Awarded highly commended for the best paper in a refereed journal by the National Institute of Forensic Science Australia.

† Front cover

Presentations

Selected aspects of the work contained within this thesis were also presented at the following conferences:

Oral Presentations

M. Maric. Characterisation and classification of automotive clear coats by attenuated total reflectance infrared spectroscopy with subsequent chemometric analysis, in *21st International Symposium on the Forensic Sciences*, 2012, Hobart (Tasmania).*

van Bronswijk, W., Maric, M., Sauzier, G., Lewis, S.W., Pitts, K., and D.E. Martin. The characterisation of automotive paints by infrared spectroscopy for forensic purposes, in *10th Australian Conference on Vibrational Spectroscopy*, 2014, Glenelg (South Australia).

* Key-note speech; awarded an honourable mention for the best talk in the chemical criminalistics stream.

Poster Presentations

van Bronswijk, W., Maric, M., Lewis, S.W., and K. Pitts, An infrared study of automotive paints in the Australian context, in *2011 Australasian Conference on Vibrational Spectroscopy*, 2011, Wellington (New Zealand).

Table of Contents

List of Figures

Chapter 1

Chapter 2

Chapter 3

Chapter 4

Chapter 5

Chapter 6

Chapter 7

Appendices

List of Tables

Chapter 1: Introduction

Over the past few decades, the general public has shown an increased interest in the application of science to crime solving. This can be largely attributed to the proliferation of television shows depicting the use of forensic science in the solving of crimes (e.g. CSI). However, the manner in which forensic science is portrayed in these programmes is highly sensationalised, especially in regards to the forensic analysis and interpretation of trace evidence. The most common misconception is that forensic science is infallible, meaning that the results from the analysis of trace contact evidence cannot be questioned.[1-3] In reality, recent inquiries undertaken by the National Academy of Sciences (NAS) in the United States, and by the British Parliamentary Committee on Science and Technology, have highlighted the need to establish impartiality in the analysis and interpretation of forensic evidence.[4, 5] In order to address these concerns, increased efforts have been made to establish a statistical basis for evaluating evidential significance. One approach is to use multivariate statistics or chemometric techniques, which offer the potential to develop rigorous statistical protocols enabling objective conclusions to be obtained from analytical data. This dissertation describes a program of research examining the use of chemometrics in the interpretation of automotive paint evidence. Whilst the research specifically relates to automotive paint, the statistical methodology developed can be universally applied to other forms of trace contact evidence.

Forensic science is largely centred on the notion of establishing associations or links between the perpetrator/s, victim/s and or crime scene/s. One of the main tenets which define forensic science is the exchange principle, initially proposed by Edmund Locard, which infers that any physical contact between person/s, object/s and locale/s will result in a mutual exchange of material, no matter how tenuous.[6-9]

> *"It is impossible for a criminal to act, especially considering the intensity of a crime, without leaving traces of this presence."*[10]

Ultimately, Locard posits that any physical contact between two entities will result in the cross-transference of traces of physical evidence, more commonly referred to as trace evidence.[7, 11] Some examples of frequently encountered trace evidence include

fingerprints, footwear impressions, hair, fibres, glass fragments, paint, soils, bodily fluids and gunshot and explosive residues. One of the widespread and most significant forms of trace contact evidence submitted to forensic science laboratories is paint.[6, 7, 9, 10]

1.1 Paint Composition

Nowadays, almost every man-made object and virtually every surface in our environment has some form of coating designed to protect, improve aesthetic characteristics or impart some functionality to the object.[12-14] One example of these coatings is paint. The origin of paint can be traced back to the Palaeolithic era, some 40, 000 years ago, where a combination of sap extracted from plants and colouring agents obtained from blood, berries and soil were employed in cave paintings.[15] Although paint technology has evolved and improved over the years, modern paint systems are still only contained of four basic components; binder/s, pigment/s, additive/s and a solvent.[13, 15-20]

1.1.1 Binder ('Resin')

The binder, or resin, is a polymeric constituent that forms the matrix of the coating as it binds the pigment/s and additive/s into place, whilst also allowing the film to strongly adhere to the substrate.[13, 15, 21] The binder forms the backbone of the solid continuous film upon curing, which can occur *via* several mechanisms; evaporation, polymerisation or coagulation.[12, 15, 21] Films formed by evaporation are known as 'non-convertible' films as the binder does not convert to a polymerised coating. The film itself is produced following evaporation of the solvent, leaving the binder, pigment/s and additive/s behind. These coatings are effectively known as lacquers and can be re-dissolved upon addition of the solvent.[15, 21]

‘Convertible’ films, on the other hand, are formed *via* polymerisation upon drying, whereby the resin is irreversibly cross-linked following oxidation, heating or by the addition of a catalyst.[15, 21] Finally, emulsion or ‘latex’ coatings form, when small particulates of resin that are dispersed in an immiscible liquid, coalesce into a networked structure as the liquid evaporates.[12, 18] Ultimately, the binder is critical to the success of the final film as it binds the pigments to the application surface, whilst also imparting most of the physical characteristics and durable qualities to the coating. The common resins used in modern paint systems include acrylics, alkyds, urethanes, epoxies and polyesters.[15, 21, 22]

1.1.2 Pigment

Pigments are finely ground particles that are dispersed in paint and have a number of different roles depending on the type of pigment employed.[10, 21, 23] Colour pigments, which can be either organic or inorganic, are utilised to impart a colour to the final coating so as to improve its aesthetic appeal. White and black inorganic colour pigments are often termed ‘hiding pigments’ as they increase the opacity and obliterate colour variation in the coating. This is of particular significance in improving the colour contrast of films added on top of the original coating.[15] Metallic and effect pigments are also utilised in automotive paint to provide the vehicle with a metallic, pearlescent or colour-shifting finish.[24] Finally, extender pigments are routinely employed to ‘extend’ or stretch the thickness of the coating at a low cost, whilst also imparting certain desirable qualities to the film.[25, 26]

1.1.3 Additive

Additives are formulated into paints in small or trace amounts to fix any deficiencies and lend additional performance characteristics to the finished coating.[23] It is common for many paint systems to contain up to ten or more additives, with the cumulative amount of additives in the paint formulation usually totalling less than three percent. There is a broad spectrum of additives that can affect and enhance

performance properties including; pigment dispersability, sag resistance, de-foaming, skinning, in-can stability, gloss, viscosity, binder cross-linking, flexibility, and ultraviolet (UV), fire and microbial resistance.[13, 18, 27]

1.1.4 Solvent

Solvents are an integral component of the paint system as they ensure that the binder/s, pigment/s and additive/s remain in the liquid form facilitating easy application to the substrate.[15, 27] The solvent does not remain in the mixture for long as it is lost during the curing process, often following the application of heat.[21, 23] Volatile organic compounds (VOCs) are scarcely used nowadays, with most paint manufacturers preferring water as their solvent for health and environmental reasons (e.g. emulsion or latex coatings). Furthermore, improvements in paint technology have led to the development of powder coatings, which contain all of the main constituents of paint, except solvent.[15, 28] Following the application of the paint to the substrate, the solvent, if any, evaporates leaving behind the final coating.

1.1.5 Paint Types

From a forensic science standpoint, paints are predominantly categorised into three main groups as a function of their use. These groups are architectural, artistic and automotive paints.[6] Architectural or structural paints broadly encompass any paint applied to a residence or a building and are commonly encountered as evidence at volume crime scenes, such as burglaries.[6, 29, 30] On the other hand, artistic paints are occasionally encountered by forensic examiners in instances of art forgery and graffiti.[30] However, by far the most commonly occurring form of paint evidence in forensic science are automotive paints; which can be located at hit-and-run accidents, vehicular homicides, automobile crashes or generally any incident where a vehicle has been used in the commission of a crime.[29, 30] This dissertation focuses solely on the analysis and interpretation of automotive paint evidence.

1.2 Automotive Paint

Automotive paint is a complex multilayered system, as depicted in Figure 1.1, designed to protect the frame of the vehicle and impart certain aesthetic properties. Each layer has unique chemical characteristics and a distinct function.[19] An original equipment manufacturer (OEM) automotive finish system is typically applied sequentially in a number of steps. Prior to paint deposition, all metal portions of the vehicle are normally pre-treated *via* zinc electroplating (~ 1 µm), in order to prevent corrosion and inhibit rust.[24, 31] The first paint layer applied to the vehicle is the electrocoat primer. The electrocoat primer is an approximately 20 µm thick epoxy based coating, which is electroplated onto the body surface of the vehicle to provide greater corrosion resistance.[7] A primer surfacer, which is usually a 35-40 µm alkyd based coating, is then applied to conceal any surface imperfections, providing a uniform foundation which will be amenable and more receptive to the application of the basecoat.[24, 32] Following the application of the primer surfacer, a roughly 15 µm thick pigment containing layer known as the basecoat is applied to achieve the desired colour.[6, 7, 30] Recently, there has been a growing trend towards the addition of metallic and effect pigments to automotive paint basecoats. The addition of metallic pigments such as aluminium flakes impart a glittering appearance to the paint surface, whilst metal oxide coated mica particles are utilised in order to provide the vehicle with a pearlescent finish. Hue-shifting pigments may also be employed to cause colour-shifting when the coating is viewed from different perspectives.[6, 24]

The final coat applied in the automotive finishing process is known as the clear coat. The clear coat is typically a 40 µm thick un-pigmented layer, consisting of UV absorbers and hindered amine light stabilisers, designed to protect the basecoat and underlying layers from UV degradation and weathering.[7] The UV absorbers present in the clear coat absorb light in the wavelength range of 290-350 nm, thereby significantly reducing the photo-degradation of the paint binders. Aside from the resistance to weathering, the clear coat also provides gloss, hardness, physical protection from road debris and resistance to solvents and chemicals.[7, 24, 32]

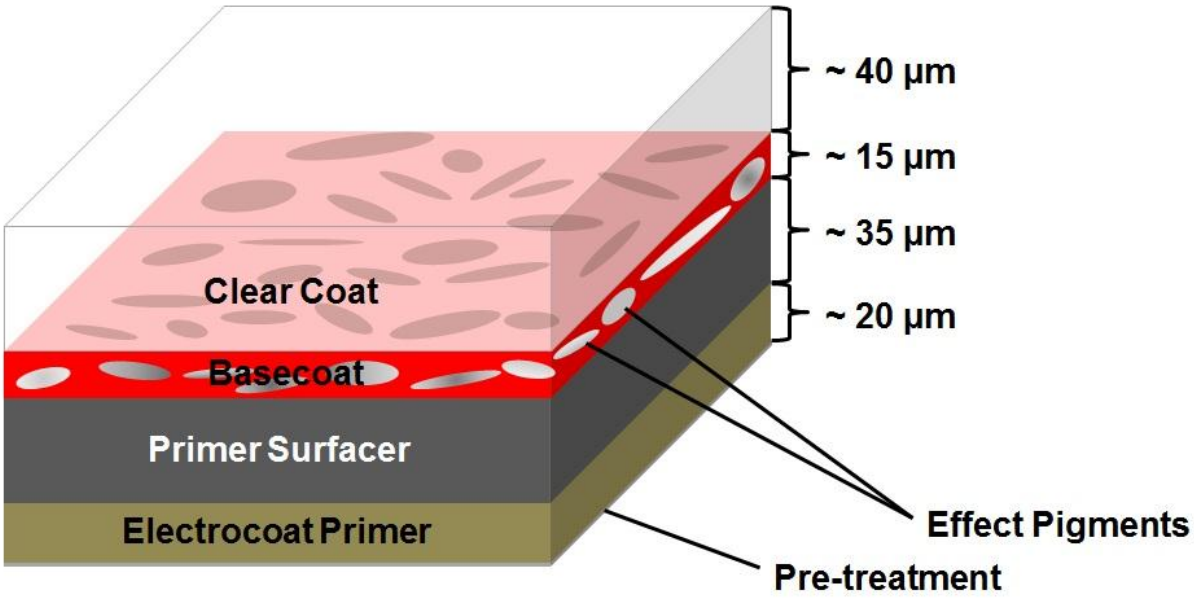

Figure 1.1: Typical OEM automotive paint system comprising four distinct layers; electrocoat primer, primer surfacer, basecoat and clear coat.

Whilst the OEM 4-coat system comprising a clear coat, basecoat, primer surfacer and electrocoat primer is the norm, there are notable exceptions, as depicted in Figure 1.2. Some older vehicles contain a monocoat paint system, with an opaque, non-metallic basecoat without clear coat.[14] Furthermore, some higher-end vehicles have a metallic finish, whereby the basecoat contains solely metallic or effect based pigments.[14, 24] If the vehicle has been damaged, or if the manufacturer isn't satisfied with the finish, it may have 6 or more OEM coatings. In these instances, the vehicle is often refinished with an OEM basecoat and clear coat atop the original finish. Similarly, aftermarket coatings are commonly encountered on vehicles that have been damaged and subsequently refinished at a body shop. Although this type of paint system also typically contains 6 layers, it differs from the OEM refinish in that the chemical composition of the aftermarket base and clear coat is almost always different than the OEM counterparts. This is illustrated in Figure 1.2, whereby it is clearly observed that the colour and morphology of the aftermarket base and clear coat differ markedly from the original coatings.

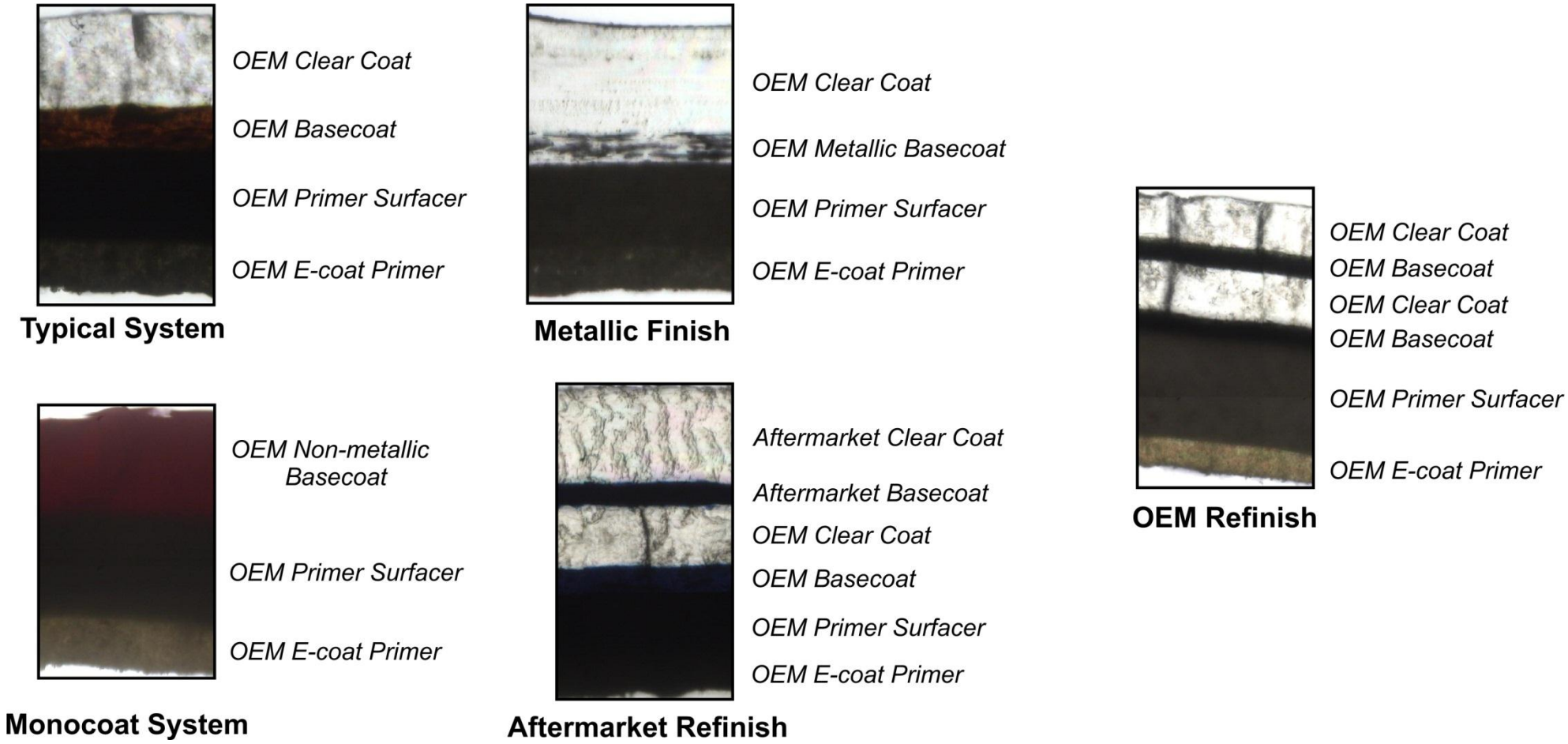

Figure 1.2: Commonly encountered vehicle paint systems. Images were obtained from thin microtomed paint cross-sections (~ 8 µm) at the infrared microspectroscopy beam-line of the Australian Synchrotron.

1.2.1 Types of Automotive Paint Evidence

Automotive paint evidence can be recovered from incident scenes in the form of either paint chips or smears.[6, 30] The nature of the paint evidence transferred is dependent on a number of factors, including the force of the contact, the nature of the recipient surface and the quality and adherence properties of the paint.[29] Paint smears may arise upon minor glancing contact between a vehicle and a substrate, typically when one vehicle side-swipes another. As a result, paint smears usually involve only the outermost layer of the paint system, which is normally the original clear coat.[6, 29] In many instances, the smear transfer is also integrated with the outer coating of the substrate, making it extremely challenging for the forensic examiner to accurately sample and characterise the smeared paint.[6] Automotive paint chips, on the other hand, typically arise upon forceful direct contact between the vehicle and the substrate, resulting in a deformation of the vehicle frame leading to paint fragments being dislodged.[29] In a forensic context, paint chips are less challenging as they contain the entire layer structure of the paint system intact, enabling analysis of all of the layers and thereby increasing the evidentiary value and significance.[30] Paint chips also offer the potential for physical fits to a known sample, which is highly individualising and would provide unambiguous evidence of association between the questioned paint sample and a source.[33]

1.3 Forensic Analysis of Automotive Paint

Although paint has widely been regarded as a valuable form of trace evidence, many forensic examiners initially questioned the validity of forensic paint examination.[34] In fact, Paul Kirk, widely recognised as one of the leading pioneers in modern criminalistics stated that;

> *"Because of the alteration of the vehicle on drying and the approximate uniformity of the dry vehicle film, little if any importance is attached to it in paint identification except as an impediment to the easy study of the solids suspended in it."*[34, 35]

This statement epitomised the approach towards forensic paint examination some 60 years ago. However, it is important to note that the analytical approach to forensic paint examination has continuously evolved over the years; with the modern outlook underlining that a significant amount of information may be extracted from automotive paint analysis. Whilst there is no current universal methodology for forensic paint examination, guidelines have been developed by the Scientific Working Group on Materials Analysis (SWGMAT)[36] and by the American Society for Testing and Materials (ASTM),[37] in order to provide a framework for the analysis of paint evidence. The guidelines advise that a combination of instrumental and spectroscopic techniques be utilised to characterise both the organic and the inorganic components of paint. These techniques include, but are not limited to, microscopical examinations, microspectrophotometry (MSP), infrared (IR) spectroscopy, Raman spectroscopy, pyrolysis-gas chromatography/mass spectroscopy (Py-GC/MS) and elemental analysis techniques.[36, 37] The analytical scheme used to characterise paint evidence follows a logical sequence of examination that is flexible and dependent on the quality, quantity, morphology and the physical and chemical complexity of the sample.

1.3.1 Microscopy

Whilst there is no single analytical scheme suited to all samples, the starting point of almost every forensic paint examination is optical microscopy.[29, 36, 37] Microscopic examination of paint fragments enables information to be ascertained regarding the layer sequence and structure, colour, pigment distribution and size, surface textures and features, morphology and appearance (Figure 1.2).[33, 38-40] It is worth noting that in order to obtain unambiguous paint layer discrimination, the paint fragments often require some form of sample preparation. The most common method of paint sample preparation is to obtain thin cross-sections *via* either a microtome or by hand using a scalpel.[36, 37, 41] When these cross sections are viewed under a high magnification microscope with varying degrees of illumination (i.e. bright and dark field), further distinctive features such as surface defects and striae are able to be observed.[29] Polarised light microscopy (PLM) and fluorescence microscopy provides

information complementary in nature to that obtained by optical microscopy. PLM allows examiners to observe and identify birefringent materials, such as inorganic pigments and extenders that are visually identical under visible light.[29, 38, 42] The use of PLM as a means for the identification of pigments and extenders has largely been superseded by a number of instrumental techniques.[33] Fluorescence microscopy aids in the discrimination between layers of multicomponent systems, by improving contrast between visually similar layers. This is achieved by illuminating the sample with light of a short wavelength (i.e. UV light) and observing the emitted fluorescence. Each layer of the paint cross section will therefore emit fluorescence of varying intensities, based upon the components within each layer.[29, 34] By using the aforementioned techniques in tandem, a comprehensive visual examination of the paint sample can be obtained, as depicted in Figure 1.3.[29]

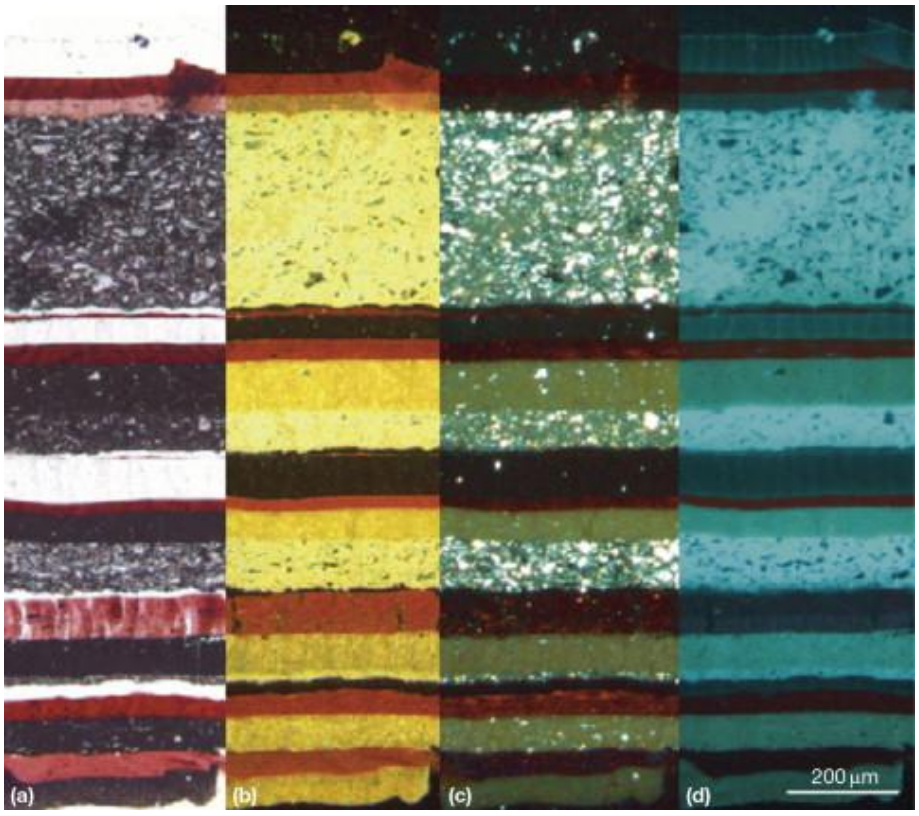

Figure 1.3: Thin re-painted automobile cross-section viewed under (a) bright field, (b) dark field, (c) polarised light and (d) UV light (excitation 340-380 nm, emission 425 nm).[29]

1.3.2 Microspectrophotometry (MSP)

The optical examination of paint is typically followed by a technique known as MSP, which is a highly discriminating method that can provide an objective assessment of colour.[33, 39] MSP is an invaluable tool in identifying and characterising dyes and pigments in paint, as it allows discrimination of samples based on their interaction with light.[43, 44] A microspectrophotometer is essentially a microscope that is interfaced with a spectrophotometer, which is capable of measuring the intensity of light as a function of wavelength of the visible and UV regions of the electromagnetic spectrum. Microspectrophotometers operate by irradiating a microscopic section of the paint sample with a controlled light source, and then measuring the intensity of the light across the spectrum that is either transmitted or reflected by the sample.[45, 46] The preferred method of choice for paint characterisation by MSP is in the transmission mode using thin microtomed cross-sections.[47]

Although the human eye is adept at colour discrimination, it is extremely subjective, with a number of variables affecting the manner in which colour is perceived.[48, 49] MSP has been proven to be inherently more sensitive in identifying subtle differences in colour than the human eye, specifically in the case of metameric paints.[49] Metameric paints are indistinguishable to the naked eye, yet are composed of different pigment combinations and thus may be readily distinguished by MSP.[48, 49] Additionally, research conducted by Kopchick and Bommarito has demonstrated that spectral information can even be obtained in some achromatic black and grey/silver basecoats using visible region MSP.[50] This is an extremely positive finding considering that achromatic materials are believed to absorb or reflect all wavelengths of visible light uniformly, and hence visible MSP has previously been excluded from the forensic analysis of achromatic paints.[50]

Whilst the use of MSP has been well established for the characterisation of pigments in paint, it has also shown potential for the analysis of UV absorbing compounds in clear coats. Stoecklein and Fujiwara demonstrated that UV MSP can discriminate between automotive clear coats based upon their corresponding UV absorption profile.[51] Whilst the features in the UV profile could be attributed to both the UV absorbers and binders, the authors concluded that the spectral characteristics are primarily attributed to the structural core of the UV absorber.[51] In spite of the research that has been conducted, a proficiency trial conducted in 2004 has indicated that only 15 % of forensic examiners routinely employ MSP in the analysis of automotive paint.[52] The reason behind this may be due to the fact that MSP lacks the chemical specificity of other spectroscopic techniques as the output is inherently simplistic, typically consisting of one or two broad spectral features, thus making discrimination between samples much more difficult.[53]

1.3.3 Infrared (IR) Spectroscopy

IR spectroscopy is unequivocally the most powerful, non-destructive technique available for the characterisation of paint, providing information pertaining to the composition and relative abundance of binder/resin, pigment and extender components.[14, 34, 54] IR spectroscopy utilises IR radiation to probe the molecular features of materials. When IR radiation is irradiated onto a sample, some, but not necessarily all of the radiation can be absorbed to render an IR spectrum that is characteristic of the molecular structure of the sample.[55] IR spectroscopy is incapable of identifying components that are present in trace amounts (less than 5 % by weight) and as a result is unlikely to detect minor co-polymers, residual solvents and most additives.[34, 54] Paint evidence in the form of chips and fragments is often quite small; as such a beam condensing and focusing device and a Fourier transform IR (FT-IR) spectrometer is essential in order to adequately characterise the sample.[29, 56] FT-IR spectroscopy has been widely used in the analysis of paint evidence, with several sampling techniques including transmission,[47, 57-60] reflection,[57] transflection,[57] diffuse reflectance[57, 61, 62] and attenuated total reflection (ATR)[63, 64] being reported in the open literature. A complicating factor

with most modern FT-IR spectrometers is that they often employ a narrow-band mercury cadmium telluride (MCT) detector, which has a spectral cut-off near 700 cm^{-1}.[34, 38, 56] Unfortunately, many inorganic pigments and extenders have key vibrational bands in the far IR region of the spectrum, well below the spectral cut-off of the MCT detector.[14, 34] Extended IR spectroscopy using caesium iodide optics and a deuterated triglycine sulfate detector has enabled spectra to be acquired down to 220 cm^{-1}.[65-70] Transmission analysis is typically preferred over reflectance techniques, even though time consuming sample preparation is required. This is because reflectance analysis typically suffers from poor signal to noise ratio, spectral distortion and issues with reproducibility.[54] Furthermore, reference databases such as the Paint Data Query (PDQ) database contain transmission data which are incompatible with spectra obtained *via* reflectance techniques.[71, 72]

1.3.3.1 ATR IR Spectroscopy

ATR FT-IR spectroscopy has shown great potential in the forensic analysis of paint smears and the individual characterisation of automotive paint layers.[14, 34] ATR FT-IR spectroscopy is a surface sensitive technique that minimises the need for sample preparation as only contact between the specimen surface and the reflectance crystal is required,[54] as depicted in Figure 1.4. This is due to the fact that the evanescent wave generated following internal reflectance of the infrared beam in the crystal, protrudes 1-2 µm out of the crystal and therefore only penetrates 1-2 µm into the specimen surface.[14, 34] Due to the surface sensitive nature of the technique it enables the *in situ* analysis of transferred paint smears on a substrate, with minimal interference from the substrate itself.[14] Additionally, the shallow penetration of the beam can be exploited to rapidly characterise original clear coats, without having to separate the coating from the underlying layers.[64] It has been demonstrated that ATR FT-IR spectroscopy can be utilised in the rapid characterisation and discrimination of automotive clear coats.[73, 74]

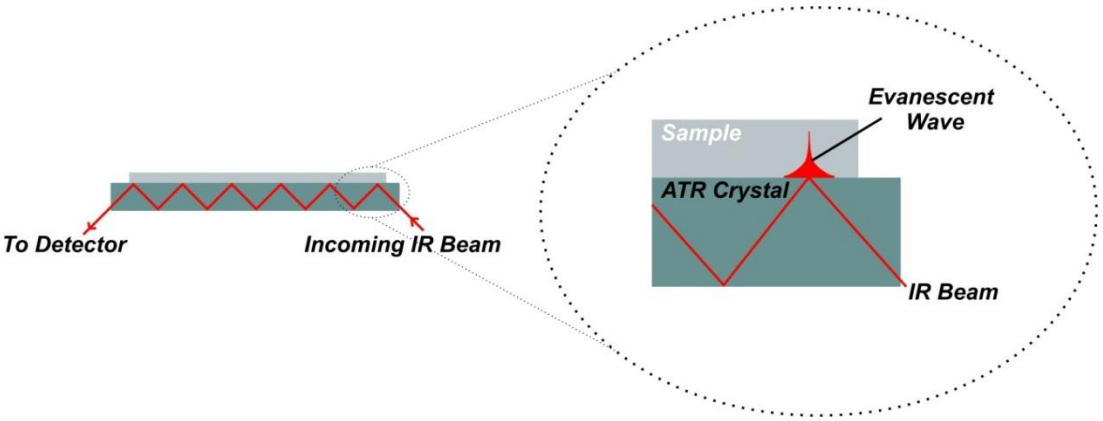

Figure 1.4: Diagrammatic representation of the analysis of a sample by multiple-bounce ATR FT-IR spectroscopy.

1.3.3.2 IR Microspectroscopy

FT-IR microspectroscopy combines the power of microscopy with the FT-IR technique and has become the foremost method of choice for the analysis of multicomponent systems, such as automotive paint, in forensic laboratories.[29, 56] This is because it allows the examiner to sequentially analyse all layers of the sample, without the need for individual separation of each layer or complex sample preparation.[57, 58] Samples analysed by transmission FT-IR microspectroscopy are normally sectioned using a microtome, to provide thin cross-sections that are 5-10 µm thick. The transverse sections are typically flattened between diamond windows and each layer is separately characterised multiple times with a small aperture.[56] FT-IR microspectroscopy is one of the most valuable tools available to the forensic paint examiner, as it enables highly reproducible, non-destructive, rapid, individual layer comparisons.[54]

1.3.3.3 IR Chemical Imaging

IR chemical imaging offers an alternative to FT-IR microspectroscopy, owing to the fact that chemical and spatial information can be obtained from the sample synchronously. In this particular instance, IR chemical imaging allows potentially hundreds of spectra to be acquired from all layers of the paint cross section simultaneously.[75, 76] Previous research by Flynn *et al* has demonstrated that focal plane array (FPA) detectors can be employed in the stratigraphic imaging of

automotive paint chips.[75] These authors noted that FPA based chemical imaging offers significant advantages over single-point infrared microspectroscopy (section 1.3.3.2), relating to the analysis of multicomponent paint chips. The advantages stem from the fact that thousands of spectra are collected across the sample, which allows the user to either visualise the distribution of chemical components across all the layers of the sample, or extract IR spectra from regions of interest. This wealth of information ultimately enables comparisons between samples to be more easily visualised.[75] However in some instances, conventional glow bar sourced IR microspectrometers, with both single element and FPA based detectors, may not display adequate sensitivity and spatial resolution required for the analysis of automotive paint traces. In these scenarios, synchrotron sourced FT-IR microspectroscopy can provide improved signal to noise ratios and spatial resolution, and thus can overcome the shortcomings associated with conventional glow bar sourced IR microspectroscopy.

1.3.3.4 Synchrotron IR Microspectroscopy

A synchrotron is a very large cyclic particle accelerator that generates intensely bright, highly collimated beams of electromagnetic radiation, which can be utilised as an alternative light source for spectroscopic analysis.[77, 78] A schematic diagram of the Australian Synchrotron in Melbourne is presented below in Figure 1.5. In a synchrotron, electrons generated by an electron gun are accelerated by a linear accelerator to relativistic speeds. The electrons are moved into the booster ring where their energy is further increased before they are transferred into the storage ring. The storage ring consists of a number of bending magnets, separated by a series of straight sections that contain insertion devices such as undulators and wigglers. As the electrons move through the storage ring, they are deflected by the bending magnets and insertion devices, resulting in the release of electromagnetic radiation. The synchrotron radiation is funnelled into a beam-line and filtered to the desired wavelength using monochromators, before being directed down to an end-station for use.[77, 78]

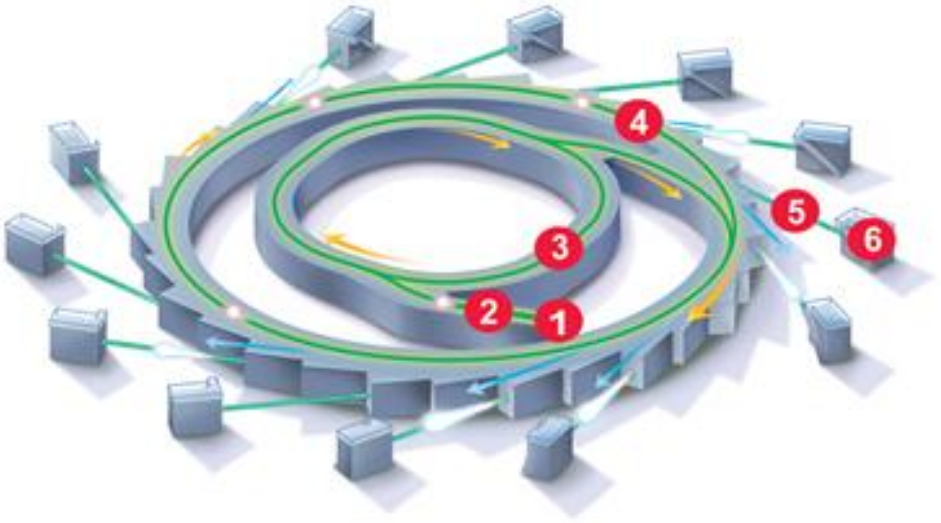

Figure 1.5: Schematic diagram of the Australian Synchrotron; (1) electron gun, (2) linear accelerator 'linac', (3) booster ring, (4) storage ring, (5) beam-line and (6) end-station.[78]

Synchrotron radiation has been used extensively in a number of disciplines including biosciences,[79, 80] medical research,[81, 82] environmental sciences,[83] materials analysis and engineering,[84-86] and forensic science.[87] A detailed review concerning the application of synchrotron light to the analysis and characterisation of forensic trace evidence has been provided by Kempson *et al*.[87] Synchrotron radiation in the mid-IR range is roughly 2-3 orders of magnitude brighter than conventional glow bar sources, which equates to a 20-40 fold improvement in the signal to noise ratio. Furthermore, the radiation is polarised and highly collimated, enabling spectra to be acquired with a greater spatial resolution (i.e. 2-5 μm) than conventional instrumentation.[87-90] Ultimately, the improved spatial resolution of synchrotron sourced IR allows the examiner to analyse smaller sample areas or regions of interest. This is highly significant, especially in instances where thin layers are encountered and the improved spatial resolution is required in order to unequivocally characterise only the layer of interest.[91] These advantageous features can potentially be highly beneficial to the analysis of multi-layered systems like automotive paint.

1.3.4 Raman Spectroscopy

Recent advances in Raman spectrometers have resulted in a renewed interest in Raman spectroscopy as an analytical technique, consequently providing an outlet for exploring this technique in forensic applications.[34] Raman spectroscopy, much like IR spectroscopy, provides information regarding the molecular structure of a sample. However, whilst IR spectroscopy is concerned with the absorption of light, Raman spectroscopy deals with the inelastic scattering of monochromatic light (i.e. laser) by a sample.[92-95] When a sample is irradiated with monochromatic light, most of the light is elastically scattered (Rayleigh scattering), such that the scattered light has the same energy as the incident light. However, a small fraction of the light is inelastically scattered, which causes the photon to either gain (anti-Stokes shift) or lose energy (Stokes shift) due to deactivation or excitation of molecular vibrations.[92-94] The shift in energy of the photon is dependent upon the chemical structure of the molecule itself and can provide knowledge regarding the structure, symmetry, electronic environment and bonding of the molecule.[93, 95, 96]

As Raman spectroscopy is based on light scattering as opposed to absorption, it provides information complementary in nature to IR spectroscopy. Raman spectroscopy, like IR spectroscopy, provides information regarding the characteristic vibrations of molecules. Whilst IR spectra arise from dipole changes, Raman spectra arise from polarisability changes that occur during vibration. Hence IR spectroscopy is more adept at detecting polar molecular features, whilst Raman spectroscopy is more suitable for the identification of less polar moieties.[34, 97] This notion is illustrated by Figure 1.6, which depicts the IR and Raman spectrum of an aftermarket refinish clear coat. By examining both spectra it is evident that the less polar aliphatic C-H stretches (blue region) are more intense in the Raman than the IR spectrum. Similarly, the polar moieties attributable to the carbonyl stretches (red region) are significantly stronger in the IR than the Raman spectrum. The complementary nature of Raman and IR for forensic analysis is best exemplified by a study conducted by Buzzini and Massonnet, detailing the discrimination of 40 similarly coloured green spray paint samples.[98] The authors noted that individually,

IR and Raman spectroscopy have a lower discriminating power than when the techniques are used in combination with each other.[98]

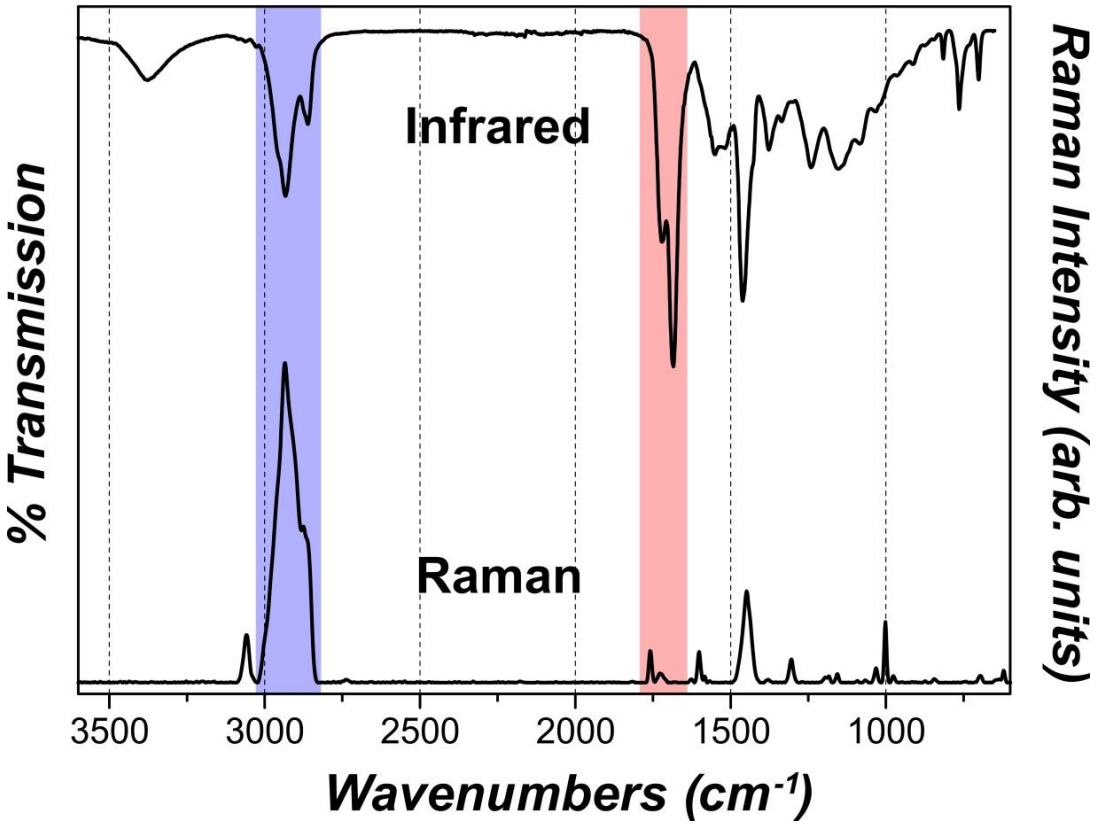

Figure 1.6: Comparison of ATR FT-IR and FT-Raman spectra of an aftermarket refinish clear coat.

Whilst Raman spectroscopy has previously been utilised to chemically interrogate the binder portion of paint systems,[99, 100] it has been employed primarily in a forensic context to provide information concerning the organic and inorganic pigments, including the extenders.[101] This is due to the fact that Raman spectrometers are routinely capable of identifying spectral features down to 100 cm^{-1}, well into the far-IR region of the electromagnetic spectrum where many pigments have key vibrational bands.[34] A study by Massonnet and Stoecklein employed FT-Raman spectroscopy to identify pigments in red automotive basecoats. These authors concluded that Raman spectroscopy was a suitable technique for the rapid, *in situ* analysis of red automotive basecoats, based upon the high discrimination power achieved for light red (0.89) and dark red (0.97) paints.[102] Whilst research has demonstrated that Raman spectroscopy could be an integral part

of the forensic analysis scheme, it is not routinely used in all forensic laboratories.[29] One issue that has limited the applicability of Raman spectroscopy to the analysis of paint is that the laser may induce fluorescence of the sample, which could potentially mask any spectral features in the Raman spectrum. By employing a near-IR laser (e.g. 1064 nm) the fluorescence emission could be somewhat mitigated; however, as longer wavelength light sources produce significantly weaker Raman scattering, a FT-Raman spectrometer needs to be employed.[93, 94]

1.3.5 Pyrolysis-Gas Chromatography/Mass Spectroscopy (Py-GC/MS)

Py-GC/MS has been established as arguably the most discriminating technique available for differentiating between similar paint binder compositions.[34, 103-105] It is a highly sensitive and discriminating method that has shown real potential in the forensic examination of polymer traces.[106-108] Py-GC/MS is a technique that pyrolytically decomposes trace amounts (5-10 µg) of paint into gaseous products which are then introduced into a gas chromatograph. The pyrolysis process thermally breaks down the polymeric macromolecules, which correspond to the paint binders, into smaller fragments. The fragments are then separated using GC and can be identified by their resulting mass spectrum.[7, 29, 107] The technique is typically employed to identify the monomer/s used in binder systems, but is also sensitive enough to characterise and identify some additives, pigments and residual solvents.[109, 110] Additionally, Py-GC/MS is capable of detecting subtle variations in binder composition and as such has the ability to differentiate between paint samples that are indistinguishable by FT-IR and Raman spectroscopy.[111, 112] Whilst the technique has a high discriminating power, it is destructive and often time consuming; consequently any chemical information obtained from non-destructive techniques always precedes Py-GC/MS. As a result, Py-GC/MS is typically one of the last techniques utilised in the forensic analysis of paint.[29, 34, 39]

1.3.6 Elemental Analysis

Elemental analysis constitutes a combination of bulk and trace instrumental techniques, including but not limited to; scanning electron microscopy energy dispersive spectroscopy (SEM-EDS), X-ray fluorescence spectroscopy (XRF) and laser ablation inductively coupled plasma mass spectroscopy (LA-ICP-MS).[33, 38, 39] Elemental analysis is primarily utilised to characterise the inorganic components and extenders present in the paint specimen. These techniques provide information complementary to IR spectroscopy and Py-GC/MS, which are typically used to analyse the organic components of paint.[29, 34, 38] SEM-EDS is a non-destructive technique that provides the examiner with information pertaining to particle sizes and distribution, morphology and bulk elemental composition of the sample. The method is sensitive down to approximately 1 % of mid-range atomic weight elements (i.e. nitrogen to bismuth), with the elemental profile being particularly useful in identifying the extenders in the sample.[113, 114] XRF is another non-destructive technique capable of determining the elemental composition of a paint sample.[115, 116] However, XRF unlike SEM-EDS is significantly more sensitive to higher atomic weight elements and as such is particularly useful in characterising drier metals, inorganic colouring and metal complex pigments.[34, 114, 117] XRF typically suffers from limited spatial resolution and is widely considered a bulk technique. However, a recent study by Ninomiya has demonstrated that synchrotron XRF microspectroscopy with high energy excitation is capable of characterising small areas of interest and is capable of discriminating between similarly coloured pearlescent coatings.[118] LA-ICP-MS is a viable technique for the forensic analysis of automotive paints, owing to the improved sensitivity over the previously described elemental techniques, as well as the ability to detect trace elements.[119]

1.3.7 X-ray diffraction (XRD)

Although X-ray diffraction (XRD) is not an elemental technique, it can also be occasionally employed by forensic examiners to perform inorganic analysis on paint. Unlike the previously mentioned techniques, XRD does not provide the user with an elemental profile per se; rather XRD assesses the crystallinity of the material and can provide definitive identification of major inorganic pigments.[114]

1.4 Interpretation of Trace Contact Evidence

1.4.1 Questioned *vs.* Known Comparisons

The approach adopted by forensic examiners in the analysis of paint evidence is dependent primarily on the presence or absence of a control material. If a control or known paint sample from a suspect vehicle is available to the examiner, then comparisons between the questioned paint sample obtained from the scene and the known paint sample may be undertaken.[29, 33] In these so-called questioned *vs.* known comparisons, both samples are compared based upon their physical and chemical characteristics *via* a suite of analytical tests, as depicted in Figure 1.7. As stated previously, the sequence of examination is dependent on the equipment available to the examiner, but is also contingent on the quantity, quality and morphology of the samples.[14, 29] Typically, microscopical examinations are conducted first, as differences in the layer colour, structure and sequence between the questioned and known sample will immediately indicate if the samples do not share a common origin. On the other hand, destructive techniques such as Py-GC/MS are normally conducted last, especially in instances where there are only trace amounts of sample to begin with.[34]

If the known and questioned paint sample cannot be discriminated using the combination of analytical techniques described above, then it can be inferred that the specimens could share a common source. Similarly, if the two samples have different physical and chemical characteristics, then the notion of a common origin can be excluded.[29] Only in the event of a physical fit between the questioned and control samples, can it be unequivocally concluded that the two paint samples are from the same source (Figure 1.7). The main issue with questioned *vs.* known comparisons, especially considering the results of spectroscopic analysis, is that they invariably rely on visual comparisons of complex spectra. These comparisons are highly subjective and have led to serious concerns within the forensic community, regarding human error and bias in the interpretation of trace evidence.[53, 120]

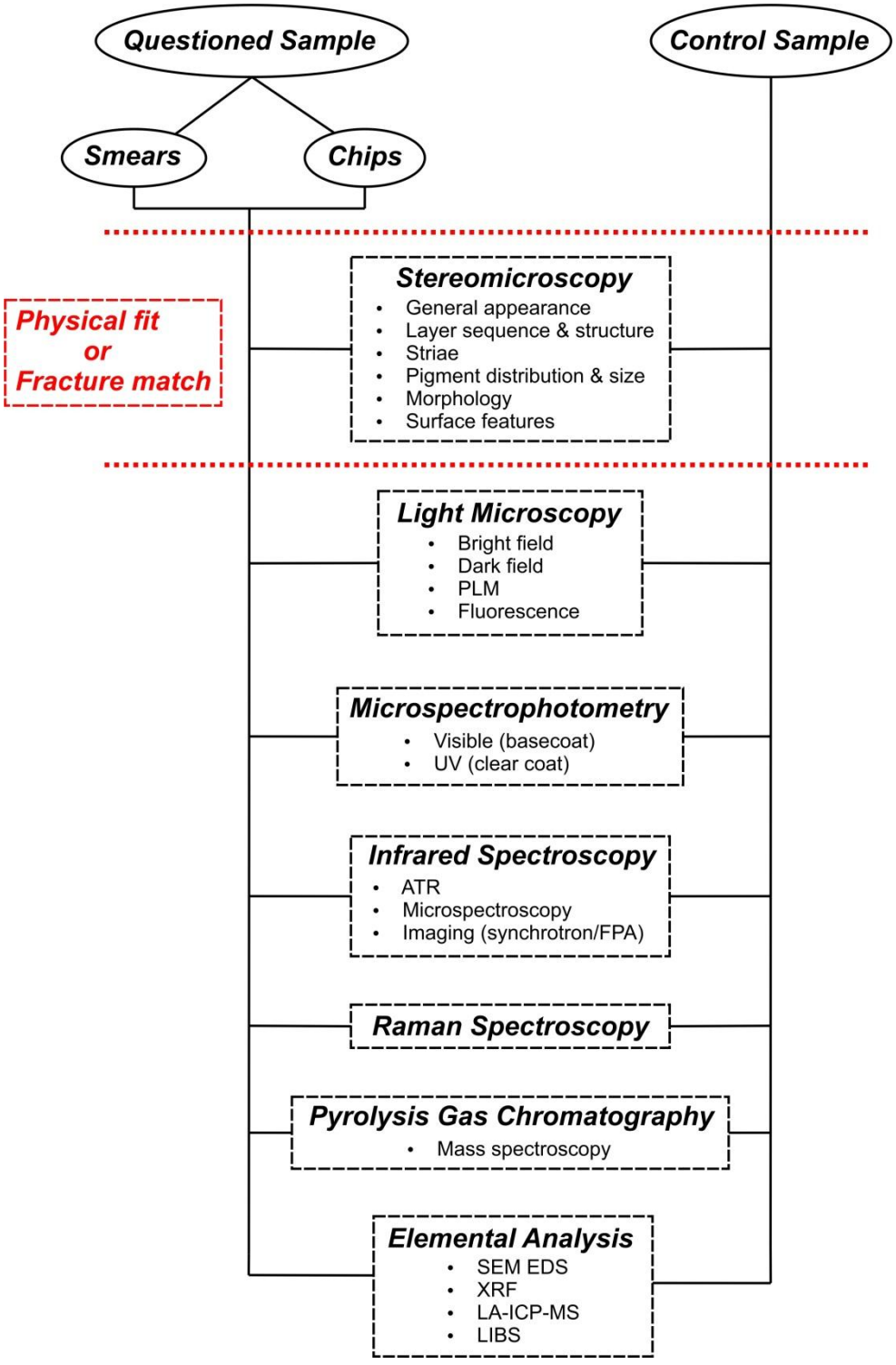

Figure 1.7: Typical analytical sequence for automotive paint evidence in the comparison of questioned and control samples. If the samples remain undifferentiated following characterisation with a specific technique, then the examiner continues with the sequence of examination. This figure was adapted from [38].

1.4.2 No Known Sample

There are some instances, such as those involving hit-and-run accidents, where a known sample is not available for a comparison. In these scenarios, the physical and chemical characteristics of the questioned sample can be compared to a database of known references in order to procure investigative leads. One such automotive paint database, known as PDQ, was established in the early 1970's by the Royal Canadian Mounted Police and is the largest automotive paint database in existence.[7, 121] At this period in time, the PDQ database contains over 19, 000 independent samples, representing paint systems from a range of global vehicle manufacturers. PDQ is a computerised text-based database that contains information regarding both the physical characteristics (i.e. layer sequence and colour) and chemical composition of each individual layer in the paint system.[121-123] Furthermore, PDQ is equipped with a library that contains IR spectra of every individual layer from the paint systems. The PDQ database is capable of direct searching of IR spectra using the IR SearchMaster add-in. However, the basic search algorithms used by IR SearchMaster provide matches based on a limited number of spectral features as opposed to the entire spectrum, and only IR data from one layer can be searched at any given time. Consequently, the forensic examiner typically translates the chemical information from the IR spectra into specific text codes, which are then inputted into the database along with information pertaining to the colour and layer sequence of the paint system, so as to provide a list of probable matches to vehicles.[56, 124] In this way, the PDQ database can be utilised for investigative purposes, as it aids in the potential identification of the make, model and year of an unknown vehicle, from a paint sample encountered at a crime scene.

However, the issue with the coding system used in the PDQ database is that it is highly generic, as it only recognises the presence or absence of chemical components in the paint system, whilst neglecting to factor in their relative amounts. This lack of specificity in the search criteria results in a significantly larger number of potential matches that the forensic examiner must work through and eliminate.[124, 125] Furthermore, the hits generated by the database have to be manually interpreted by

visually comparing the IR spectra from each coating in the unknown paint sample, against the library spectra from the individual layers of the database matches.[125] This presents a similar problem to that observed in questioned *vs.* known comparisons, in that it still requires manual interpretation of the spectra by the examiner, which is again subject to human error and bias. As a result, one of the main issues that need to be addressed by the forensic science community is the subjective nature of the interpretation of forensic trace evidence.

1.4.3 Issues in the Interpretation of Forensic Evidence

Recent inquiries undertaken by the Science and Technology Committee in the UK, and the NAS in the US, have attempted to highlight issues pertaining to the forensic community. Both of these investigations revealed that there is the potential for bias in the current interpretational protocols for forensic trace evidence.[4, 5] Specifically, the NAS report identified the need to establish strict rigorous protocols for the interpretation of forensic evidence.[5]

> *"A body of research is required to establish the limits and measures of performance and to address the impact of sources of variability and potential bias. Such research is sorely needed, but it seems to be lacking in most of the forensic disciplines that rely on subjective assessments of matching characteristics."*[5]

Furthermore, the NAS recommended that research be undertaken to address issues of accuracy, reliability and validity in forensic science, which includes research concerning human observer bias and sources of human error in forensic examinations.[5] The use of multivariate statistics or chemometrics has the potential to address the aforementioned recommendations, enabling meticulous statistical and scientific approaches to the interpretation of forensic evidence.

1.5 Chemometrics in Forensic Data Analysis

As mentioned previously, when attempting to determine if a questioned and known paint sample could share a common source, the forensic examiner often relies principally on the visual comparison of complex spectra. Consequently, the examiner lacks a statistical basis for evaluating the validity or significance of the evidence in question.[126] Chemometrics is a discipline that uses mathematical and statistical approaches to design and optimise experimental procedures, extract maximum chemical information from data, and procure knowledge about chemical systems.[127, 128] Chemometrics has previously been utilised in forensic science in order to mitigate bias and partiality in the interpretation of analytical data obtained from trace evidence.[129-131]

Chemometrics eliminates the subjectivity associated with the visual comparison of complex spectra from questioned and known samples, as it ensures that quantitative, impartial measures of the data are obtained. This is extremely significant considering forensic science is a discipline centred on the notion of forming objective conclusions, based upon the analysis of physical evidence.[129] Chemometrics provides a statistical measure of how similar or dissimilar samples are thus improving the reproducibility, reliability and discrimination of the data, whilst simultaneously addressing issues such as human error and bias.[129, 131] There is a myriad of chemometric techniques that may be suitable in the interpretation of analytical data obtained from forensic evidence. These include, but are not limited to; cluster analysis, principal component analysis (PCA), linear discriminant analysis (LDA), soft independent modelling of class analogy (SIMCA) and artificial neural networks.[129-131] In this study, a combination of PCA and LDA was utilised to interpret spectroscopic data obtained from automotive paint evidence. The approach was adopted as it enables much of the relevant, discriminating portions of the data to be extracted, whilst also allowing accurate predictions to be made about the data.[131] It should be noted that multivariate statistical analysis can be used in conjunction with Bayesian statistics to develop likelihood ratios. The Bayesian method has been previously used in the interpretation of automotive paint evidence.[33, 34]

1.5.1 Principal Component Analysis (PCA)

It is not uncommon for modern spectroscopic techniques to generate anywhere from hundreds to several thousands of variables, with the sheer volume of data making it difficult for structure and patterns to be discerned. Exploratory data analysis in the form of PCA enables the user to identify patterns in multivariate data.[132-134] PCA is the general workhorse of modern chemometrics, as it forms the foundation for many of the other multivariate statistical techniques.[135, 136] PCA is an unsupervised technique that requires no user input in regards to sample groupings and is primarily concerned with reducing the dimensionality of the original dataset, whilst still retaining as much of the variance in the data as possible.[137, 138] In PCA, the original data is transformed into principal components (PCs); which are essentially latent, orthogonal, uncorrelated pseudo-variables generated *via* the linear combination of the original, interrelated variables, for each sample in the dataset.[129, 131, 134, 138, 139] Each PC accounts for an amount of the total variance contained in the original data, with the first PC describing the greatest proportion of the variance in the dataset. Every successive PC accounts for less variation than the previous one, thus enabling a significant proportion of the variance in the data to be described in the first few PCs. A small number of these PCs can then be utilised to reconstruct the dataset, revealing patterns and structure that would not have been readily visible in the raw data.[132, 137, 140]

PCA can be performed by analysing either a correlation or a covariance matrix, with the latter being utilised throughout the entirety of this thesis. In the correlation method, the original dataset is mean centred and scaled, such that each variable in the transformed dataset is weighted equally. This approach is desirable in instances where variables have different measurement units, or when some components have significantly larger variances than others. In the covariance method, the data is mean centred but not scaled, with this approach being preferred in instances where the magnitude of the variance and the metric of the variables are comparable.[131, 133, 134]

PCA transforms the original data matrix (X), into a score (T) and a loadings (P) matrix, as given by the following equation:

$$\mathbf{X = T.P + E}$$

The combined scores and loadings for the first few PCs contain all or most of the systematic variation from the original dataset. Therefore, by multiplying the scores and the loadings matrices together, the original dataset can be reconstructed, minus a residual or error (E), which contains negligible relevant information and noise.[132] Every sample contains a score on each PC, with the score acting as a co-ordinate reflecting the sample position on that PC. By plotting the scores for the first two or three PCs (2D or 3D scores plot), it is possible to visualise or map the position of the samples, which ultimately enables structure and patterns to be discerned.[132-134] The scores plot allows the user to visually identify and cluster similar samples into groups, whilst also discriminating between samples that have markedly different scores. The formation of groupings within the scores plot is often indicative of samples sharing similar chemical characteristics.[138] Further information may be extracted from the scores plot by examining the loadings, which reflects the variables in the original data that have a significant weighting (either positive or negative) on a PC. Variables that have large positive or negative values have a significant impact on a PC, whilst low values indicate that those variables are less significant to that PC.[132, 133]

1.5.2 Linear Discriminant Analysis (LDA)

One of the main goals of pattern recognition is in the classification of samples. LDA is a form of supervised pattern recognition that uses pre-specified groupings to develop and build classification rules.[129, 131] The use of LDA is often preceded by a data reduction technique typically in the form of PCA. LDA generates a discriminant function *via* a linear combination of variables, which maximises the ratio of between to within class variance (i.e. Fisher ratio), thereby providing maximum separation between groupings.[133, 134, 140] The resultant model is then utilised to reassess and reclassify the samples from the original dataset, thereby providing the user with a percentage correct classification. The LDA model can then be used to assign

unknown samples into the most probable grouping, enabling the predictive power of the model to be gauged.[131, 137] The classification accuracy of the developed model can be determined through the use of cross-validation procedures.[133] The most common form of validation is the leave-one-out method, which is an iterative process whereby the first sample is omitted from the dataset and a discriminant model is generated based upon the remaining data. The resultant model predicts the classification of the test sample and the exact procedure is then repeated for every other sample in the dataset.[132, 133]

The simplest form of cross-validation, known as the re-substitution method, utilises the entire dataset as a training set to develop a discriminant model based upon the pre-specified groupings.[141] The classification rules are then used to re-classify each sample, such that the predicted grouping can be compared to the actual grouping. The major drawback with the re-substitution method is that it employs exactly the same data to both define and evaluate the model. In view of this, the discriminant model tends to be overoptimistic, which ultimately has a detrimental effect on the classification accuracy of the model when applied to new datasets.[133, 134, 141]

The most reliable and robust method of validation is test set validation, whereby the entire original dataset is segregated into two distinct datasets; a calibration or training set and a validation or test set.[132, 133] The training set, which preferably is around twice as large as the test set, is employed to develop and define the model; with the resultant model being used to predict the classification of test samples. The predicted classification of the test samples can then be compared with their actual grouping to afford a prediction error, which gives an estimation of the efficacy of the model. Test set validation is the most effective and accurate form of cross-validation as it uses two independent datasets to both develop and test the model.[132, 133, 139] This form of cross-validation has been used throughout the entirety of this thesis.

1.5.3 Chemometrics in the Analysis of Trace Evidence

A combination of PCA and LDA has been applied in the discrimination and classification of forensic evidence; including fibres,[142-144] glass,[145, 146] inks,[147, 148] soil,[149, 150] hair,[151] accelerants,[152-154] photocopy and printer toners,[155-158] paper,[159] electrical tapes[160, 161] and paint.[53, 124, 162-164] Chemometrics has been employed previously in paint analysis, with research demonstrating the applicability of PCA and discriminant analysis to the quality control of paint coatings.[165] In a forensic context, chemometrics has been utilised in the analysis of both architectural[164] and spray paints.[163] Similarly, a number of studies have started to use chemometrics in the analysis of automotive paints.[53, 124, 162] The main limitation with all of these studies can be primarily attributed to the small sample sizes, which limit the significance and minimises the predictive capabilities of the statistical models.

1.5.4 Chemometrics in the Analysis of Automotive Paint

A study conducted by Liszewski *et al*[53] utilised UV MSP in conjunction with multivariate statistics, in order to assess the extent of diversity within a number of automotive clear coats. Cluster analysis and PCA revealed that three distinct groupings were present within the sample population; however no discernible relationship could be made between the groupings and the make, model or year of the corresponding vehicles. As a result, this method is limited in that it can only really be used in the comparison of questioned and known samples and cannot procure investigative leads.[53] A further study conducted by Mendlein applied the same statistical protocols to Raman spectra obtained from automotive clear coats, with similar results.[166]

Research undertaken by Kochanowski and Morgan[162] utilised Py-GC/MS in combination with PCA and LDA (canonical variate analysis), to characterise and discriminate between 100 automotive paint samples, representing 5 different colours.

The authors noted that LDA performed on the spectra is capable of differentiating between paint samples as a function of their colour, with only minor overlap observed between blue and silver paint groupings. Additionally, PCA subplots generated from samples of the same colour demonstrated that the variance between samples is much greater than that within the sample (replicates), potentially enabling further discrimination to be achieved between vehicles of a similar colour, but different make and model.[162]

A study by Lavine and co-workers[124] has utilised search pre-filters to aid in searching the IR spectral libraries of the PDQ database. The authors utilise a two-step procedure to develop these search pre-filters. The first step involves applying wavelets to decompose FT-IR spectra of clear coats in the PDQ library into wavelet coefficients. A genetic algorithm consisting of both supervised (LDA) and unsupervised (PCA) forms of pattern recognition analysis identifies wavelet coefficients characteristic of the model and manufacturer of the automobile. Using this approach, the authors were able to distinguish between samples from Chrysler vehicles from a similar production year range, as a function of the manufacturing plants where the vehicles were assembled.[124]

1.6 Aims

In spite of recent developments, chemometric techniques have not been routinely employed by the forensic science community for the analysis and interpretation of automotive paint evidence. The focus of this dissertation is to utilise a number of spectroscopic techniques in conjunction with chemometrics, in order to develop a statistically reliable means of comparison and differentiation in the analysis of automotive paint evidence. Whilst this thesis is principally concerned with the analysis of automotive paint, the methodology developed is universal and may potentially be applied to other forms of trace contact evidence. This thesis

dissertation involves five main streams of investigation. The first, detailed in Chapter 3, utilises conventional ATR FT-IR spectroscopy in combination with multivariate statistical techniques (i.e. PCA and LDA) to characterise and classify a statistically large population of automotive clear coats. Chemometric methods were employed to identify patterns and structure within the data, in an effort to provide information regarding the potential make, model or year of the vehicle, as a function of the chemical composition of the clear coat. Further discussion in Chapter 4 focuses on fundamental chemical studies that may affect the classification model generated in the previous chapter. Synchrotron FT-IR microspectroscopy was used to obtain high spatial resolution stratigraphic chemical images of automotive paint cross-sections, with a view to examining the extent of migration of chemical components between layers. Additional studies utilising ATR FT-IR spectroscopy examined the effect environmental conditions such as heat, humidity and UV light have on the degradation of automotive clear coats.

To date, the forensic analysis of paint has primarily been limited to the analysis of the base and clear coat. In fact, the public domain is seemingly devoid of any research examining the variability in the chemical composition of the underlying layers, such as the electrocoat primer, primer surfacer and basecoat. Consequently, Chapter 5 examines the chemical diversity in a large sample set of basecoats, primer surfacers and electrocoat primers, using a combination of synchrotron FT-IR microscpectroscopy and PCA. Chapter 6 investigates the comparisons between statistical models developed following characterisation of the automotive clear coats using IR and FT-Raman spectroscopy. As previous research has shown that a combination of IR and Raman spectroscopy attains a much higher discriminating capability than both techniques used in isolation; Chapter 7 examines the potential of developing an all-encompassing, highly discriminating statistical model that incorporates chemical information obtained from both techniques.

Chapter 2: Experimental Considerations

2.1 Sampling

All automotive paint exemplars were obtained from a sunroof fitting company (Prestige Sunroofs WA, Australia) from roof panels removed during the process of sunroof installation, as illustrated in Figure 2.1. The make, model, year and Vehicle Identification Number (VIN) were recorded for each vehicle.

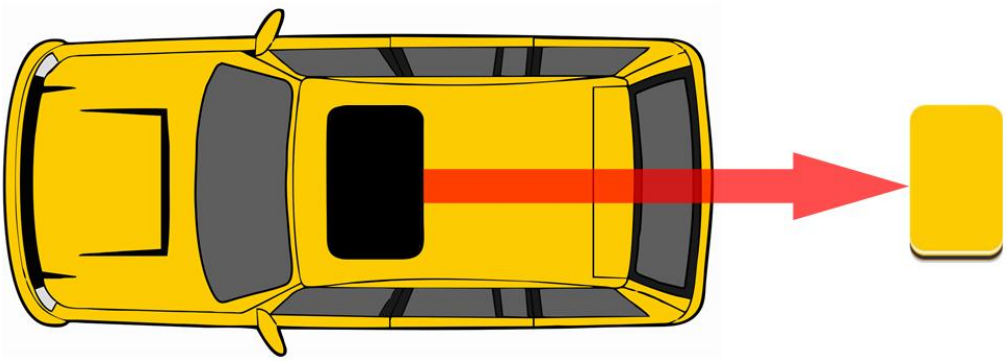

Figure 2.1: Diagrammatic representation depicting the position on the vehicle where samples were obtained.

In studies outlined in this dissertation, statistically relevant sample populations were utilised, consisting of 139 individual vehicles covering a range of Australian and international manufacturers. The sample collection consists of a diverse range of vehicles with 17 different manufacturers and 45 different models being represented, as shown in Table 2.1. Whilst there are 17 different manufacturers represented in the sample population, roughly 60 % of the sample population consists of only Holden and Holden Special Vehicles (HSV), Ford, Toyota and Mazda vehicles. This was anticipated considering a sales report commissioned by the Federal Chamber of Automotive Industries, revealed that the cumulative sales for these manufacturers totalled approximately 45 % of the Australian market in 2013.[167] Although this deviates slightly from the value in the sample population, it signifies that the collection of samples is generally characteristic of the average vehicle in Australia.

Table 2.1: A complete breakdown of the vehicle types, model/s and origin of manufacture for every vehicle in the sample population.

Manufacturer	No. Samples		Model(s)	Origin of Manufacture
BMW	**3**		325i/135i Coupe	Germany
Dodge	***7***	5	Nitro	US (Toledo, Ohio)
		2	Journey	Mexico (Toluca, Mexico State)
Ford	**17**	10	Falcon/Territory	Australia (Broadmeadows, Victoria)
		5	Focus	Germany
		2	Mondeo	Germany
Holden	**38**	36	Commodore/Calais/Adventra/Caprice/Cruze	Australia (Elizabeth, South Australia)
		2	Captiva	South Korea
Holden Special Vehicles (HSV)	**9**		Grange/GTS/Clubsport	Australia (Clayton, Victoria)
Honda	**8**	3	Accord	Japan
		2	CRV	Poland
		2	City	Thailand
		1	Civic	UK
Hyundai	**5**		i30/Elantra	South Korea
Jaguar	**1**		X-Type	UK
Jeep	**3**		Cherokee	US (Detroit)
Mazda	**12**		Mazda 3/Mazda 6	Japan
Mitsubishi	**8**	4	Pajero	Japan (Nagoya)
		3	Lancer	Japan (Mizushima)
		1	Colt	Japan
Nissan	**5**	2	Maxima	Thailand
		2	Navara	Spain
		1	X-Trail	Japan
Saab	**2**		Saab 93	Sweden
SsangYong	**2**		Kyron	South Korea
Subaru	**5**		Impreza	Japan
Suzuki	**1**		Grand Vitara	Japan
Toyota	**13**	6	Celica/Corolla/Prado/Kluger	Japan
		4	Camry	Australia (Altona, Victoria)
		3	Hilux	Thailand

2.2 Decoding the VIN

Important information utilised throughout this body of work regarding the country of origin, as well as other common vehicle descriptors (Table 2.1), were obtained by decoding the VIN. The VIN is a 17-digit alphanumeric code that not only uniquely identifies a vehicle, but also provides latent information about the vehicle itself.[168-170] The VIN is composed of three sections; the world manufacturer identifier (WMI), the vehicle descriptor section (VDS) and the vehicle identification section (VIS). The WMI contains the first three characters of the VIN, with the first two digits signifying the country of origin of the vehicle.[169, 170] In this study, the origin of manufacture of the vehicle was decoded by using a list of country codes, which is given in Table 2.2 below.

Table 2.2: Partial list of common country codes. The bolded country codes were encountered in this study.[170]

	Code	Country
Africa (A-H)	AA-AH	South Africa
Asia (J-R)	**J**	**Japan**
	KL-KR	**South Korea**
	L	China
	ML-MR	**Thailand**
Europe (S-Z)	**SA-SM**	**United Kingdom**
	SN-ST, W	**Germany**
	SU-SZ	**Poland**
	VF-VR	France
	VS-VW	**Spain**
	YS-YW	**Sweden**
	ZA-ZR	Italy
North America (1-5)	**1, 4, 5**	**United States**
	2	Canada
	3A-3W	**Mexico**
Oceania (6-7)	**6A-6W**	**Australia**
	7A-7E	New Zealand
South America (8-9)	8A-8E	Argentina
	9A-9E, 93-99	Brazil
	9F-9J	Columbia

The remaining characters in the VIN often contain information pertaining to the manufacturing plant and platform where the vehicle was assembled, the vehicle model/series, body style, transmission, chassis and engine type and the sequential production number (Table 2.3).[169, 170] Unfortunately, the VIN positions of the characters corresponding to the aforementioned vehicle descriptors vary markedly depending upon the manufacturer.[170] As this study required specific information concerning the manufacturing plant where the vehicle was assembled, individual manufacturer VIN books were used to decipher and obtain this information.

Table 2.3: Example VIN broken down into individual segments and decoded.[170]

WMI	VDS	Check Digit	VIS
JT8	BH22F	4	T0048456
J = Japan **T** = Toyota Motor Corporation **8** = Lexus Division	**BH2** = LS400 4-door Sedan; 4.0 L V8 Engine **2F** = Restraint System; Dual Airbags		**T** = 1996 Model Year **0** = Tahara (Japan) Assembly Plant **048456** = Sequential Production Number

2.3 ATR FT-IR Spectroscopy

ATR FT-IR spectroscopy was utilised to characterise the original manufacturer clear coat of all automotive paint exemplars, which contain either a typical 4-coat or OEM refinish paint system. A scalpel was utilised to pry chips of paint off the underlying metal ensuring all paint layers were present in the sample. The paint chip was then positioned so that the clear coat was in contact with the reflectance crystal of the ATR attachment. IR spectra of the automotive clear coats were recorded with a Perkin Elmer® Spectrum™ FT-IR spectrometer, equipped with a universal single-bounce Diamond-ZnSe crystal ATR sampling accessory. The ATR accessory is equipped with a pressure arm in order to consistently maintain the sample and crystal interface contact at a force of 80 N. Perkin Elmer software, Spectrum® (v. 6.3.2), was employed to perform an ATR correction on the entire spectral dataset, to

account for the change in the depth of penetration with wavelength, so that the collected spectra were visually comparable to transmission spectra. All spectra were acquired over a range of 4000-650 cm^{-1}, with a spectral resolution of 4 cm^{-1} and 4 accumulated scans. Five replicate scans were recorded at different locations for each paint sample, as replicate measurements are essential in chemometric studies to accurately measure *intra*-sample versus *inter*-sample variation. Between sample acquisitions, the crystal was thoroughly cleaned to remove contaminants and particulate matter using an ethanol soaked piece of lint free tissue. A background scan of the clean Diamond-ZnSe crystal was acquired before each sample scan.

2.4 Synchrotron FT-IR spectroscopy

2.4.1 Cross-section Preparation

Paint chips were obtained by using a scalpel to flake the paint off the underlying metal, being careful to ensure that all paint layers were present in the sample. The chips of paint were then sandwiched between two rigid pieces of plastic prior to transverse sectioning with a microtome equipped with a stainless steel blade. The paint chips could not be sectioned as is because they are brittle in nature and tend to fracture easily. Similarly, samples were not embedded in a resin prior to microtoming as previous research indicated the infiltration of the embedding media into the paint chips, leading to interference bands in the resultant IR spectra.[171] The microtomed cross sections obtained from all paint samples were 8 µm thick. The paint sections were then separated from the plastic and pressed flat between two micro-diamond cell windows (Thermo Scientific). As the samples remained flat the top window was removed prior to spectra acquisition.

2.4.2 Sample Characterisation

All experiments were conducted on the IR microspectroscopy (IRM) beam-line of the Australian Synchrotron, Melbourne, Australia. The mechanics of the IRM beam-line are outlined in detail by Creagh *et al*.[172] The beam-line consists of a Bruker Vertex V80v FT-IR spectrometer, equipped with a liquid nitrogen cooled narrow-band MCT detector in conjunction with a Bruker Hyperion 2000 microscope (Bruker Optik GmbH, Ettlingen, Germany). The microscope is equipped with a motorised sample stage that allows spectral mapping of regions of interest, and an atmospheric purge box to minimise background variation over the mapping time. The paint sections were mapped in transmission mode using an X-Y step size of 2.5 µm, with a 5 µm x 5 µm sampling aperture. Spectra were acquired over the range of 3900-730 cm^{-1} at a spectral resolution of 4 cm^{-1} with 64 co-added scans. 2-dimensional false colour chemical maps were then generated for specific IR bands of interest by correlating integrated peak areas to specific positions in the measured grid. Data acquisition and processing was performed *via* Bruker Opus software (version 7.0). The process is illustrated in Figure 2.2.

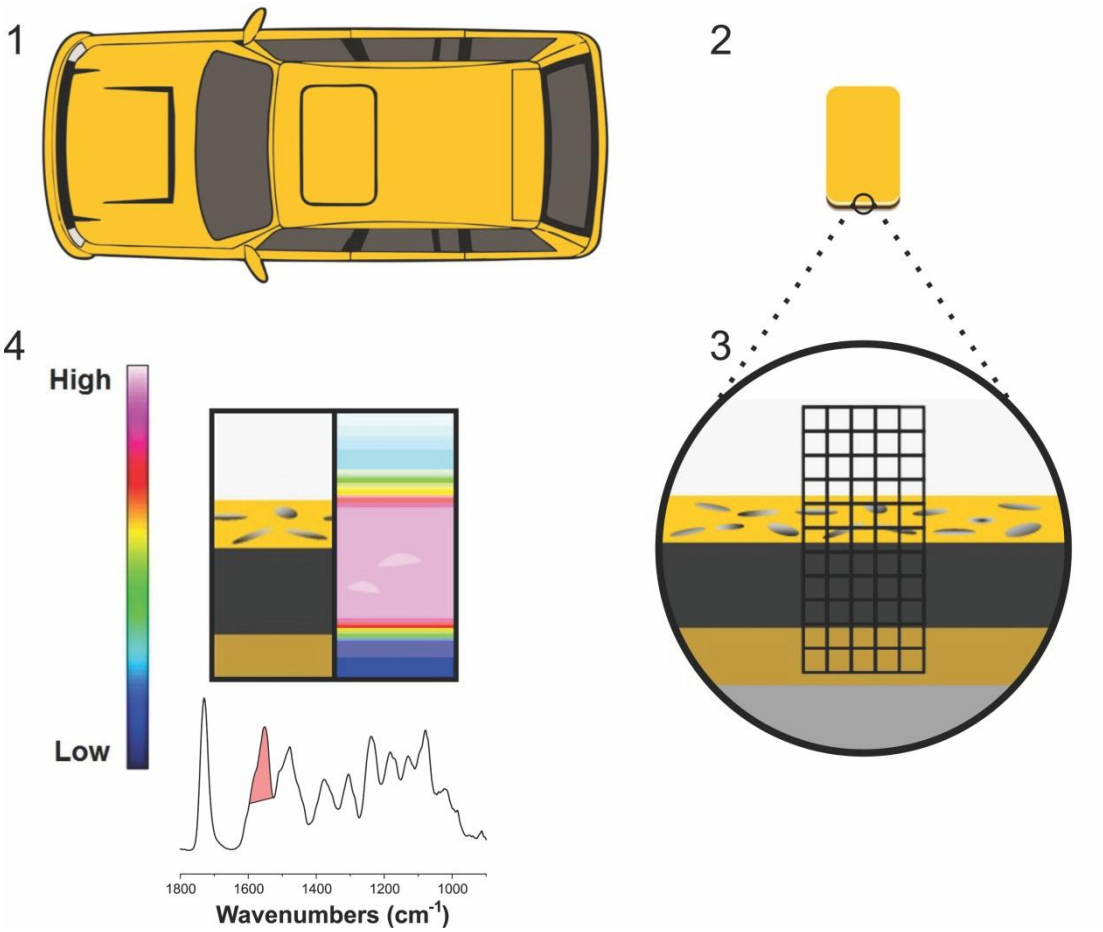

Figure 2.2: Diagrammatic representation of the stratigraphic imaging of automotive paint cross-sections via synchrotron FT-IR microspectroscopy. Paint samples were obtained from roof panels (2) removed from the vehicle during the process of sunroof installation (1). Synchrotron FT-IR microspectroscopy was then utilised to map an area across the paint section (3), whereby an IR spectrum was collected at each grid-point in the map. 2D chemical images were then generated by integrating specific peaks, thereby enabling the distribution of select chemical components to be visualised (4).

2.4.3 Interference Fringe Removal

IR transmission spectra obtained from thin films such as automotive paint cross-sections are convoluted by the presence of interference fringes, which often mask small spectral features and make quantification of components problematic.[173-175] In this particular instance, the interference fringes are caused by multiple reflections of IR radiation within the sample, resulting in a sine wave pattern propagated

throughout the spectrum.[176] These fringes may affect both the qualitative and quantitative interpretation of the spectra and thus need to be eliminated.[175] As a result, interference fringes were removed from the spectra by spectral subtraction of a sinusoidal wave with the same frequency as the fringes of the original data, as depicted in Figure 2.3.

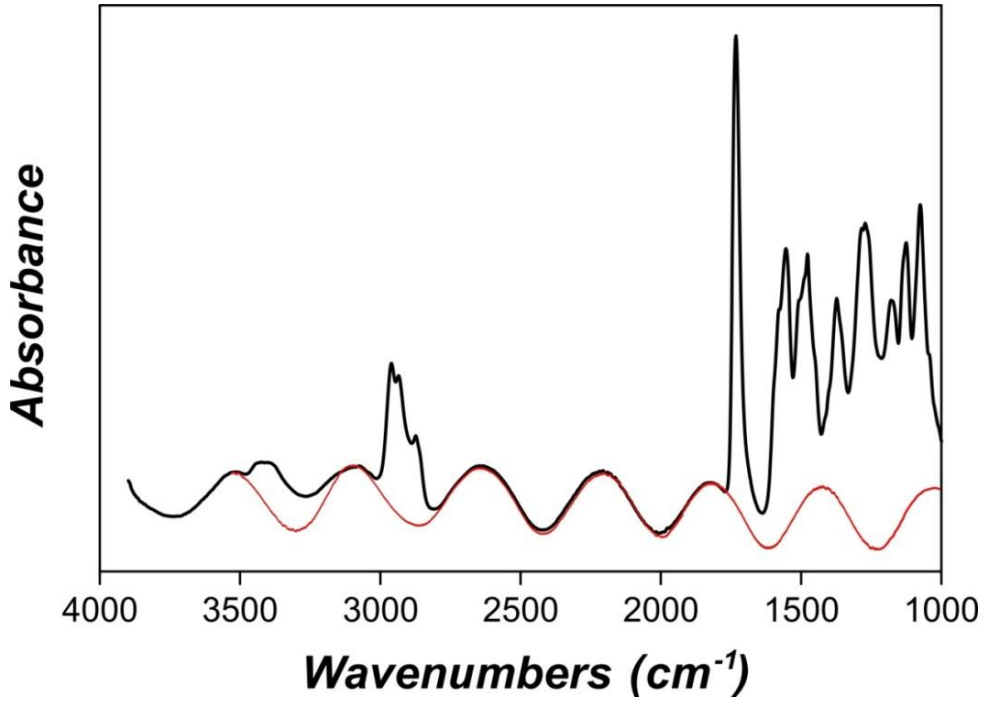

Figure 2.3: Interference fringes were removed from IR spectra by subtracting the sine wave function (red) from the original IR spectrum (black).

2.5 Chemometrics

Prior to the use of chemometric techniques the data was pre-processed, in order to eliminate systematic noise and any variation arising from the characterisation of the sample. For each stream of investigation in this dissertation, all spectra were assembled and stored in a single data matrix, whereby every column signified a variable and each row represented a sample. All spectra in the dataset were then linearly baseline corrected and range normalised, unless otherwise specified. Additionally, the data was truncated to a range of 1800-650 cm^{-1}, unless otherwise specified, so as to only retain chemically relevant information from the 'fingerprint'

region of the spectra. Furthermore, truncation of the dataset also eliminates extraneous variables, such as those pertaining to aliphatic C-H stretches, which contain negligible relevant information. All pre-processing and subsequent statistical analysis of the data was performed using the Unscrambler® X 10.2 software (CAMO Software AS, Oslo, Norway).

2.5.1 Principal Component Analysis

PCA was performed on the truncated pre-processed data matrices in order to visualise groupings and enable relationships to be discerned. In this study, mean-centred data was analysed by PCA using the non-linear iterative partial least squares (NIPALS) algorithm. 3-dimensional scores plots were generated by using the scores from as many as the first five PCs, in order to visualise the grouping of samples within the dataset. The loadings corresponding to these PCs were then employed to identify characteristic spectral features that give rise to the discrimination between samples.

2.5.2 Linear Discriminant Analysis

The discriminant models generated in this study were validated using test set validation. In this method, the entire spectral dataset was segregated into two independent sets of data; a calibration or training set and a validation set. The training set (490 spectra; 98 vehicles) was roughly 2.5 times larger than the validation set (205 spectra; 41 vehicles). As some groupings in the dataset contained more samples than others, the data was separated in a manner such that the training set contained approximately 2.5 times more samples per grouping than the validation set. The training set was used to generate the discriminant model, whilst the validation set was then used to classify unknown test samples and gauge the predictive performance of the model. The efficacy of the models was evaluated by comparing the actual grouping to the predicted grouping of each sample in both datasets. This information was presented in a table in the form of a confusion matrix.

Chapter 3: Characterisation and classification of automotive clear coats using attenuated total reflectance infrared spectroscopy and chemometrics

---

Portions of this chapter have been published in the journal *Analytical Methods*:

Maric, M., van Bronswijk, W., Lewis, S.W., and K. Pitts, *Rapid characterisation and classification of automotive clear coats by attenuated total reflectance infrared spectroscopy*. Analytical Methods, 2012. **4**(9): p. 2687-2693.

3.1 Introduction

Automotive clear coats are principally utilised in order to protect the basecoat from the effects of weathering, chemical agents, solvent and mechanical impact.[7, 24] Clear coat technology was first instituted in the early 1970's, when the single layer topcoat system was replaced by a pigmented basecoat and clear coat. Over the years, the clear coat has gained popularity and unsurprisingly is still utilised in automotive paint systems. In fact, less than 2 % of all automotive paint systems worldwide have no OEM clear coat.[24] Clear coat technology is ever-evolving and has changed extensively since its inception, with different paint binders and lower concentrations of VOCs being utilised, so as to comply with new environmental standards and regulations.[51] Modern OEM clear coats applied to the painted metal portions of the vehicle typically consist of only one of two possible formulations; a combination of melamine, acrylic and styrene, or melamine, acrylic, styrene and polyurethane.[125]

Paint smears often arise when less forceful contact occurs between a vehicle and a substrate.[6, 29] Due to the relatively large thickness of the clear coat layer, in comparison to the thinner underlying layers, most paint smears consist only of the clear coat.[124, 125] In instances where clear coat paint smears are encountered at crime scenes, obtaining investigative leads from this evidence has often proved challenging. Whilst databases such as PDQ have been implemented in these situations, they have often found limited success.[124] Although direct searching of IR spectra in the PDQ database is possible with the IR SearchMaster add-in program, the program provides matches based upon a limited number of peaks rather than the entire spectrum. Consequently, the IR data is typically manually interpreted and coded, with the coded information being utilised to search against the codes in the database. The generic nature of the coding system, in conjunction with the fact that OEM clear coats typically only have two possible formulations, makes it difficult to obtain conclusive information about the vehicle (due to the large number of potential matches) from clear coat smears.[124, 125] As searching of the PDQ database relies heavily on large variations in the chemical composition and colour of the coating, this significantly limits the applicability of the PDQ database in the identification

and characterisation of the automotive paint evidence. Additionally, both the text-based and spectral searches are restricted by the samples in the database, which predominantly consists of North American vehicles. Subsequently, the PDQ system is somewhat limited in obtaining information from OEM clear coats in an Australian context.

An approach based upon multivariate statistics may aid in procuring investigative leads in an Australian context, under the provision that a statistically relevant sample population is used. Consequently, this chapter investigated the use of ATR FT-IR spectroscopy in combination with chemometric techniques, in order to assess the chemical diversity of a statistically large population of automotive clear coats. ATR FT-IR spectroscopy was employed to characterise the outermost surface of the paint system (i.e. OEM clear coat), with PCA and LDA being applied to the resultant data. Although discrimination between the samples was based solely upon their resultant IR spectra, in some instances it was difficult to correlate a subtle change in the IR spectra with changes in the composition of the coating. Thus, Py-GC/MS was utilised to aid primarily in elucidating the acrylic components that discriminate between select groups of samples. The novelty in this stream of investigation lies in the methodology and statistical approach, in conjunction with the large sample size of individual vehicles, which ultimately enables patterns and relationships to be discerned that would otherwise prove impracticable.

3.2 Experimental

ATR FT-IR spectra were obtained from the automotive clear coats as described in section 2.3. The resultant IR data was collated and pre-processed according to section 2.5. PCA and LDA were then conducted on the data as described in section 2.5.1 and 2.5.2 respectively.

3.2.1 Py-GC/MS

A Curie point pyrolysis unit (Horizon Instruments) was coupled with a Hewlett Packard 6890 gas chromatograph mass spectrometer. The samples (~ 5 µg) were mounted on a flattened, bent Curie point wire and pyrolysed at 770 °C, for a duration of 5 s, in the pyrolyser head. The pyrolysis products were directly transferred by a stream of helium (18 psi) into an Agilent J&W vitreous silica DB1701 (cyanopropyl phenyl methylsilicone) capillary column (30 m, i.d. 0.25 mm) and detected by the mass spectrometer. The GC conditions and temperature program are summarised below in Table 3.1. The mass spectrometer was operated in positive electron impact mode and the resultant data was interpreted using mass spectral databases. The analysis of automotive paint samples by Py-GC/MS was conducted by Kari Pitts at the ChemCentre.

Table 3.1: Summary of the GC conditions and temperature program utilised in the characterisation of automotive clear coats by Py-GC/MS.

GC Conditions		Temperature Program	
Mode	Splitless	***Initial Temp.***	35 °C
Initial Temp.	250 °C (On)	***Time at Initial Temp.***	1 min
Pressure	9.50 psi (On)	***Initial Ramp Rate***	8 °C/min
Purge Flow	500.0 mL/min	***Intermediate Temp.***	150 °C
Purge Time	0.50 min	***Final Ramp Rate***	20 °C/min
		Final Temp.	270 °C
		Time at Final Temp.	10 min

3.3 Results & Discussion

3.3.1 Principal Component Analysis

PCA performed on the entire spectral dataset (695 spectra) revealed that 98.1 % of the total variance of the data was accounted for in the first five PCs, as depicted in the Scree plot below (Figure 3.1). The Scree plot is highly significant as it provides the user with an indication of the appropriate number of PCs to be utilised.[177] This is important because if too few PCs are examined, information pertaining to variation within the dataset may be overlooked.[177, 178] Likewise, if extraneous PCs are employed, systematic noise may potentially be incorporated into the model.[134] Thus, the Scree plot was ultimately used as a screening method, so as to determine the optimal number of PCs required to model the data. This was accomplished by identifying the location of the plot where there is a natural break or where the curve is plateauing or levelling off.[134, 177, 178] In this particular instance, the Scree plot clearly indicates that as many as five PCs could be employed to reconstruct the data. Although the first three PCs account for 96.0 % of the variance in the data, as the spectral variation may be subtle, the first three PCs may not be sufficient to model the dataset. Consequently, the influence of the fourth and fifth PC was evaluated.

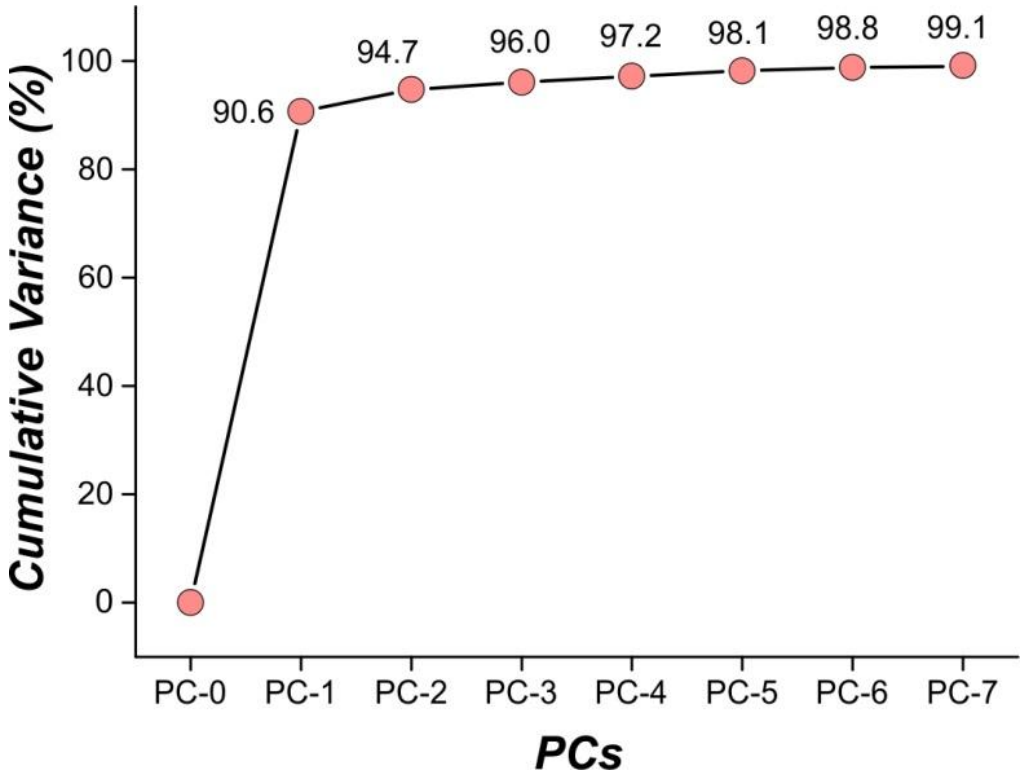

Figure 3.1: Scree plot depicting the variance in the dataset retained by each PC.

3-dimensional PCA scores plots were generated by plotting the scores of the projected objects from the relevant PCs. 3-dimensional scores plots created using a number of combinations of the first five PCs (Figure 3.2 and Figure 3.3), revealed that there visually appear to be 17 groupings in the dataset. A strong correlation was made between the sample groupings as a function of common vehicle descriptors; including vehicle origin, manufacturer, model/s, assembly plant and in some instances the year of vehicle manufacture.

Interestingly, upon examination of the scores plot generated from the first three PCs (Figure 3.2), it was observed that the samples in classes 1-3, cannot be visually discriminated, as the samples are projected too close together. However, upon substituting the scores from the third PC with the fifth PC in the scores plot, it can be seen that PC5 can be utilised to discriminate between these groupings (Figure 3.3). Whilst the fifth PC individually accounts for only 0.9 % of the variance in the dataset, it was integral in providing additional discrimination between samples. The influence of the fourth PC was also examined; however, PC4 was determined to have a diminished influence on the model, as it afforded no additional group separation. It is also worth noting the impact of the third PC on the scores plot (Figure 3.2). The third PC also only accounts for a small percentage of the variance (1.3 %) in the data, however, it is responsible for segregating the samples in classes 7-9 from the other groupings. More importantly, as the samples in class 8 do not have significant negative or positive scores on PC1 and PC2, the third PC is primarily responsible for describing these samples. This is not the case with the samples in classes 7 and 9, as they are also both tenuously accounted for by PC2 (Figure 3.2).

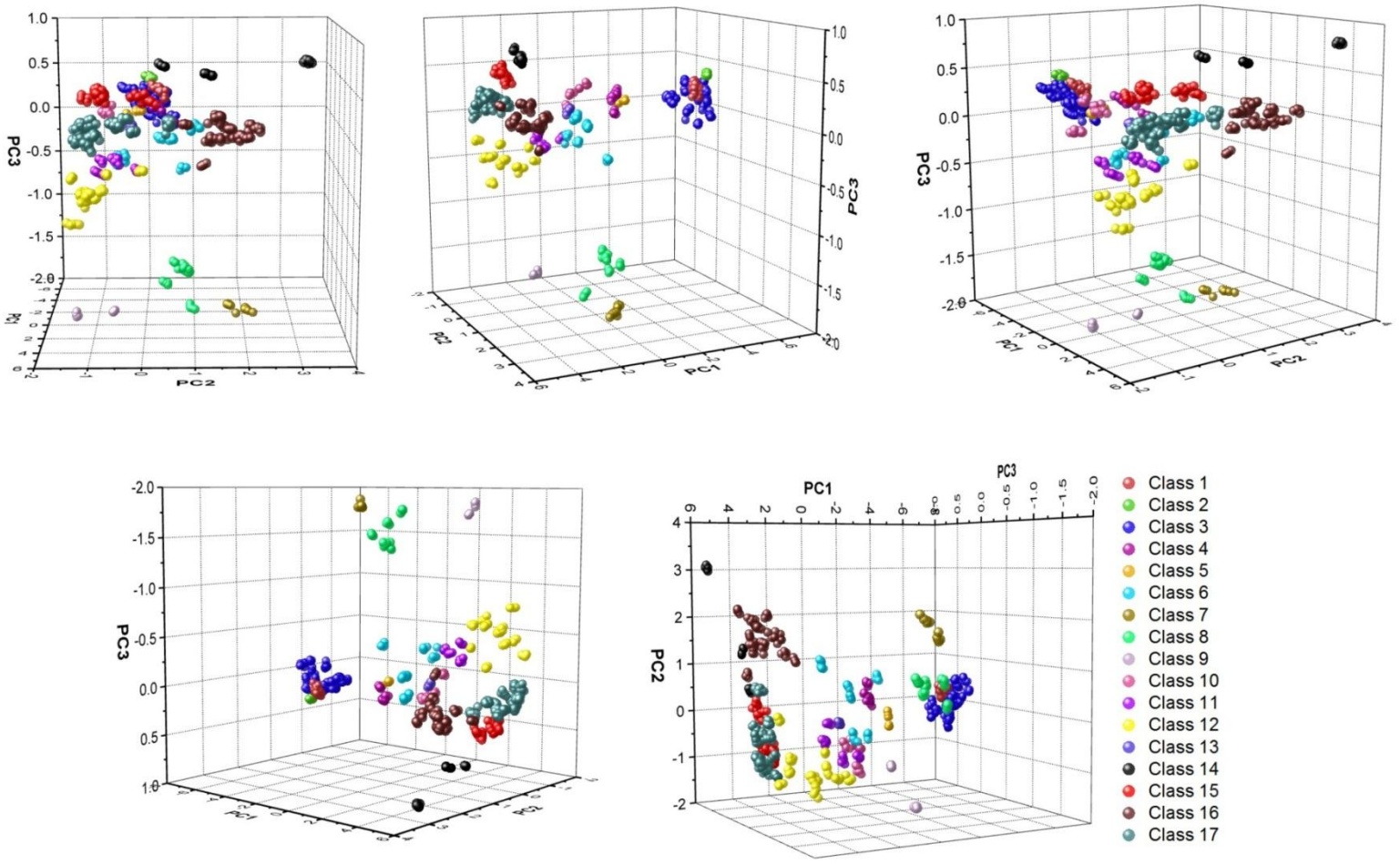

Figure 3.2: A 3-dimensional PCA scores plot from a number of different perspectives, generated using the first three PCs, highlighting the distribution of a population of automotive clear coats based upon their corresponding IR spectra.

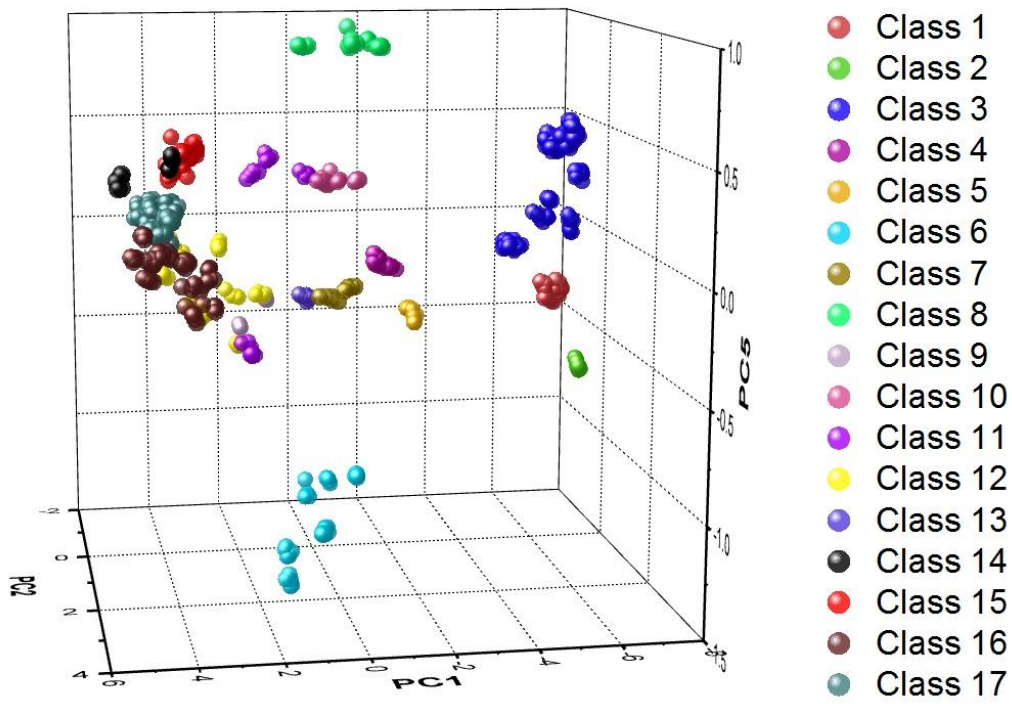

Figure 3.3: 3-dimensional PCA scores plot, consisting of PC1, PC2 and PC5. The fifth PC enables discrimination between the samples in classes 1, 2 and 3.

Based upon the PCA scores plots depicted in Figure 3.2 and Figure 3.3, it is evident that 17 groupings are present in the spectral data. A complete breakdown of the vehicles represented in each class is provided below in Table 3.2. The first grouping consists of samples obtained from the US-manufactured Dodge and Jeep vehicles. Whilst both these Dodge and Jeep vehicles were assembled in different regions and manufacturing plants in the US, it is not surprising that they group together considering they fall under the flagship Chrysler brand. With that being said, Dodge vehicles that were manufactured in Mexico were not grouped with the samples in class 1, but rather formed their own distinct grouping (class 5). Class 2 contained samples representing the German-manufactured BMW vehicles. The samples in class 3 signified Australian and Japanese-manufactured Toyota; and Japanese-made Mazda and Mitsubishi vehicles. Interestingly, the Mitsubishi vehicles represented in this class were Mitsubishi Lancers, which are assembled at the Mizushima manufacturing plant. This differs to the Mitsubishi Pajero vehicles from class 4, which are manufactured in Nagoya, thereby highlighting inherent diversity within an automotive manufacturer as a function of the plant where the vehicle was assembled.

Table 3.2: Summary of the samples that comprise every PCA grouping.

Class No.	No. of Samples	Vehicles Represented
Class 1	8	US (Dodge/Jeep)
Class 2	3	BMW
Class 3	25	Japan (Mazda/Mitsubishi Lancer); Australia/Japan (Toyota)
Class 4	4	Mitsubishi Pajero
Class 5	2	Mexico (Dodge)
Class 6	7	Japan (Subaru/Mitsubishi Colt/Nissan)
Class 7	2	Germany (Ford Mondeo)
Class 8	5	Hyundai
Class 9	2	South Korea (Holden)
Class 10	6	Germany (Ford Focus)
Class 11	5	Poland (Honda); Sweden (Saab); UK (Jaguar)
Class 12	11	Thailand (Nissan/Toyota); Japan (Honda/Suzuki)
Class 13	2	SsangYong
Class 14	4	Australia (Ford) [2004-2009]
Class 15	9	Australia (Ford) [2009-present]; Spain (Nissan)
Class 16	15	Australia (Holden/HSV) [2001-2009]
Class 17	29	Australia (Holden/HSV) [2009-present]

It is important to note that four classes exist within the dataset signifying samples obtained from Ford vehicles (classes 7, 10, 14 and 15). Classes 7 and 10 contain samples from the German-manufactured Ford Mondeo and Focus respectively, whilst classes 14 and 15 contain predominantly Australian-made Ford vehicles. The primary distinction between the two Australian Ford classes can be attributed to the period in time when the vehicles were manufactured. In particular, class 14 contains samples from Ford vehicles manufactured from 2004 up until 2009, whilst samples in class 15 represent Ford vehicles produced from 2009 until present day. Interestingly, class 15 also includes samples obtained from Spanish-manufactured Nissan Navara vehicles. Similarly, there are three classes in the dataset that contain samples obtained from General Motors-manufactured Holden vehicles (classes 9, 16 and 17). It is not surprising that the South Korean-manufactured Holden vehicles (class 9) differ from the Australian-made Holden vehicles (classes 16 and 17).

However, a relationship was also identified within the samples obtained from Australian factory-made Holden vehicles as a function of the year the vehicles were manufactured. Specifically, samples obtained from class 16 signified vehicles manufactured from 2001 up until 2009, whereas samples in class 17 represented vehicles manufactured from 2009 onwards. The significance of this relationship will be discussed in detail later. Class 8 and class 13 contain samples representing the South Korean-manufactured Hyundai and SsangYong vehicles respectively.

Class 6 principally consists of samples obtained from Japanese-manufactured Subaru vehicles. Whilst there are solitary samples in this grouping signifying Japanese-made Mitsubishi Colt and Nissan vehicles, the number of paint samples representing these vehicles is far too small for patterns or generalisations to be inferred. Consequently, these samples are not able to form stand-alone groupings and thus must be grouped with samples that attain similar scores. It is anticipated that as the dataset continues to expand and the subsequent model becomes more defined, the model will most likely compensate for this change, effectively producing more classes corresponding to these vehicles. This was also observed to an extent with select samples in classes 11 and 12. Class 11 consisted of samples representing select vehicles manufactured in Europe; including the Polish-manufactured Honda CRV, the Swedish-made Saab and the UK factory-made Jaguar. Finally, class 12 represents both Toyota and Nissan utility vehicles manufactured in Thailand, as well as the Japanese-manufactured Honda and Suzuki.

To evaluate the discrimination veracity and basis of the statistical techniques, the IR spectra of the central samples of each grouping were visually examined and their chemical constituents were identified, as displayed in Figure 3.4. Predictably only two formulations were identified in the automotive clear coat population, with either an acrylic, melamine, styrene, or an acrylic, melamine, styrene, and polyurethane enamel being utilised.[125] However, relative differences in the abundance of components were observed in the centroid IR spectra of each grouping (Figure 3.4).

In all instances the main type of binder was identified as acrylic; but, subtle differences within the acrylic 'fingerprint' region (i.e. 1300-1000 cm^{-1}) were observed, suggesting variations in the acrylic co-polymers utilised to create the backbone of the enamel.[14] Melamine was another component present in all automotive clear coats, as it is an amino resin principally utilised to cross-link the acrylic backbone.[14, 15, 24] Styrene was also identified in virtually all acrylic enamels of the automotive clear coats, with its continual use being predicated on the favourable qualities such as gloss and hardness, it imparts to the finished film.[24] It is important to note that whilst all automotive clear coats contain these three fundamental components, the abundance of these components can vary significantly. On the other hand, polyurethane was only unequivocally observed in the clear coats of the German-made Ford Mondeo (class 7) and South Korean-manufactured Hyundai vehicles (class 8). Interestingly, a large abundance of polyurethane was also observed in aftermarket respray clear coats and the significance of this will be discussed in detail shortly. Although the chemical composition of the clear coats were comparable, variations between spectra typically arise from differences in the relative amounts of acrylic, melamine, polyurethane and styrene present, as well as differences in the acrylic co-polymers used. These differences can often be difficult to distinguish *via* the use of visual comparisons (Figure 3.4), reinforcing the need for a multivariate statistical approach.

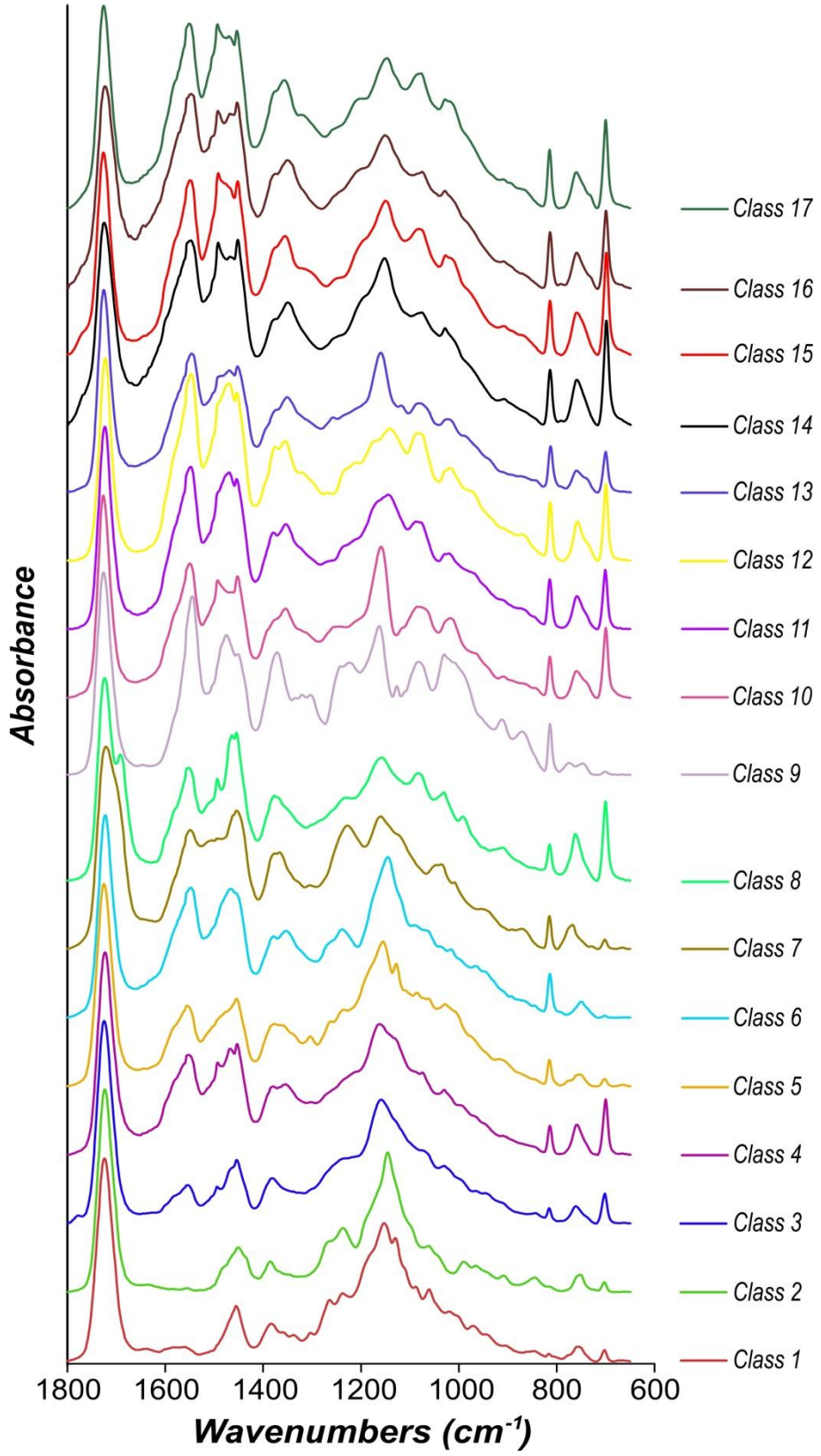

Figure 3.4: The IR spectra obtained from the central objects of each class, showing the spectral differences between the groupings.

The factor loadings for the first five PCs were utilised to identify the spectral regions contributing to the variance in the dataset. In particular, the loadings plot for PC1 (Figure 3.5), revealed a significant positive correlation at approximately 1550 cm^{-1} and a region of significant positive correlation between 1490 and 1450 cm^{-1}. The intense broad absorption at 1550 cm^{-1} is indicative of an in-plane triazine ring expansion attributable to melamine.[14, 55, 56, 179] Furthermore, the intense peaks *ca.* 1490 and 1450 cm^{-1} are characteristic for both ring and side chain C-N stretches and C=C aromatic ring stretches, which could be symptomatic of both melamine and styrene. By examining the scores plot in Figure 3.5, it can be observed that samples which have relatively large intensities of these peaks, and thus a large abundance of melamine and styrene, attain significant positive scores on PC1 (e.g. classes 14-17). Conversely, samples that have relatively low intensities of these variables have significant negative scores on PC1 (e.g. classes 1-3). As a result, discrimination between classes on PC1 is achieved based primarily upon the relative abundance of melamine in the clear coat.

The loadings plot for PC2 depicted in Figure 3.6 revealed zones of significant positive correlation in the 1700 and 1635 cm^{-1} regions of the IR spectrum. It is important to note that the dominant vibrational stretch in all the IR spectra in the sample population was the band near 1730 cm^{-1}, which is principally attributed to the ester carbonyl stretch of the acrylic component.[14] Consequently, the large positive correlation at 1700 cm^{-1} is most likely indicative of a shift in the peak position of the carbonyl stretch associated with the acrylic binder, thereby implying a probable change in the acrylic binder composition. On the other hand, the significant positive correlation at 1635 cm^{-1} relates to a shoulder on the melamine peak. Whilst the loadings plot for PC2 describes very subtle differences in the IR spectra, PC2 is influential in the model as it is solely responsible for the discrimination between the two classes representing the Australian-manufactured Holden and Ford vehicles. The significance of this result will be discussed in detail shortly.

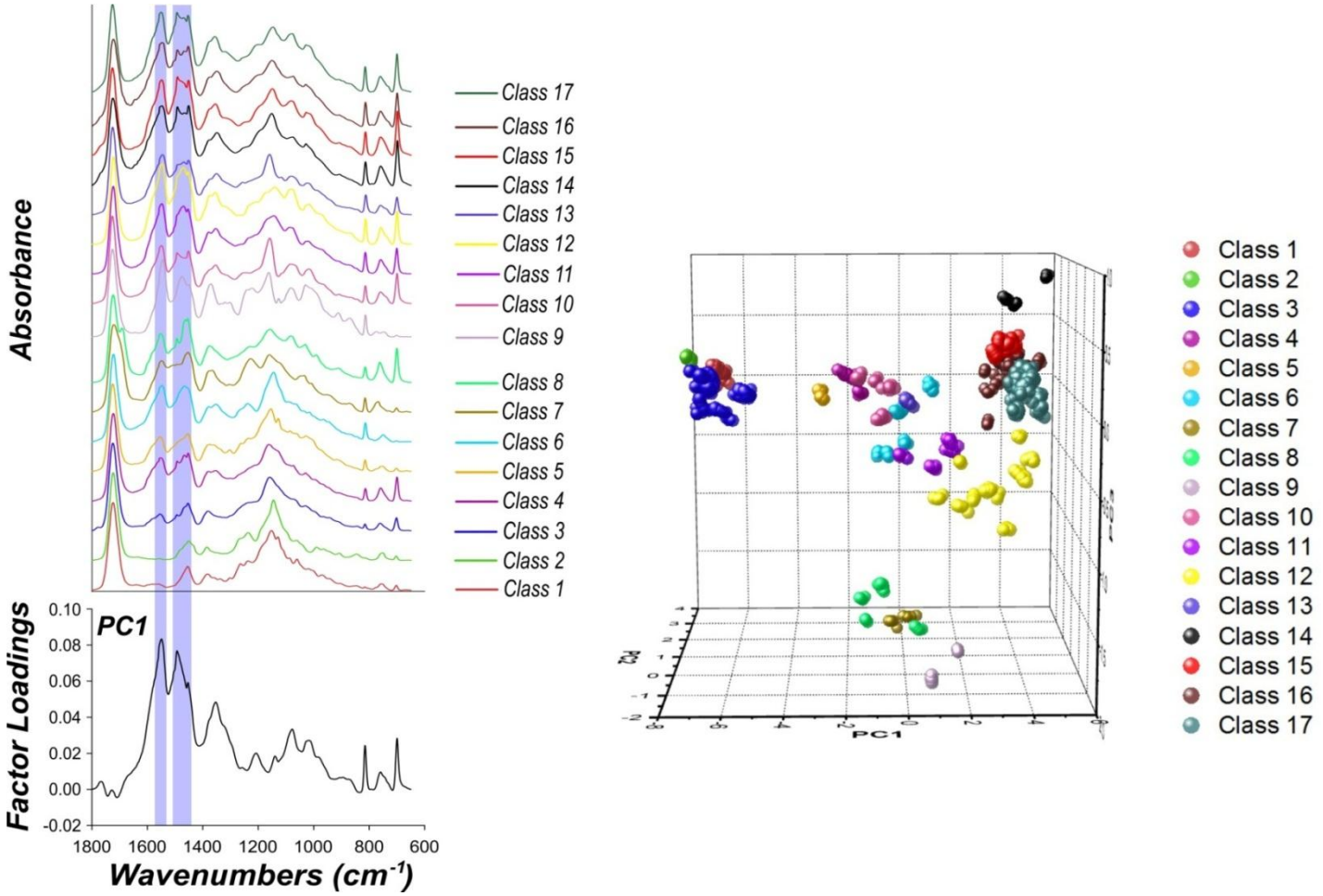

Figure 3.5: Factor loadings plot for PC1. The blue regions superimposed on the representative IR spectra for each class, denote spectral regions significantly positively correlated with PC1.

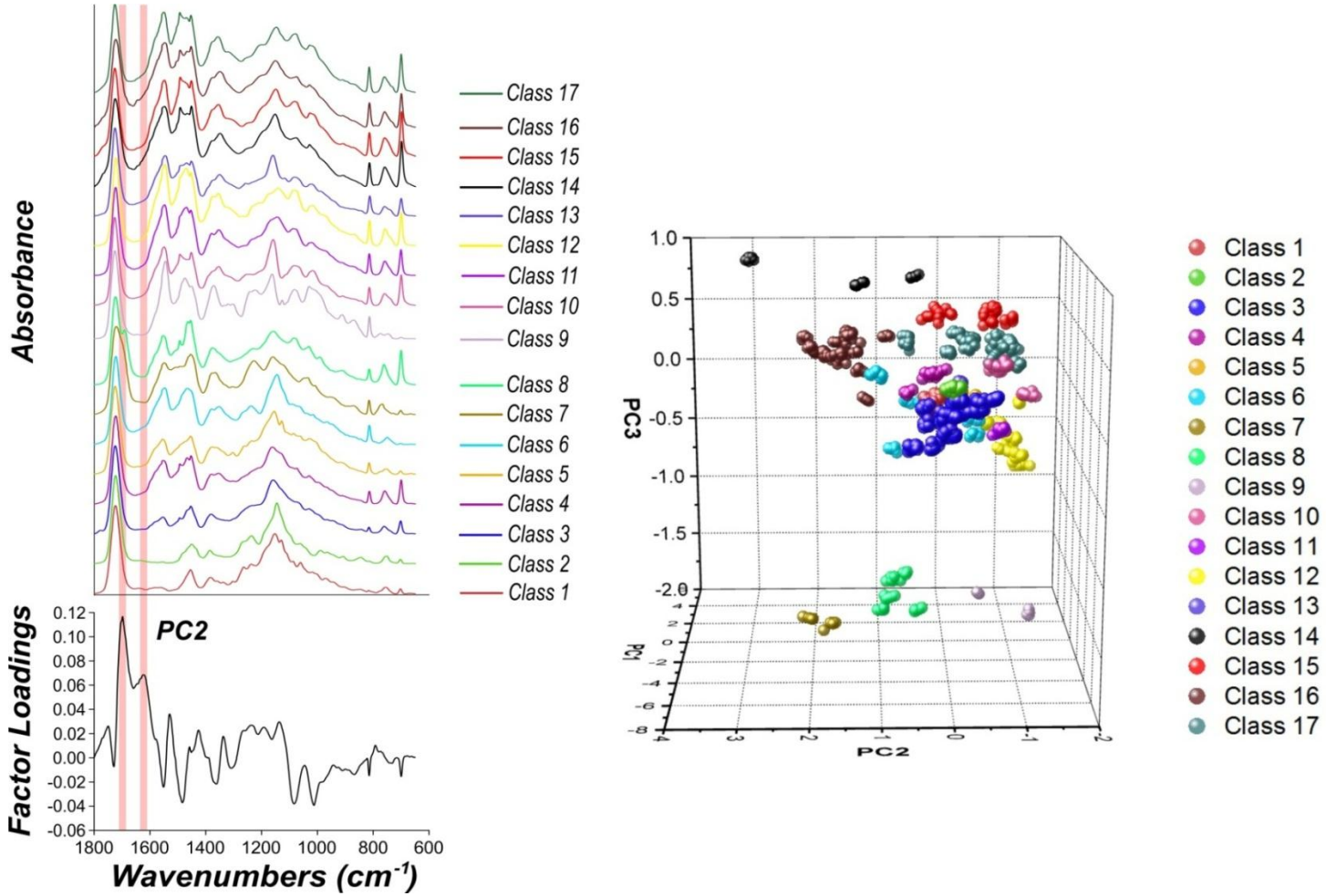

Figure 3.6: Factor loadings plot for PC2. The red regions overlaid on the representative IR spectra for each class, denote spectral regions significantly positively correlated with PC2.

The loadings plot for PC3 (Figure 3.7) revealed a significant negative correlation at approximately 1690 cm^{-1} and a large band of positive correlation at 1150 cm^{-1}. The large negative loading *ca.* 1690 cm^{-1} is a characteristic absorption attributable to the C=O vibrational stretch of polyurethane.[14, 179] Conversely, the positively correlated loading is characteristic for the acrylic binder. The key peaks associated with the acrylic component are the ester C=O stretch at 1730 cm^{-1} and a series of C-O stretching absorptions between 1300 and 1000 cm^{-1} (i.e. acrylic 'fingerprint' region).[14, 56] As a result, the positive loading *ca.* 1150 cm^{-1} is most likely indicative of compositional changes of the acrylic backbone. Relating the loadings for PC3 to the scores plot (Figure 3.7), samples in classes 7-9 attain large negative scores on PC3 due either to the large abundance of polyurethane or the presence of specific acrylic binder/s compositions. Conversely, samples that obtained significant positive scores on PC3 contained no polyurethane, and a large abundance of specific acrylic binder/s or distinct permutations of acrylic co-polymers. Importantly, PC3 is primarily responsible for discriminating between the Australian-manufactured Ford and Spanish-manufactured Nissan vehicles (classes 14 and 15) from the Australian-manufactured Holden vehicles (classes 16 and 17); based upon subtle differences in the acrylic fingerprint region of the IR spectra.

Although discrimination between these samples arises from subtle differences in the acrylic 'fingerprint' region of the spectra, it is virtually impossible to attribute these changes to specific acrylic components based solely upon the IR spectra. Consequently, Py-GC/MS was conducted on select centroid samples, which were separated on PC3, so as to provide unequivocal characterisation and identification of the acrylic polymers utilised in the coatings and thus enable separation of groupings to be attributed to specific acrylic components (Table 3.3). As displayed in Table 3.3, it is evident that automotive clear coats contain a combination of acrylic co-polymers as opposed to a single polymeric acrylic component. Additionally, the information provided in this table enables the discrimination between PCA sample groupings to be explained based upon chemical compositional differences in the acrylic component.

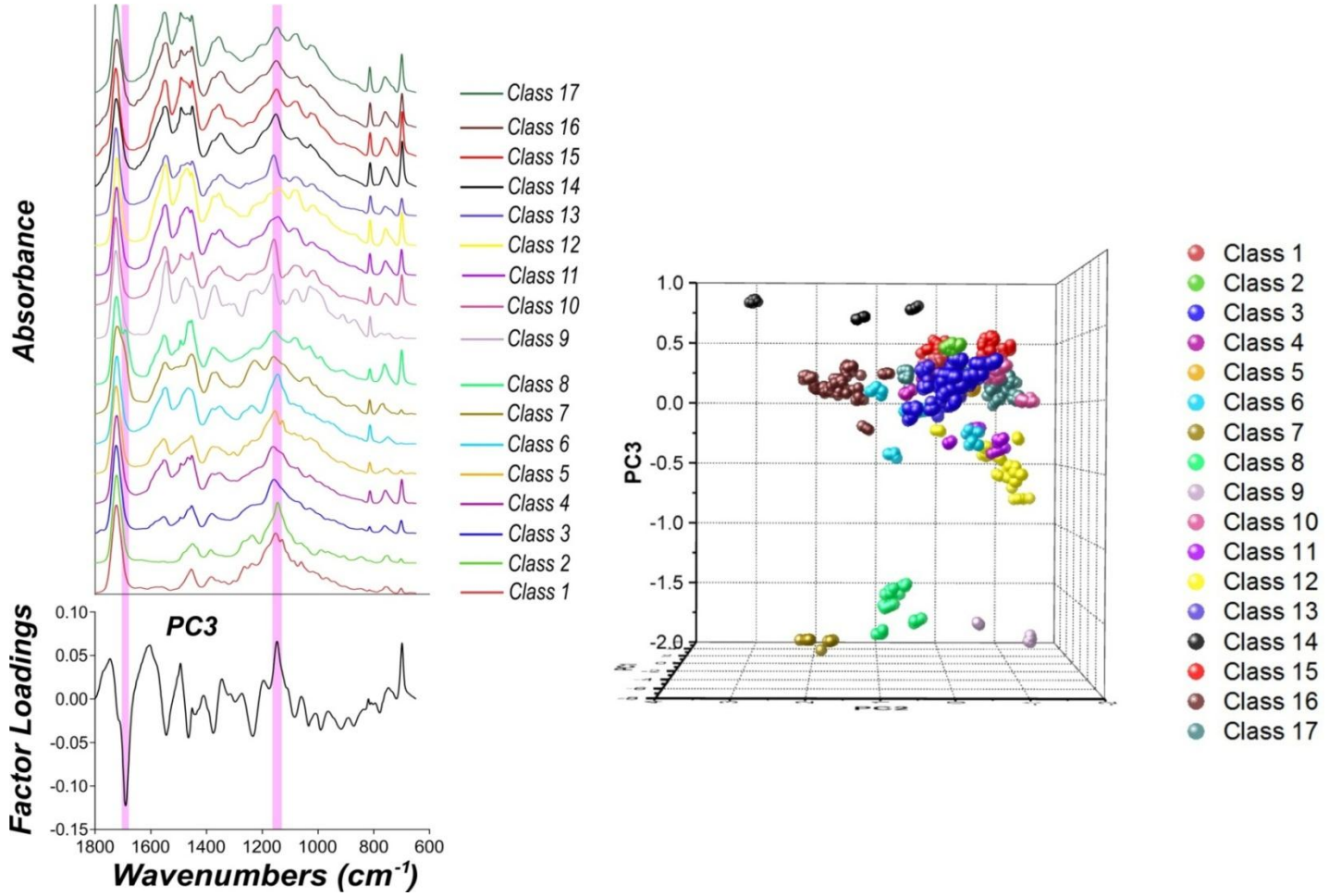

Figure 3.7: Factor loadings plot for PC3. The purple regions superimposed on the representative IR spectra for each class, designate spectral regions significantly correlated with PC3.

Take the example given above; whereby samples obtained from Australian-manufactured Ford and Spanish-made Nissan vehicles (classes 14 and 15) attain slightly larger positive values on PC3 than the Australian-manufactured Holden vehicles (classes 16 and 17). By examining Table 3.3 it is evident that the discrimination between the two sets of groupings on PC3 can be attributed to differences in the acrylic backbone. In this instance, the samples in classes 14 and 15 are primarily composed of a combination of ethylhexylacrylate (EHA) and pentylmethacrylate (PMA). This deviates from the composition of samples in classes 16 and 17 which predominantly consist of EHA and hydroxyethylmethacrylate (HEMA). Similarly, the samples in class 12 have scores on PC1 and PC2 that are comparable to the samples in class 17. These samples are ultimately discriminated from the samples in class 17 based upon their scores on PC3, which are significantly lower and can again be credited to different permutations of the acrylic components. In this particular instance, the samples in class 12 contain a combination of octylmethacrylate (OMA) and n-butylmethacrylate (nBMA), which differs from the acrylic composition of the samples in class 17. Thus, the Py-GC/MS data has demonstrated that the separation of samples on PC3, based upon the acrylic fingerprint region of the IR spectra, can be ascribed to specific changes in the acrylic co-polymers used.

Table 3.3: Pyrolysis results for select centroid samples of the PCA groupings separated on PC3. A list of abbreviations for the compounds is provided in Table 3.4.

	Pyrolysis Products		
Class	**Strong**	**Moderate**	**Weak**
Class 1	nBMA, Sty	MAE, BP, BMB	unresolved MBs
Class 3	Sty, Ca, isobMA, HEMA	BMA, EHA, OMA, Ehexol, MAE, OA	aMS, HEA
Class 4	Sty, nBMA, DMA	C13, BMA, OMA, HEMA, C10	HEA
Class 7	EHA, OMA, Ehexol	HEMA, Sty, HPMA	BI
Class 8	Sty, BMA, DMA	HEMA, HPA, BA	aMS, C10
Class 10	Sty, BA	HEA, DMA, aMS, unresolved MBs	BI, OMA
Class 12	OMA, Sty, nBMA	HEMA, DMA, C13	Ehexol, C10
Class 14	Sty, EHA, PMA	Ehexol, OMA, C10	aMS, HEA
Class 15	Sty, EHA, PMA	DMA, Ehexol, OMA, C10	aMS, HEA
Class 16	Sty, EHA, HEMA	Ehexol	aMS
Class 17	Sty, EHA, HEMA	Ehexol	aMS, BEol, BI

Table 3.4: Abbreviations for the compounds identified in the pyrolysate.

Abbreviations		
Sty - Styrene	MMA - methylmethacrylate	BMA – i-butylmethacrylate
nBMA – n-butylmethacrylate	PMA - pentylmethacrylate	OMA – octylmethacrylate
EHMA - ethylhexylmethacrylate	HEMA - hydroxyethylmethacrylate	HPMA - hydroxypropylmethacrylate
DMA - decylmethacrylate	isobMA - isobornylmethacrylate	aMS – alpha methylstyrene
EHexol – 2-ethyl 1-hexanol	BEol - butoxyethoxyethanol	EHA – ethylhexyacrylate
HPA - hydroxypropylacrylate	HEA - hydroxyethylacrylate	BA - butylacrylate
BP – butyl 2-methylpentanoate	BMB – butyl 2-methylbutanoate	MAE - methacrylic acid 2,3-epoxypropylester
BI – benzyl isocyanate	C10 - dodecene	C13 – tridecane
Ca - camphene	OA - dimethyloctylamine	MB – methylbenzene

As mentioned previously, exploratory analysis of the IR data was conducted with the first five PCs. Models built with only three PCs were unable to discriminate between the first three classes, as seen in Figure 3.2. The factor loadings for PC4, which is displayed in Figure A.1 of the appendix, did not provide any additional discrimination between the samples. However, total discrimination between the first three groupings was achieved by utilising the fifth PC (Figure 3.3). The factor loadings for PC5 which are depicted in Figure 3.8 revealed that there is a significant positive loading at approximately 700 cm^{-1}. This large positive correlation *ca.* 700 cm^{-1} is indicative of a =C-H out-of-plane bending vibration, which is the main diagnostic peak characteristic of styrene.[55] Ultimately, these three classes are differentiated based upon the relative intensity of this peak; with the samples in class 3 having a larger intensity than the samples in class 1, which has a larger intensity than the samples in class 2. Thus, the samples in class 3 attain more positive scores on PC5 than the samples in class 1, which similarly have more positive scores on PC5 than the samples in class 2.

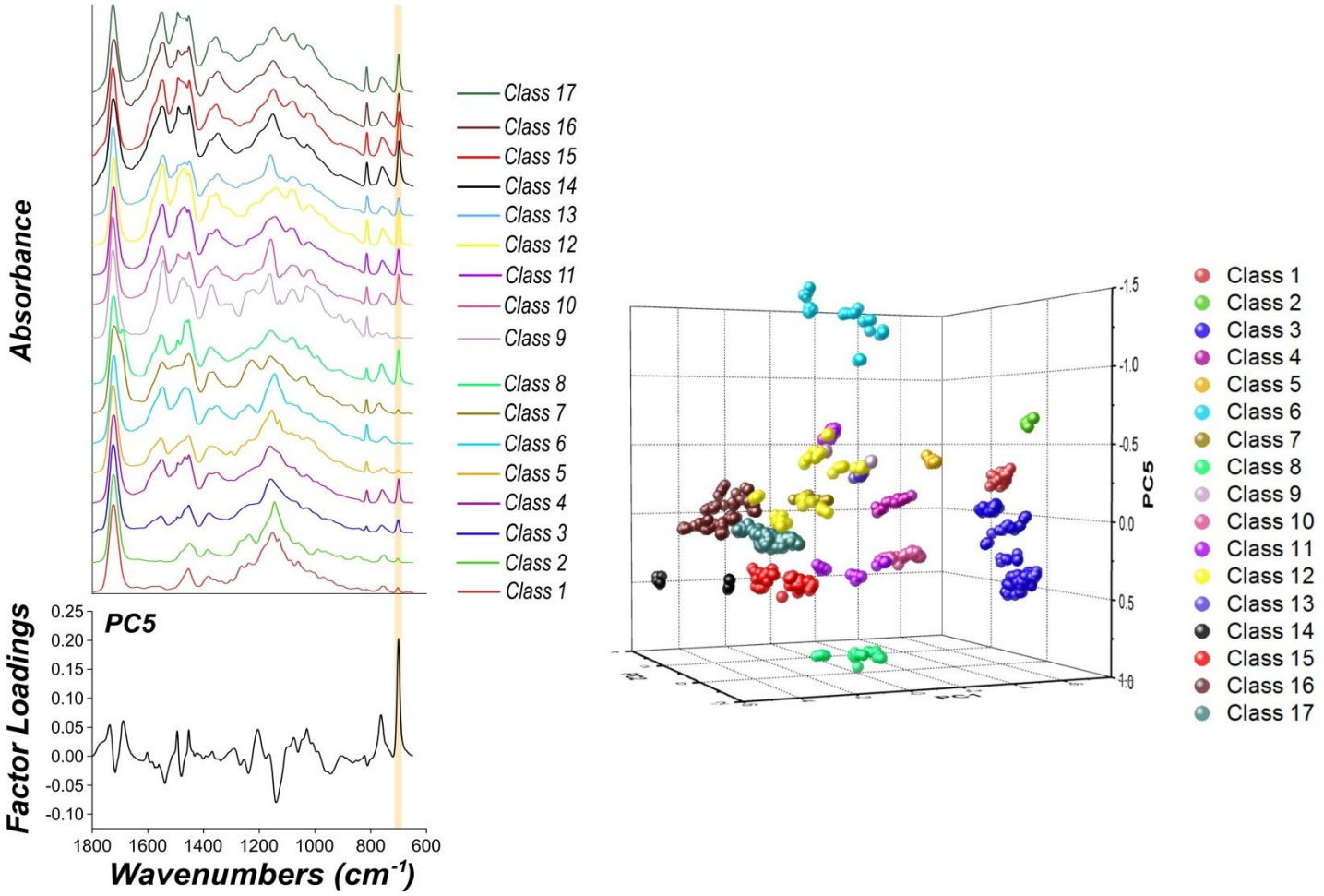

Figure 3.8: Factor loadings plot for PC5. The orange region overlaid on the representative IR spectra for each class, shows a spectral region substantially positively correlated with PC5.

Whilst the loadings plots are useful in identifying the regions of the spectra that are the most variable for a given PC, univariate Fisher ratio plots are capable of discerning the individual spectral features that are the most discriminating for the separation of the specified groups.[144, 155, 156] Fisher ratio plots are generated by using the analysis of variance (ANOVA) technique to determine the F-statistic for every spectral wavelength in the dataset. The F-value is defined as the ratio of the between group variance to within group variance and these values are subsequently plotted as a function of wavenumber to produce the Fisher ratio plot. The F-value can range from zero to an unbounded upper limit, with larger F-values denoting more discriminating spectral features.[144, 155, 156]

Figure 3.9 depicts the Fisher ratio plot, with the shaded blue regions superimposed on the representative IR spectra from the centroid of each grouping, signifying spectral features with higher F-values and thus denotes regions of the spectra that are highly discriminating. In this particular instance, the plot of the F-statistic against wavenumber shows that significant differences between the IR spectra of the 17 different classes are present at approximately 1550 cm^{-1}, 1490-1450 cm^{-1}, 1400-1300 cm^{-1}, 815 cm^{-1} and 740 cm^{-1}.[179] All of the vibrational bands in these regions can be attributed for the most part to the melamine cross-linking agent. The main diagnostic peaks for melamine at *ca.* 1550 and 815 cm^{-1} are indicative of the in-plane and out-of-plane triazine ring deformation respectively.[14, 56] Interestingly, the Fisher ratio plot indicates that only the vibrational bands characteristic for the melamine resin were highly discriminating for the separation of the classes. In comparison to the loadings plots from PCA, the Fisher ratio plot indicates that the regions in the spectra indicative of acrylic, polyurethane and styrene are far less significant to the discrimination between classes than melamine. This finding is consistent with the loadings plot for PC1, which accounts for the most significant portion of the variance in the dataset (90.6 %), and is primarily responsible for discriminating between samples on the basis of melamine abundance.

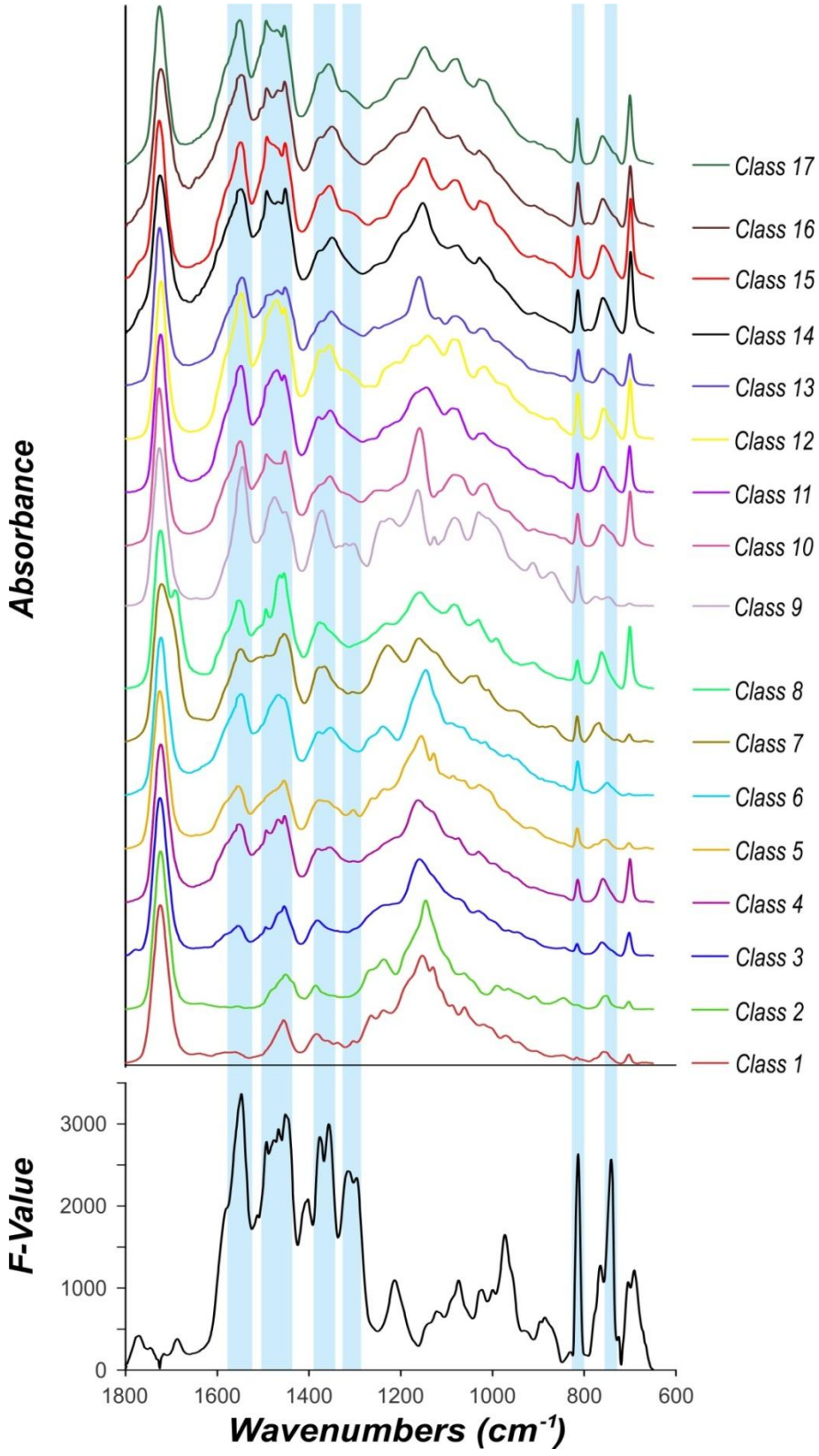

Figure 3.9: Fisher ratio plot. The blue regions superimposed on the IR spectra of each class represent spectral features with large F-values, indicative of their relative importance for discriminating between the groupings.

3.3.2 Linear Discriminant Analysis

LDA was conducted using the data obtained from PCA. As mentioned previously, the entire spectral dataset was divided into two portions; a calibration or training set and a validation set, which were mutually exclusive. By segregating the data used to generate the discriminant model from the data used to estimate its performance, an unbiased robust evaluation of the classification accuracy can be obtained.[134, 139]

The LDA calibration model was created by employing the first five PCs and the classifications derived from PCA of the calibration dataset. The five PC-score LDA model successfully classified 100 % of the training dataset and 97.6 % of the test set, as portrayed in the calibration and validation confusion matrices provided in Table 3.5 and Table 3.6 respectively. As evident in Table 3.6, only one sample and its subsequent replicates were misclassified; with a Honda Accord from class 12 being categorised into class 11 by the discriminant model. This result was corroborated upon inspection of the discriminant values, with smaller discriminant values indicating that the projected samples lie closer to the centroid of a given class. As a result, a sample is classified to the specific class which has the smallest discriminant value. In this particular instance, the misclassified sample lies closer to the class 11 centroid than the class 12 centroid, based upon the discriminant values provided in Table A.1 of the appendix. Additionally, it is important to inspect the discriminant values in order to assess the level of confidence in the classification, because in LDA an unknown sample must be categorised into one of the pre-specified groupings. Therefore, if the discriminant values for a given sample are large for all of the groupings, it can be concluded that the sample is not well-represented in the model. These discriminant values infer that although the sample is misclassified it is still adequately represented in the model. Furthermore, the discriminant values for a select sample and its replicates are consistent, inferring that the *intra*-sample variability is small in comparison to the *inter*-sample variability (Table A.1). Ultimately, based upon the results obtained from the test set validation, it can be concluded that the overall performance of the classification model is highly discriminating, which is of considerable significance in eliminating the ambiguity when predicting the classification of unknown samples.

Table 3.5: Confusion matrix displaying the results from LDA of the samples within the calibration dataset.

Actual

Predicted Class	1	2	3	4	5	6	7	8	9	10	11	12	13	14	15	16	17	Total	% Correct
1	***25***	*0*	*0*	*0*	*0*	*0*	*0*	*0*	*0*	*0*	*0*	*0*	*0*	*0*	*0*	*0*	*0*	***25***	***100***
2	*0*	***15***	*0*	*0*	*0*	*0*	*0*	*0*	*0*	*0*	*0*	*0*	*0*	*0*	*0*	*0*	*0*	***15***	***100***
3	*0*	*0*	***80***	*0*	*0*	*0*	*0*	*0*	*0*	*0*	*0*	*0*	*0*	*0*	*0*	*0*	*0*	***80***	***100***
4	*0*	*0*	*0*	***15***	*0*	*0*	*0*	*0*	*0*	*0*	*0*	*0*	*0*	*0*	*0*	*0*	*0*	***15***	***100***
5	*0*	*0*	*0*	*0*	***10***	*0*	*0*	*0*	*0*	*0*	*0*	*0*	*0*	*0*	*0*	*0*	*0*	***10***	***100***
6	*0*	*0*	*0*	*0*	*0*	***20***	*0*	*0*	*0*	*0*	*0*	*0*	*0*	*0*	*0*	*0*	*0*	***20***	***100***
7	*0*	*0*	*0*	*0*	*0*	*0*	***10***	*0*	*0*	*0*	*0*	*0*	*0*	*0*	*0*	*0*	*0*	***10***	***100***
8	*0*	*0*	*0*	*0*	*0*	*0*	*0*	***15***	*0*	*0*	*0*	*0*	*0*	*0*	*0*	*0*	*0*	***15***	***100***
9	*0*	*0*	*0*	*0*	*0*	*0*	*0*	*0*	***10***	*0*	*0*	*0*	*0*	*0*	*0*	*0*	*0*	***10***	***100***
10	*0*	*0*	*0*	*0*	*0*	*0*	*0*	*0*	*0*	***25***	*0*	*0*	*0*	*0*	*0*	*0*	*0*	***25***	***100***
11	*0*	*0*	*0*	*0*	*0*	*0*	*0*	*0*	*0*	*0*	***15***	*0*	*0*	*0*	*0*	*0*	*0*	***15***	***100***
12	*0*	*0*	*0*	*0*	*0*	*0*	*0*	*0*	*0*	*0*	*0*	***35***	*0*	*0*	*0*	*0*	*0*	***35***	***100***
13	*0*	*0*	*0*	*0*	*0*	*0*	*0*	*0*	*0*	*0*	*0*	*0*	***10***	*0*	*0*	*0*	*0*	***10***	***100***
14	*0*	*0*	*0*	*0*	*0*	*0*	*0*	*0*	*0*	*0*	*0*	*0*	*0*	***20***	*0*	*0*	*0*	***20***	***100***
15	*0*	*0*	*0*	*0*	*0*	*0*	*0*	*0*	*0*	*0*	*0*	*0*	*0*	*0*	***25***	*0*	*0*	***25***	***100***
16	*0*	*0*	*0*	*0*	*0*	*0*	*0*	*0*	*0*	*0*	*0*	*0*	*0*	*0*	*0*	***50***	*0*	***50***	***100***
17	*0*	*0*	*0*	*0*	*0*	*0*	*0*	*0*	*0*	*0*	*0*	*0*	*0*	*0*	*0*	*0*	***110***	***110***	***100***
Total	***25***	***15***	***80***	***15***	***10***	***20***	***10***	***15***	***10***	***25***	***15***	***35***	***10***	***20***	***25***	***50***	***110***	***490***	***100***

Table 3.6: Confusion matrix showing predicted vs. actual classifications for the samples within the validation set. Note: bolded diagonal numbers indicate correctly classified samples, whilst the bolded red number denotes a misclassified sample.

Actual

Predicted: Class	1	2	3	4	5	6	7	8	9	10	11	12	13	14	15	16	17	Total	% Correct
1	**15**	0	0	0	0	0	0	0	0	0	0	0	0	0	0	0	0	**15**	**100**
2	0	**0**	0	0	0	0	0	0	0	0	0	0	0	0	0	0	0	**0**	**-**
3	0	0	**45**	0	0	0	0	0	0	0	0	0	0	0	0	0	0	**45**	**100**
4	0	0	0	**5**	0	0	0	0	0	0	0	0	0	0	0	0	0	**5**	**100**
5	0	0	0	0	**0**	0	0	0	0	0	0	0	0	0	0	0	0	**0**	**-**
6	0	0	0	0	0	**15**	0	0	0	0	0	0	0	0	0	0	0	**15**	**100**
7	0	0	0	0	0	0	**0**	0	0	0	0	0	0	0	0	0	0	**0**	**-**
8	0	0	0	0	0	0	0	**10**	0	0	0	0	0	0	0	0	0	**10**	**100**
9	0	0	0	0	0	0	0	0	**0**	0	0	0	0	0	0	0	0	**0**	**-**
10	0	0	0	0	0	0	0	0	0	**5**	0	0	0	0	0	0	0	**5**	**100**
11	0	0	0	0	0	0	0	0	0	0	**10**	**5**	0	0	0	0	0	**15**	**66.7**
12	0	0	0	0	0	0	0	0	0	0	0	**15**	0	0	0	0	0	**15**	**100**
13	0	0	0	0	0	0	0	0	0	0	0	0	**0**	0	0	0	0	**0**	**-**
14	0	0	0	0	0	0	0	0	0	0	0	0	0	**0**	0	0	0	**0**	**-**
15	0	0	0	0	0	0	0	0	0	0	0	0	0	0	**20**	0	0	**20**	**100**
16	0	0	0	0	0	0	0	0	0	0	0	0	0	0	0	**25**	0	**25**	**100**
17	0	0	0	0	0	0	0	0	0	0	0	0	0	0	0	0	**35**	**35**	**100**
Total	**15**	**0**	**45**	**5**	**0**	**15**	**0**	**10**	**0**	**5**	**10**	**20**	**0**	**0**	**20**	**25**	**35**	**205**	**97.6**

As mentioned previously, classes 16 and 17 contain samples obtained from Australian-manufactured Holden vehicles. The distinction between the samples in the two classes can be attributed to the time period in which the Holden vehicles were manufactured. Samples in class 16 represent Holden vehicles manufactured prior to May/June of 2009, whilst samples in class 17 signify vehicles manufactured after this time period. This result is significant, considering that this relationship could potentially be utilised in order to obtain more specific information concerning the vehicle model. It is important to note that this information can only be procured upon determining when the manufacturer ceased production on specific lines of vehicles. A timeline highlighting the production years of specific models under the General Motor's Holden umbrella is depicted below in Figure 3.10. The dashed red line on the timeline denotes the point of distinction between the two groupings. Consequently, samples in class 16 were obtained from vehicles manufactured prior to mid-2009, and thus must only represent specific models of Holden vehicles manufactured before this point in time. Conversely, samples in class 17 were obtained from Holden vehicles manufactured post mid-2009 and thus solely signify Holden models manufactured in this time period.

For example, consider an instance whereby a questioned paint sample is obtained from a crime scene and there is no control or known sample for comparison. In this particular scenario, the questioned paint sample can be incorporated into the statistical model in order procure an investigative lead. If the questioned paint sample was obtained from an Australian-made Holden vehicle then it should only be categorised into classes 16 or 17. Depending upon which class the sample is assigned to may enable the examiner to infer specific information regarding the potential vehicle model, whilst also excluding several other models in the process (Figure 3.10). Additionally, the discriminating capability of this relationship can be enhanced when utilised in combination with partial eyewitness accounts. Consider a situation whereby a partial account of the suspect vehicle is obtained and it is determined to be from a compact vehicle. Consequently, if the questioned paint sample obtained from the suspect vehicle is categorised into class 16 it is most likely from a Holden Astra, whereas if it is classified in group 17 it infers it was obtained from a Holden Cruze.

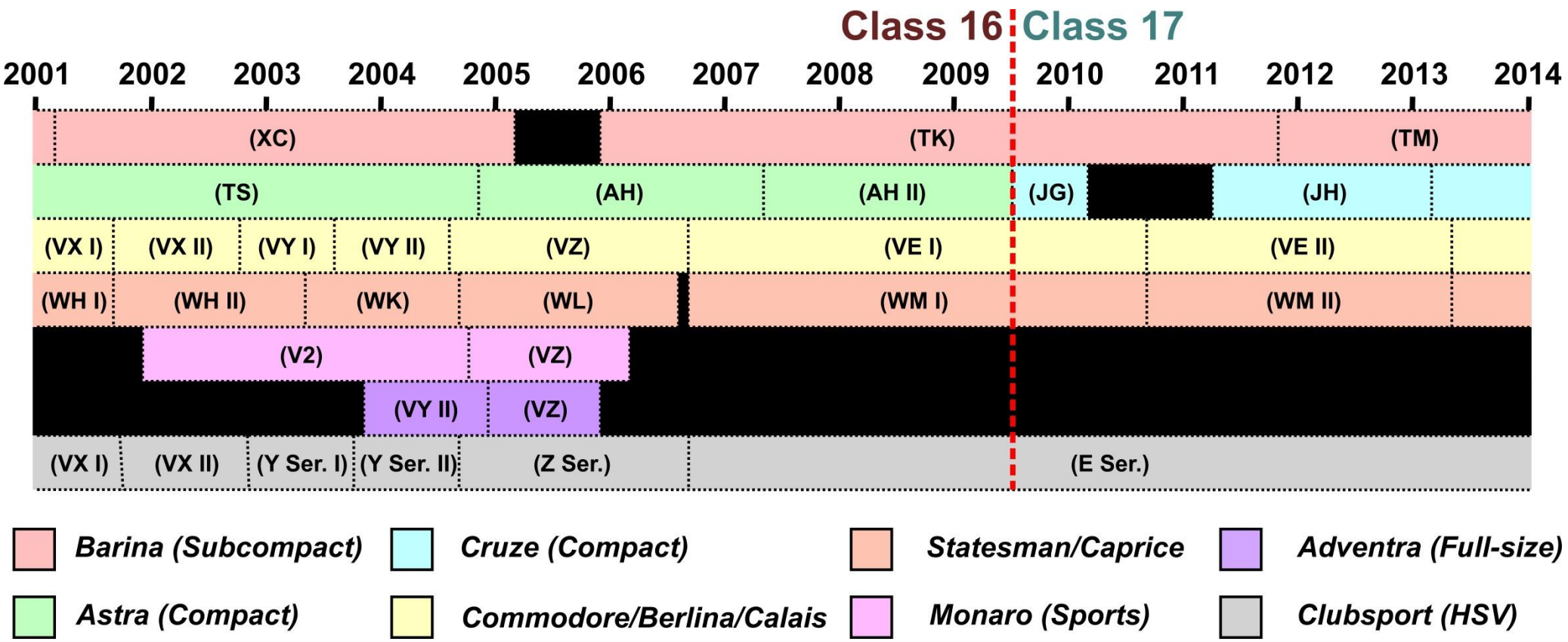

Figure 3.10: Timeline of select Holden vehicles. The dashed red line denotes the demarcation between the two groupings containing Australian-manufactured Holden vehicles in the ATR FT-IR model.

Additionally, some lines of Holden vehicles had only limited production years; including the sports utility Adventra and the performance based Monaro. As both these lines of vehicles were only manufactured prior to 2009, these vehicles can unequivocally be excluded from any samples categorised into class 17. Whilst this pattern is extremely significant from a forensic standpoint, it was only discerned in the Australian-made Holden vehicles and to a lesser extent in the Australian-manufactured Ford vehicles of classes 14 and 15. This might be due to the fact that the number of Australian-made Holden vehicles in the sample population is significantly larger than any of the other manufacturers (Table 2.1). Furthermore, these samples are inherently more diverse than those from the other manufacturers, with a significant range of models and production years being represented. Subsequently, it is anticipated that as the other classes become more defined and diverse, similar relationships will be discerned with respect to the other vehicle manufacturers. Whilst the spectral differences between classes 16 and 17 have previously been discussed in terms of the loadings, it is believed that the change in composition and the resultant differentiation between the two classes may have arisen from a recent change in the paint formulation. More specifically, it is postulated that the change in paint formulation may be attributed towards the use of water based paints, in order to meet current environmental regulations.[180, 181]

3.3.3 Aftermarket clear coats

It is important to note that the statistical model was built and defined with IR data obtained solely from OEM automotive clear coats. However, as mentioned previously some vehicles contain aftermarket respray coatings over the original paint system. As the aftermarket respray clear coat is the outermost coating of the paint system, ATR FT-IR spectroscopy will characterise the aftermarket respray clear coat as opposed to the OEM clear coat. Aftermarket respray coatings are typically applied in order to conceal damage or degradation to the original paint system, or to alter the colour and finish of the vehicle. Aftermarket respray base and clear coats are customarily enamels composed of acrylic/alkyd and polyurethane, which deviates considerably from the typical composition of OEM clear coats.[24, 34] This can primarily be attributed to the fact that aftermarket coatings have to be able to cure

without the assistance of elevated temperatures.[24] A typical IR spectrum of a respray clear coat is provided below in Figure 3.11. The respray clear coats are recognisable from their corresponding IR spectra, based upon a distinctively large abundance of polyurethane resin and a low abundance of melamine resin. As a result, it is important to determine the effect incorporating spectra obtained from respray clear coats will have on the current statistical model.

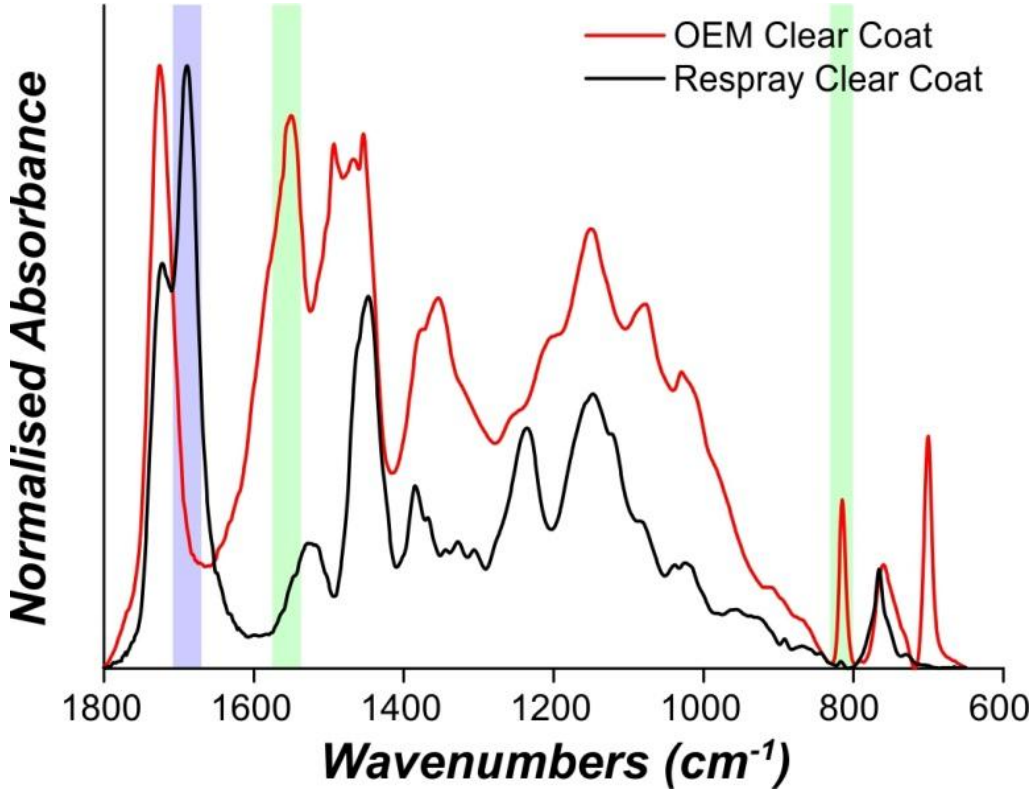

Figure 3.11: Representative IR spectra of an aftermarket acrylic-polyurethane refinish clear coat (black) and a typical OEM acrylic-melamine clear coat (red). The blue highlighted region is indicative of polyurethane and the green regions are characteristic of melamine.

PCA was conducted on the spectral dataset containing IR data from both the OEM and aftermarket respray clear coats (740 spectra, 148 samples). In order to assess the impact the aftermarket clear coats had on the developed model, the same 17 groupings were utilised, with a new class being attributed to the respray clear coats. Upon examination of the PCA scores plot depicted in Figure 3.12, it is evident that the addition of respray clear coats significantly impacts the statistical model. As can be seen in Figure 3.12, the respray clear coats attain large positive scores on PC2, whilst the remaining samples from the OEM clear coats obtain either small positive

or negative scores on PC2. The loadings plot for PC2, provided in Figure A.2 of the appendix, revealed a significant positive correlation at 1690 cm^{-1} that is indicative of the carbonyl vibrational stretch characteristic of the polyurethane resin.[14, 55, 56] Consequently, samples which have a large abundance of polyurethane (i.e. respray clear coats) attain large positive scores on PC2, whilst the remaining samples which contain either a moderate amount of or no polyurethane attain small positive or negative scores on PC2, and are effectively compressed into one half of the scores plot. This result is significant as it potentially increases the likelihood of misclassification between samples from the remaining classes.

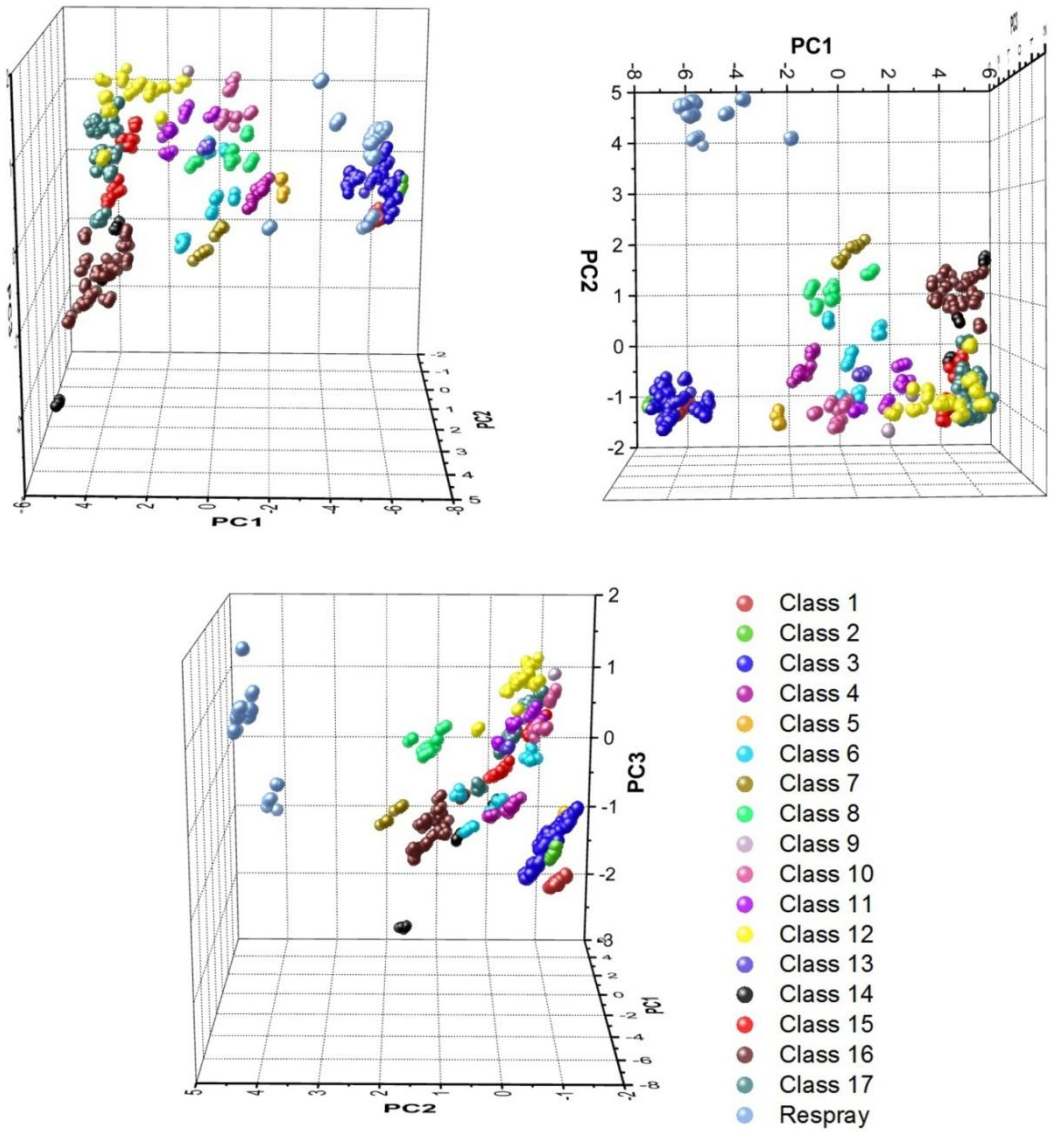

Figure 3.12: 3-dimensional PCA scores plot from a number of different perspectives, highlighting the disparity between spectra obtained from respray and OEM clear coats.

By incorporating the IR spectra obtained from the respray coatings into the model, it can be observed from the scores plot that the samples representing these aftermarket coatings have a large effect or influence on the model. This notion was reinforced upon examining the influence plot for PC2, which is depicted in Figure 3.13. The influence plot, which is a plot of the sample's residual variance against leverage, is typically utilised to objectively identify samples which are outliers or that may overly influence the PCA model.[182] Samples that have a high residual variance are often poorly described by the model and can be classified as outliers. Conversely, samples with a high leverage have a high influence on the model.[183] The worst case scenario is when a sample attains both a high residual variance and leverage, and is classed as a dangerous outlier as it distorts the model to better describe itself.[182, 184] These samples need to be removed otherwise the model will focus primarily on the differences between the outlier/s and the remaining samples, as opposed to describing differences between the other samples.

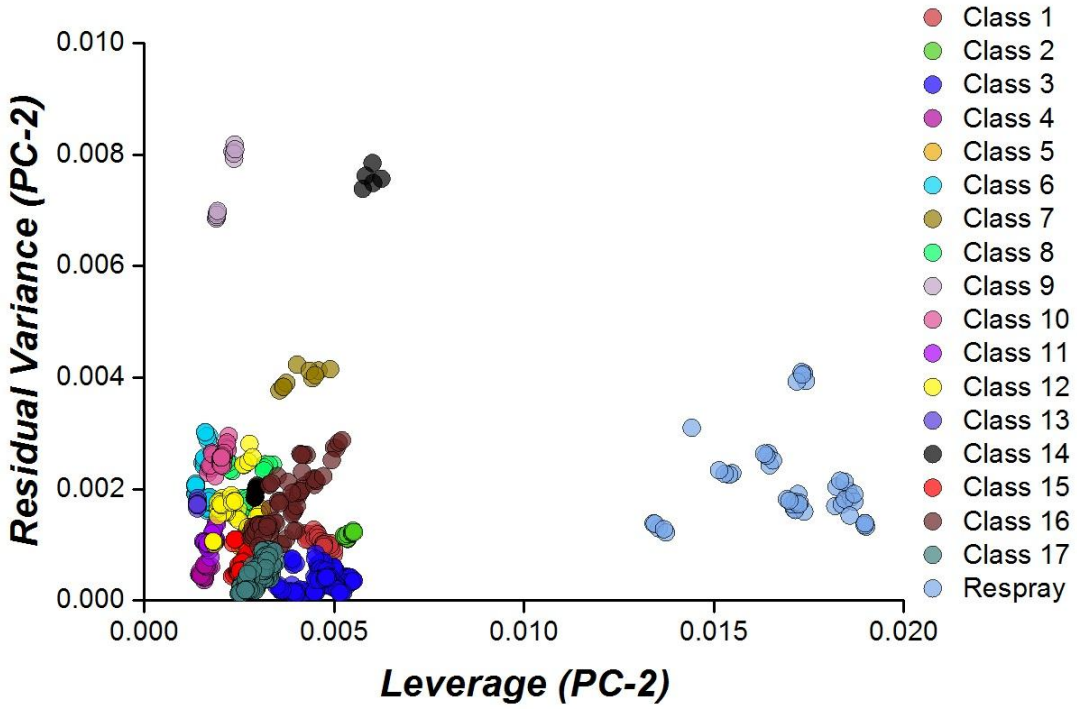

Figure 3.13: Influence plot for PC2.

It can be seen from Figure 3.13 that the respray samples have a high leverage on PC2 and therefore can be categorised as influential samples. A sample's influence on the model should be measured in terms of relative leverage. In this particular instance, the respray samples had absolute leverage values 3 to 4 times greater in magnitude than the remaining samples, thereby indicating that these samples are very influential to the model. The reason behind the high leverage of the respray samples is principally attributed to the large values for the variable *ca.* 1690 cm^{-1}, which is characteristic of the polyurethane resin.

LDA was performed on the entire spectral dataset including the data obtained from the respray clear coats. This was undertaken so as to assess the impact incorporating this data has on the classification accuracy of the resultant model. It is worth mentioning that the calibration dataset (535 spectra, 107 samples) consisted of the same samples as the original training set; with the addition of 9 respray samples. Similarly, the validation dataset (220 spectra, 44 samples) is identical to the original test set with the addition of 3 respray samples. It was important to ensure that the same samples from the 17 classes were used to construct both the original and new calibration and validation datasets, in order for a valid comparison to be made between the original model and the model containing the respray clear coats. The five-PC score LDA model successfully classified 97.2 % and 95.5 % of the samples in the calibration and validation datasets respectively, as depicted in the confusion matrices portrayed in Table 3.7 and Table 3.8. Whilst the classification accuracy is still excellent, with only 5 samples and their corresponding replicates being misclassified, the classification accuracy is lower for both these datasets relative to the original calibration and validation sets which solely consist of OEM clear coats. This suggests that the addition of the IR data from the respray clear coats into the statistical model influences the model sufficiently so as to increase the potential for misclassification.

Table 3.7: Confusion matrix displaying the results from LDA of the calibration dataset containing data obtained from respray and OEM clear coats. The bolded red values signify misclassified samples.

Predicted \ Actual	1	2	3	4	5	6	7	8	9	10	11	12	13	14	15	16	17	Respray	Total	% Correct
1	25	0	**5**	0	0	0	0	0	0	0	0	0	0	0	0	0	0	0	30	**83.3**
2	0	15	**5**	0	0	0	0	0	0	0	0	0	0	0	0	0	0	0	20	**75**
3	0	0	70	0	0	0	0	0	0	0	0	0	0	0	0	0	0	0	70	100
4	0	0	0	15	0	0	0	0	0	0	0	0	0	0	0	0	0	0	15	100
5	0	0	0	0	10	0	0	0	0	0	0	0	0	0	0	0	0	0	10	100
6	0	0	0	0	0	20	0	0	0	0	0	0	0	0	0	0	0	0	20	100
7	0	0	0	0	0	0	10	0	0	0	0	0	0	0	0	0	0	0	10	100
8	0	0	0	0	0	0	0	15	0	0	0	0	0	0	0	0	0	0	15	100
9	0	0	0	0	0	0	0	0	10	0	0	0	0	0	0	0	0	0	10	100
10	0	0	0	0	0	0	0	0	0	25	0	0	0	0	0	0	0	0	25	100
11	0	0	0	0	0	0	0	0	0	0	15	**5**	0	0	0	0	0	0	20	**75**
12	0	0	0	0	0	0	0	0	0	0	0	30	0	0	0	0	0	0	30	100
13	0	0	0	0	0	0	0	0	0	0	0	0	10	0	0	0	0	0	10	100
14	0	0	0	0	0	0	0	0	0	0	0	0	0	20	0	0	0	0	20	100
15	0	0	0	0	0	0	0	0	0	0	0	0	0	0	25	0	0	0	25	100
16	0	0	0	0	0	0	0	0	0	0	0	0	0	0	0	50	0	0	50	100
17	0	0	0	0	0	0	0	0	0	0	0	0	0	0	0	0	110	0	110	100
Respray	0	0	0	0	0	0	0	0	0	0	0	0	0	0	0	0	0	45	45	100
Total	25	15	80	15	10	20	10	15	10	25	15	35	10	20	25	50	110	45	535	97.2

Table 3.8: Confusion matrix showing the predicted vs. actual classifications for the samples in the new validation dataset. The bolded red values signify misclassified samples.

Actual

Predicted	1	2	3	4	5	6	7	8	9	10	11	12	13	14	15	16	17	Respray	Total	% Correct
1	**15**	0	0	0	0	0	0	0	0	0	0	0	0	0	0	0	0	0	**15**	**100**
2	0	**0**	0	0	0	0	0	0	0	0	0	0	0	0	0	0	0	0	**0**	**-**
3	0	0	**45**	0	0	0	0	0	0	0	0	0	0	0	0	0	0	0	**45**	**100**
4	0	0	0	**5**	0	0	0	0	0	0	0	0	0	0	0	0	0	0	**5**	**100**
5	0	0	0	0	**0**	0	0	0	0	0	0	0	0	0	0	0	0	0	**0**	**-**
6	0	0	0	0	0	**15**	0	0	0	0	0	0	0	0	0	0	0	0	**15**	**100**
7	0	0	0	0	0	0	**0**	0	0	0	0	0	0	0	0	0	0	0	**0**	**-**
8	0	0	0	0	0	0	0	**10**	0	0	0	0	0	0	0	0	0	0	**10**	**100**
9	0	0	0	0	0	0	0	0	**0**	0	0	0	0	0	0	0	0	0	**0**	**-**
10	0	0	0	0	0	0	0	0	0	**5**	0	0	0	0	0	0	0	0	**5**	**100**
11	0	0	0	0	0	0	0	0	0	0	**10**	**5**	0	0	0	0	0	0	**15**	**66.7**
12	0	0	0	0	0	0	0	0	0	0	0	**10**	0	0	0	0	0	0	**10**	**100**
13	0	0	0	0	0	0	0	0	0	0	0	0	**0**	0	0	0	0	0	**0**	**-**
14	0	0	0	0	0	0	0	0	0	0	0	0	0	**0**	0	0	0	0	**0**	**-**
15	0	0	0	0	0	0	0	0	0	0	0	0	0	0	**20**	0	0	0	**20**	**100**
16	0	0	0	0	0	0	0	0	0	0	0	**5**	0	0	0	**25**	0	0	**30**	**83.3**
17	0	0	0	0	0	0	0	0	0	0	0	0	0	0	0	0	**35**	0	**35**	**100**
Respray	0	0	0	0	0	0	0	0	0	0	0	0	0	0	0	0	0	**15**	**15**	**100**
Total	**15**	**0**	**45**	**5**	**0**	**15**	**0**	**10**	**0**	**5**	**10**	**20**	**0**	**0**	**20**	**25**	**35**	**15**	**220**	**95.5**

The reason behind the decrease in the classification accuracy is most likely attributable to the distortion of the model caused by the respray samples. In particular, the samples obtained from the respray clear coats are so influential that they cause the samples from the remaining classes to be projected much closer together than in the original model. Consequently, the distances between the classes are smaller and thus the potential for misclassification is much higher. As a result, respray clear coats, which are readily identifiable from their IR spectra, should be excluded from the statistical model and no attempt should be made to classify them with the OEM only based model.

In instances where a vehicle contains a respray base and clear coat over the OEM paint system, transmission IR spectra of paint cross-sections can be obtained from the original clear coat and incorporated into the model. This is because the model was generated from ATR corrected spectra. These are comparable to spectra obtained *via* transmission IR microspectroscopy as the correction accounts for the change in depth of penetration as a function of wavelength.

3.4 Conclusions

Summarising the findings from this statistical model, a correlation was readily discerned between the formation of the classes as a function of the vehicle origin, manufacturer, specific models, and in some instances the manufacturing plant where the vehicle was assembled. The model generated can be utilised to rapidly classify unknown samples with a high degree of confidence, and afford information that may procure investigative leads in an Australian context. Whilst statistical analysis in the form of pair-wise comparisons is a viable option when conducting known *vs.* questioned comparisons (i.e. K *vs.* Q), a problem arises when there are no known paint samples (i.e. no suspect vehicles) to compare to the questioned sample. Furthermore, when dealing with incidents in the nature of hit-and-run accidents and vehicular homicides, with the exception of closed circuit television footage or eyewitness accounts, paint is typically the most significant form of physical evidence located at these scenes. In these instances, increased significance is placed on the results obtained from the analysis of paint evidence. Hence, the statistical model is of particular importance in providing rapid classification information pertaining to unknown samples obtained from incident scenes in order to yield investigative leads, as the information can be directly employed to elucidate vehicle origin, manufacturer/s, model/s and or assembly plant where the vehicle was made. Using the model generated, the information can be obtained and conveyed to law enforcement within 10 minutes of the sample being received.

It is important to note that the statistical model generated in this study was developed using a range of Australian and international manufacturers, with the international cars representing only models commonly exported to Australia. Therefore, at this period in time the model can only be employed readily in an Australian context, and further research is required in order to incorporate a larger number of internationally manufactured vehicles. The strategy that was utilised is universal and by extension could be employed in other jurisdictions if they were to generate statistically significant data sets. Based upon these findings it can be concluded that ATR FT-IR spectroscopy in combination with chemometrics is a simple, rapid and inexpensive technique, which can rapidly provide information resulting in the procuring of investigative leads from questioned paint samples located at crime scenes.

Chapter 4: The effect of chemical component migration and environmental weathering on the classification of automotive clear coats

Portions of this chapter have been previously published in the journals *Forensic Science International* and *Analytical Methods*:

Maric, M., van Bronswijk, W., Lewis, S.W., Pitts, K., and D.E. Martin, *Characterisation of chemical component migration in automotive paint by synchrotron infrared imaging*. Forensic Science International, 2013. **228**(1-3): p. 165-169.

Sauzier, G., Maric, M., van Bronswijk, W., and S.W. Lewis, *Preliminary studies into the effect of environmental degradation on the characterisation of automotive clear coats by attenuated total reflectance infrared spectroscopy*. Analytical Methods, 2013. **5**(19): p. 4984-4990.

4.1 Introduction

As described in Chapter 3, ATR FT-IR spectroscopy was utilised to characterise a statistically large population of OEM automotive clear coats, with the resultant spectral data being classified using multivariate statistics. 17 distinct classes were discerned in the statistical model and a relationship was identified between the formation of the groupings as a function of a number of common vehicle descriptors (i.e. vehicle origin, manufacturer, model/s and manufacturing plants). The statistical model generated may potentially be used to procure investigative leads from questioned paint samples obtained at crime scenes. However, before this model can be applied in a forensic setting, fundamental chemical studies need to be undertaken in order to assess the impact chemical change of automotive clear coats, be it from the migration of chemical components or degradation, will have on the ATR-based model.

Synchrotron FT-IR microspectroscopy was utilised to assess the extent of component migration amidst the layers of automotive paint cross-sections, with particular emphasis on the cross-linking agent melamine. Melamine is a reactive chemical component frequently utilised by automotive manufacturers in their formulation to initiate cross-linking of the binders during the curing process, to form extended networks, thus affording a hard and durable coating.[13, 14, 24, 33] Whilst a number of analogous amino cross-linkers are occasionally employed, melamine is undeniably the most commonly encountered cross-linking additive in automotive paint systems.[27, 32] Based upon the Fisher ratio plot presented in Chapter 3, melamine is the most significant component discriminating between the classes in the ATR-based model. Previous research has revealed that low molecular weight UV absorbers and hindered amine light stabilisers are capable of migrating between the clear coat and basecoat layers during paint curing.[51] It is therefore also feasible that low molecular weight cross-linkers (e.g. melamine), additives and pigments may also migrate between the layers. It is recognised by the forensic community that interlayer migration of melamine can occur from the basecoat into the clear coat. However, at this point in time there is no direct supporting evidence available in the

literature. As a result, this study examined whether chemical component migration exists in automotive paint systems, and the resultant impact this migration may have in relation to the ATR-based model.

Another potential limitation of the statistical model described in Chapter 3 is that the exemplars used to define the model were obtained principally from factory new or relatively new vehicles. Whilst the model has been shown to be promising in categorising samples from new or near-new factory finished vehicles, its applicability to samples that have undergone extensive weathering has not been fully investigated. Studies examining the weathering of automotive coatings have been previously documented in the literature from a paint technology viewpoint, with the intention of maximising the service life of automotive coatings. Such research has demonstrated that acrylic melamine enamels, identified in original automotive clear coats and other outdoor paint systems, are susceptible to degradation following exposure to environmental factors.[185-188] These studies have shown that the degradation of acrylic melamine coatings is influenced by UV radiation, humidity and air pollutants.[185-188] Additionally, a comprehensive review conducted by Mohseni *et al* has investigated the effect mechanical and biological factors have on the chemical integrity of automotive coatings.[187]

However, there is a lack of reports in the scientific literature examining the influence of degradation on automotive coatings within a forensic context. One such study undertaken by Chang *et al.* investigated the influence of environmental degradation on automotive base and clear coats over a three year period.[189] In this study, paint samples obtained from automobile manufacturers in Taiwan were exposed to the elements for three years, with the samples being periodically characterised using IR spectroscopy. The resultant spectra were then searched against an IR database using a peak table search algorithm, with the majority of the coatings being correctly assigned to their non-weathered counterpart. However, some base and clear coats exhibited changes in their spectra attributable to environmental exposure, thereby lowering the hit quality index of the sample.[189] It is important to note that the

samples utilised in the study by Chang and co-workers were mounted in an embedding resin and cross-sectioned prior to analysis. This approach has been proven to potentially facilitate infiltration of the embedding media into the paint sample itself, resulting in interference bands in the IR spectra, which ultimately may impact the results of this study.[171] Additionally, the study was conducted in the Taiwanese setting, with paint samples obtained from their domestic manufacturers and the resultant exemplars aged under their ambient environmental conditions. This is significant as Taiwan on average has much higher temperatures and humidity year round than Australia, which could alter the degradation process. Consequently, the impact of environmental factors on automotive clear coats needs to be assessed in an Australian context. Hence, this chapter also examines the effects of environmental exposure on the automotive clear coats and the resultant impact this would have on the ATR-based model.

4.2 Experimental

4.2.1 Infrared Spectroscopy

Chemical component migration was assessed by characterising automotive paint cross-sections *via* synchrotron FT-IR microspectroscopy as outlined in section 2.4. For the degradation study, the clear coats were characterised using ATR FT-IR spectroscopy, as detailed in section 2.3.

4.2.2 Degradation Regime

Three automotive paint exemplars, as described in Table 4.1, were fastened to the roof of the chemistry building at Curtin University to undergo natural exposure to the environment, as depicted in Figure 4.1.

Table 4.1: Vehicle information for the samples exposed to the environment.

Vehicle Type & Model	VIN	Class
Mazda 3	JM0BK10F200356037	3
Ford Focus XR5	WF0PXXGCDPAR45974	10
Holden VE SV6	6G1EK6EV6BL519455	17

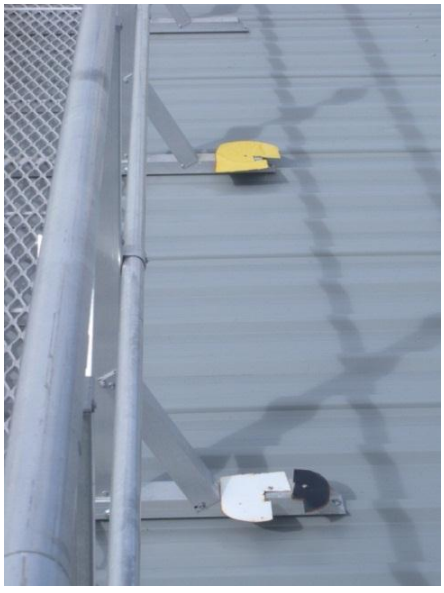

Figure 4.1: Segments from automotive panels placed on the roof of the chemistry department, so as to undergo natural exposure to the elements.

The samples were attached to metal struts on the roof (Figure 4.1) and were left to endure continuous exposure over an 18 month period, from the beginning of February 2012 until the end of July 2013. Sampling of the clear coats was performed at intervals of 2, 4, 6, 8 and 18 months.

4.2.3 Statistical Analysis of Degraded Samples

As described in Chapter 3, the discriminant model was developed *via* test set validation, whereby the entire spectral dataset was segregated into mutually exclusive training and test sets. For the degradation study, the entire original dataset was modelled in order to maximise its robustness. Thus, the entire spectral dataset from Chapter 3 was treated as the training (calibration) set, and the spectra obtained from the degradation samples following environmental exposure formed the foundation of the test (unknown) set. The samples in the test set were projected onto the model generated from the calibration set, to enable comparisons to be made of the samples following a change (i.e. environmental exposure). Projection is a technique that is essentially the PCA equivalent of prediction in regression methods. Additionally, a five PC-score LDA model was generated using the complete 'calibration' dataset (695 spectra, 139 samples), and the resultant model was used to predict the classifications of the samples in the test set that had undergone exposure to the environment.

4.3 Results & Discussion

4.3.1 Chemical component migration

Synchrotron FT-IR microspectroscopy was utilised to chemically image thin automotive paint cross-sections. Unfortunately, only a small subset (75 vehicles) of the total sample population (139 vehicles) could be chemically imaged, due to limitations regarding the user time available at the IRM beam-line. Nevertheless, it was clearly evident from the exemplars analysed that chemical component migration can and does occur. Figure 4.2 depicts the optical micrograph of an area of interest taken from a cross-sectioned paint chip obtained from a Mazda 3. Interestingly, the image of the paint section clearly reveals bleeding of the red organic pigment from the basecoat into the clear coat, as indicated by the diffusion of the red colour across the base/clear coat interface. In this particular instance, the red pigment is from a broad class of pigments known as diketo-pyrollo pyrroles, which was identified by the presence of two dominant characteristic IR absorption bands *ca.* 1641 and 1605 cm^{-1} in the resultant IR spectra of the basecoat.[190]

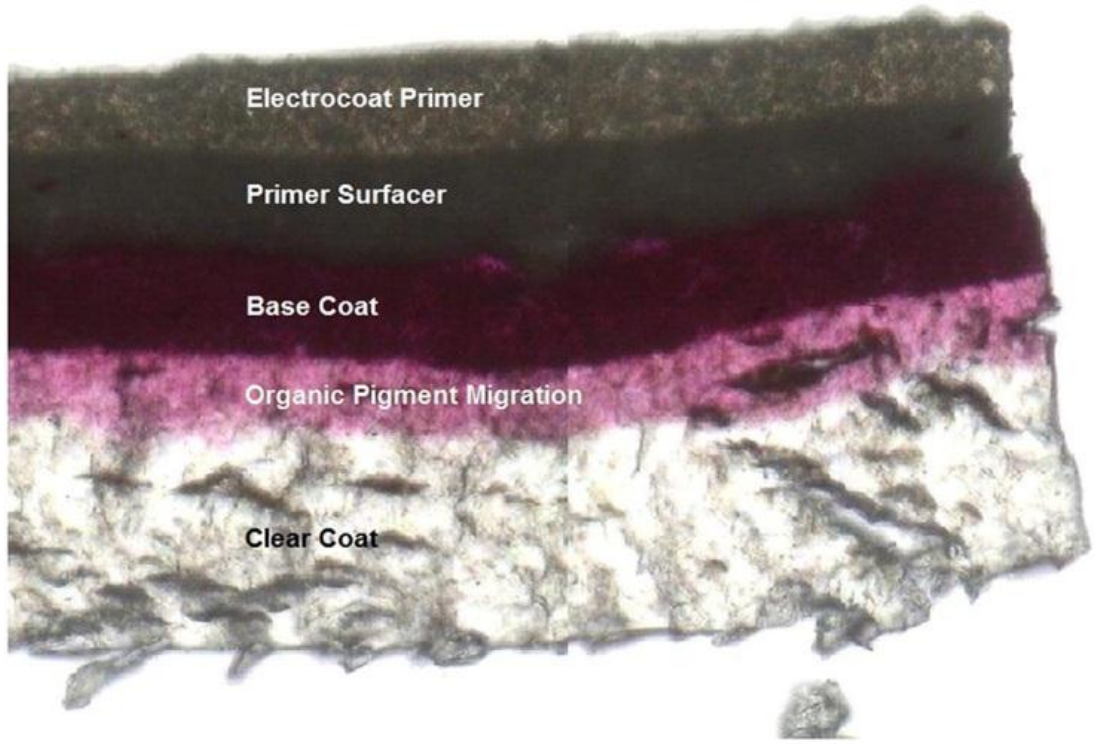

Figure 4.2: Optical micrograph of an automotive paint cross-section obtained from a red Mazda 3.

This migration was confirmed spectroscopically in the corresponding 2-dimensional chemical map shown in Figure 4.3. The map displays a spatial distribution pattern for the amide C=O stretch (1641 cm^{-1}) and is comparable with the observed visible migration of the pigment. In this particular instance, it is evident that relatively strong absorption of the pigment amide C=O stretch persists well beyond the base/clear coat interface, adding further credence to the notion of interlayer migration of paint components.

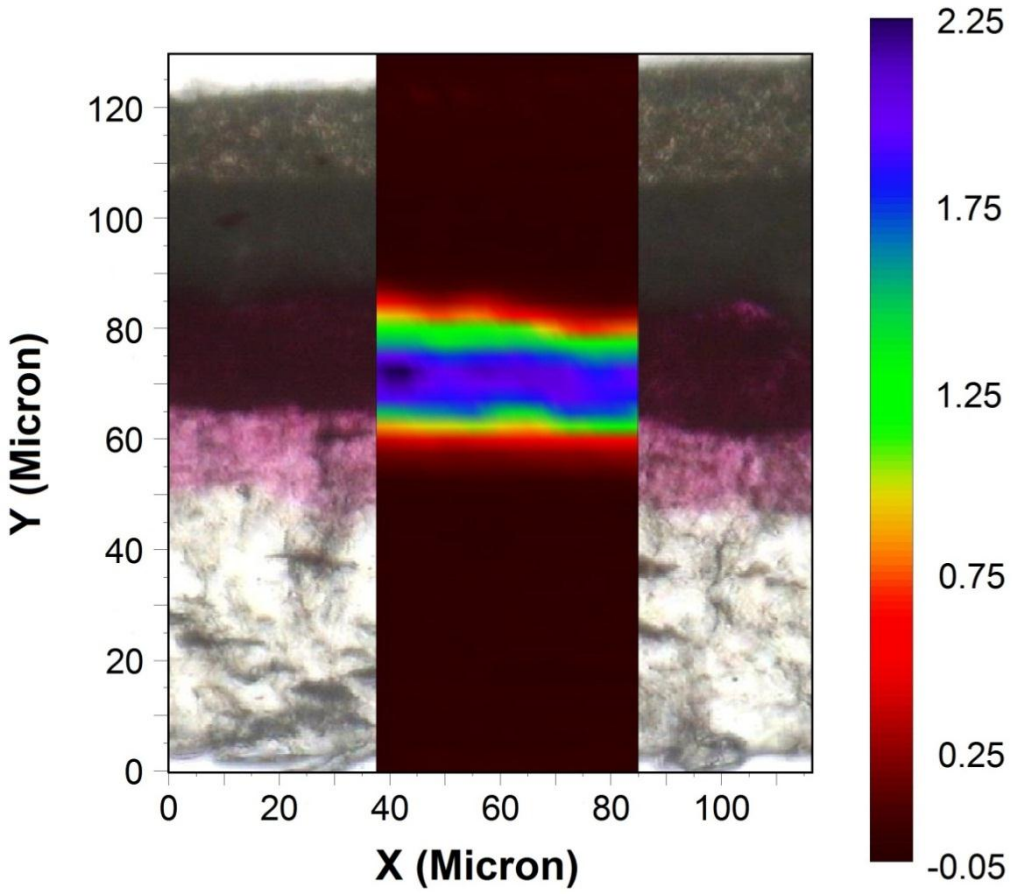

Figure 4.3: 2-dimensional FT-IR chemical image from a paint cross-section (Mazda 3) following integration of the amide C=O stretching vibrational band of the organic pigment (~ 1641 cm^{-1}). The purple regions of the contour map infer areas of high pigment abundance, whilst the red zones are characteristic of regions with lower negligible pigment concentrations.

To further investigate the extent of interlayer component migration, Figure 4.4 depicts a 2-dimensional chemical map demonstrating the melamine abundance across the sample, as melamine is also a significant basecoat constituent. The map was produced by integrating the band *ca.* 1550 cm^{-1}, which is indicative of an in-plane triazine ring stretch for melamine.[14, 55, 56, 179] The main diagnostic peak for melamine, which occurs near 815 cm^{-1} and is characteristic for the out-of-plane triazine ring deformation, could not be utilised because it is too near the lower limit of the spectral cut-off for the MCT detector.

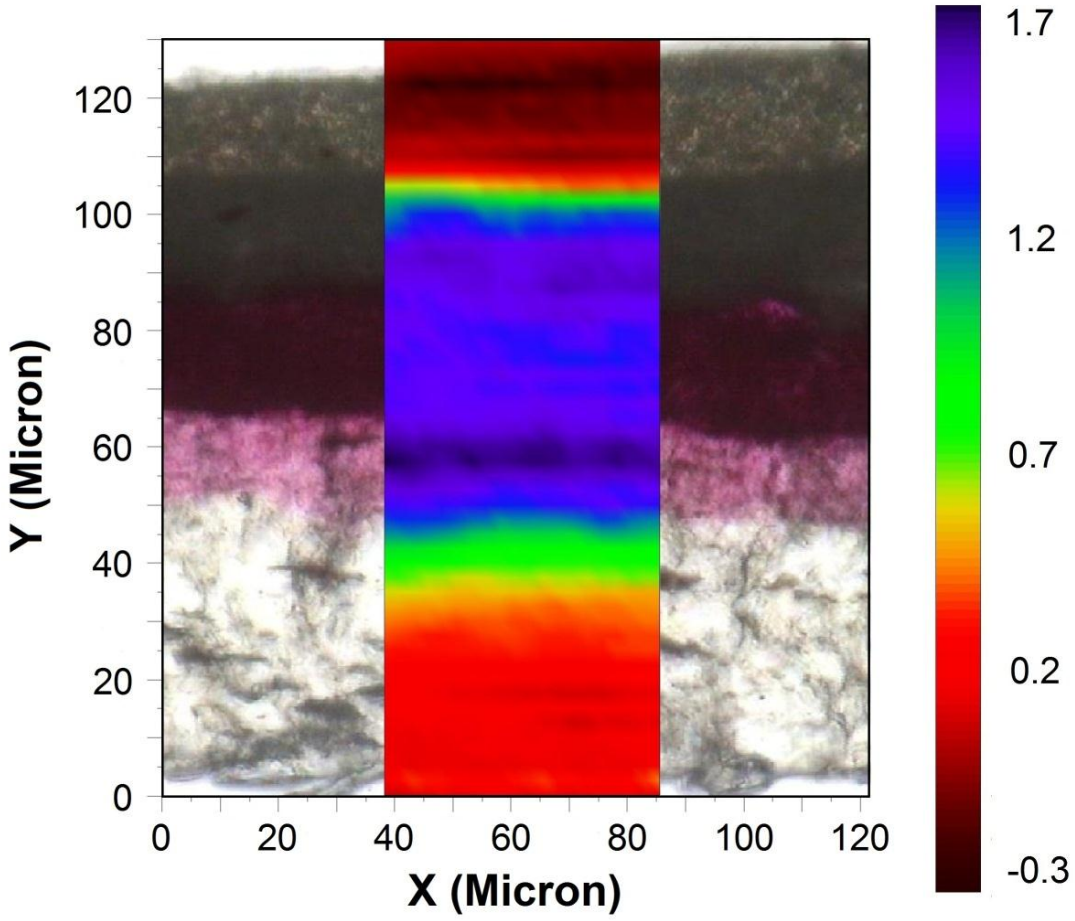

Figure 4.4: 2-dimensional FT-IR chemical image from a paint cross-section (Mazda 3) following integration of the in-plane triazine (1550 cm^{-1}) band of melamine.

Figure 4.4 clearly illustrates a significant decrease in melamine abundance in the clear coat of the paint section from the base/clear coat boundary. In particular, the initial 20 μm of the clear coat displays a strong IR response for melamine, which substantially diminishes when approaching the surface of the clear coat. Similarly, Figure 4.5 shows the intensity distribution of melamine across a paint section obtained from a Mazda 6. In this instance, the IR response of melamine is strong in the primer surfacer and basecoat but consistently and incrementally decreases through the clear coat. This indicates that the melamine cross-linking agent has migrated from the basecoat before diminishing halfway through the clear coat.

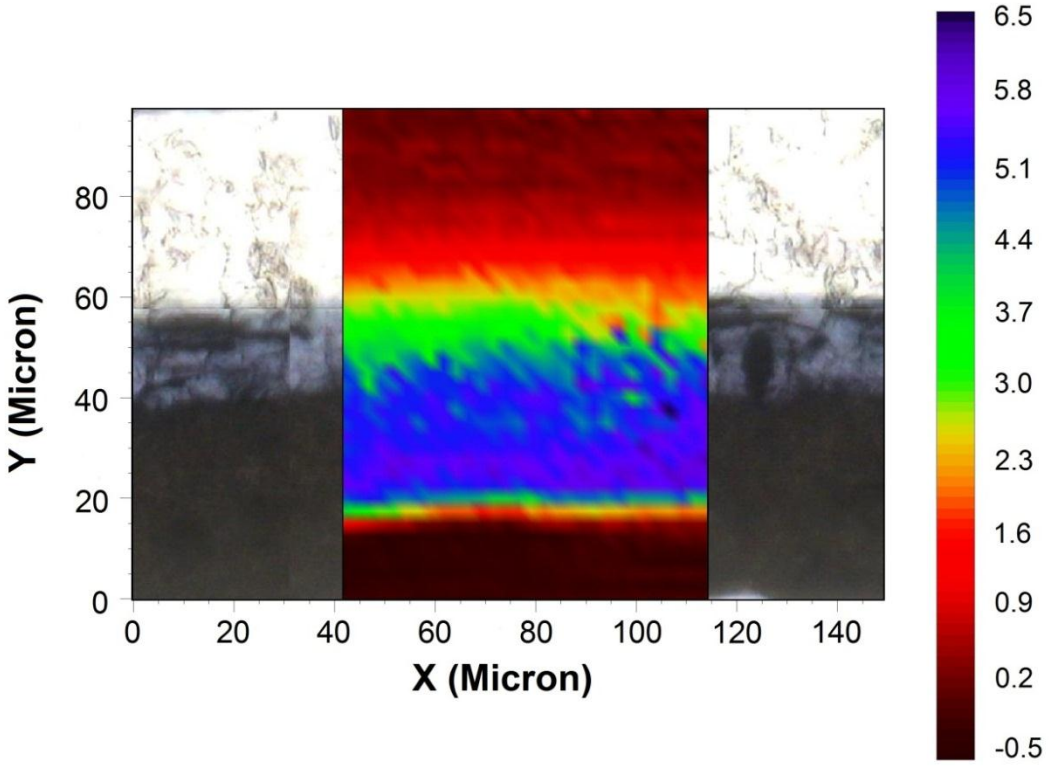

Figure 4.5: 2-dimensional FT-IR chemical image of a paint cross section from a Mazda 6 contrasted using the integrated absorbance of the in-plane triazine (~ 1550 cm^{-1}) band of melamine.

It is worth noting the migration of melamine was only unequivocally observed in Mazda vehicles from class 3, which naturally have a low abundance of melamine in the clear coat, thereby allowing subtle variations in the melamine distribution to be readily discerned. It should also be noted that this effect was only observed with melamine and low molecular weight organic pigments (e.g. diketo-pyrollo pyrolles) and was not seen with any of the other chemical components typically present in automotive clear coats; such as acrylic binders, polyurethane and styrene. It is believed that the diffusion of paint components is size mediated, with larger polymeric species being incapable of interlayer migration, whilst small low molecular weight components and pigments are able to readily diffuse between coatings. This idea of paint component migration between the base and clear coat is supported by an earlier study conducted by Stoecklein and Fujiwara, which revealed that UV absorbers may potentially migrate between coatings in instances of wet on wet applications.[51]

The observed migration of melamine may well be attributed to the manner in which the vehicle is painted. Recent advances in automotive coating technology has resulted in the development of a wet paint system, which is a one-step baking and drying method consisting of the successive application of the primer surfacer, base and clear coat, all whilst wet.[191] This method employs water based paints thereby significantly reducing the emission of VOCs. Moreover, by eliminating the required drying process after every coat, carbon dioxide production and energy consumption is greatly diminished. This technology was initially developed by Mazda and is likely to be instituted by other manufacturers in the future as a more environmentally friendly automobile coating process.[191] It is believed that this wet paint system is directly responsible for the interlayer infiltration of melamine, which is further substantiated by the fact that this effect has at this time only been encountered in Mazda vehicles, where this painting process is implemented.

The implications of these results are significant. Based upon the extent of melamine dissemination observed from the underlying layers and into the clear coat, it is evident that caution must be reserved when characterising specific individual layers (mainly the clear coat) so as to obtain an IR spectrum truly representative of the composition of the coating. This may have a significant impact especially in instances where investigative leads need to be procured by library searching databases or *via* the use of chemometrics. A demonstration of this is shown in Figure 4.6, which depicts two IR spectra that have been extracted from a point in the outermost surface of the clear coat, and a point near the base/clear coat interface of the paint cross-section obtained from the Mazda 3. Each spectrum is dominated by the characteristic vibrational bands associated with acrylic binders as well as melamine and styrene.[56] It is evident that the main source of variation between the two spectra is the relative intensity of the peak *ca.* 1550 cm^{-1} attributable to melamine, which could easily reduce the accuracy with which questioned paint samples could be identified against a library database search or a statistical model. As the proportion of melamine has been shown to fluctuate within the clear coat of a specified sample (Figure 4.6), the heterogeneity of the IR data obtained may invariably result in a discrepancy in the hits generated by the database.

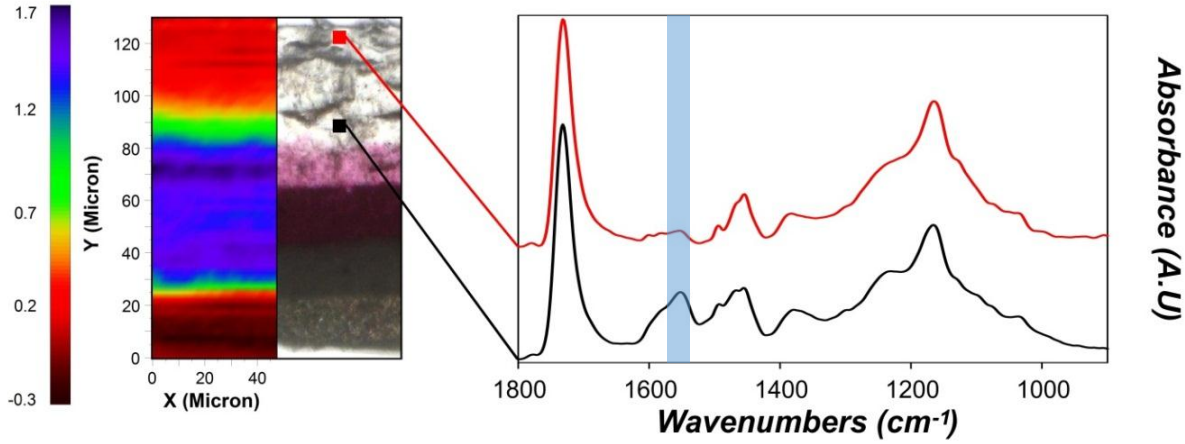

Figure 4.6: IR spectra extracted from an area of the clear coat previously shown to be affected by melamine migration (black) and a region of the clear coat unaffected by melamine migration (red). The highlighted peak corresponds to melamine and illustrates the variability in the proportion of melamine within the clear coat. Interference fringes were removed from the spectra depicted in this figure, as detailed previously in section 2.4.3.

However, as ATR spectra arise from only the first few microns (0-3 μm) of the clear coat, it is highly unlikely that spectra in the previously described ATR-based clear coat model will be affected by melamine migration issues. The same may not necessarily be true for spectra obtained in transmission mode from paint cross-sections. If this model were to be applied to transmission spectra from paint cross-sections with an inconsistent melamine concentration across the different layers, it would most likely result in a misclassification of the sample, as demonstrated in Figure 4.7.

Figure 4.7 illustrates the potential impact melamine migration could have on the classification of select samples. Relating this to the ATR-based clear coat model described in Chapter 3, PC1 accounts for 90.6 % of the variance in the original dataset and is significantly positively correlated to the peak *ca.* 1550 cm^{-1}, which is characteristic for melamine. Consequently, as PC1 in the model is principally responsible for describing the differences in the relative abundance of melamine in the clear coat, if FT-IR transmission spectra of Mazda vehicles from class 3 were acquired from melamine contaminated areas of the clear coat, then the samples will be projected such that they attain more positive scores on PC1, potentially resulting in misclassification with samples from class 4 and class 5 (Figure 4.7). The outcomes of this misclassification is significant, as this would potentially result in misleading information being conveyed to law enforcement regarding the potential make and model of the offending vehicle.

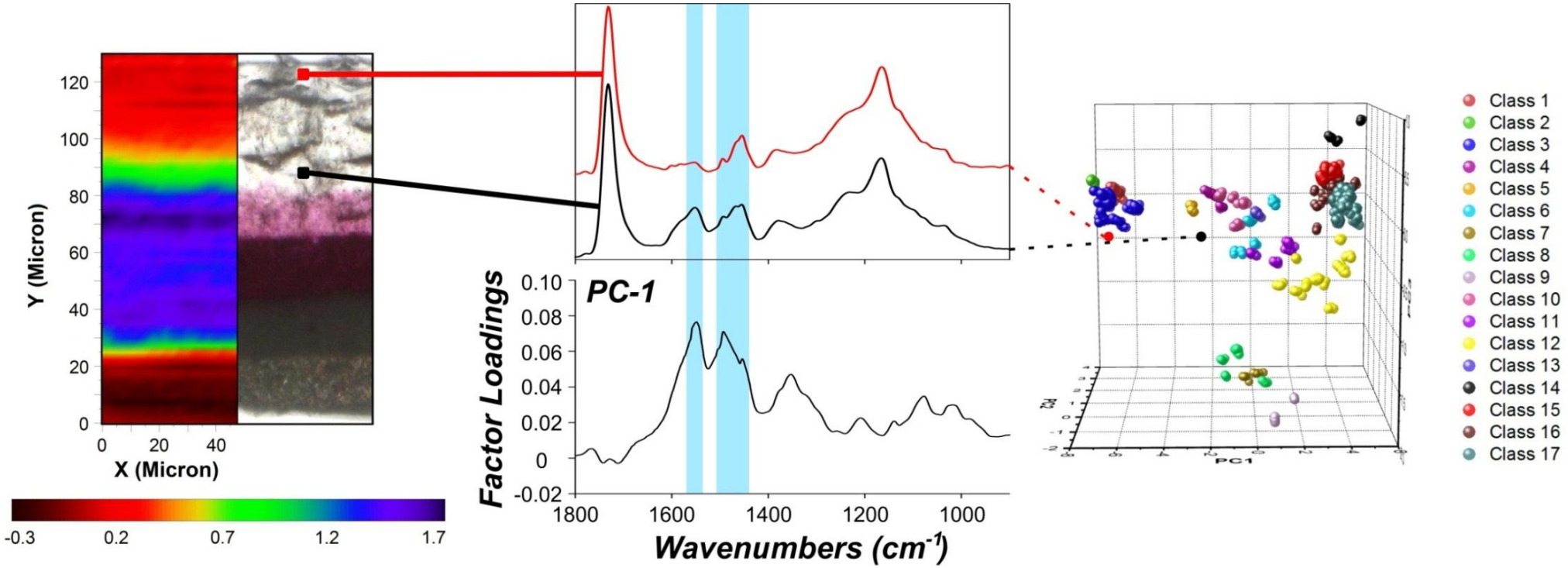

Figure 4.7: Illustration depicting the effect melamine migration could potentially have on the classification of samples using the ATR-based statistical model previously described in Chapter 3.

Based upon these results, stringent analytical protocols need to be developed in order to ensure that the migration of paint components does not affect the analysis and characterisation of paint layers. In particular, in instances where IR microspectroscopy is employed to sequentially analyse individual layers of a paint cross-section, it is vital that a sampling aperture size be chosen to limit the area of analysis towards the surface of the clear coat. For the remaining underlying layers the spectra should be measured as far from the adjacent layers as possible (i.e. mid-centre of the coating). It will also be efficacious to use as small a sampling aperture size as is feasible and take measurements from a number of separated spots. Furthermore, precautions must be taken when analysing thin peels or shavings of individual layers, to ensure the sections are taken from an area truly representative of the composition of the coating and devoid from any melamine contamination.

4.3.2 Environmental Degradation of Clear Coats

To evaluate the impact of environmental conditions on the classification of samples within the model, three exemplars were left to undergo ambient environmental exposure over an 18 month period. Due to the vastness of Australia, the climatic conditions can vary drastically from tropical or sub-tropical in the north to temperate in the south.[192] This stream of investigation was conducted in Perth, which is in the south-west region of Western Australia. The climate at this location is classified as Mediterranean, typically characterised by very hot, dry summers and mild, wet winters.[192] Meteorological data obtained over this time interval revealed that the samples experienced approximately 4700 hours of bright measurable sunshine, with temperatures ranging from -0.7 °C to 42.2 °C, and approximately 950 mm of rainfall.[193] A complete monthly breakdown of the climatic conditions over the time period is provided in Table 4.2.[193, 194] By examining the statistics provided in Table 4.2, it can be clearly seen that during the time interval, the exemplars endured conditions typical of the Perth climate.

Table 4.2: A summary of the major climate statistics recorded at the Perth airport weather station, over the time period of this study (red – summer, yellow – autumn, blue – winter and green – spring).[193, 194]

	Time Period																	
	2012											2013						
Statistics	**Feb**	**Mar**	**Apr**	**May**	**Jun**	**Jul**	**Aug**	**Sep**	**Oct**	**Nov**	**Dec**	**Jan**	**Feb**	**Mar**	**Apr**	**May**	**Jun**	**Jul**
Mean Maximum Temp. (°C)	31.3	31.6	26.4	23.0	19.3	19.2	20.0	21.4	24.9	26.1	31.4	32.3	34.6	28.4	28.7	21.7	19.9	18.7
Mean Minimum Temp. (°C)	18.3	15.6	14.0	10.2	10.1	5.6	8.2	8.8	11.7	12.7	16.8	18.5	18.6	15.2	16.1	10.6	7.8	6.6
No. days Temp. above 35 °C	6	7	1	0	0	0	0	0	1	2	11	8	14	1	4	0	0	0
Total Rainfall (mm)	19.0	0.0	53.2	39.8	134.4	30.6	117.8	103.8	13.8	84.8	24.8	8.2	1.0	60.2	7.8	112.2	23.0	119.2
Mean No. hours Sunshine	10.5	10.6	7.9	7.6	4.4	7.4	7.5	8.7	9.8	10.6	10.8	11.3	11.0	9.2	6.9	7.3	7.0	6.5
Mean global solar exposure (MJ/m^2)	24.8	24.2	15.1	11.9	8.3	11.0	13.4	18.2	21.7	25.4	28.3	29.5	26.9	20.4	13.8	11.4	10.1	10.1
Mean UV Index	10.3	8.6	5.9	3.9	2.7	3.1	4.4	6.4	8.3	10.1	11.1	11.7	10.2	8.2	5.4	3.8	3.1	3.4
No. days extreme UV levels	15	0	0	0	0	0	0	0	0	9	25	30	8	0	0	0	0	0

Throughout the summer (i.e. December to February) the samples were exposed to high temperatures as well as extreme UV levels. During the 547 days of exposure, the samples had to endure 55 days with temperatures exceeding 35 °C and 87 days with an extreme UV index level ($\geq$ 11).[193, 194] It is important to note that following 2 months of exposure to the conditions, the samples began to show visible signs of degradation, owing primarily to the rust formed on the exposed metal edges and the subsequent discoloration of the clear coat. Whilst there are obvious visual signs of degradation, this can most likely be attributed to the fact that flakes of paint were removed from the panels periodically for analysis, thereby leaving exposed metal surfaces that will ultimately corrode. It is important to note that the clear coats of the exemplars were characterised from regions of the panels that were unaffected by corrosion.

The spectra obtained from the automotive paint exemplars over the 18 month time period were projected onto the PCA model described in Chapter 3. The resultant scores plot depicted in Figure 4.8 revealed that from a purely visual standpoint, the spectra obtained from the three samples following extensive environmental exposure grouped together with the corresponding samples expected class. It is difficult to visually differentiate between the first three classes without utilising the scores from the fifth PC. Consequently, in order to unequivocally ascertain which class the degraded samples from class 3 are projected into, a new 3-dimensional scores plot was generated utilising PC5 in lieu of PC3 (Figure 4.9). As can be seen from Figure 4.9, the degraded samples predicted to be from class 3 are categorically projected into this grouping. Additionally, the scores plot revealed slight variation in the position of the projected samples and this will be discussed later.

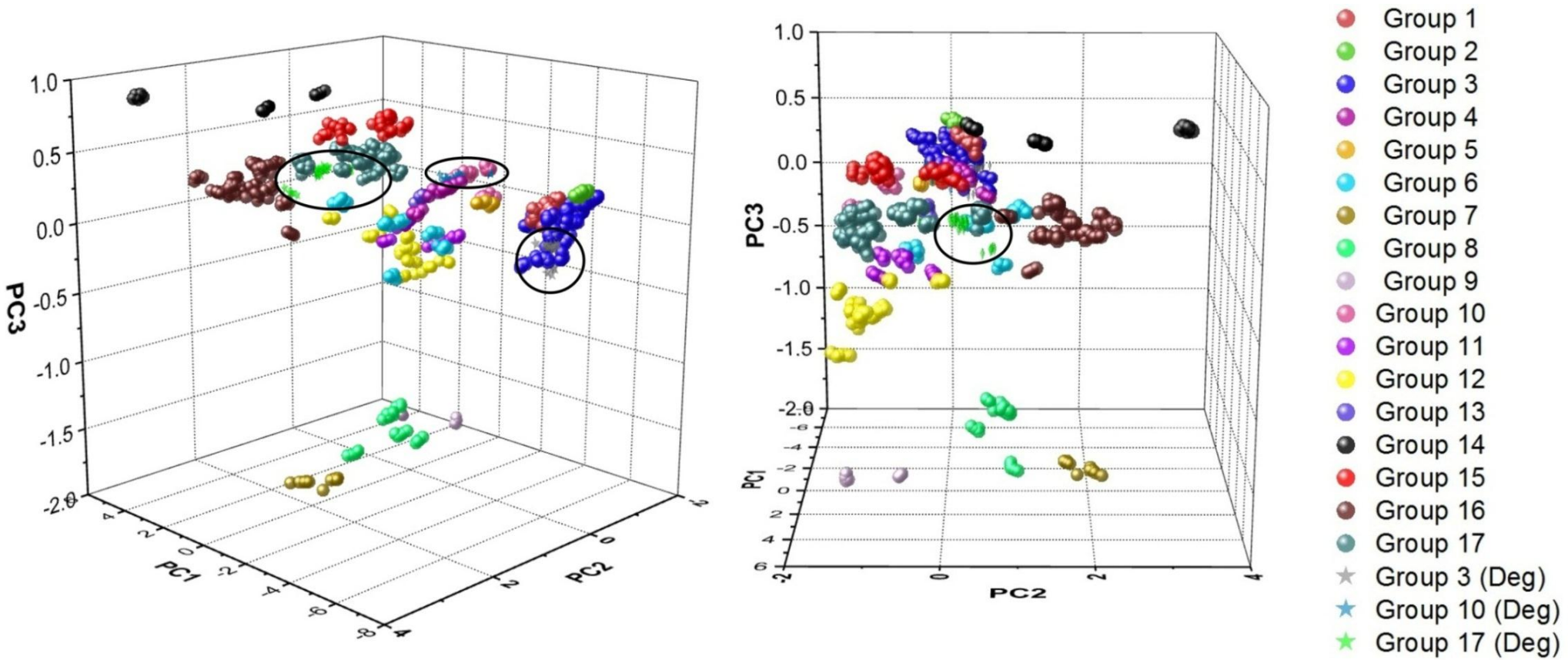

Figure 4.8: 3-dimensional PCA scores plot showing the distribution of the projected samples on the pre-existing PCA model.

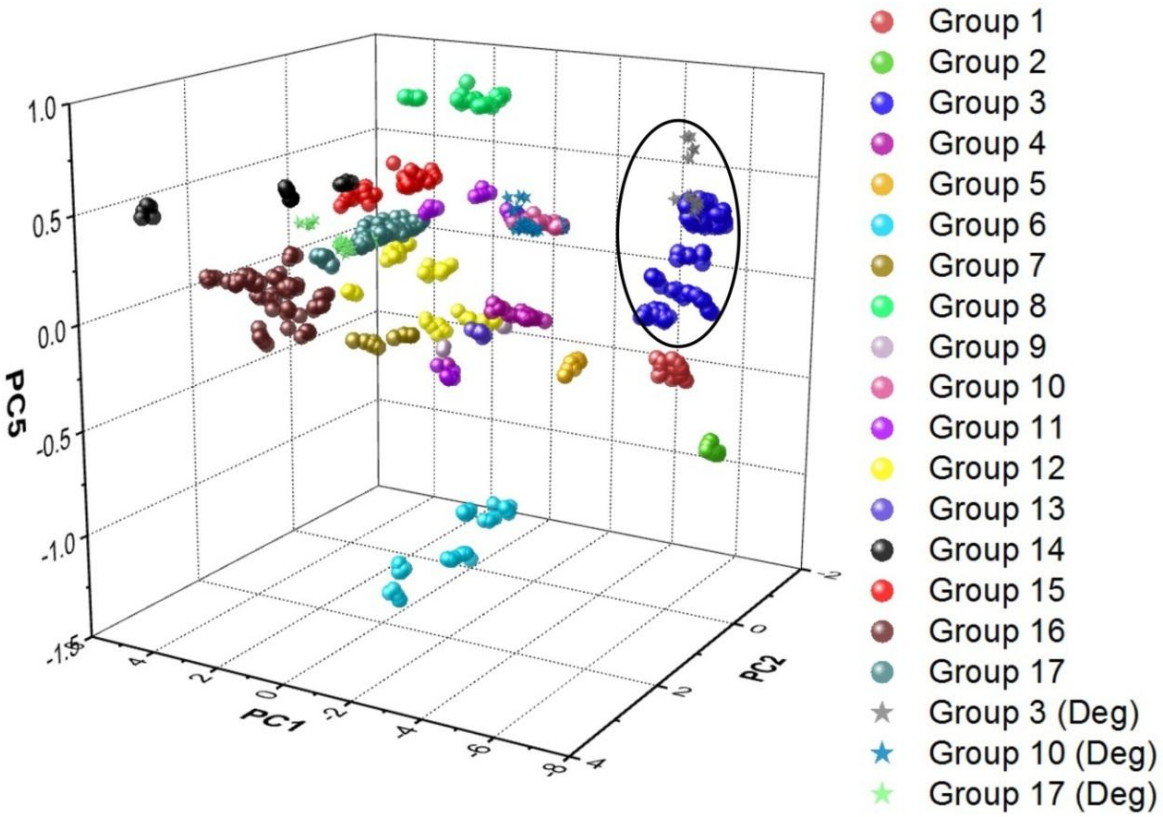

Figure 4.9: 3-dimensional PCA scores plot consisting of PC1, PC2 and PC5 highlighting that the degraded samples from class 3 are projected with the samples from class 3.

LDA was performed by utilising the first five PCs along with the classifications derived from PCA of the entire spectral dataset described in Chapter 3 (695 spectra). The results of this new LDA model are tabulated below in Table 4.3, with the model generated from the entire dataset successfully classifying all of the data. Unsurprisingly, the classification accuracy is higher with this new model relative to the discriminant model described in Chapter 3. In this study, this new discriminant model was employed in all subsequent LDA classifications.

Table 4.3: Confusion matrix showing predicted vs. actual classifications for the entire spectral dataset.

Actual

Predicted Class	1	2	3	4	5	6	7	8	9	10	11	12	13	14	15	16	17	Total	% Correct
1	***40***	*0*	*0*	*0*	*0*	*0*	*0*	*0*	*0*	*0*	*0*	*0*	*0*	*0*	*0*	*0*	*0*	***40***	***100***
2	*0*	***15***	*0*	*0*	*0*	*0*	*0*	*0*	*0*	*0*	*0*	*0*	*0*	*0*	*0*	*0*	*0*	***15***	***100***
3	*0*	*0*	***125***	*0*	*0*	*0*	*0*	*0*	*0*	*0*	*0*	*0*	*0*	*0*	*0*	*0*	*0*	***125***	***100***
4	*0*	*0*	*0*	***20***	*0*	*0*	*0*	*0*	*0*	*0*	*0*	*0*	*0*	*0*	*0*	*0*	*0*	***20***	***100***
5	*0*	*0*	*0*	*0*	***10***	*0*	*0*	*0*	*0*	*0*	*0*	*0*	*0*	*0*	*0*	*0*	*0*	***10***	***100***
6	*0*	*0*	*0*	*0*	*0*	***35***	*0*	*0*	*0*	*0*	*0*	*0*	*0*	*0*	*0*	*0*	*0*	***35***	***100***
7	*0*	*0*	*0*	*0*	*0*	*0*	***10***	*0*	*0*	*0*	*0*	*0*	*0*	*0*	*0*	*0*	*0*	***10***	***100***
8	*0*	*0*	*0*	*0*	*0*	*0*	*0*	***25***	*0*	*0*	*0*	*0*	*0*	*0*	*0*	*0*	*0*	***25***	***100***
9	*0*	*0*	*0*	*0*	*0*	*0*	*0*	*0*	***10***	*0*	*0*	*0*	*0*	*0*	*0*	*0*	*0*	***10***	***100***
10	*0*	*0*	*0*	*0*	*0*	*0*	*0*	*0*	*0*	***30***	*0*	*0*	*0*	*0*	*0*	*0*	*0*	***30***	***100***
11	*0*	*0*	*0*	*0*	*0*	*0*	*0*	*0*	*0*	*0*	***25***	*0*	*0*	*0*	*0*	*0*	*0*	***25***	***100***
12	*0*	*0*	*0*	*0*	*0*	*0*	*0*	*0*	*0*	*0*	*0*	***55***	*0*	*0*	*0*	*0*	*0*	***55***	***100***
13	*0*	*0*	*0*	*0*	*0*	*0*	*0*	*0*	*0*	*0*	*0*	*0*	***10***	*0*	*0*	*0*	*0*	***10***	***100***
14	*0*	*0*	*0*	*0*	*0*	*0*	*0*	*0*	*0*	*0*	*0*	*0*	*0*	***20***	*0*	*0*	*0*	***20***	***100***
15	*0*	*0*	*0*	*0*	*0*	*0*	*0*	*0*	*0*	*0*	*0*	*0*	*0*	*0*	***45***	*0*	*0*	***45***	***100***
16	*0*	*0*	*0*	*0*	*0*	*0*	*0*	*0*	*0*	*0*	*0*	*0*	*0*	*0*	*0*	***75***	*0*	***75***	***100***
17	*0*	*0*	*0*	*0*	*0*	*0*	*0*	*0*	*0*	*0*	*0*	*0*	*0*	*0*	*0*	*0*	***145***	***145***	***100***
Total	***40***	***15***	***125***	***20***	***10***	***35***	***10***	***25***	***10***	***30***	***25***	***55***	***10***	***20***	***45***	***75***	***145***	***695***	***100***

The new discriminant model was capable of successfully classifying all of the samples over the 18 month exposure period into their respective class. The confusion matrix presented in Table 4.4, revealed that there is no change in the sample classifications over the exposure period, with all the spectra being correctly assigned to the pre-ordained expected groupings.

Table 4.4: Confusion matrix depicting the predicted vs. actual classifications for the environmental exposure samples.

		Actual				
Predicted	**Class**	**3**	**10**	**17**	**Total**	**% Correct**
	3	***30***	*0*	*0*	***30***	***100***
	10	*0*	***30***	*0*	***30***	***100***
	17	*0*	*0*	***30***	***30***	***100***
	Total	***30***	***30***	***30***	***90***	***100***

Whilst the LDA model correctly classified all of the samples following an extended period of environmental exposure, the discriminant values need to also be inspected so as to verify and validate the classification. Discriminant values are measures of the distance of a given sample from the class centroid. Smaller magnitude discriminant values indicate that samples lie closer to the centre of the grouping and vice versa. By examining the discriminant values of the three exemplars utilised in this study, it can be seen that there are variations in the magnitude of the discriminant values, throughout the period of exposure. Table 4.5 contains the discriminant values from the samples obtained from the Ford Focus vehicle over the 18 month exposure period. Firstly, it is evident based upon the magnitude of the discriminant values that all the samples were correctly classified to class 10. This is due to the fact that the discriminant values for all the samples are the smallest for class 10, relative to all the other groupings, thereby indicating that the samples are much closer to the class 10 centroid than the remaining groupings.

Table 4.5: Discriminant values for the Ford Focus (class 10) vehicle over the 18 month exposure period.

Discriminant Values

	Cl. 1	Cl. 2	Cl. 3	Cl. 4	Cl. 5	Cl. 6	Cl. 7	Cl. 8	Cl. 9	Cl. 10	Cl. 11	Cl. 12	Cl. 13	Cl. 14	Cl. 15	Cl. 16	Cl. 17
Initial-1	-320.0	-292.2	-197.0	-45.6	-138.4	-110.5	-309.2	-183.8	-327.6	**-4.2**	-30.9	-70.9	-20.1	-112.3	-79.8	-76.3	-81.8
Initial-2	-320.4	-292.8	-196.9	-46.0	-138.8	-111.2	-307.8	-182.6	-326.3	**-4.2**	-31.0	-71.1	-20.2	-113.1	-80.7	-76.7	-82.6
Initial-3	-322.9	-294.8	-199.1	-46.7	-140.4	-111.9	-311.0	-185.2	-328.8	**-4.1**	-31.4	-71.1	-20.2	-112.4	-80.2	-76.4	-82.2
Initial-4	-287.7	-266.4	-173.2	-34.5	-116.6	-103.2	-298.5	-169.4	-325.6	**-6.5**	-26.8	-69.4	-23.9	-103.0	-68.3	-74.1	-72.6
Initial-5	-319.6	-292.3	-196.3	-45.6	-138.1	-110.8	-306.9	-181.8	-325.5	**-4.2**	-30.6	-70.7	-20.2	-112.8	-80.2	-76.5	-82.1
2Months-1	-327.6	-301.9	-201.5	-46.5	-144.3	-111.9	-296.9	-175.0	-323.8	**-5.3**	-30.9	-71.7	-19.3	-105.0	-82.0	-68.3	-83.2
2Months-2	-318.1	-293.0	-194.7	-43.0	-138.2	-108.9	-297.1	-174.3	-326.7	**-5.6**	-30.4	-72.3	-19.9	-102.7	-79.2	-68.0	-81.3
2Months-3	-318.1	-293.0	-194.3	-43.3	-138.4	-109.7	-297.0	-173.9	-326.4	**-5.6**	-30.7	-72.8	-20.2	-103.9	-80.0	-69.1	-82.2
2Months-4	-319.6	-293.7	-195.6	-43.9	-140.0	-110.2	-300.5	-177.1	-330.5	**-5.8**	-31.8	-74.2	-20.4	-103.7	-80.7	-69.2	-83.2
2Months-5	-323.6	-298.1	-198.8	-44.9	-141.2	-109.0	-293.3	-173.0	-321.0	**-5.4**	-30.0	-70.9	-18.7	-104.7	-81.6	-67.7	-82.5
4Months-1	-322.4	-300.0	-198.4	-43.2	-138.6	-106.5	-282.4	-163.8	-312.4	**-5.9**	-26.7	-66.3	-18.0	-98.1	-77.1	-61.5	-77.1
4Months-2	-321.5	-298.8	-197.6	-43.1	-138.8	-107.3	-285.1	-165.5	-316.2	**-6.1**	-27.7	-68.1	-18.7	-98.1	-77.6	-62.3	-78.2
4Months-3	-324.1	-300.7	-200.2	-43.6	-141.0	-108.1	-291.2	-170.3	-323.5	**-6.5**	-28.8	-69.3	-19.0	-95.1	-76.3	-60.8	-77.5
4Months-4	-321.3	-298.3	-197.5	-43.0	-138.6	-107.0	-286.1	-166.5	-317.1	**-6.1**	-27.7	-68.1	-18.6	-98.0	-77.3	-62.3	-78.0
4Months-5	-319.9	-297.2	-195.5	-43.3	-138.2	-108.2	-283.4	-163.9	-314.1	**-6.0**	-28.2	-69.1	-19.1	-101.6	-79.9	-65.0	-80.4
6Months-1	-323.0	-298.9	-197.7	-44.7	-140.9	-109.7	-288.7	-168.6	-318.5	**-5.9**	-29.7	-70.8	-19.3	-103.4	-81.5	-66.6	-82.4
6Months-2	-315.2	-289.8	-191.8	-42.7	-137.1	-108.8	-295.1	-173.1	-325.8	**-6.0**	-31.3	-74.2	-20.4	-105.7	-82.0	-70.4	-84.2
6Months-3	-315.1	-290.7	-191.9	-42.1	-136.9	-108.5	-293.4	-171.3	-325.9	**-6.3**	-30.8	-73.6	-20.5	-102.5	-80.4	-68.0	-82.7
6Months-4	-319.0	-295.3	-195.5	-42.8	-137.7	-107.1	-288.1	-168.1	-318.5	**-5.8**	-28.5	-69.6	-18.9	-101.0	-78.9	-65.1	-79.9
6Months-5	-293.9	-276.1	-177.1	-33.7	-120.5	-101.5	-279.2	-155.6	-317.5	**-7.9**	-24.7	-67.6	-22.1	-90.6	-67.7	-61.3	-70.7
8Months-1	-308.6	-288.8	-187.1	-39.1	-130.7	-105.7	-278.7	-157.7	-313.9	**-7.0**	-26.5	-68.5	-20.5	-96.2	-74.8	-62.6	-76.4
8Months-2	-309.3	-288.5	-187.9	-39.4	-130.9	-105.9	-283.1	-161.2	-316.1	**-6.3**	-26.6	-68.3	-20.2	-97.4	-74.4	-63.9	-76.2
8Months-3	-314.4	-292.9	-191.2	-41.4	-134.5	-107.6	-282.8	-161.7	-314.4	**-6.1**	-27.3	-68.7	-19.9	-100.0	-77.3	-64.9	-78.5
8Months-4	-310.8	-290.6	-188.7	-40.0	-131.5	-106.1	-278.9	-158.1	-311.4	**-6.3**	-26.0	-67.3	-19.9	-98.2	-75.3	-63.6	-76.4
8Months-5	-308.3	-288.0	-186.9	-39.2	-130.1	-105.7	-280.2	-158.7	-313.1	**-6.3**	-26.1	-67.8	-20.2	-97.9	-74.6	-64.0	-76.1
18Months-1	-260.0	-251.0	-150.1	-26.3	-101.4	-105.5	-274.7	-140.9	-324.8	**-14.4**	-26.6	-74.8	-33.9	-86.5	-60.4	-67.5	-68.1
18Months-2	-247.6	-244.0	-142.0	-23.1	-92.8	-101.1	-256.4	-126.4	-314.3	**-19.7**	-25.2	-73.9	-37.4	-81.9	-58.4	-64.0	-65.4
18Months-3	-259.6	-248.1	-151.4	-25.0	-102.0	-102.4	-284.2	-150.4	-337.3	**-14.7**	-28.2	-77.3	-33.2	-82.3	-59.1	-65.0	-67.8
18Months-4	-273.0	-260.8	-160.9	-28.2	-108.9	-102.0	-273.7	-145.5	-323.1	**-12.5**	-25.8	-72.3	-28.7	-84.2	-62.8	-61.5	-68.6
18Months-5	-263.3	-254.4	-152.8	-27.0	-103.6	-106.3	-275.9	-141.7	-326.5	**-14.5**	-26.6	-74.5	-33.7	-84.1	-59.5	-65.5	-67.3

It is apparent from Table 4.5 that the magnitude of the discriminant values for the samples increases notably over the exposure period. Up until the 8 month period, the discriminant values for the tested samples showed no significant variation for their respective class, thereby intimating that there is no change in the distribution of samples. However, following 18 months of ambient exposure the discriminant values increase by approximately 2 fold. Whilst this does not affect the classification of the samples, it does indicate that these samples are much further from the group centroid than the samples aged over a short to medium-term time period. Furthermore, these samples begin to approach other classes (i.e. class 4), suggesting that with further exposure to the environment the samples might be misclassified (Table 4.5). A similar effect was observed with the two other samples, and their tabulated discriminant values are provided in Table A.2 and Table A.3 of the appendix. Whilst it is possible that the discrepancy in the discriminant values may be attributed to physical changes in the sample surface texture over the exposure period; it is more likely that the longer term environmental exposure (*ca.* 18 months) is chemically altering the outermost surface of the clear coat.

Thermoset acrylic melamine coatings, which are widely utilised in automotive clear coat technology, are susceptible to degradation following exposure to weathering conditions.[186] In particular, acrylic melamine coatings have been shown to undergo photo-degradation following significant exposure to UV radiation, resulting in chain scission and the formation of various amine and carbonyl derivative degradation products.[186, 195] Due to the substantial UV exposure these samples endured throughout the course of the 18 month period (Table 4.2), it is feasible that the photo-degradation of the acrylic and melamine binders is responsible for the observed differences in the discriminant values. This notion was reinforced upon examination of the averaged IR spectra for the samples obtained from the Ford Focus vehicle after every sampling interval, as depicted in Figure 4.10.

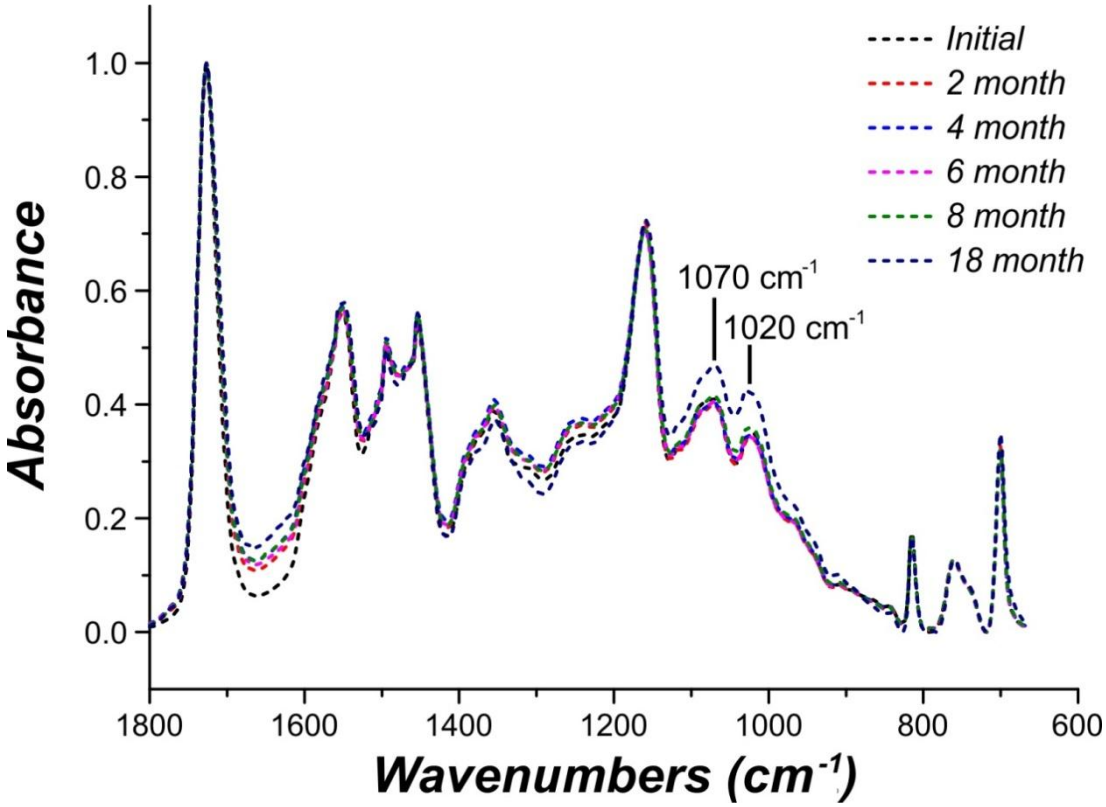

Figure 4.10: Averaged ATR FT-IR spectra obtained from the clear coat of the Ford Focus vehicle after every sampling interval. Note the changes in the intensity of the vibrational stretches at 1170 and 1020 cm^{-1} following 18 months of environmental exposure.

Visual inspection of the IR spectra in Figure 4.10 revealed that there is no significant change in the clear coat composition within the first 8 months of environmental exposure. However, discernible differences were observed in the acrylic fingerprint region (1300-1000 cm^{-1}) of the spectra obtained from samples following 18 months of environmental exposure. In particular, there are two peaks in the acrylic fingerprint region (*ca.* 1070 and 1020 cm^{-1}) representing C-O symmetric vibrations, which are more intense in the sample after 18 months of environmental degradation. However, photo-degradation of acrylic-melamine clear coats that leads to chain scission would unequivocally result in an observed decrease in the intensity of the corresponding C-O stretches.[186, 195]

The results obtained from this ambient weathering study, depicted in Figure 4.10 and Figure A.3 and A.4 of the appendix, contradict those of previous studies.[186, 195] This may be due to the fact that the studies reported in the open literature, artificially aged their samples in a controlled system by manipulating only a few variables such as temperature, humidity and UV irradiance. However, these studies neglected to investigate the effect other natural environmental factors, such as the presence of biological materials, have on the weathering of these coatings. Biological materials in the form of bird droppings, plant sap, insect bodies and other microorganisms are commonly encountered in the surroundings, and thus will affect the chemical, visual and mechanical properties of automotive coatings.[187, 196]

Recent studies have revealed that artificially aging acrylic-melamine clear coats which have previously been subjected to various biological materials, chemically deteriorates the composition of the coating in a manner mirroring ambient environmental degradation. Artificial weathering of these coatings solely in climate chambers, causes hydrolytic reactions to cleave the ether linkages formed between the melamine and acrylic binder during curing; thereby resulting in a decrease in the observed intensity of the vibrational bands attributable to this ether linkage (*ca.* 1100-1000 cm^{-1}).[197, 198] Conversely, the synergistic effect of biological substances and weathering on the clear coats, promotes self-condensation reactions thereby forming new ether linkages between acrylic and melamine, resulting in amplification in the intensity of these same C-O vibrational stretches.[197, 198] A similar chemical response was also observed in the remaining samples utilised in this study that were exposed to the ambient environment (Figure A.3-A.4 of the appendix). Whilst the samples used in this study were not deliberately subjected to biological materials prior to exposure, they will more than likely have come into contact with some form of bio-source throughout the duration of natural environmental exposure. Based upon the results of this study, acrylic-melamine coatings respond differently when aged artificially in climate chambers relative to the natural surroundings. This indicates that although climate chambers can accelerate the degradation process, studies involving natural weathering of the

samples needs to be undertaken, in order to obtain an accurate representation of the effect of weathering on automotive clear coats.

This study ultimately concluded that environmental exposure over an 18 month period does not affect sample classification. Although differences in the IR spectra and projection of samples were observed following 18 months of ambient environmental exposure, it is worth reiterating that all of these samples were still correctly classified into their corresponding class. It is important to note that the average age of registered vehicles on the Australian roads is approximately 10 years, therefore extensive weathering studies that span this lifetime need to be conducted in order to assess the applicability of this model.[199] Whilst previous studies have employed climate chambers to artificially accelerate the ageing process by simulating the outdoor conditions, it has been demonstrated that the clear coats respond differently when aged in climate chambers as opposed to the natural surroundings. Consequently, in order to obtain an accurate assessment of the impact of environmental degradation on the model, these samples need to be exposed to the natural surroundings for a period of 10 years. Another issue that warrants further investigation is the potential effect of uneven weathering across different portions of the vehicle.

4.4 Conclusion

Based upon the results of this study, it is evident that the migration of components between the various layers can and does occur. In particular, the cross-linking agent melamine and pigments were shown to consistently migrate from the underlying layers into the clear coat of select vehicles. From a forensic science viewpoint, these results are significant as the relative abundance of melamine and pigments in the clear coat will vary greatly depending upon the region of the layer analysed. Relating this to the ATR-based model, melamine migration may lead to misclassification of samples if spectra are obtained from regions of the coating affected by component migration. Consequently, appropriate analytical protocols must be established to negate the effects of component migration, so as to obtain a true representation of the composition of the coating for forensic identification purposes. Another potential limitation of the ATR model, which warranted further investigation, was the influence of environmental factors on the characterisation and classification of automotive clear coats. The results of this stream of investigation revealed that samples exposed to the environment over an 18 month time period did not affect the classification of the samples in the model. However, subtle differences were observed in the acrylic fingerprint region of the IR spectra following 18 months of environmental exposure, suggesting that longer periods of weathering are necessary in order to gauge the limits of the model.

It is important to note that the clear coat model previously described in Chapter 3 was generated solely from ATR FT-IR spectra, which is ultimately representative chemically of the outermost surface of the clear coat. In this particular instance, if ATR FT-IR spectroscopy is utilised to characterise the clear coats, the issue regarding chemical component migration is mitigated; as IR spectra used to generate and test the model are solely obtained from areas of the coating unaffected by component migration. However, in situations where transmission IR spectra need to be acquired from shavings or thin peels, caution must be exercised to ensure spectra obtained from regions of the sample are truly representative of the composition of

the coating. Whilst ATR FT-IR spectroscopy can be used to prevent chemical component migration from significantly influencing the model, the same cannot be said for the study examining the effect of environmental degradation. This is due to the fact that the degradation of the coating may be more pronounced at the surface of the clear coat. This implies that differences observed in the ATR spectra may not be indicative of significant changes in the bulk composition of the coating and this needs to be investigated further.

Chapter 5: Characterisation of the underlying paint layers of automotive paint systems using synchrotron FT-IR microspectroscopy

Portions of this chapter have been published in the journal *Talanta*:

Maric, M., van Bronswijk, W., Lewis, S.W., and K. Pitts. *Synchrotron FTIR characterisation of automotive primer surfacer paint coatings for forensic purposes.* Talanta, 2014. **118**: p. 156-161.

5.1 Introduction

Whilst the model generated from the IR spectra obtained from automotive clear coats displayed potential in procuring investigative leads from questioned paint samples, there are situations that preclude the use of this model. Although most vehicles contain a typical 4-coat paint system, a small proportion, less than 2 % of vehicles worldwide, contain a single-stage topcoat or monocoat paint system, which consists of only an electrocoat primer, primer surfacer and basecoat.[24, 32] Subsequently, as there is no clear coat in this paint system, it would be impossible in this situation to utilise the model described in Chapter 3 to provide information about the questioned paint sample.

Where IR spectra are unable to be obtained from original automotive clear coats or are inconclusive, further information can be obtained from underlying automotive paint layers. There appears to be no published research available in the open literature examining the chemical variability in the composition of the underlying automotive paint layers for forensic purposes. From a paint technology viewpoint, modern automotive clear coats generally only consist of four main components (i.e. acrylic, melamine, styrene and/or polyurethane). The underlying coatings contain a range of similar chemical components, but also contain inorganic pigments and extenders. This is of significance as the chemical formulation of these coatings will consist of a much larger number of chemical components, which can potentially be utilised to discriminate between samples. Consequently, the main aim of this study was to employ synchrotron FT-IR microspectroscopy in combination with multivariate statistics to assess the diversity in a large population of automotive electrocoat primer, primer surfacer and basecoat layers; with a view to identifying relationships between the chemical composition of the coatings and the potential make, model and year of manufacture of the vehicle.

5.2 Experimental

Thin automotive paint cross-sections were obtained from all automotive paint exemplars as outlined in section 2.4.1. A small segment of the resultant cross-sections was chemically imaged using synchrotron FT-IR microspectroscopy, as described in section 2.4.2. For every sample, 2-dimensional distribution maps were generated from key vibrational bands representing each individual component in the cross-section. Six single point IR spectra were extracted from chemically uniform regions of these underlying layers. The spectral datasets for each layer were then linearly baseline corrected and the interference fringes were removed as outlined in section 2.4.3. The datasets were mean normalised, thereby eliminating any variability attributable to sample texture. Finally, the datasets were truncated to a range of 1800-900 cm^{-1} as minimal variance in the spectra was observed outside of this region. PCA was then performed on the spectral datasets as defined in section 2.5.1. The key components of the process are diagrammatically summarised in Figure 5.1.

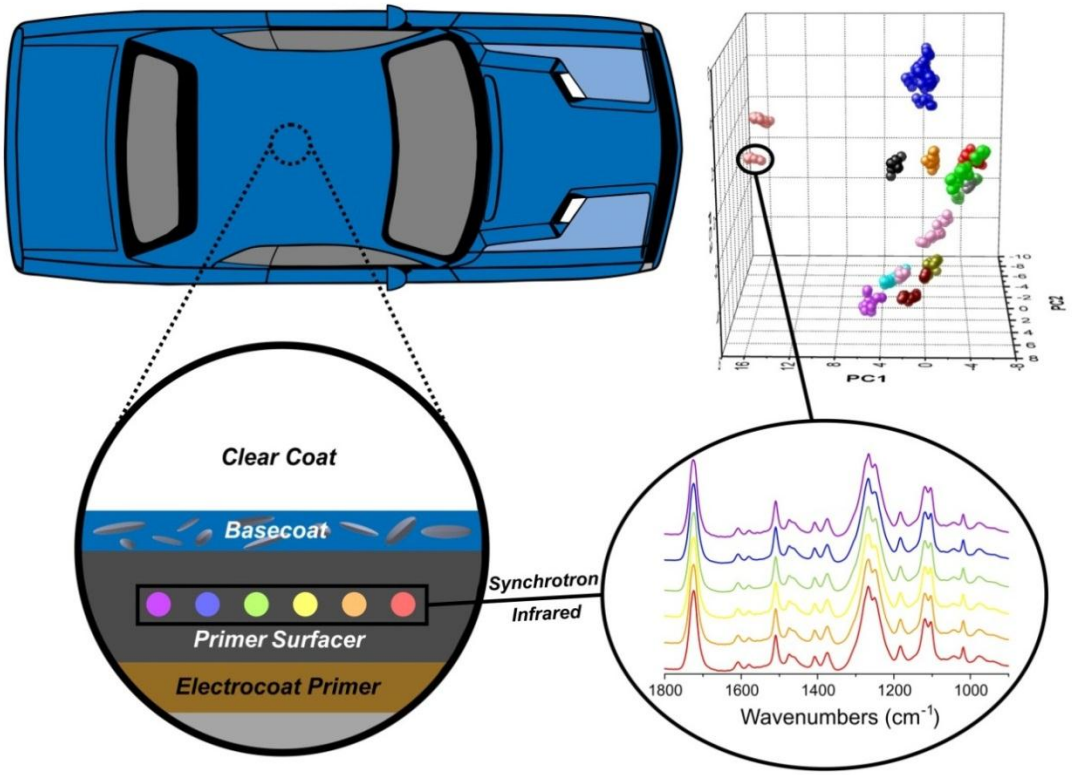

Figure 5.1: Illustration detailing the methodology involved in the evaluation of synchrotron FT-IR data obtained from the primer surfacer.

5.3 Results & Discussion

It is important to note that PCA assessment of synchrotron FT-IR spectra extracted from the electrocoat primer and basecoat, revealed no identifiable patterns or trends. The composition of the basecoat was determined to be entirely dependent on the colour and/or finish of the vehicle, which is to be expected as it is characterised by the pigments in the coat. No significant variability was observed in the IR data obtained from the electrocoat primer. However, significant diversity was observed in the synchrotron FT-IR data from the primer surfacer layers. Synchrotron IR imaging was utilised in the stratigraphic imaging of automotive paint cross-sections, with a view to identifying sections of the primer surfacer that are chemically uniform and are thus truly representative of the composition of the coating. Figure 5.2(e) is the combined image of Figure 5.2(b-d), such that the three chemical images are overlapped to produce a red-green-blue (RGB) map. RGB mapping is a form of component imaging, whereby each individual component (1b-d) is colour-coded as red, green or blue.

The RGB map adds the colour portions of the selected chemical components allowing visualisation of the local distribution of all the components based upon the fundamentals of additive colour mixing. As the additive mixing of all three primary colours yields white, this region of the RGB map represents the area where all three components of the surfacer are the most abundant and therefore corresponds to the region of the coating unaffected by interlayer paint component migration. In this particular instance, it is evident that the white region in Figure 5.2(e) correlates with the mid-centre of the primer surfacer (Figure 5.2(a)). Subsequently, synchrotron FT-IR spectra were extracted predominantly from the chemically uniform centre of the primer surfacer; however, this was constantly re-evaluated on a case by case basis. In this particular study, the spectral dataset contained a total of 450 spectra consisting of 75 distinct vehicles, covering a range of Australian and international manufacturers. The dataset encompassed a diverse range of vehicles, with 13 makes and 45 different models being represented.

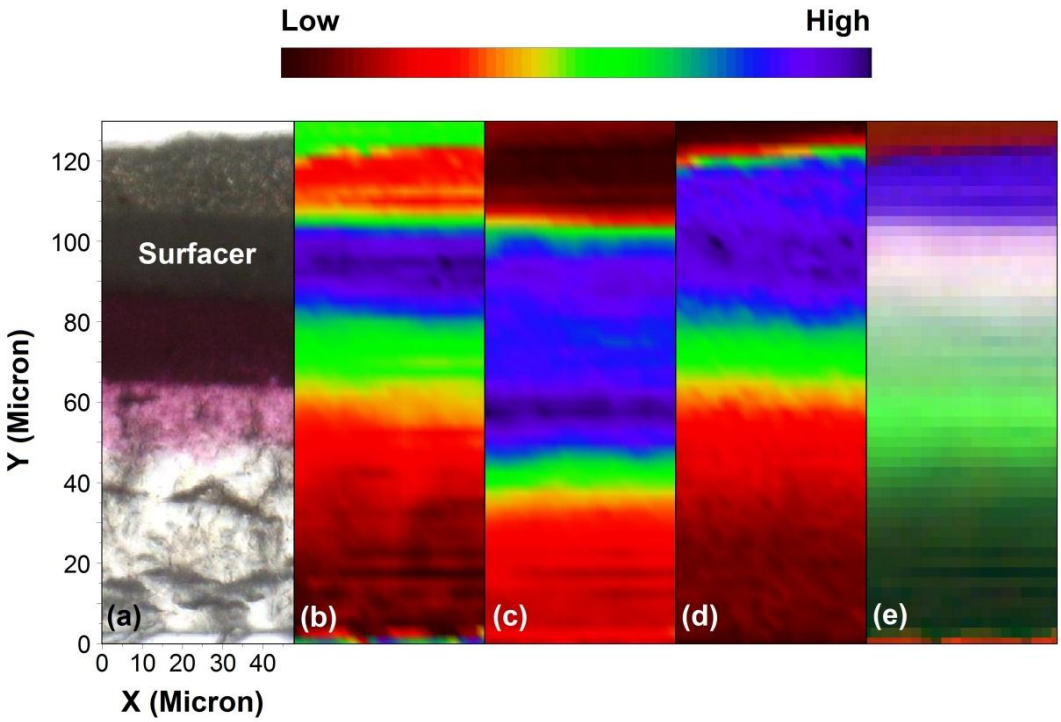

Figure 5.2: (a) Optical image of an automotive paint cross-section obtained from a Mazda 3. (b) Synchrotron FT-IR chemical image highlighting the distribution of polyurethane (ca. 1690 cm^{-1}), (c) melamine (ca. 1550 cm^{-1}), and (d) isophthalic alkyd (ca. 1236 cm^{-1}). (e) An RGB image produced by combining and overlapping the previous three chemical images (b-d), thereby allowing visualisation of the local distribution of all three components. The polyurethane trace is depicted as red, melamine is displayed as green and isophthalic alkyd is presented as blue.

PCA performed on the primer surfacer spectral dataset revealed that 74.7 % of the total variance in the dataset was accounted for in the first three PCs. The Scree plot shown in Figure 5.3 advocated the utilisation of as many as five PCs. A number of combinations of the first five PCs were examined, with the scores plot containing the first three PCs detailed in Figure 5.4, as the fourth and fifth PC did not offer any additional discrimination of samples.

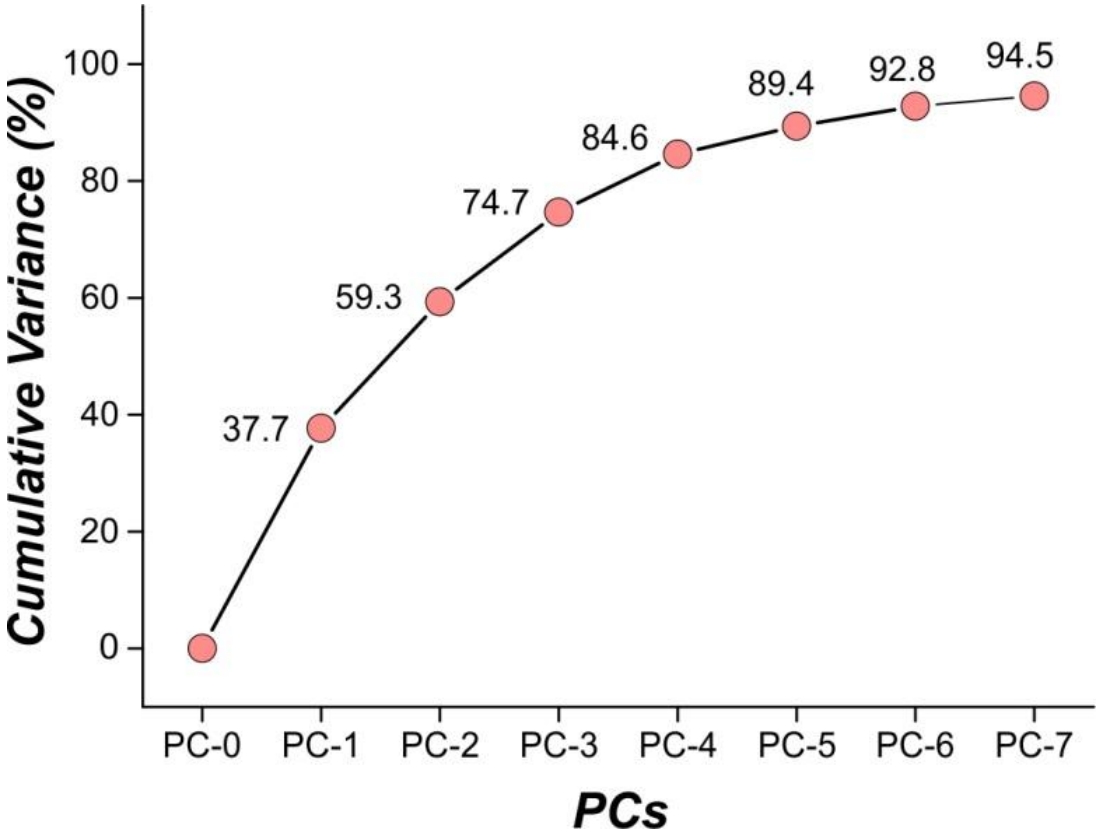

Figure 5.3: Scree plot depicting the variance in the primer surfacer spectral dataset retained by each PC.

The 3-dimensional PCA scores plot, generated from the first three PCs, revealed that 14 distinct classes are present in the dataset and a correlation exists between the classes and the country of manufacture, the specific manufacturer and manufacturing plant (Table 5.1 and Figure 5.4). In addition to the samples classified into these 14 classes, there are samples in the dataset representing single vehicles manufactured by Nissan, Chrysler, and Jaguar. Unfortunately, the number of samples signifying these vehicles is far too small for generalisations or relationships to be deduced and as such they were excluded from the model. It is anticipated that as the dataset continues to expand, the statistical model will become more defined, consequently producing more classes corresponding to these vehicles. There are two distinct groupings for both the German-manufactured Ford Focus and for the South Korean-made Hyundai. The reason for this will be discussed in detail later.

As mentioned beforehand, five replicate spectra were extracted from each sample so as to assess the intra-sample variability within the surfacer layer. The differences between the replicate spectra are insignificant providing representative spectra are obtained from the chemically uniform regions of the coating; thereby ensuring compositional differences within a sample are minimal.

Table 5.1: Classes revealed following PCA of the primer surfacer spectral dataset.

Class	No. of samples	Vehicle/s represented
Class 1	3	Mitsubishi Pajero
Class 2	3	SsangYong
Class 3	15	Australia (Holden/HSV) [2006-present]
Class 4	10	Australia (Ford)
Class 5	4	Mitsubishi Lancer
Class 6	3	South Korea (Holden)
Class 7	10	Toyota/Honda
Class 8	5	Mazda
Class 9	2	Germany (Ford Focus)
Class 10	5	Australia (Holden/HSV) [2001-2005]
Class 11	5	Hyundai
Class 12	4	Hyundai
Class 13	2	Germany (Ford Focus)
Class 14	4	US (Dodge/Jeep)

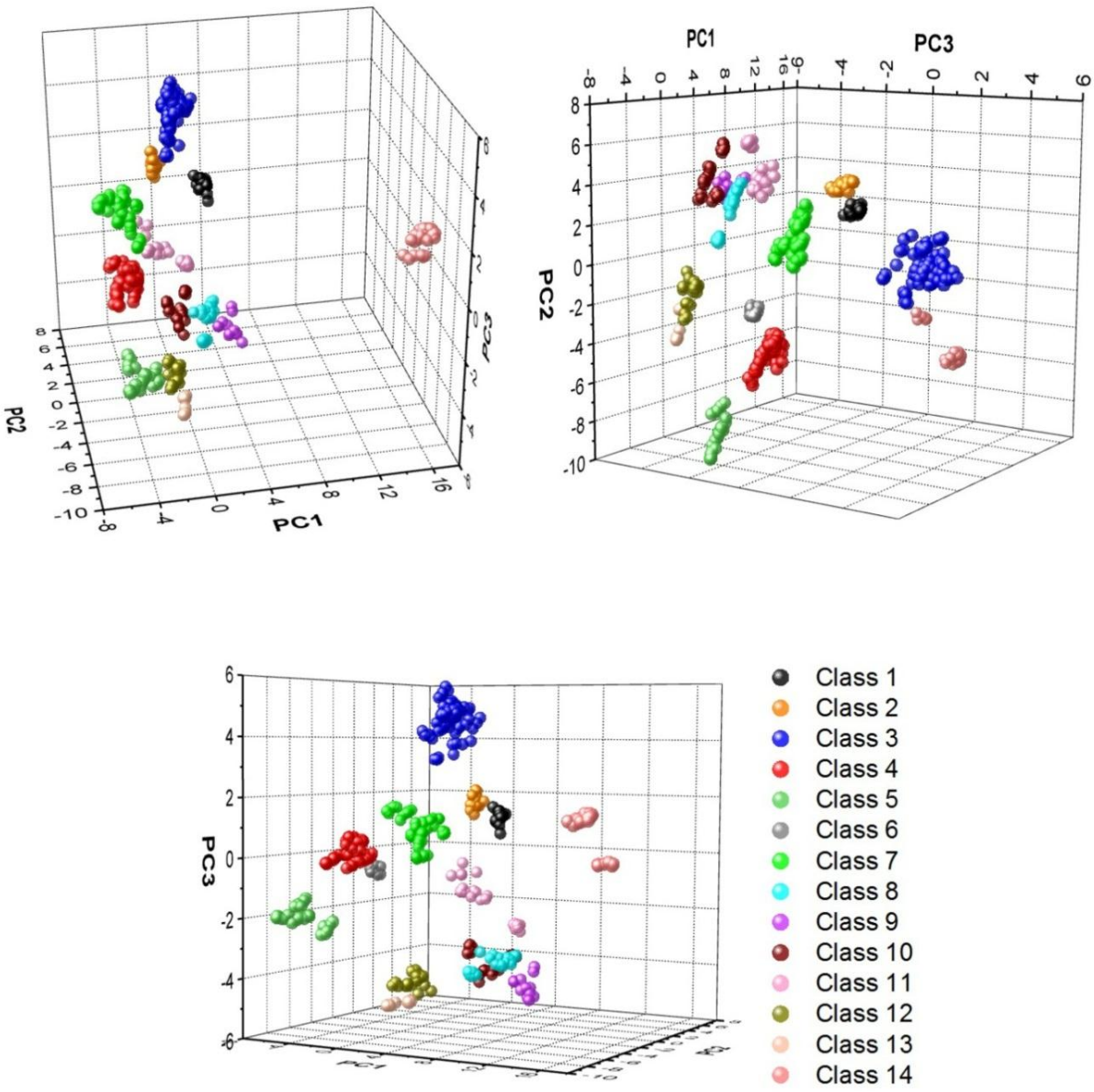

Figure 5.4: Three different perspectives of a 3-dimensional PCA scores plot highlighting the distribution of a population of automotive primer surfacers based upon their corresponding synchrotron FT-IR spectra. Note: classes representing vehicles, which contain only one sample, were removed from the scores plot to provide clarity.

It is important to note that the spectral dataset was derived from 75 distinct vehicles, which is only a small subset of the total sample population (139 vehicles), due to restrictions on user beam-time at the Australian Synchrotron. Consequently, the number of groupings in this model could be fewer and much less defined than the groupings in the ATR-based clear coat model. However, there are a number of groupings common to both models; including classes representing the US-manufactured Dodge and Jeep, SsangYong, South Korean-manufactured Holden, and Mitsubishi Pajero vehicles. Whilst there are shared groupings within both models, there are additional classes in the primer surfacer model corresponding to specific manufacturers. In fact, generally speaking the clear coat model was mainly capable of providing information regarding the origin of the vehicle. On the other hand, as can be seen from Table 5.1 and Figure 5.4, the model based on the primer surfacer is capable of providing more specific information regarding the potential manufacturer. For instance, whilst class 3 of the clear coat model represents Japanese and Australian-made Toyota, Japanese-manufactured Mazda and Mitsubishi Lancer vehicles, these three types of vehicles have their own distinct groupings in the primer surfacer model, thereby highlighting the increased discriminating power of this statistical model.

Three classes exist in the dataset representing samples obtained from General Motors-manufactured Holden vehicles (classes 3, 6 and 10). It is not surprising that chemical differences in the primer surfacer are evident between the South Korean and Australian-made Holden vehicles, as similar differences were also observed in the clear coats. However, a relationship was also discerned within the samples obtained from Australian factory-made Holden/HSV vehicles as a function of the year the vehicles were manufactured. Although this trend was also observed in the clear coats, in this particular instance, samples obtained from class 3 represented vehicles manufactured from 2006 onwards, whereas samples in class 10 signify vehicles manufactured up until 2006. The significance of this relationship will be discussed in further detail below. Furthermore, there are two Mitsubishi classes present in the dataset (classes 1 and 5), with the distinction between these two

groupings occurring as a function of the plant in which the vehicles were manufactured. In this particular instance, the samples from class 1 represent Mitsubishi Pajero vehicles manufactured at the Nagoya plant, whilst the samples from class 5 signify Mitsubishi Lancer vehicles produced at the Mizushima plant, thereby highlighting diversity within the manufacturer. This correlation was also observed in the ATR-based clear coat model.

Similarly, there are also two groupings in the dataset which are representative of samples obtained from the German-manufactured Ford Focus (classes 9 and 13), and Hyundai vehicles (classes 11 and 12). However, there is no observable correlation between the two sets of classes and the common vehicle descriptors; which includes but is not limited to, the model and year of the vehicle as well as the plant and platform used to manufacture the vehicle. The rationale behind the discrimination between these two sets of groupings will be discussed in detail later. It is important to note that class 7 contains samples representing both Toyota and Honda vehicles, irrespective of the country of manufacture. Consequently, class 7 includes Toyota vehicles manufactured in Japan, Australia, and Thailand, as well as Honda vehicles manufactured in Japan, Poland, and the UK. This deviates considerably from the groupings in the clear coat model, with the Thai-manufactured Toyota vehicles being classified separately from the Australian and Japanese-manufactured Toyota vehicles. Similarly, the Japanese-made Honda vehicles are classified differently to the Polish and UK-made Honda vehicles in the clear coat model.

Based upon the PCA scores plot depicted in Figure 5.4, it is evident that 14 distinct classes are present in the spectral data. In order to ascertain which features of the spectra give rise to the discrimination between the classes, the IR spectra of the central sample of each class was visually examined (Figure 5.5) and their chemical constituents were identified (Table 5.2).

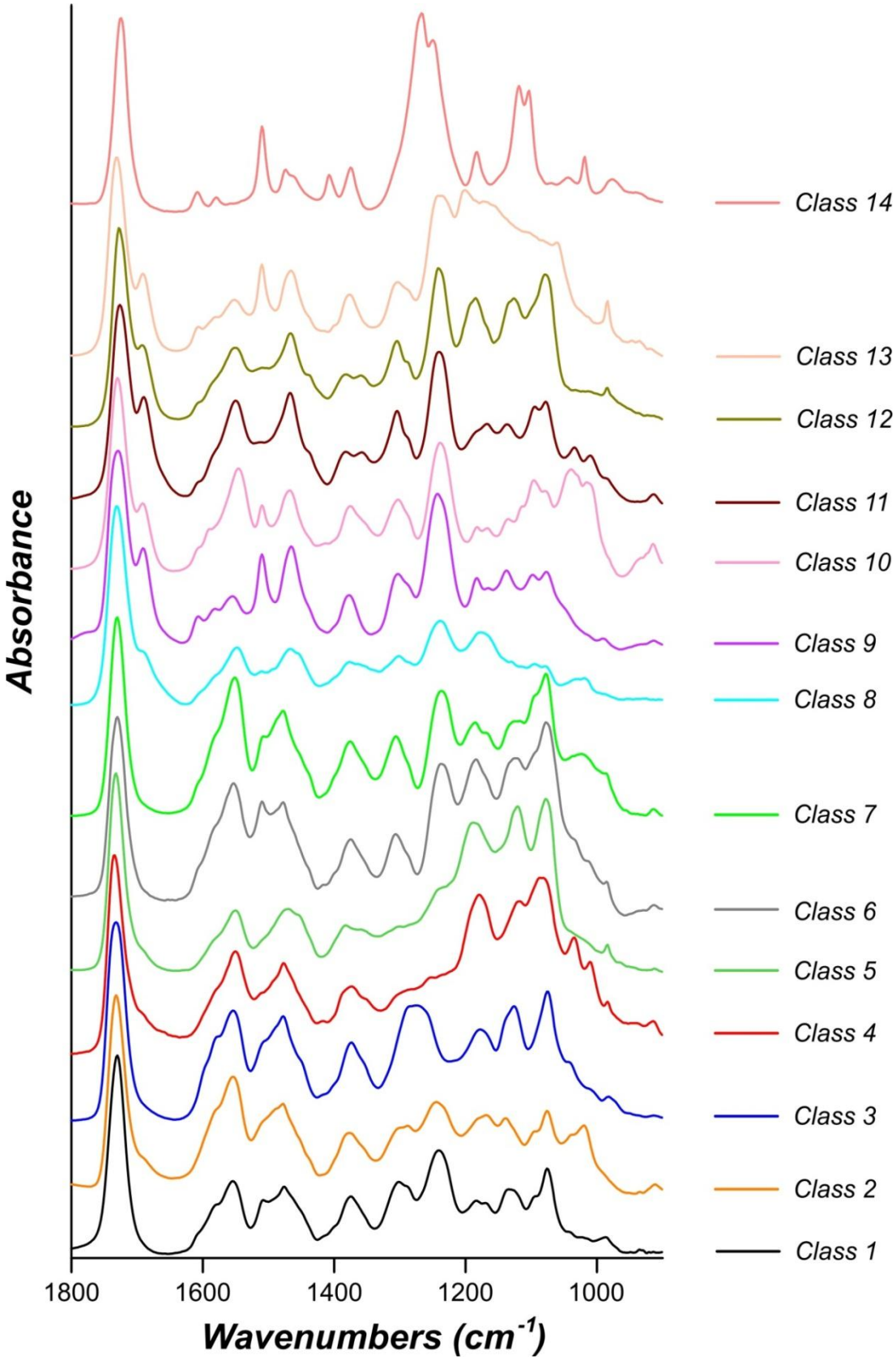

Figure 5.5: Synchrotron FT-IR spectra obtained from the central sample of each class highlighting the chemical differences between the classes.

Table 5.2: Frequencies (cm^{-1}) for synchrotron FT-IR spectra obtained from the centroid of each grouping. Note: s – strong, m – moderate, w – weak, b – broad, h – high, l - low.

Class	IR Absorption Frequencies (cm^{-1})	Composition
Class 1	1731 (s), 1554 (m), 1508(m), 1476 (m), 1375 (m), 1301 (m), 1242 (m), 1183 (m), 1135 (m), 1076 (m), 986 (w)	Isophthalic alkyd (m), Melamine (m), Epoxy (m), Barium sulfate (m)
Class 2	1731 (s), 1553 (m), 1478 (m), 1376 (m), 1289 (m), 1245 (m), 1168 (m), 1139 (m), 1076 (m), 1020 (m), 912 (w)	Isophthalic alkyd (m), Melamine (m), Magnesium silicate (m)
Class 3	1732 (s), 1554 (m), 1478 (m), 1374 (m), 1272 (bm), 1177 (m), 1126 (m), 1075 (s), 983 (w)	Orthophthalic alkyd (m), Melamine (m), Barium sulfate (m),
Class 4	1735 (s), 1550 (m), 1477 (m), 1374 (m), 1238 (m), 1179 (m), 1114 (m), 1086 (s), 1035 (m), 1010 (m), 984 (m), 914 (w)	Isophthalic alkyd (m), Melamine (m), Barium sulfate (m), Aluminium silicate (m)
Class 5	1732 (s), 1551 (w), 1469 (w), 1383 (w), 1301 (w), 1236 (m), 1184 (s), 1120 (s), 1074 (s), 984 (w)	Isophthalic alkyd (m), Melamine (l), Barium sulfate (h)
Class 6	1730 (s), 1554 (m), 1510 (m), 1478 (m), 1375 (m), 1306 (m), 1237 (s), 1184 (s), 1125 (s), 1076 (s), 1036 (m), 1013 (m), 986 (w), 914 (w)	Isophthalic alkyd (m), Melamine (m), Epoxy (m), Barium sulfate (h), Aluminium silicate (m)
Class 7	1730 (s), 1551 (s), 1508 (m), 1478 (m), 1376 (m), 1305 (m), 1237 (s), 1182 (m), 1171 (m), 1130 (m), 1079 (s), 985 (w)	Isophthalic alkyd (m), Melamine (h), Epoxy (m), Barium sulfate (m)
Class 8	1731 (s), 1691 (w), 1548 (w), 1511 (w), 1467 (w), 1377 (w), 1302 (w), 1239 (m), 1176 (m), 1095 (w), 1078 (w), 1031 (w), 1019 (w)	Isophthalic alkyd (m), Melamine (l), Polyurethane (l), Epoxy (l), Aluminium silicate (l)
Class 9	1729 (s), 1691 (m), 1607 (w), 1581 (w), 1553 (w), 1510 (m), 1466 (m), 1377 (w), 1303 (m), 1243 (s), 1182 (m), 1138 (m), 1098 (m), 1077 (m), 915 (w)	Isophthalic alkyd (m), Melamine (l), Polyurethane (m), Epoxy (m)
Class 10	1730 (s), 1691 (m), 1546 (s), 1510 (m), 1468 (m), 1376 (m), 1303 (m), 1238 (s), 1182 (m), 1166 (m), 1136 (m), 1095 (m), 1078 (m), 1034 (s), 1012 (m), 915 (m)	Isophthalic alkyd (m), Melamine (h), Polyurethane (m), Epoxy (m), Aluminium silicate (h)
Class 11	1725 (s), 1690 (m), 1552 (m), 1468 (m), 1382 (w), 1358 (w), 1304 (m), 1240 (s), 1165 (w), 1138 (w), 1096 (m), 1078 (m), 1035 (w), 1010 (w), 915 (w)	Isophthalic alkyd (m), Melamine (m), Polyurethane (m), Aluminium silicate (l)
Class 12	1725 (s), 1692 (m), 1551 (m), 1509 (m), 1466 (m), 1382 (m), 1359 (m), 1304 (m), 1240 (s), 1184 (s), 1124 (s), 1079 (s), 984 (w), 915 (w)	Isophthalic alkyd (m), Melamine (m), Polyurethane (m), Epoxy (m), Barium Sulfate (m)
Class 13	1731 (s), 1691 (m), 1607 (w), 1580 (w), 1551 (w), 1510 (m), 1466 (m), 1377 (w), 1303 (m), 1240 (s), 1201 (s), 1170 (s), 1061 (m), 984 (w)	Isophthalic alkyd (m), Melamine (l), Polyurethane (m), Epoxy (m), Barium sulfate (h)
Class 14	1724 (s), 1608 (w), 1580 (w), 1510 (m), 1474 (w), 1408 (w), 1375 (w), 1269 (s), 1249 (s), 1183 (w), 1120 (m), 1105 (m), 1044 (w), 1019 (w), 976 (w)	Terephthalic alkyd (h), Epoxy (m)

The backbone of every primer surfacer was polyester based; however, subtle differences were observable in the form of polyester employed (i.e. orthophthalic, isophthalic and terephthalic alkyd). Melamine was another component observed in almost all types of primer surfacers as it is commonly utilised as a cross-linking agent.[13, 32, 200] Another common constituent in the surfacer is polyurethane, which is due in part to the constructive effect it has on the dispersibility of the film in a waterborne system, whilst also producing exceptional film properties.[32, 200, 201] Epoxy resin was found in over half of the surfacers as a result of the mechanical and technological features it affords the coating.[200, 201] Extenders are also widely employed in the manufacture of the primer surfacers as they affect performance parameters such as gloss, stone-chip resistance and even rheology.[32] The extenders encountered in this particular study were barium sulfate, aluminium silicate and magnesium silicate. Ultimately, discrimination between classes was achieved due to distinctive permutations of the chemical components listed above, or as a result of variations in the relative abundance of the components in the system (Table 5.2).

The factor loadings for the first three PCs were examined to identify the spectral regions in the dataset responsible for the differentiation between samples on the scores plot. The loadings plot for PC1 revealed regions of high positive correlation at 1722, 1270 and 1251 cm^{-1}, which are characteristic of the C=O and C-O vibrational stretches attributable to the terephthalic alkyd resin (Figure 5.6).[56] As only the US-manufactured Dodge and Jeep vehicles from class 14 contain terephthalic alkyd in the primer surfacer these samples attain large positive values on PC1. Similarly, the remaining samples which are based on an entirely different alkyd system attain significant negative scores on PC1, and are subsequently compressed into one half of the scores plot, as depicted in Figure 5.6.

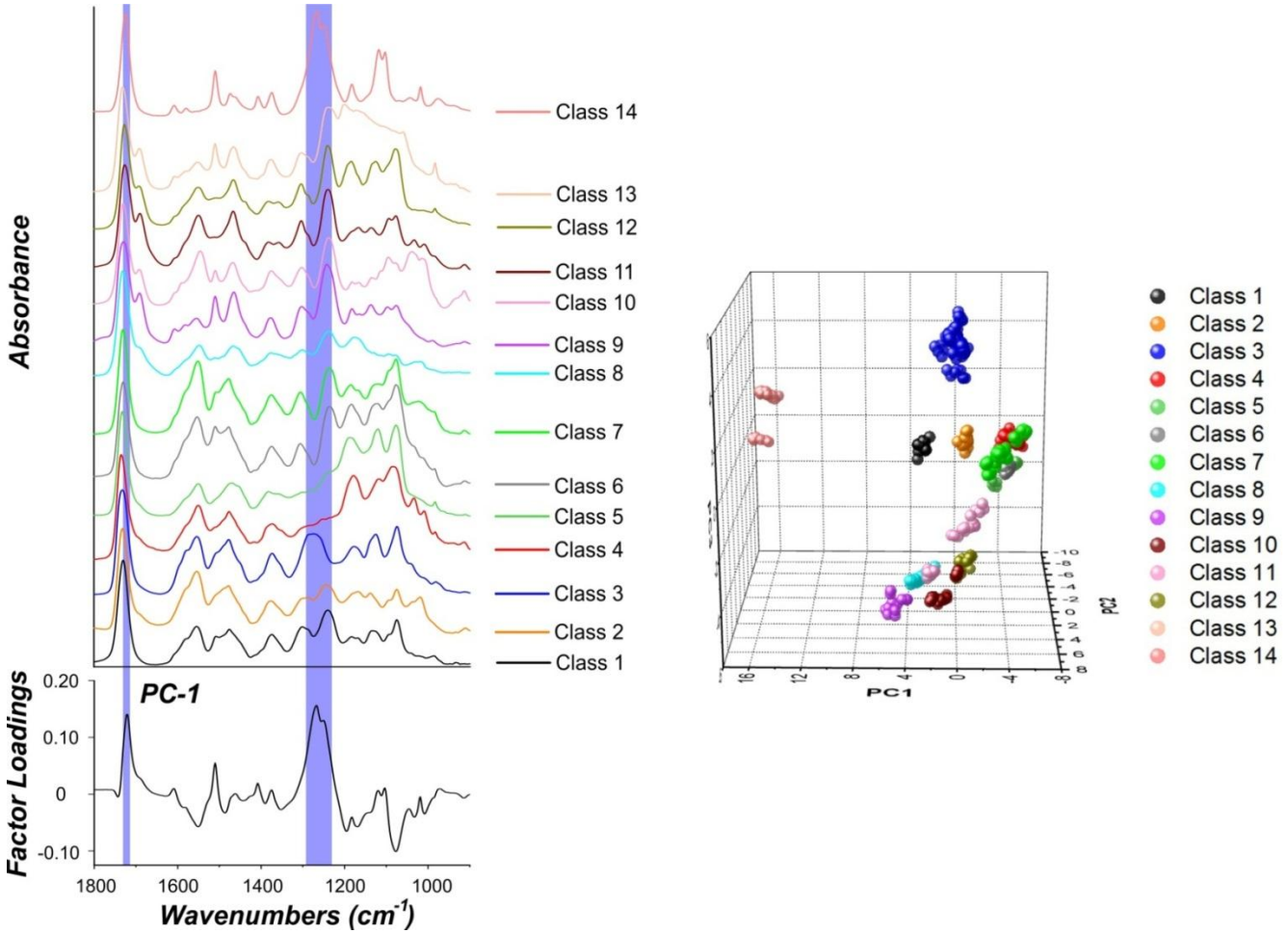

Figure 5.6: Factor loadings for PC1. The blue regions superimposed on the representative IR spectra for each grouping, signify spectral regions that are significantly positively correlated with PC1.

The factor loadings for PC2 revealed a strong positive correlation at 1551 cm^{-1}, which is indicative of an in-plane vibration of the triazine ring characteristic for the melamine cross-linking agent. Additionally, the two significant negative loadings *ca.* 1182 and 1119 cm^{-1} are distinctive for the barium sulfate extender. Therefore, discrimination between samples on PC2 is achieved based upon the relative abundance of melamine and barium sulfate in the primer surfacer, as displayed in Figure 5.7. As can be seen from Figure 5.7, samples with a relatively large abundance of the barium sulfate extender and low abundance of melamine in the primer surfacer, attain significant negative scores on PC2 (e.g. samples in class 5). Conversely, samples that contain a large abundance of melamine and a low abundance of barium sulfate will have large positive scores on PC2 (e.g. classes 2, 10 and 11).

The loadings plot for PC3 revealed two zones of significant negative correlation; one at approximately 1689 cm^{-1} which is consistent with the C=O stretch attributable to polyurethane, and the other at 1236 cm^{-1} which is the main diagnostic peak representing the isophthalic alkyd resin. A broad zone of positive correlation was also observed at 1273 cm^{-1}, which denotes the C-O stretch attributable to the orthophthalic alkyd resin. Therefore, samples are separated on PC3 based upon the presence of the orthophthalic and isophthalic alkyd resin and the abundance of polyurethane. By examining Figure 5.8, it is evident that the reason why samples from class 3 attain significant positive scores on PC3 is due to the large abundance of orthophthalic alkyd, and the absence of isophthalic alkyd and polyurethane in the surfacer. Conversely, the samples with large negative scores on PC3 contain a relatively large abundance of isophthalic alkyd and polyurethane, with little to no orthophthalic alkyd (e.g. classes 11-13).

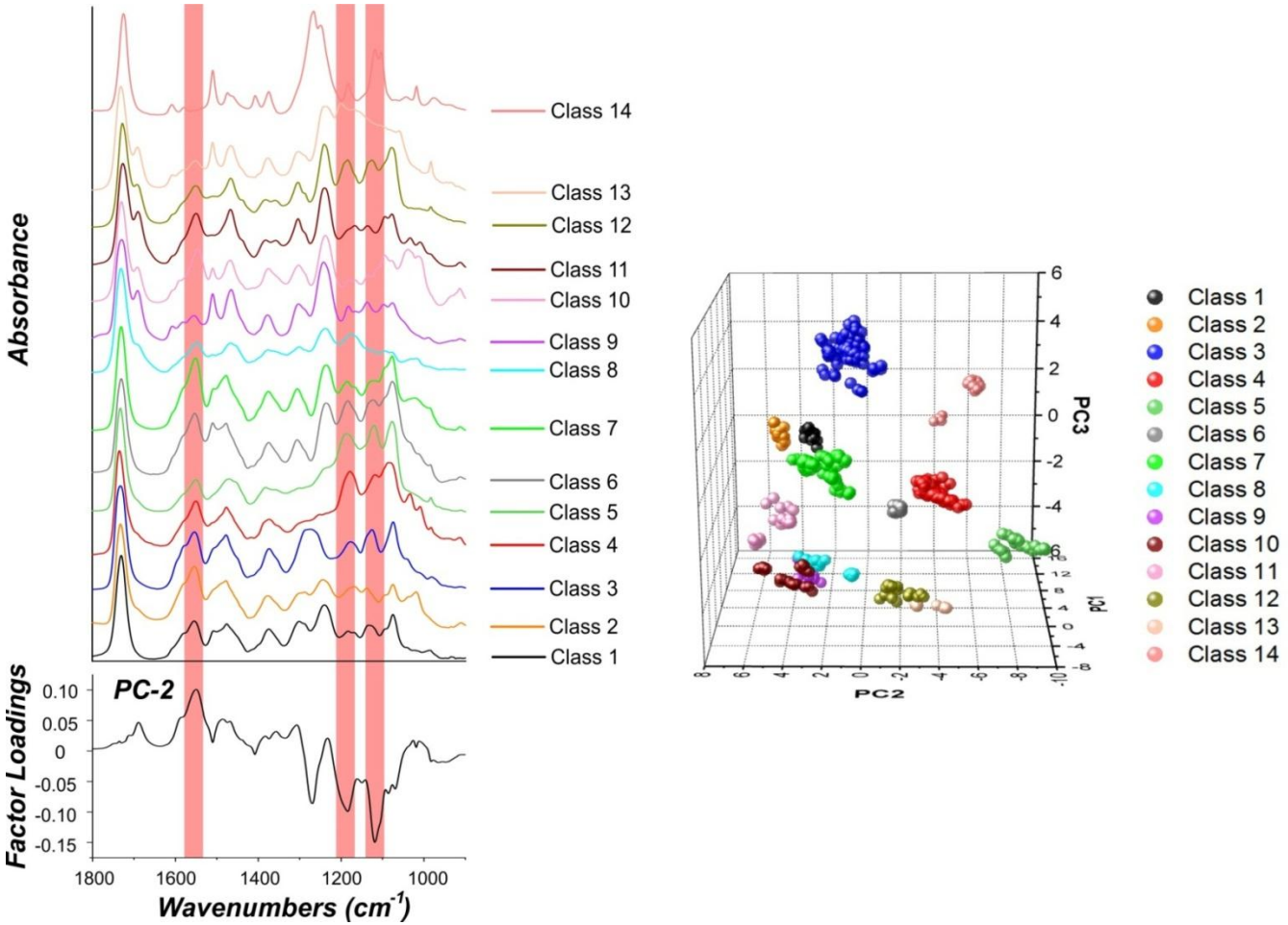

Figure 5.7: Factor loadings plot for PC2. The red regions overlaid on the representative IR spectra for each class centroid, denote regions of significant correlation with PC2.

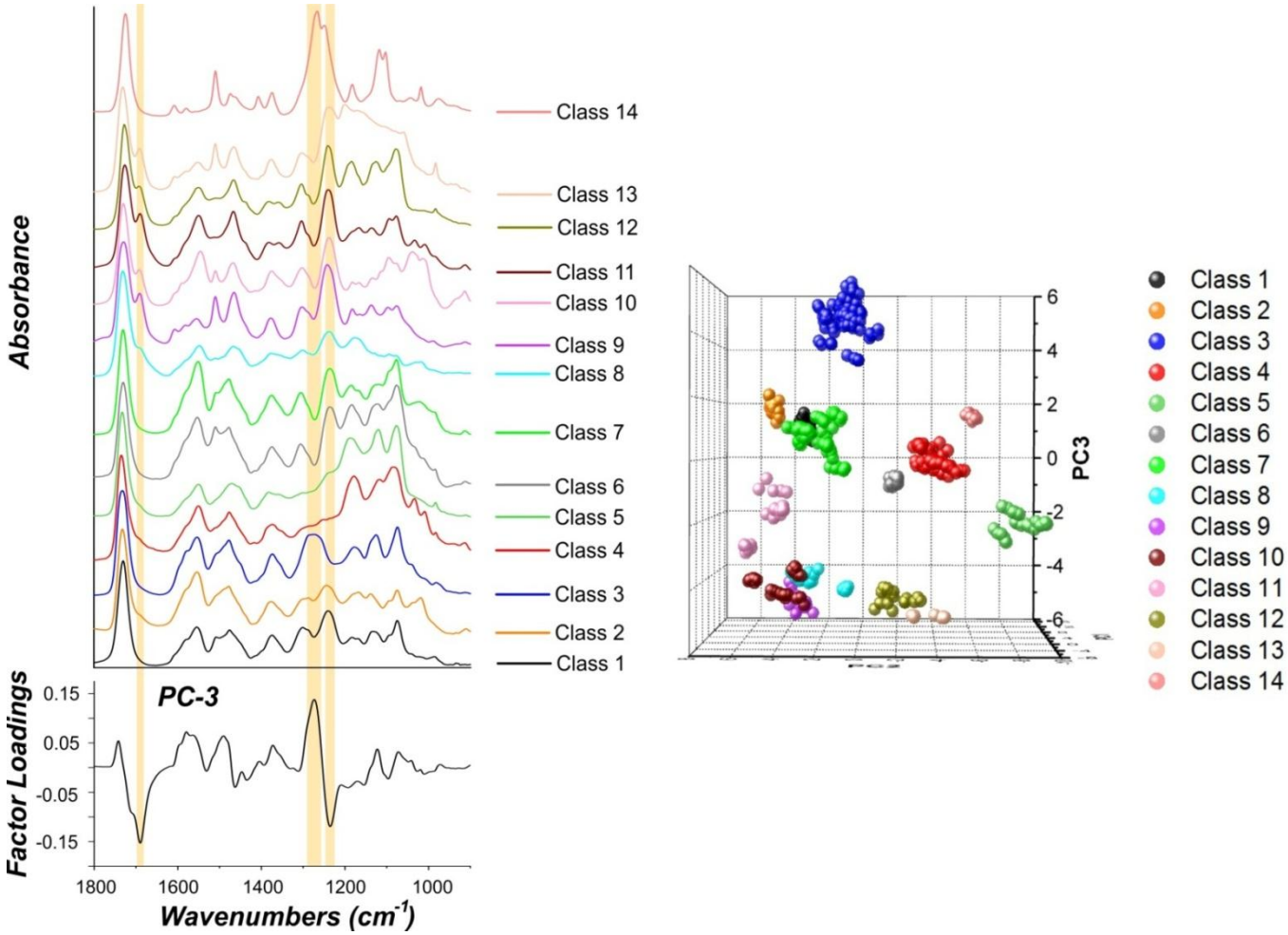

Figure 5.8: Factor loadings plot for PC3. The orange regions superimposed on the representative IR spectra for each class, signify spectral regions significantly correlated with PC3.

The Fisher ratio plot based on the PCA groupings revealed that the most important spectral feature in the dataset is an intense, sharp vibrational band *ca.* 1270 cm^{-1}. This peak is indicative of the terephthalic alkyd resin and the presence of this band is a distinguishing characteristic between the representative IR spectra of the PCA groupings, as depicted in Figure 5.9. This result is consistent with the factor loadings for PC1, which accounts for 37.7 % of the total variance in the dataset, and is solely responsible for discriminating samples based primarily on the presence of terephthalic alkyd in the primer surfacer.

As mentioned previously, there are two sets of groupings present in the model representing the German-manufactured Ford Focus, and Hyundai vehicles. No discernible correlation was observed between the groupings as a function of the common vehicle descriptors. However, upon closer examination, a trend was observed between the two classes and the nature and layer structure of the paint samples. Specifically, class 13 consists of Ford Focus vehicles that contain the typical 4-layered paint system, whilst the samples from class 9 represent Ford Focus vehicles containing 6 OEM coatings. As depicted in Figure 5.10, it is evident that the two paint systems have roughly the same total thickness, presumably to meet certain internal specifications and requirements. In this particular instance, the 4-coat system contains a much thicker primer surfacer to compensate for the fact that the 6-layered OEM paint system contains an additional original manufacturer base and clear coat. The main chemical difference between the surfacers of both systems is due solely to the much higher abundance of barium sulfate present in the 4-layered system. Barium sulfate is an extender, which is used primarily to extend or stretch the primer surfacer layer further at a low cost.[201] Thus, the chemical difference between both surfacers is attributable to the fact that a large amount of barium sulfate was employed to extend the primer surfacer of the 4-layered system, so that the total thickness of the 4 and 6-layered systems are comparable. As a result, the subtle differences in the chemical composition of the two surfacers can directly be correlated with the number of layers in the paint system.

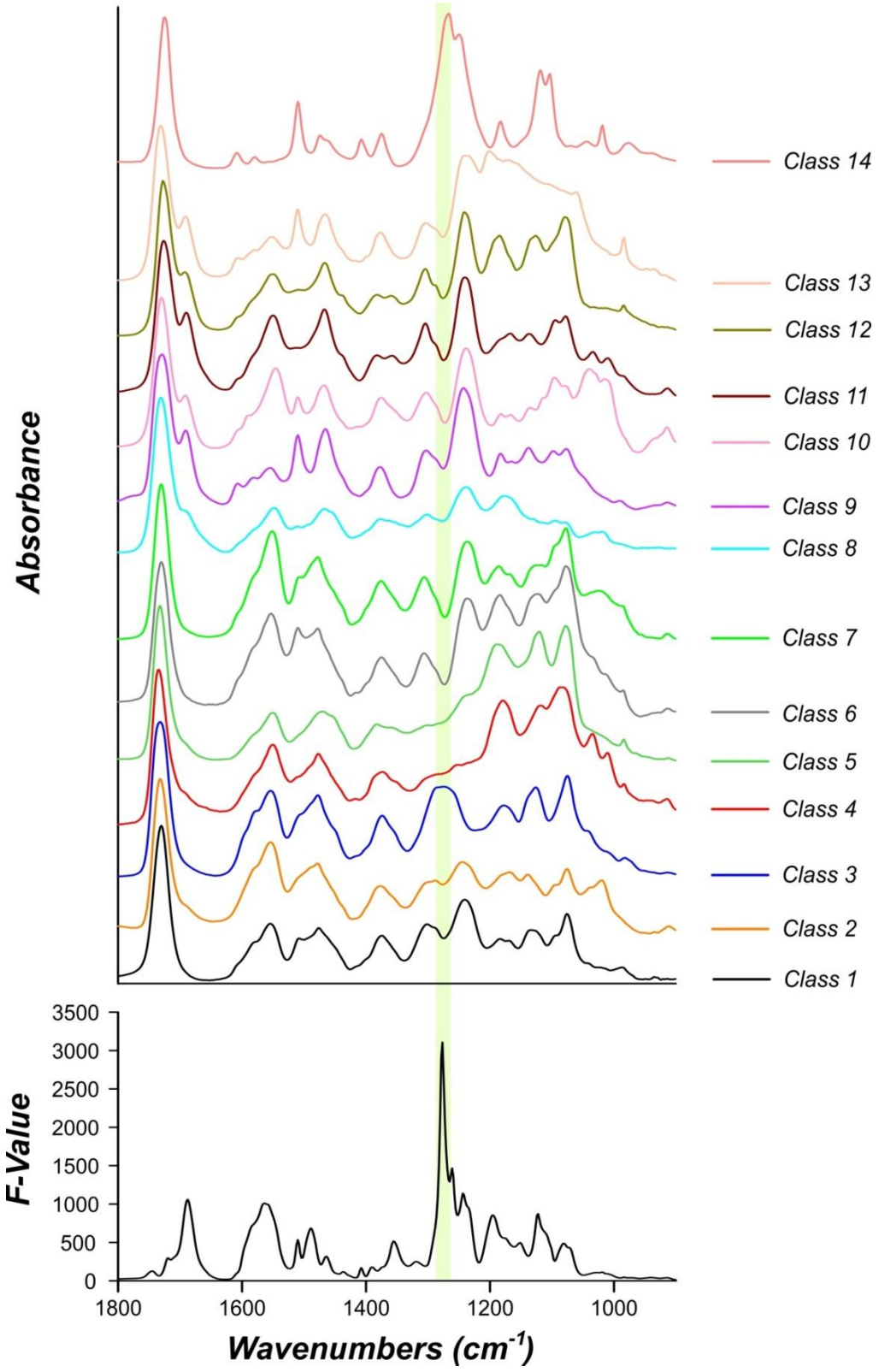

Figure 5.9: Representative IR spectra for all PCA groupings and Fisher ratio plot. Note the green region superimposed on the IR spectra which is indicative of a peak with a large F-value and thus highly significant in discriminating between the groupings.

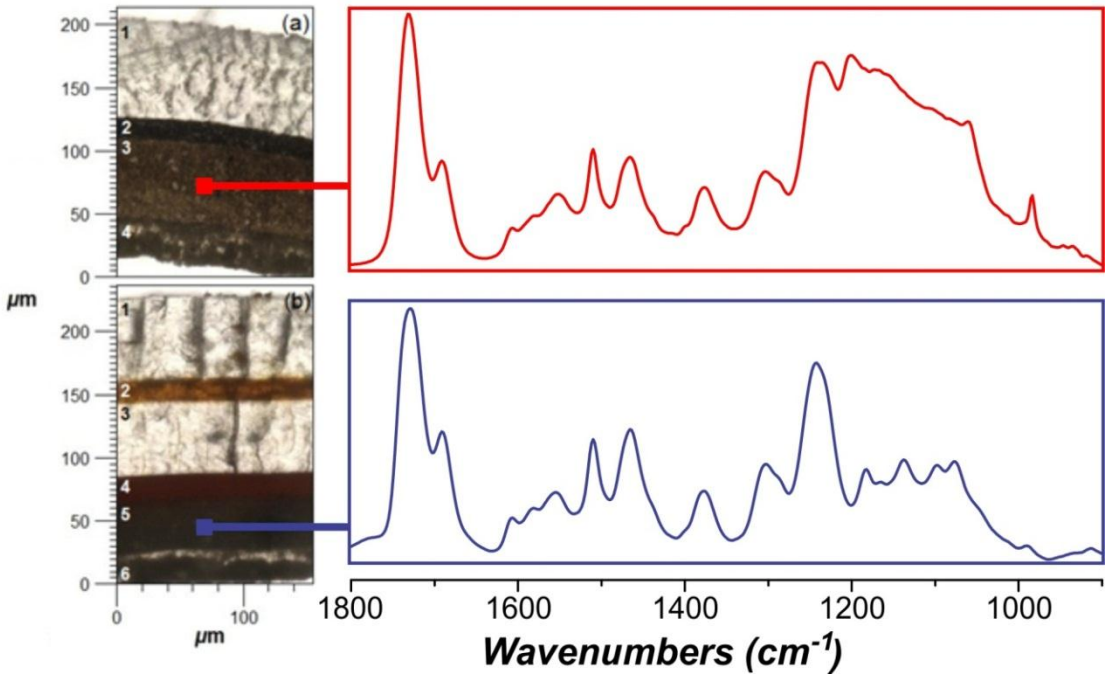

Figure 5.10: Synchrotron FT-IR spectra extracted from the primer surfacer of (a) sample from class 13 and (b) a sample from class 9.

Additionally, there are two groupings in the dataset representing samples obtained from Hyundai manufactured vehicles. Similarly, there is no observable pattern between the two sets of classes and the typical vehicle descriptors. However, once again, a trend is observed between the chemical compositions of the surfacers from the two sets of samples, as a function of the layer structure of the automotive paint samples. Specifically, the samples obtained from class 11 represent vehicles that contain an atypical monocoat system with no original manufacturer clear coat, whilst the samples from class 12 comprise the typical 4-layered scheme. As the 3-layered paint systems contain no original manufacturer clear coat the function of the primer surfacer in this particular instance is inherently more significant, as now the onus is primarily on the primer surfacer to prevent corrosion and protect the underlying metal body. Hence, it is not surprising that the chemical composition of the surfacer coating varies from 3-layered and 4-layered paint systems obtained from Hyundai vehicles. This finding ultimately reinforces the fact that different primer surfacers are tailored for specific applications.[202]

From a comparative standpoint, the model generated from the primer surfacer may potentially offer a number of advantages over the previously described clear coat model. Firstly, the primer surfacer model affords more specific information concerning the potential vehicle manufacturer, whilst the clear coat model may in some instances only provide general information regarding the origin of the vehicle. Secondly, the primer surfacer model employs chemical information which is not, or only minimally, impacted by deleterious effects of long-term environmental exposure. Although long-term continuous exposure (10 years or more) to the environmental conditions will likely impact on the clear coat model, it is less likely to affect the model generated from primer surfacers, as this layer is sandwiched between two other coatings and as such is not directly exposed to the environment. Ultimately, this minimises the risk of environmental degradation, enabling an accurate representation of the composition of the surfacer to be obtained from older or aged vehicles.

Whilst there are circumstances in which it will be beneficial to utilise one model over the other, the synergistic effect of both models enables more information to be obtained from questioned paint samples. Consider a situation whereby a questioned paint sample is characterised and based upon the composition of the surfacer the sample is grouped with the samples in class 7. In this scenario, the primer surfacer model is incapable of identifying the exact vehicle manufacturer, as it is unable to differentiate between samples obtained from Toyota and Honda vehicles. However, in this instance, the clear coat model described in Chapter 3 can be utilised in conjunction with the primer surfacer model to obtain specific vehicle manufacturer identification. This is because automotive clear coats from Japanese and Australian-made Toyota vehicles are grouped into class 3, whilst samples obtained from Thai-manufactured Toyota vehicles are classified into class 12 of the clear coat model. Therefore, by using both statistical models in tandem, more information concerning the questioned paint sample may be elucidated.

As mentioned previously, there are two groupings in the primer surfacer model representative of Australian-manufactured Holden vehicles (classes 3 and 10). Samples that grouped into class 3 signify vehicles manufactured post-2006, whereas samples in class 10 represent vehicles manufactured up until 2006. This relationship is significant as it enables the forensic examiner to deduce potential vehicle models, based upon sample groupings as well as pre-existing knowledge of when the specific manufacturer (i.e. Holden) ceased production on certain lines of vehicles. In this particular situation, samples in class 3 were obtained from Holden vehicles manufactured after 2006 and thus can only represent specific vehicle models manufactured after this period in time, as depicted in Figure 5.11. Conversely, samples in class 10 were obtained from Holden vehicles manufactured prior to 2006 and therefore can only represent specific models manufactured before this time period. For example, a sample obtained from either a first or second generation VE Commodore will be categorised into class 3, as this model was only commissioned for production in July 2006 (Figure 5.11). Likewise, primer surfacers characterised from the earlier Commodores (e.g. VX) will be classified into class 10, as Holden ceased production on these specific vehicles well before 2006.

As described in Chapter 3, a similar relationship was also observed with the Holden/HSV vehicles on the basis of the composition of the clear coat. However, in this situation a change in the composition of the clear coat was detected mid-2009; with samples from class 16 signifying vehicles manufactured prior to May/June of 2009, and samples from class 17 representing samples manufactured after this time period. Once again, the synergistic effect of the two models can be utilised to obtain more specific model information from a questioned paint sample obtained from an Australian-manufactured Holden/HSV vehicle, as depicted in Figure 5.11. For example, if a questioned paint sample obtained from a Holden vehicle is characterised and categorised into class 10 of the primer surfacer model and class 16 of the clear coat model, it can be inferred that the sample was obtained from a vehicle model manufactured prior to 2006.

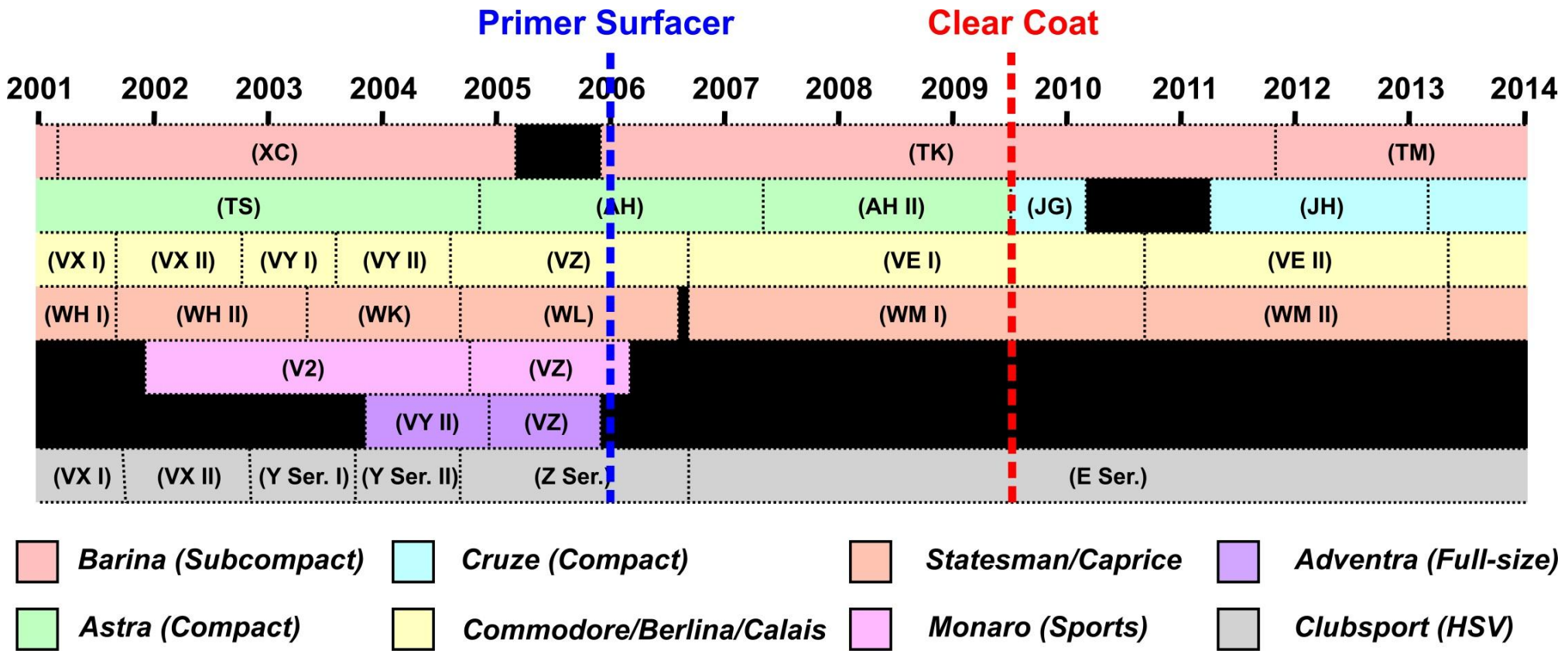

Figure 5.11: Timeline of select lines of Holden vehicles. The red dashed line denotes the distinction between classes 16 and 17 in the clear coat model, whilst the blue dashed line signifies the discrimination between samples contained in classes 3 and 10 of the primer surfacer model.

Similarly, if a questioned paint sample was categorised into class 3 and class 16 of the primer surfacer and clear coat model respectively, this would indicate that the vehicle was made between 2006 and mid-2009; thereby further limiting the potential vehicle types. Finally, if a paint sample was characterised and classified into class 3 of the primer surfacer and class 17 of the clear coat model, then it can be inferred with some degree of certainty that the vehicle was manufactured after 2009. Ultimately, this result reinforces the notion that the two models should be employed together, in order to extract the maximum amount of information from the sample in question.

5.4 Conclusions

A statistical model was developed using synchrotron FT-IR data obtained from the primer surfacer, and a pattern was discerned between the PCA groupings in the dataset as a function of vehicle manufacturer. No discernible variation was observed in the composition of the basecoat and electrocoat primer. However, from a forensic standpoint useful information may be acquired regarding a suspect vehicle from questioned paint samples by interrogating the primer surfacer. The statistical model generated from the primer surfacer offers a few advantages over the model generated from clear coats. Firstly, the primer surfacer model can afford specific information pertaining to the vehicle manufacturer, whilst in some situations the clear coat model can only provide more generalised information concerning vehicle origin. Additionally, whilst long-term environmental exposure (i.e. $\geq$ 10 years) is likely to impact the clear coat model, this is not much of an issue with the primer surfacer model, as this coating is routinely sandwiched between other layers and in essence shielded from the deleterious effects of the environment. Whilst there are benefits to only employing the model generated from the primer surfacers, the discriminatory power of the model is enhanced when used in combination with the ATR-based model.

The statistical model was defined from vehicles representing a range of Australian and international manufacturers. It is important to note that the international vehicles contained vehicle models only commonly exported to Australia. As a result, this statistical model can only be utilised in an Australian context. However, other jurisdictions could utilise the same methodology as long as statistically significant datasets were generated. Furthermore, due to limitations involving beam-time at the Australian Synchrotron, the following model was not as well-defined as the clear coat model and as such LDA was not conducted on the dataset. Whilst the PCA groupings are distinct, the numbers of samples in the groupings are small, making it difficult to perform test set validation on the dataset. Thus, a larger number of samples need to be characterised in order to better define the model, such that LDA can be performed and an estimation of the predicative performance of the model can be obtained.

Chapter 6: Characterisation and classification of automotive clear coats with Raman spectroscopy and chemometrics

6.1 Introduction

Raman spectroscopy has enormous potential for the forensic analysis of paints, owing to its ability to characterise both the organic and inorganic components of the paint system at a very high spatial resolution and with minimal sample preparation.[34, 101] Whilst Raman spectroscopy has been extensively applied to the examination of artistic paints (e.g. in instances of art forgery),[203-210] there is less published work in the literature using this technique to characterise architectural[99, 100, 211, 212] and automotive[102, 213-219] paints, which are commonly encountered in forensic casework. Furthermore, of the handful of studies that employed Raman spectroscopy to examine automotive paint systems, the majority have used the technique solely to characterise the organic and inorganic pigments in the basecoat, or the fillers and extenders in the primer surfacer.[102, 213, 215-219]

From a forensic science standpoint, there is only one study in the open literature that has employed Raman spectroscopy to chemically interrogate automotive clear coats. De Gelder and co-workers[214] used Raman spectroscopy to characterise all of the layers, including the clear coat, in automotive paint cross-sections. The authors discovered that although reproducible spectra could be obtained from clear coats, the basecoat of the paint system provided the best spectra with which to discriminate between paint samples.[214] Due to the paucity of research in the literature and because IR and Raman spectroscopy are complementary techniques, this chapter will explore the potential of Raman spectroscopy for the characterisation of a large population of automotive clear coats with subsequent chemometric analysis to interpret the resultant data. This statistical model can then be compared to the equivalent model generated from ATR data (Chapter 3), in order to determine which vibrational spectroscopic technique is better suited to this application.

6.2 Experimental

Automotive paint exemplars were obtained as previously described in section 2.1.

6.2.1 Raman Spectroscopy

Raman spectra were acquired with a Bruker RFS 100 FT-Raman spectrometer (Bruker Optik GmbH, Ettlingen, Germany) equipped with a liquid-nitrogen cooled, high sensitivity germanium diode detector. A near-IR Nd:YAG continuous wave laser, operating with an excitation wavelength of 1064 nm and with a maximum power of 800 mW, was used to characterise the clear coats. Analysis of the clear coat layer was achieved by employing a scalpel to obtain thin shavings of the coating, which were then tightly packed into a stainless steel sample cup (Figure 6.1). Extreme care was taken to ensure that the shavings were obtained from the outer surface of the clear coat, such that the shavings were unaffected by chemical component migration (section 4.3.1) and thus truly representative of the composition of the coating. Five spectra were collected from each sample using 180 ° back-scattering sampling mode at a focal position of 0.0 mm, over a range of 3600-75 cm^{-1} (Stokes shift), with a spectral resolution of 4 cm^{-1}, and 1024 accumulated scans (~ 30 min).

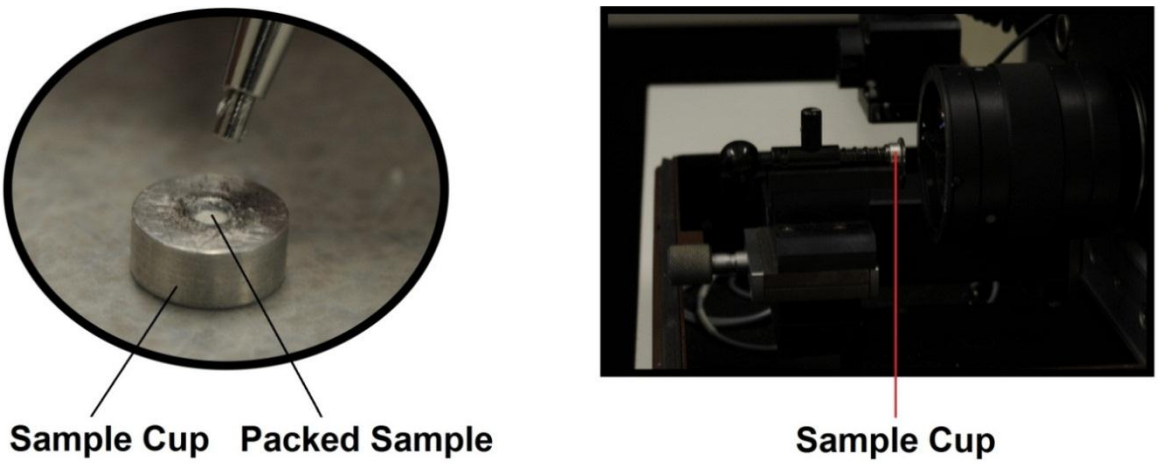

Figure 6.1: (Left) Tightly packed clear coat shavings in a stainless steel sample cup; (Right) Sample mounted into the sampling compartment setup for 180 ° back-scattering geometry in a FT-Raman spectrometer.

6.2.2 Chemometrics

All spectra were collated into a single matrix dataset and were pre-processed according to section 2.5. The dataset was then truncated between 1800 and 600 cm^{-1}, as no significant information was observed outside of this spectral range. PCA and LDA were then conducted on the dataset as described in Section 2.5.1 and 2.5.2 respectively.

6.3 Results & Discussion

6.3.1 Principal Component Analysis

A dispersive Raman spectrometer equipped with visible lasers (e.g. 514 nm and 633 nm) was initially utilised to chemically interrogate the automotive clear coats. Unfortunately, high levels of fluorescence were observed in the spectra that masked the Raman bands and this fluorescence interference was not able to be overcome by changing the excitation wavelength and laser power. Consequently, FT-Raman spectroscopy with a near-IR laser (1064 nm) was employed in this situation. This technique offers a significant advantage over dispersive Raman spectrometers that employ visible excitation, in that it is able to overcome the issue of fluorescence in materials by using an IR excitation source.[220-222]

PCA performed on the Raman spectral dataset (695 spectra) revealed that 96.7 % of the total variance in the dataset was accounted for by the first five PCs, as seen below in Figure 6.2. Based upon Figure 6.2, it can be clearly seen that as many as five PCs could be employed to reconstruct and model the data. Whilst the first three PCs (93.6 %) may be capable of adequately describing the data, additional PCs also need to be evaluated, as the spectral variation may be quite subtle.

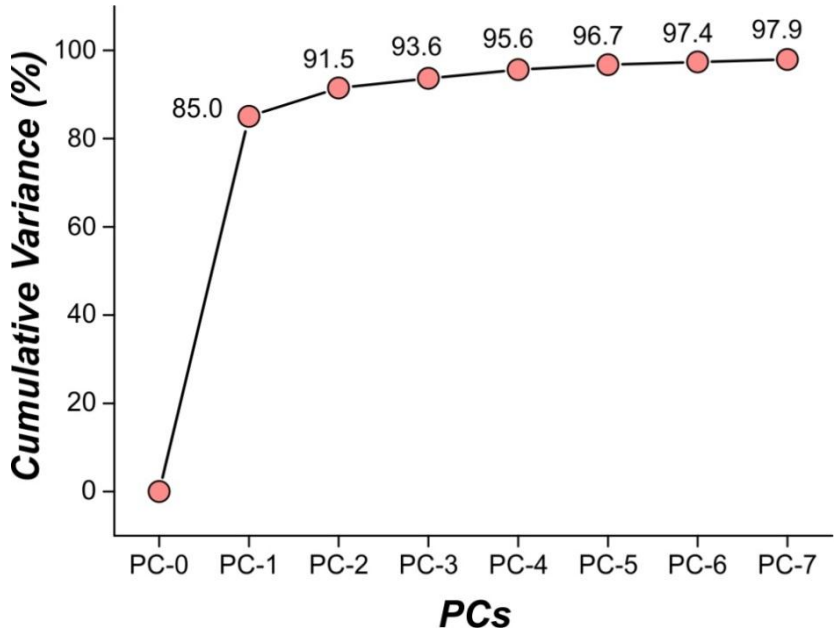

Figure 6.2: Scree plot detailing the variance in the dataset explained by each PC.

A 3-dimensional scores plot generated using the first three PCs indicated that there visually appear to be 19 groupings in the dataset (Figure 6.3). Scores plots were also created from a number of combinations of the first five PCs, in order to examine the influence of PC4 and PC5. The fourth and fifth PCs were determined to afford no additional discrimination between samples, thereby justifying the use of only three PCs. The scores plot depicted in Figure 6.3 illustrates the separation of the data into 19 groupings, with the discrimination between sample groupings being attributable to common vehicle descriptors; including vehicle origin, manufacturer, specific models, year of manufacture, and in some instances the manufacturing plant where the vehicle was assembled. A comprehensive summary of the samples that comprise each grouping in the dataset is provided below in Table 6.1.

Table 6.1: Summary of the samples contained within each grouping following PCA of the Raman spectral dataset.

Class No.	No. Samples	Vehicles Represented
Class 1	8	US (Dodge/Jeep)
Class 2	2	Mexico (Dodge)
Class 3	6	Japan (Subaru/Nissan)
Class 4	2	Germany (Ford Mondeo)
Class 5	3	South Korea (Holden); Japan (Mitsubishi Colt)
Class 6	3	BMW
Class 7	12	Japan (Mazda/Mitsubishi Lancer/Toyota)
Class 8	4	Australia (Toyota)
Class 9	9	Japan (Mazda/Toyota)
Class 10	4	Mitsubishi Pajero
Class 11	2	SsangYong
Class 12	13	Thailand (Nissan/Toyota); Honda; Suzuki
Class 13	5	Hyundai
Class 14	3	Sweden (Saab); UK (Jaguar)
Class 15	5	Australia (Holden/HSV) [2001-2004]
Class 16	6	Germany (Ford Focus)
Class 17	29	Australia (Holden/HSV) [2009-Present]
Class 18	10	Australia (Holden/HSV) [2004-2009]
Class 19	13	Australia (Ford); Spain (Nissan)

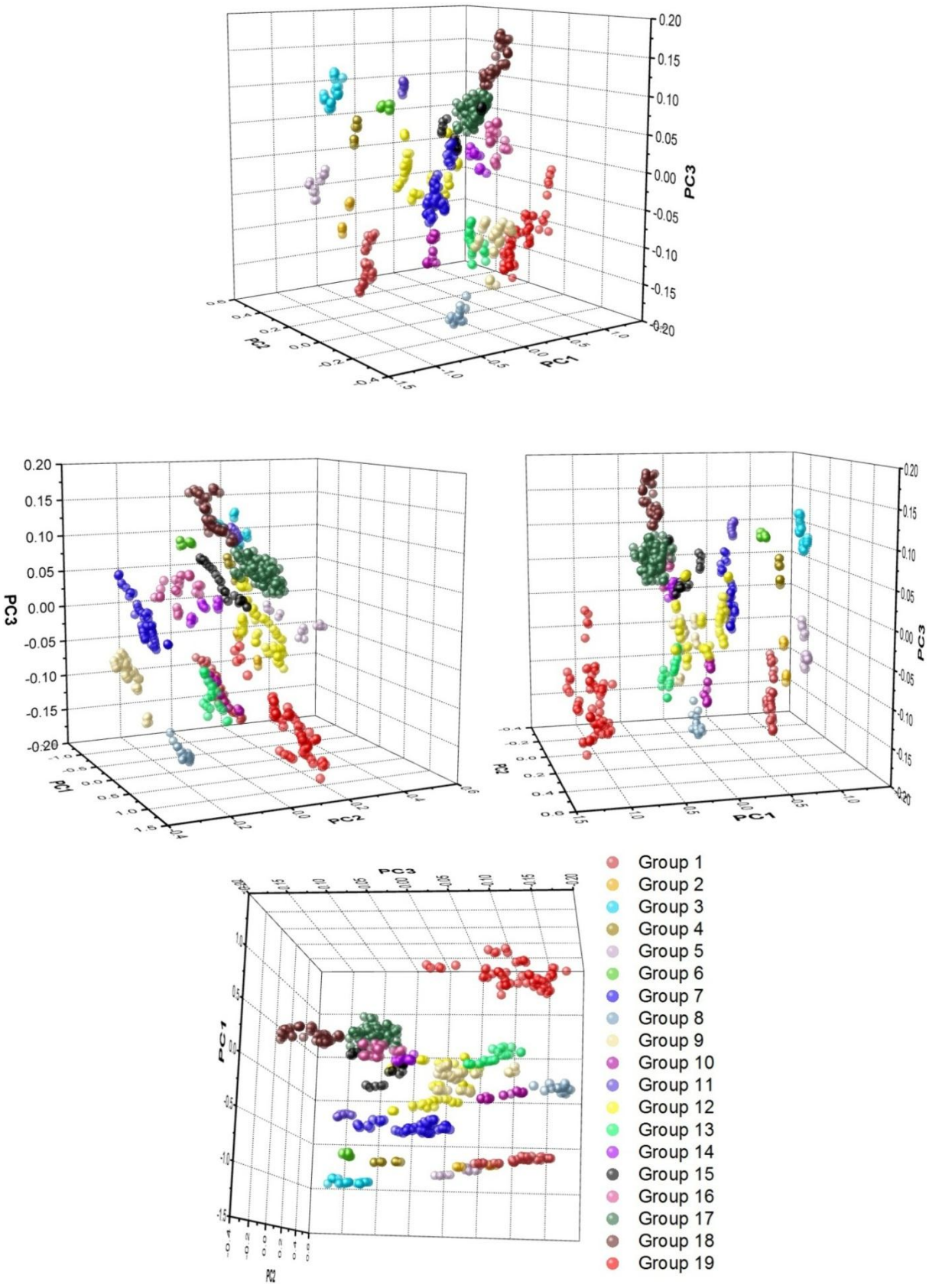

Figure 6.3: A number of different perspectives of a 3-dimensional PCA scores plot depicting the distribution of samples based upon their resultant Raman spectra.

Whilst there are groupings common to both the ATR-based clear coat model (described in Chapter 3) and the corresponding model produced from Raman spectra, there are also noticeable differences in the number of groupings between both statistical models (Table 6.2). The statistical model generated from IR data obtained from automotive clear coats was only able to visually discern 17 groupings; whereas PCA performed on the Raman data obtained from the same sample collection enabled 19 groupings to be visualised. Groupings common to both statistical models include the samples obtained from the US-manufactured Dodge and Jeep, Mexican-made Dodge, German-manufactured Ford Mondeo, BMW, Mitsubishi Pajero, SsangYong, Hyundai, German-manufactured Ford Focus, and the post-2009 Australian-made Holden/HSV vehicles (Table 6.2). Furthermore, the vehicles represented in classes 3 and 5 of the Raman statistical model are almost identical to classes 6 and 9 of the ATR-based model, with the sole difference relating to the grouping of the lone Mitsubishi Colt vehicle (Table 6.2).

This is not a major issue as it is anticipated that as the model becomes more defined, individual groupings may begin to emerge that represent these singular vehicles in the dataset. Similarly, groupings 12 and 14 in the Raman model principally contain the same samples as classes 11 and 12 in the ATR-based model. The only difference in the arrangement of samples within these groupings is attributable to the samples obtained from the Polish-manufactured Honda vehicles, which are grouped together with the other European vehicles in the ATR model (class 11). However, in the Raman model these samples are instead projected into class 12, alongside the samples obtained from the Thai-manufactured utility, Honda and Suzuki vehicles.

Table 6.2: Comparison of the grouping structure of the ATR-based model described in Chapter 3 and the equivalent model generated from Raman data.

ATR		Raman	
Class 1	US (Dodge/Jeep)	***Class 1***	US (Dodge/Jeep)
Class 2	BMW	***Class 6***	BMW
Class 3	Japan (Mazda/Mitsubishi Lancer); Australia/Japan (Toyota)	***Class 7***	Japan (Mazda/Toyota/Mitsubishi Lancer)
		Class 8	Australia (Toyota)
		Class 9	Japan (Mazda/Toyota)
Class 4	Mitsubishi Pajero	***Class 10***	Mitsubishi Pajero
Class 5	Mexico (Dodge)	***Class 2***	Mexico (Dodge)
Class 6	Japan (Subaru/Nissan/**Mitsubishi Colt**)	***Class 3***	Japan (Subaru/Nissan)
Class 7	Germany (Ford Mondeo)	***Class 4***	Germany (Ford Mondeo)
Class 8	Hyundai	***Class 13***	Hyundai
Class 9	South Korea (Holden)	***Class 5***	South Korea (Holden); **Mitsubishi Colt**
Class 10	Germany (Ford Focus)	***Class 16***	Germany (Ford Focus)
Class 11	**Poland (Honda)**; Sweden (Saab); UK (Jaguar)	***Class 14***	Sweden (Saab); UK (Jaguar)
Class 12	Thailand (Nissan/Toyota); Japan (Honda/Suzuki)	***Class 12***	Thailand (Nissan/Toyota); **Honda**; Suzuki
Class 13	SsangYong	***Class 11***	SsangYong
Class 14	Australia (Ford) [2004-2009]	***Class 19***	Australia (Ford); Spain (Nissan)
Class 15	Australia (Ford) [2009-present]; Spain (Nissan)		
Class 16	Australia (Holden/HSV) [2001-2009]	***Class 15***	Australia (Holden/HSV) [2001-2004]
		Class 18	Australia (Holden/HSV) [2004-2009]
Class 17	Australia (Holden/HSV) [2009-present]	***Class 17***	Australia (Holden/HSV) [2009-present]

The main differences between the two statistical models can be predominantly attributed to additional groupings in the Raman model that were formed following subdivision of select groupings within the ATR model (Table 6.2). For example, there is a singular grouping in the ATR-based model representing Australian-made Holden vehicles manufactured prior to 2009 (class 16). However, in the statistical

model generated from the Raman data, these same samples are distributed over two groups; with the samples representing Holden/HSV vehicles assembled prior to 2004 in class 15 and the samples signifying Holden/HSV vehicles manufactured between 2004 and 2009 contained within class 18. The significance of this result will be discussed in detail later. Similarly, there is only one grouping in the ATR model representing Toyota, Mazda, and Mitsubishi Lancer vehicles (class 3); however the samples in this grouping were distributed into three distinct groupings in the Raman model (classes 7-9). Class 7 contained samples obtained from Japanese-manufactured Mazda and Toyota vehicles, as well as the Mitsubishi Lancer vehicles. Likewise, the samples in class 9 also represented specific Japanese-manufactured Mazda and Toyota vehicles. Whilst the discrimination between these two groupings is evident, no discernible correlation could be made between the samples in the groupings and the vehicle descriptors (i.e. vehicle model and type, year, manufacturing plant and platform). Class 8 consists of samples obtained solely from Toyota vehicles manufactured at the Altona plant in Australia. Consequently, the Raman model is capable of discriminating between Toyota vehicles manufactured in Japan and Australia, thus enabling increased discrimination between samples over the analogous IR model. Conversely, it is important to note that only one grouping was visually discerned in the Raman model representing Australian-manufactured Ford and Spanish-manufactured Nissan vehicles (class 19). However, these samples were distributed over two groupings in the ATR-based model (classes 14 & 15).

In spite of this, based upon the number of groupings it can be concluded that the stand-alone Raman model is more discriminating than the corresponding IR model. By examining the Raman spectra obtained from the centroids of each grouping as depicted in Figure 6.4, it can be observed that the Raman vibrational bands tend to be sharper than the equivalent IR bands. This narrow spectral line width in the Raman spectra not only enables the assignment of the band frequency to be more accurate and precise, but also ensures minimal band overlap comparative to IR spectra (Table 6.3).[222-224] These advantageous features of Raman spectra could account for the increased discrimination observed between samples.

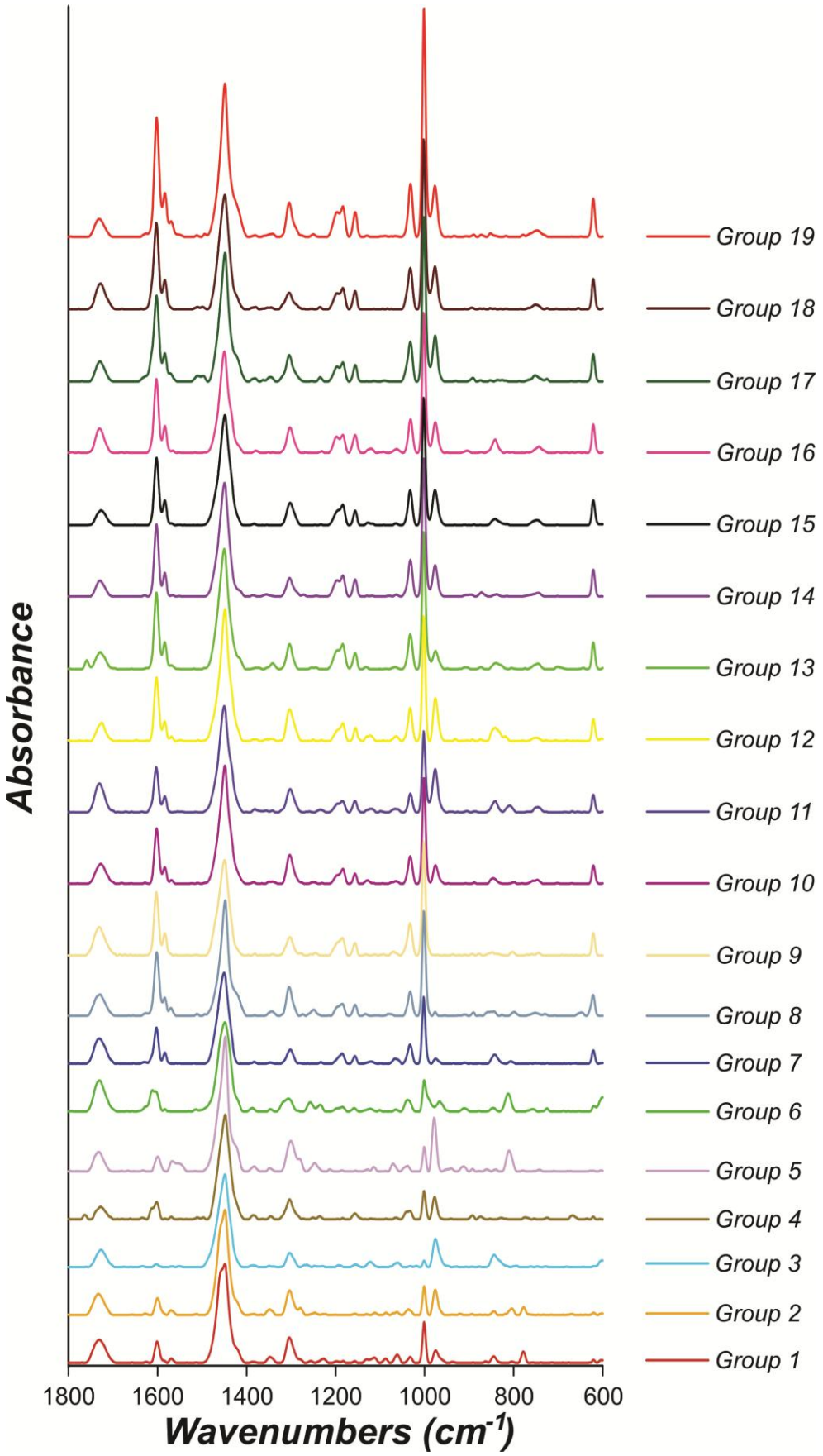

Figure 6.4: Raman spectra obtained from the centroid of each grouping.

Table 6.3: Raman frequencies (cm^{-1}) for the centroid spectra of each grouping. Note: s – strong, m – moderate, w – weak.

Class	Raman Wavenumber (cm^{-1})
Class 1	1732 (m), 1624 (w), 1601 (m), 1570 (w), 1449 (s), 1384 (w), 1349 (w), 1304 (m), 1254 (w), 1230 (w), 1157 (w), 1113 (w), 1088 (w), 1061 (w), 1032 (w), 1001 (m), 975 (w), 845 (w), 778 (w), 620 (w), 601 (w)
Class 2	1732 (m), 1625 (w), 1600 (m), 1570 (w), 1449 (s), 1385 (w), 1349 (w), 1303 (m), 1279 (w), 1249 (w), 1129 (w), 1111 (w), 1086 (w), 1063 (w), 1038 (w), 1001 (m), 976 (m), 845 (w), 804 (w), 778 (w), 620 (w), 601 (w)
Class 3	1727 (m), 1601 (w), 1567 (w), 1449 (s), 1385 (w), 1350 (w), 1303 (m), 1264 (w), 1194 (w), 1154 (w), 1122 (w), 1063 (w), 1001 (w), 976 (m), 844 (m), 600 (w)
Class 4	1762 (w), 1728 (m), 1602 (m), 1569 (w), 1496 (w), 1448 (s), 1384 (w), 1364 (w), 1348 (w), 1303 (m), 1251 (w), 1238 (w), 1156 (w), 1034 (w), 1001 (m), 978 (m), 892 (w), 875 (w), 830 (w), 775 (w), 725 (w), 668 (w), 620 (w)
Class 5	1732 (m), 1600 (m), 1567 (m), 1448 (s), 1385 (m), 1350 (w), 1301 (m), 1247 (w), 1214 (w), 1114 (w), 1070 (w), 1040 (w), 1001 (m), 979 (s), 915 (w), 895 (w), 859 (w), 841 (w), 811 (m)
Class 6	1730 (m), 1612 (m), 1604 (m), 1585 (w), 1449 (s), 1388 (w), 1346 (w), 1305 (m), 1257 (w), 1236 (w), 1185 (w), 1158 (w), 1122 (w), 1103 (w), 1063 (w), 1039 (w), 1001 (m), 966 (m), 912 (w), 845 (w), 813 (m), 757 (w), 725 (w), 619 (w), 601 (m)
Class 7	1729 (m), 1626 (w), 1603 (m), 1584 (m), 1451 (s), 1385 (w), 1346 (w), 1301 (m), 1238 (w), 1185 (w), 1157 (w), 1120 (w), 1065 (w), 1033 (m), 1002 (s), 975 (w), 843 (w), 804 (w), 621 (w)
Class 8	1730 (m), 1602 (s), 1584 (m), 1571 (m), 1512 (w), 1448 (s), 1344 (w), 1304 (m), 1274 (w), 1250 (w), 1185 (m), 1156 (w), 1081 (w), 1032 (m), 1002 (s), 977 (w), 891 (w), 849 (w), 799 (w), 752 (w), 732 (w), 648 (w), 621 (m)
Class 9	1730 (m), 1603 (s), 1584 (m), 1450 (s), 1342 (w), 1303 (m), 1248 (w), 1185 (w), 1157 (w), 1070 (w), 1033 (m), 1002 (s), 851 (w), 804 (w), 751 (w), 621 (m)
Class 10	1727 (m), 1625 (w), 1602 (s), 1584 (m), 1570 (w), 1449 (s), 1386 (w), 1303 (m), 1254 (w), 1184 (w), 1156 (w), 1129 (w), 1032 (m), 1002 (s), 976 (m), 844 (w), 803 (w), 751 (w), 621 (w)
Class 11	1730 (m), 1603 (m), 1584 (m), 1450 (s), 1380 (w), 1358 (w), 1302 (m), 1260 (w), 1234 (w), 1184 (w), 1157 (w), 1121 (w), 1065 (w), 1002 (s), 976 (m), 841 (w), 811 (w), 745 (w), 621 (w)
Class 12	1726 (m), 1602 (m), 1584 (m), 1569 (w), 1449 (s), 1382 (w), 1351 (w), 1303 (m), 1230 (w), 1184 (w), 1156 (w), 1126 (w), 1064 (w), 1032 (m), 1002 (s), 976 (m), 872 (w), 842 (w), 750 (w), 621 (m), 602 (w)
Class 13	1758 (w), 1729 (m), 1602 (s), 1584 (m), 1569 (w), 1450 (s), 1379 (w), 1341 (w), 1304 (m), 1257 (w), 1184 (m), 1156 (w), 1065 (w), 1032 (m), 1002 (s), 977 (m), 909 (w), 872 (w), 840 (w), 804 (w), 746 (w), 699 (w), 621 (m)
Class 14	1729 (m), 1602 (s), 1584 (m), 1450 (s), 1383 (w), 1355 (w), 1303 (m), 1196 (m), 1184 (m), 1156 (m), 1064 (w), 1032 (m), 1002 (s), 977 (m), 896 (w), 872 (w), 838 (w), 748 (w), 621 (m), 602 (w)
Class 15	1726 (m), 1602 (s), 1584 (m), 1449 (s), 1381 (w), 1355 (w), 1302 (m), 1184 (m), 1156 (w), 1126 (w), 1065 (w), 1032 (m), 1002 (s), 977 (m), 842 (w), 749 (w), 621 (m), 602 (w)
Class 16	1730 (m), 1603 (s), 1584 (m), 1450 (s), 1377 (w), 1353 (w), 1303 (m), 1198 (m), 1184 (m), 1156 (m), 1119 (w), 1088 (w), 1066 (w), 1032 (m), 1002 (s), 976 (m), 903 (w), 842 (w), 744 (w), 621 (m)
Class 17	1729 (m), 1602 (s), 1584 (m), 1496 (w), 1449 (s), 1383 (w), 1348 (w), 1304 (m), 1258 (w), 1236 (w), 1196 (m), 1184 (m), 1156 (m), 1032 (m), 1002 (s), 977 (m), 892 (w), 851 (w), 837 (w), 827 (w), 751 (w), 621 (m)
Class 18	1728 (m), 1603 (s), 1584 (m), 1496 (w), 1449 (s), 1380 (w), 1348 (w), 1304 (m), 1195 (m), 1184 (m), 1156 (m), 1032 (m), 1002 (s), 977 (m), 894 (w), 750 (w), 621 (m)
Class 19	1731 (m), 1602 (s), 1584 (m), 1569 (m), 1509 (w), 1449 (s), 1384 (w), 1342 (w), 1305 (m), 1252 (w), 1196 (m), 1184 (m), 1156 (m), 1032 (m), 1001 (s), 977 (m), 890 (w), 873 (w), 852 (w), 752 (w), 621 (m)

Moreover, because vibrations of polymer backbones typically do not generate significant changes in the dipole moment, but rather create drastic changes in polarisability, Raman spectroscopy is usually more amenable to the analysis of polymeric coatings such as automotive clear coats.[179, 225] As depicted in Figure 6.4 and displayed in Table 6.3, all automotive clear coats tend to be composed of the same chemical components (i.e. acrylic, melamine, styrene and polyurethane), with variations in the spectra arising from differences in the relative abundance of these constituents in the system.

The factor loadings for the first three PCs were examined to identify spectral regions responsible for the discrimination of samples on the scores plot. The loadings plot for PC1, shown below in Figure 6.5, revealed two peaks of significant positive correlation *ca.* 1602 and 1002 cm^{-1}. The peak at approximately 1602 cm^{-1} is part of a doublet of bands indicative of ring stretching attributable to styrene.[214, 226] Similarly, the intense, sharp peak at roughly 1002 cm^{-1} is characteristic for trigonal ring breathing also ascribable to styrene.[214, 226] Consequently, the discrimination between samples on PC1 is primarily attributable to the abundance of styrene in the clear coat. For example, samples in classes 1-6, as can be seen from Figure 6.5, have a relatively low abundance of styrene in the clear coat and thus attain significant negative scores on PC1. Conversely, samples obtained from the Australian manufactured-Ford and Spanish-made Nissan vehicles of class 19, have comparatively larger intensities of these peaks than the other samples and subsequently have larger positive scores on PC1.

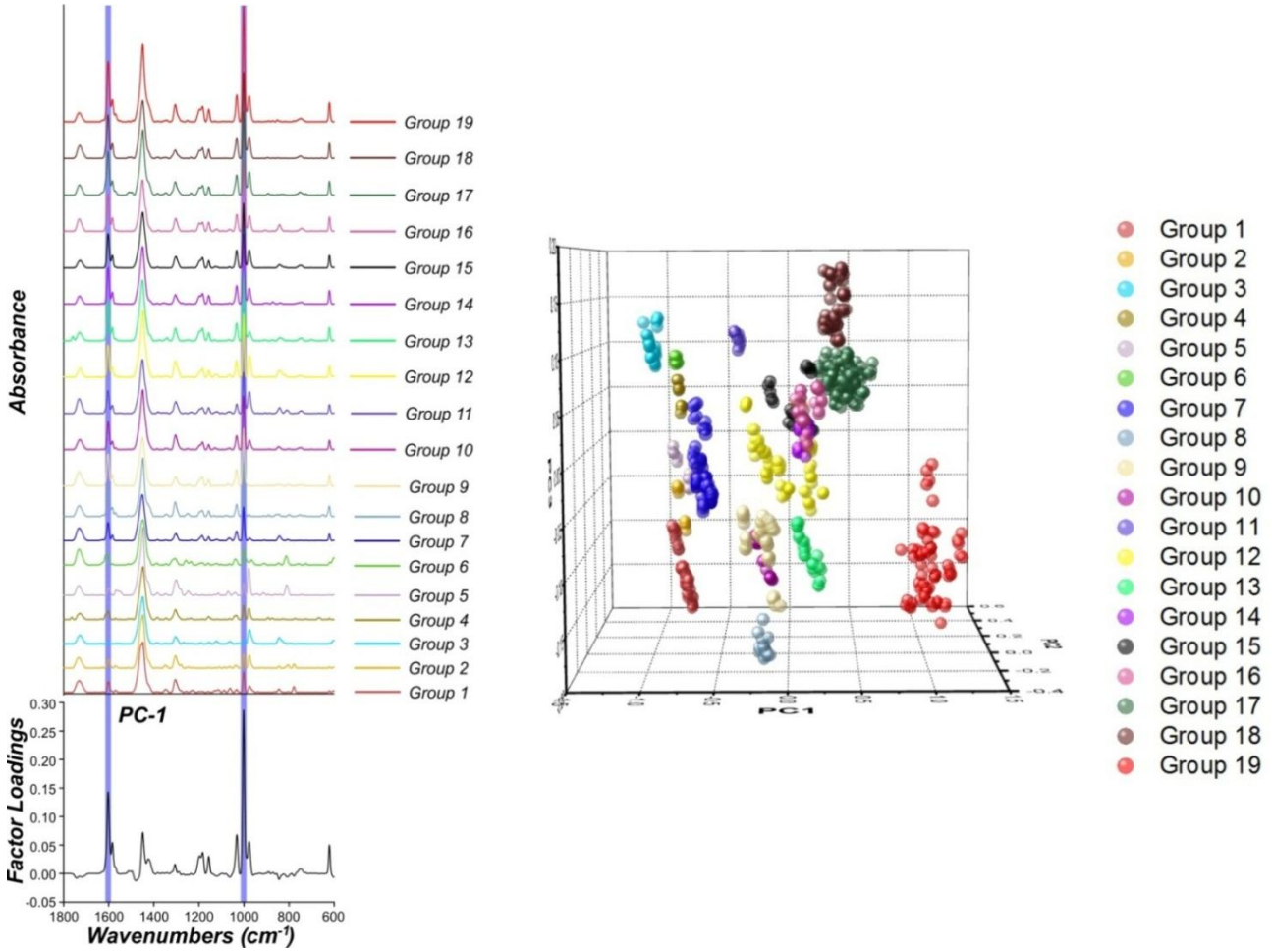

Figure 6.5: Factor loadings plot for PC1. The blue regions superimposed on the representative Raman spectra for each grouping, denote spectral regions significantly positively correlated with PC1.

The loadings plot for PC2, depicted in Figure 6.6, revealed regions of positive correlation *ca.* 1447 cm^{-1}, 1425 cm^{-1} and 977 cm^{-1}. Additionally, there was also a peak of significant negative correlation at approximately 1004 cm^{-1}, which denotes a slight band shift in the peak indicative of trigonal ring breathing characteristic of styrene. This signifies that PC2 is accounting for a subtle variation in the wavenumber shift of the styrene peak, suggesting a slight modification to the styrene binder, presumably due to the chemical component it is linking or polymerising with. The large positive loading at approximately 1447 cm^{-1} signifies CH_3 and CH_2 deformations that may be attributed to the acrylic backbone.[214, 226] Similarly, the positive loading at 1425 cm^{-1}, which corresponds to a shoulder on the main acrylic peak at 1447 cm^{-1}, is indicative of the methylene ($=CH_2$) deformation vibration also characteristic for certain acrylic polymers.[179] Finally, the significant positive loading at approximately 977 cm^{-1} signifies the triazine ring breathing of the melamine cross-linking agent.[214, 226] Consequently, samples are differentiated on PC2 based upon the presence and intensity of acrylic peaks at 1447 cm^{-1} and 1425 cm^{-1} and the melamine peak at 977 cm^{-1}, in addition to a slight band shift variation of the main diagnostic peak for styrene. For example, samples that attain large positive scores on PC2 (e.g. class 5) have relatively large intensities of peaks at 1447 cm^{-1}, 1425 cm^{-1} and 977 cm^{-1}, including no band shift in the styrene peak. Conversely, samples with large negative scores on PC2 (e.g. class 9) have relatively low intensities of the acrylic (1447 cm^{-1} and 1425 cm^{-1}) and melamine (977 cm^{-1}) peaks and or a large intensity of the band-shifted styrene peak (1004 cm^{-1}).

The factor loadings for PC3, depicted below in Figure 6.7, revealed peaks of significant positive correlation at 1613 cm^{-1} and 977 cm^{-1}, in addition to regions of large negative correlation at 1449 cm^{-1} and 1305 cm^{-1}. The large negative loadings at 1449 cm^{-1} and 1305 cm^{-1} can be assigned to the CH_3 and CH_2 deformations, and CH_2 in-phase twisting vibrations of the acrylic component respectively.[214, 226] Interestingly, the negative loading *ca.*1449 cm^{-1} represents a slight band shift in the acrylic peak, most likely inferring variation in the acrylic co-polymer utilised to form the backbone. As described previously, the large positive loading at approximately 977 cm^{-1} is indicative of triazine ring breathing of melamine.[214, 226]

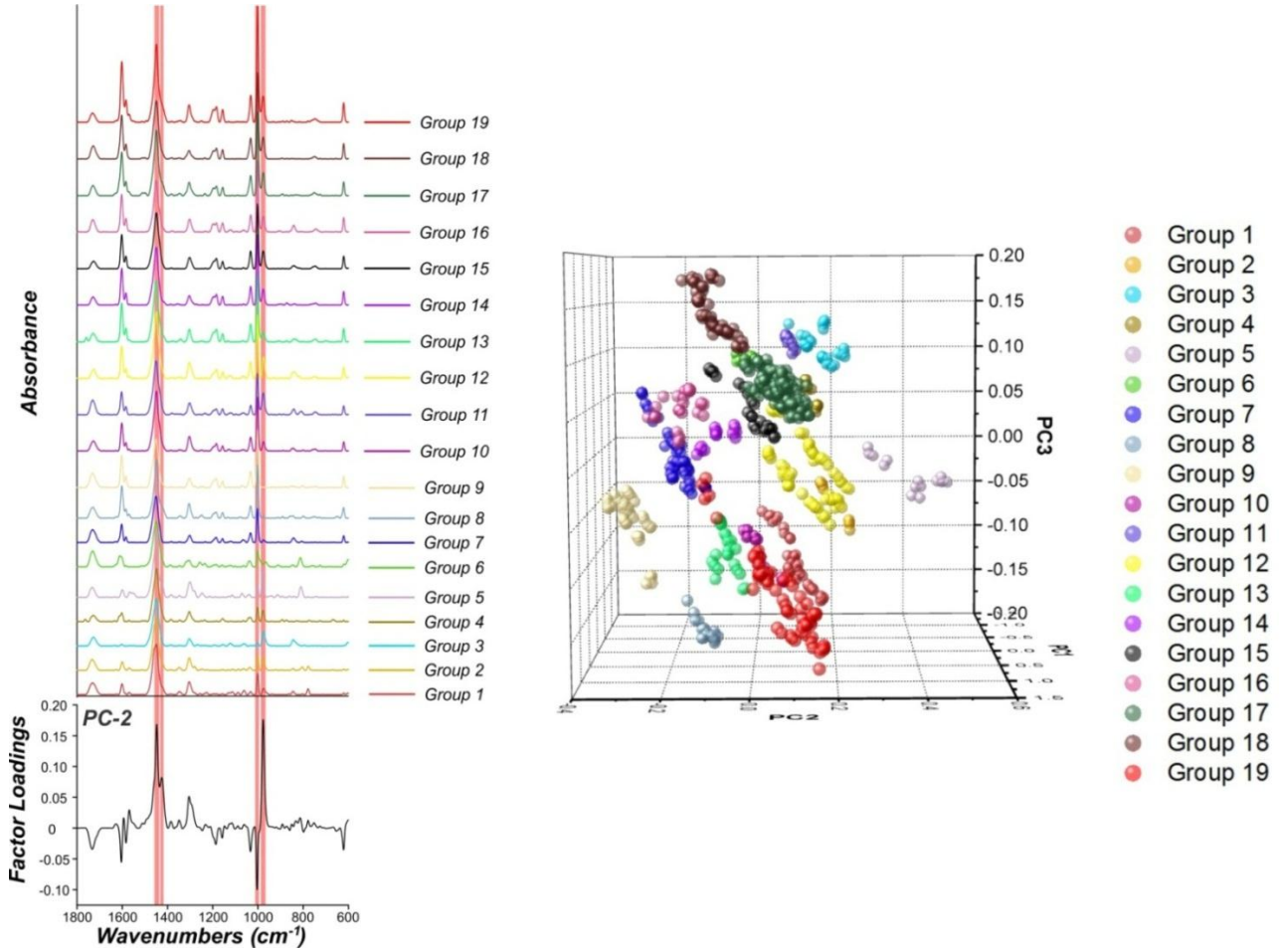

Figure 6.6: Factor loadings plot for PC2. The red zones overlaid on the Raman spectra obtained from each class centroid, signify regions of substantial correlation with PC2.

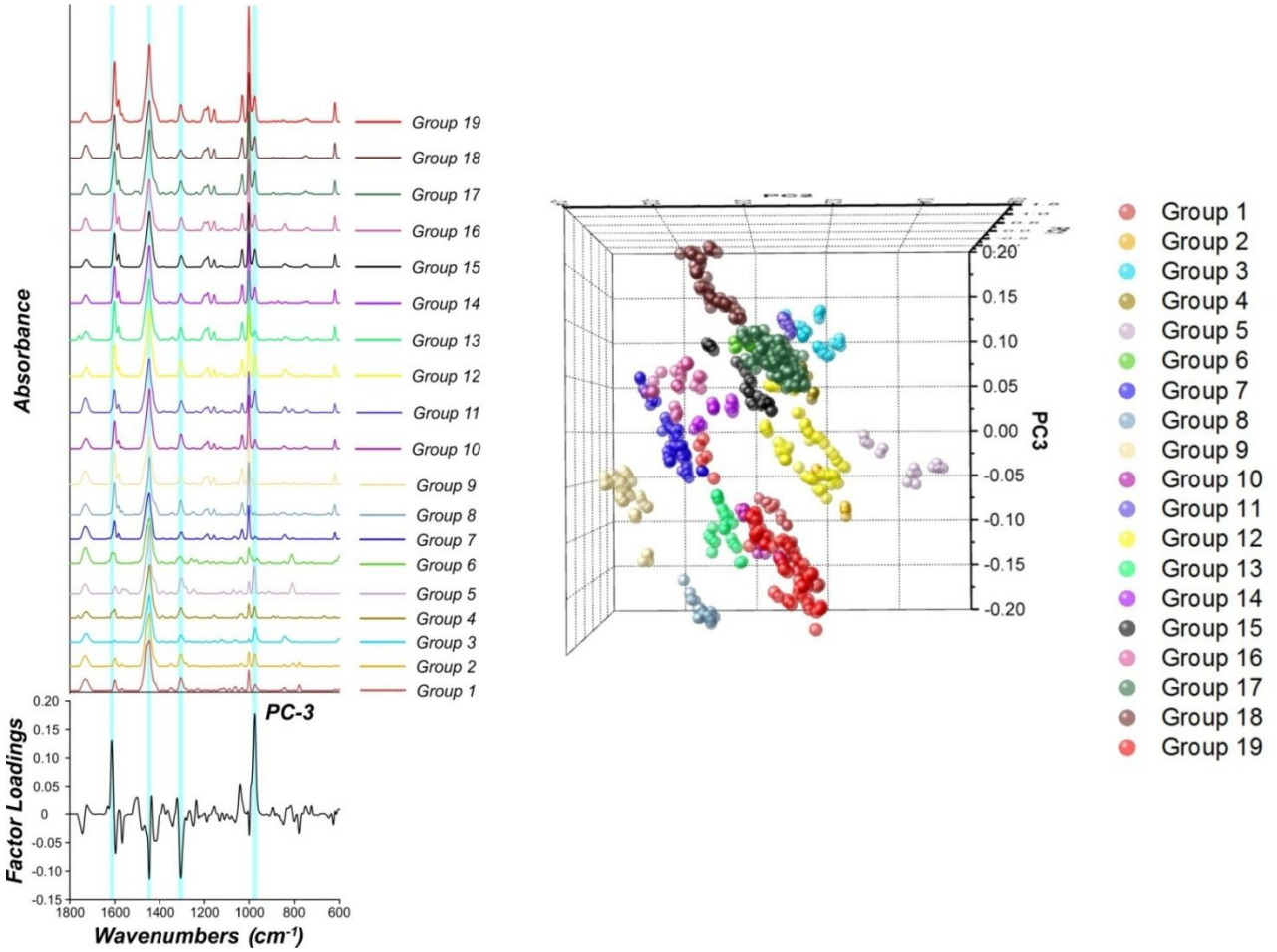

Figure 6.7: Factor loadings plot for PC3. The light blue regions superimposed on the representative Raman spectra of each PCA grouping, denote spectral regions significantly correlated with PC3.

Finally, the large positive loading at approximately 1613 cm^{-1} corresponds to a shoulder on the larger doublet peak *ca.*1602 cm^{-1} that was previously assigned to the quadrant ring stretching of styrene. This shoulder can also be attributed to ring stretching of aromatics, most likely from modifications to the styrene binder or from other aromatic additives (e.g. xylene and methylbenzenes).[226] Therefore, separation of samples on PC3 is achieved based upon the relative intensities of peaks characteristic for the cross-linking agent melamine, acrylic and styrene binder. For example, samples from classes 8 or 19 attain large negative scores on PC3, based upon the relatively more intense peaks *ca.* 1449 cm^{-1} and 1305 cm^{-1}, signifying either a larger abundance or a specific combination of acrylic binder/s. Importantly, the distinction between the samples in the two Australian-made Holden groupings (classes 17 and 18) can be made based upon the position of these samples on PC3. The samples from class 17, which represents Holden vehicles manufactured from 2009 onwards, attain less positive scores on PC3 than the samples from class 18 (Holden vehicles manufactured between 2004-2009). These samples from class 17 have comparatively less positive scores on PC3 because of the more intense vibrational bands at approximately 1449 cm^{-1} and 1305 cm^{-1}. This suggests that the samples from class 17 most likely have a much larger abundance of the same acrylic binder, or have a different acrylic backbone than those in class 18.

Interestingly, the Fisher ratio plot depicted below in Figure 6.8 revealed that the most significant spectral feature in the Raman dataset was a small peak at approximately 779 cm^{-1}. This peak can most likely be assigned to ring vibrations from *para*-disubstituted benzenes caused by either a modification to the styrene component or from another additive entirely (e.g. *p*-xylene).[226] Comparatively, the Fisher ratio plot determined the spectral regions significantly positively or negatively correlated to the first three PCs (Figures 6.5-6.7) to be far less significant than the region *ca.* 779 cm^{-1}. Although this peak was only unequivocally observed in the IR spectra of samples obtained from classes 1, 2 and 4, the large F-value for this peak emphasises its class distinguishing capabilities.

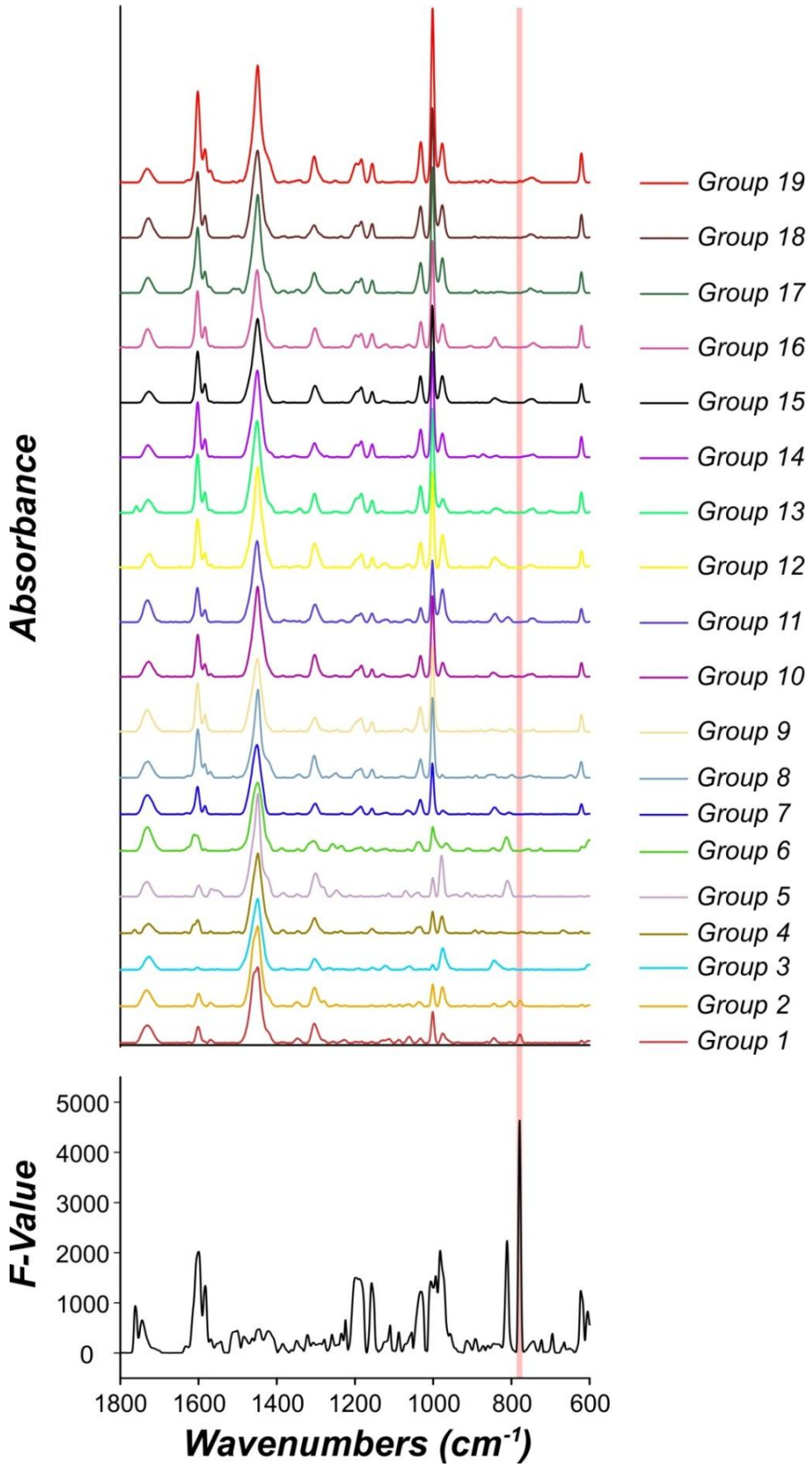

Figure 6.8: Fisher ratio plot and the Raman spectra obtained from the central sample of each PCA grouping. The red region is indicative of a peak with a large F-value, thereby indicating its significance in the dataset.

6.3.2 Linear Discriminant Analysis

A LDA model was generated by utilising the first three PCs and the groupings derived from PCA of the calibration data. The three PC-score LDA model successfully classified 96.9 % of the data in the calibration set, with only 3 samples and their corresponding replicates being misclassified (Table 6.4). Two of the three samples misclassified were obtained from a Japanese-manufactured Suzuki Grand Vitara, and a Honda Civic made in the UK. Both samples were visually projected into class 12; however, the model predicted these samples to be classified in class 15 and 14 respectively, based upon their discriminant values presented in Table A.4 of the appendix. Whilst these samples were misclassified, it is important to note that these samples represent singular vehicles in the dataset and are thus not well defined in the model. It is likely that as the size of the model increases, and more importantly, the number of samples representing these vehicles increases, specific groupings representing these vehicles may be formed. Although these samples are not adequately defined in the model, they still need to be classified into one of the pre-specified groupings, thus accounting for their misclassification. The final misclassified sample in the calibration set was obtained from a Holden VE Commodore manufactured in 2007. Whilst the sample should group with the other samples in class 18, the LDA model classifies the sample into group 17 with the Holden vehicles made from 2009 onwards. The discriminant values for this particular sample (Table A.4 of the appendix), revealed that this sample is only slightly closer to the centroid of class 17 relative to class 18, suggesting that there is a small degree of overlap between the two groupings.

The LDA model successfully classified 97.6 % of the data in the test set, with only one sample and the corresponding replicates being misclassified (Table 6.5). The sample in question was obtained from a Thai-manufactured Toyota Hilux vehicle from class 12, which was classified by the model into class 15. This result was reinforced upon examination of the discriminant values for this sample (Table A.4 of the appendix). Whilst some samples were misclassified, it can be concluded that the overall performance of the model is highly discriminating, with only minimal overlap between select groupings.

Table 6.4: Confusion matrix displaying the results from LDA of the samples within the calibration dataset.

Actual

Predicted Class	1	2	3	4	5	6	7	8	9	10	11	12	13	14	15	16	17	18	19	Total	% Correct
1	25	0	0	0	0	0	0	0	0	0	0	0	0	0	0	0	0	0	0	25	100
2	0	10	0	0	0	0	0	0	0	0	0	0	0	0	0	0	0	0	0	10	100
3	0	0	15	0	0	0	0	0	0	0	0	0	0	0	0	0	0	0	0	15	100
4	0	0	0	10	0	0	0	0	0	0	0	0	0	0	0	0	0	0	0	10	100
5	0	0	0	0	15	0	0	0	0	0	0	0	0	0	0	0	0	0	0	15	100
6	0	0	0	0	0	15	0	0	0	0	0	0	0	0	0	0	0	0	0	15	100
7	0	0	0	0	0	0	35	0	0	0	0	0	0	0	0	0	0	0	0	35	100
8	0	0	0	0	0	0	0	10	0	0	0	0	0	0	0	0	0	0	0	10	100
9	0	0	0	0	0	0	0	0	35	0	0	0	0	0	0	0	0	0	0	35	100
10	0	0	0	0	0	0	0	0	0	15	0	0	0	0	0	0	0	0	0	15	100
11	0	0	0	0	0	0	0	0	0	0	10	0	0	0	0	0	0	0	0	10	100
12	0	0	0	0	0	0	0	0	0	0	0	30	0	0	0	0	0	0	0	30	100
13	0	0	0	0	0	0	0	0	0	0	0	0	15	0	0	0	0	0	0	15	100
14	0	0	0	0	0	0	0	0	0	0	0	5	0	10	0	0	0	0	0	15	66.7
15	0	0	0	0	0	0	0	0	0	0	0	5	0	0	15	0	0	0	0	20	75
16	0	0	0	0	0	0	0	0	0	0	0	0	0	0	0	25	0	0	0	25	100
17	0	0	0	0	0	0	0	0	0	0	0	0	0	0	0	0	110	5	0	115	95.7
18	0	0	0	0	0	0	0	0	0	0	0	0	0	0	0	0	0	30	0	30	100
19	0	0	0	0	0	0	0	0	0	0	0	0	0	0	0	0	0	0	45	45	100
Total	25	10	15	10	15	15	35	10	35	15	10	40	15	10	15	25	110	35	45	490	96.9

Table 6.5: Confusion matrix depicting the accuracy with which samples in the test set were classified by the LDA model.

Actual

Predicted

Class	1	2	3	4	5	6	7	8	9	10	11	12	13	14	15	16	17	18	19	Total	% Correct
1	15	0	0	0	0	0	0	0	0	0	0	0	0	0	0	0	0	0	0	15	100
2	0	0	0	0	0	0	0	0	0	0	0	0	0	0	0	0	0	0	0	0	-
3	0	0	15	0	0	0	0	0	0	0	0	0	0	0	0	0	0	0	0	15	100
4	0	0	0	0	0	0	0	0	0	0	0	0	0	0	0	0	0	0	0	0	-
5	0	0	0	0	0	0	0	0	0	0	0	0	0	0	0	0	0	0	0	0	-
6	0	0	0	0	0	0	0	0	0	0	0	0	0	0	0	0	0	0	0	0	-
7	0	0	0	0	0	0	25	0	0	0	0	0	0	0	0	0	0	0	0	25	100
8	0	0	0	0	0	0	0	10	0	0	0	0	0	0	0	0	0	0	0	10	100
9	0	0	0	0	0	0	0	0	10	0	0	0	0	0	0	0	0	0	0	10	100
10	0	0	0	0	0	0	0	0	0	5	0	0	0	0	0	0	0	0	0	5	100
11	0	0	0	0	0	0	0	0	0	0	0	0	0	0	0	0	0	0	0	0	-
12	0	0	0	0	0	0	0	0	0	0	0	20	0	0	0	0	0	0	0	20	100
13	0	0	0	0	0	0	0	0	0	0	0	0	10	0	0	0	0	0	0	10	100
14	0	0	0	0	0	0	0	0	0	0	0	0	0	5	0	0	0	0	0	5	100
15	0	0	0	0	0	0	0	0	0	0	0	5	0	0	10	0	0	0	0	15	66.7
16	0	0	0	0	0	0	0	0	0	0	0	0	0	0	0	5	0	0	0	5	100
17	0	0	0	0	0	0	0	0	0	0	0	0	0	0	0	0	35	0	0	35	100
18	0	0	0	0	0	0	0	0	0	0	0	0	0	0	0	0	0	15	0	15	100
19	0	0	0	0	0	0	0	0	0	0	0	0	0	0	0	0	0	0	20	20	100
Total	15	0	15	0	0	0	25	10	10	5	0	25	10	5	10	5	35	15	20	205	97.6

From a comparative standpoint, the classification accuracy of the IR model is slightly greater than the equivalent model generated from Raman data. This can most likely be attributed to the fact that there are more overall groupings in the Raman model, indicating that there is a potential for more overlap between the groupings. Additionally, it is worth noting that due to differences in the number and structure of the groupings, an effective comparison of the predictive performance between the two models could not be made, as the samples used to constitute the calibration and validation sets were different.

The model generated from Raman data is potentially more discriminating than the equivalent clear coat model obtained from IR data. This is best exemplified by the discrimination between the Australian-made Holden and HSV vehicles. In the IR model previously described in Chapter 3, there are only two groupings in the dataset representing these vehicles; with samples in class 16 signifying vehicles manufactured prior to mid-2009, whilst samples in class 17 denote vehicles made after this time period. However, in the Raman model the samples contained in class 16 of the IR model are further subdivided into two distinct groupings. The samples in class 15 of the Raman model signify vehicles manufactured from a time period between 2001 until the end of 2003. The samples in class 18 represent Holden vehicles manufactured from the start of 2004 until mid-2009. This potentially enables increased discrimination between Holden and HSV vehicle models, which would not otherwise be discerned from the IR model (Figure 6.9). Take for example, a situation whereby a questioned paint sample was obtained from a Holden commodore. The original clear coat of the specimen could be characterised by Raman spectroscopy, and subsequently classified into one of the three groupings representing Australian-made Holden vehicles. If the sample was classified into class 15, it indicates that the sample was obtained from either a VX or VY commodore. Similarly, if the sample was classified into class 18 it infers that the sample most likely came from a series II VY, VZ or series I VE commodore. Finally, if the sample was classified into class 17 it indicates that the sample was obtained from a VE commodore.

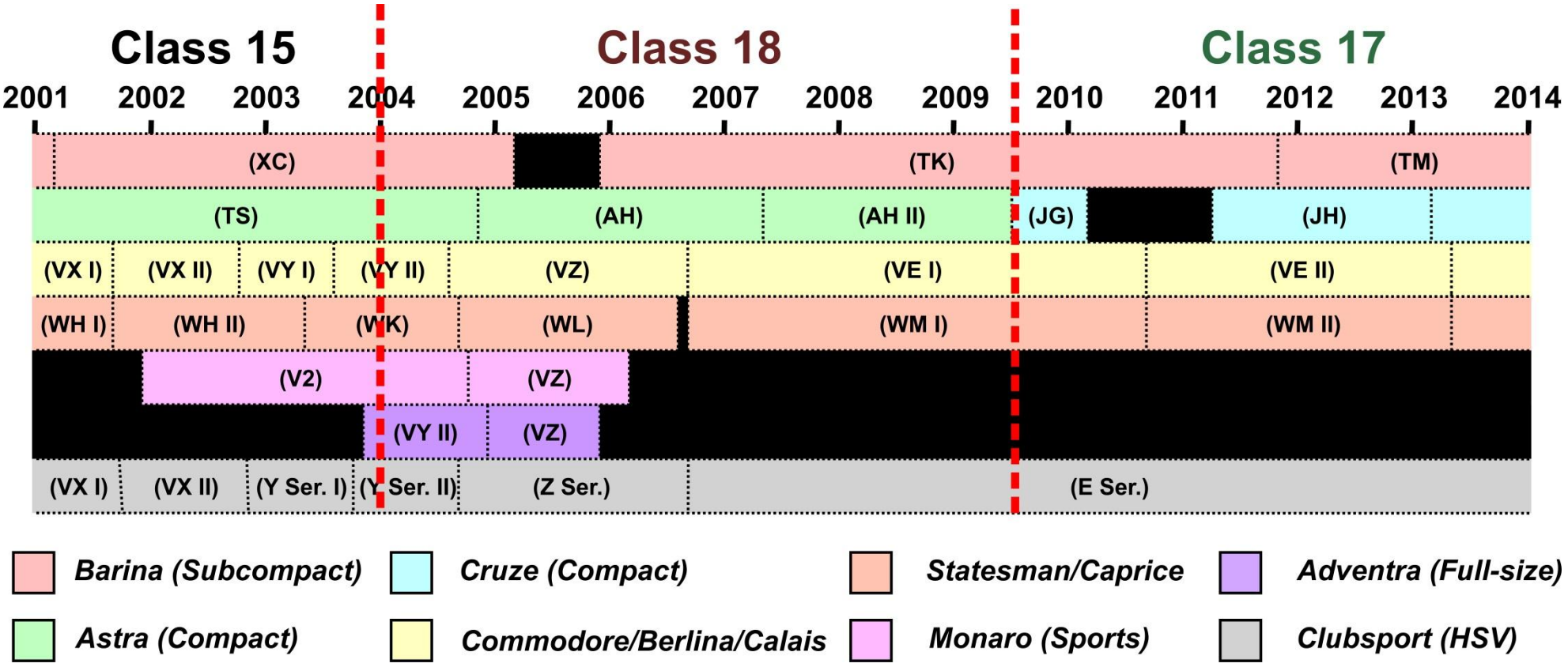

Figure 6.9: Timeline of select lines of Holden vehicles. The red dashed line denotes the demarcation between samples in groupings 15, 17 and 18 of the Raman statistical model.

6.4 Conclusions

A statistical model was developed from Raman data obtained from automotive clear coats. A comparison between this model and the equivalent model generated from IR data (Chapter 3) revealed that the Raman model was more discriminating than the corresponding IR model. This was based upon the comparatively greater discriminating ability of the Raman model (19 groupings) to the IR model (17 groupings). This result infers that Raman spectroscopy may be of more use to the forensic examiner in the characterisation of automotive paint specimens than IR spectroscopy. Ultimately, this finding is significant as it may potentially enable more information to be obtained regarding the suspect vehicle, from questioned paint specimens.

Chapter 7: Discrimination of automotive clear coats using a combined FT-Raman and FT-IR statistical approach

7.1 Introduction

The characterisation of a large population of automotive clear coats by ATR FT-IR and FT-Raman spectroscopy in conjunction with chemometric techniques has been previously described in Chapters 3 and 6 respectively. The stand-alone statistical models generated from IR and Raman data have been shown to enable discrimination between samples on the basis of common vehicle descriptors (e.g. make, model and year of vehicle manufacture). Furthermore, as described in Chapter 6 the individual Raman model provided improved discrimination over the analogous ATR-based model. Previous research by Buzzini and Massonnet have demonstrated that IR and Raman spectroscopy complement each other and their combination enables improved discrimination between similarly coloured green spray paint samples.[98] Consequently, the main objective of this study was to combine or couple the data obtained from both spectroscopic techniques (i.e. IR and Raman), which could potentially permit a larger amount of information to be extracted from each sample.

Recent studies by Pallipurath *et al*[227], and Bueno and Lednev[228] have demonstrated that PCA performed on combined data obtained from two complementary spectroscopic techniques, enables increased discrimination between samples. The first study, which combined Raman and fibre-optic reflectance spectra from the same samples, revealed improved discrimination of medieval paint mixtures.[227] The more recent study by Bueno and Lednev combined FT-IR and Raman spectra obtained from organic gunshot residues and provided a similar conclusion.[228] The work described in this chapter involves concatenating FT-IR and FT-Raman data obtained from the original automotive clear coats, so as to potentially increase the sensitivity and specificity of the statistical analysis.

7.2 Experimental

The IR dataset described in Chapter 3 and the Raman dataset described in Chapter 6 were pre-processed separately, so as to ensure that the spectral contribution of the two analytical techniques were similar. The raw IR data was linearly baseline corrected, range normalised and then truncated (1800-650 cm^{-1}) as described previously. The raw Raman data was also linearly baseline corrected, range normalised and truncated (1800-600 cm^{-1}). As the Raman dataset was normalised to the large aliphatic stretches (i.e. ~ 3000 cm^{-1}) the truncated fingerprint region of the Raman dataset was also scaled, to provide comparable intensities with the IR data. The Raman dataset was also interpolated, such that the interval between data points was 1 cm^{-1} and was therefore commensurate with the IR data.

The 1390 total pre-processed IR and Raman spectra were then combined to afford 695 spectra, generating five replicate single vector IR-Raman spectra for each of the 139 total vehicles. Arbitrary wavenumbers were assigned to the combined IR-Raman spectra, such that the IR data ranged from 2951-1801 cm^{-1} and the Raman data ranged from 1800-600 cm^{-1}. As depicted in Figure 7.1 the IR spectrum (black trace) was coupled with the corresponding Raman spectrum (blue trace) for each sample. It is important to note that both sets of data (IR and Raman) were individually pre-processed, so that there was no significant difference at the point of attachment in the combined spectra (Figure 7.1). This was imperative in order to ensure that the chemometric techniques utilised on the corresponding dataset do not account for any variability attributable to the concatenation point in the combined spectra. PCA and LDA were then conducted on the combined dataset as described in section 2.5.1 and 2.5.2 respectively.

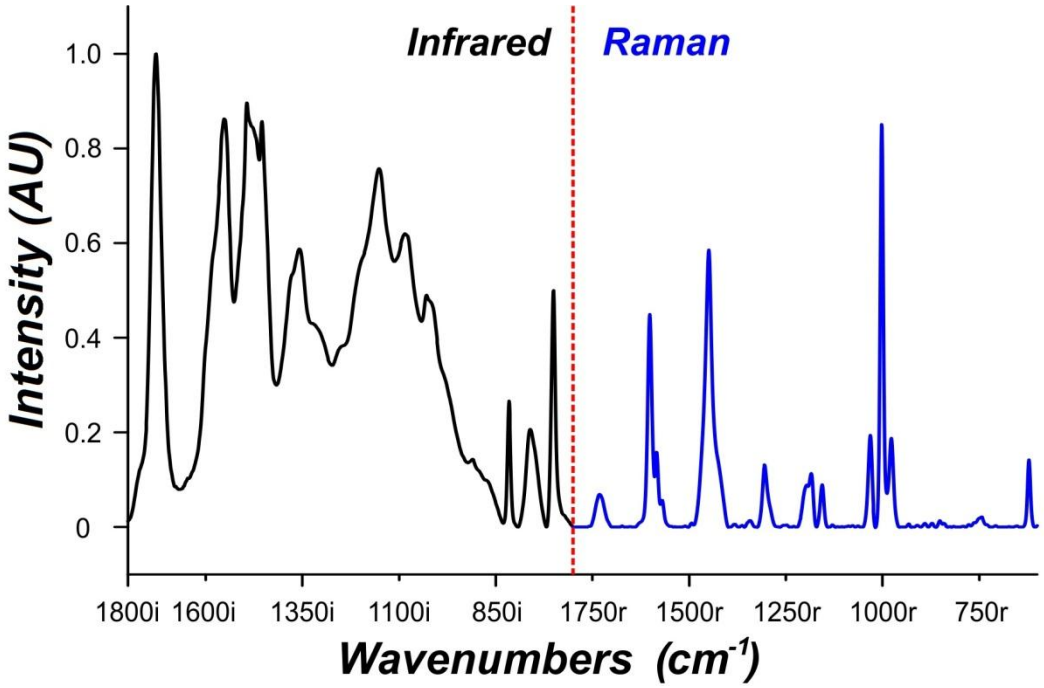

Figure 7.1: Combined IR (black) and Raman (blue) spectrum obtained from the clear coat of a Holden VZ Commodore. The demarcation line (red) depicts the point of attachment between the two spectra.

7.3 Results & Discussion

Generally speaking, the discrimination and classification accuracy of samples are typically enhanced when more information is provided to describe the samples under investigation. Consequently, a statistical model generated from a combination of Raman and IR data should provide greater classification accuracy than the corresponding individual IR and Raman models. In order to corroborate this notion, an all-encompassing combined dataset was created by concatenating individually pre-processed IR and Raman spectra for each sample (Figure 7.1). A previous study conducted by Bueno and Lednev normalised the raw IR and Raman datasets by area, such that the area under each IR and Raman spectrum of a given sample was the same.[228] The authors were able to utilise this approach because the intensity and peak width of the vibrational bands in the raw Raman and IR spectra were comparable. However, in this situation, the IR spectra of automotive clear coats are characterised by very broad peaks, with the average area under the raw IR spectra being significantly larger than that of the raw Raman spectra. Subsequently, if area normalisation was utilised the combined IR-Raman spectra would be distorted in a manner that would assign more weight to the Raman spectra, which would have significantly larger intensities (Figure 7.2).

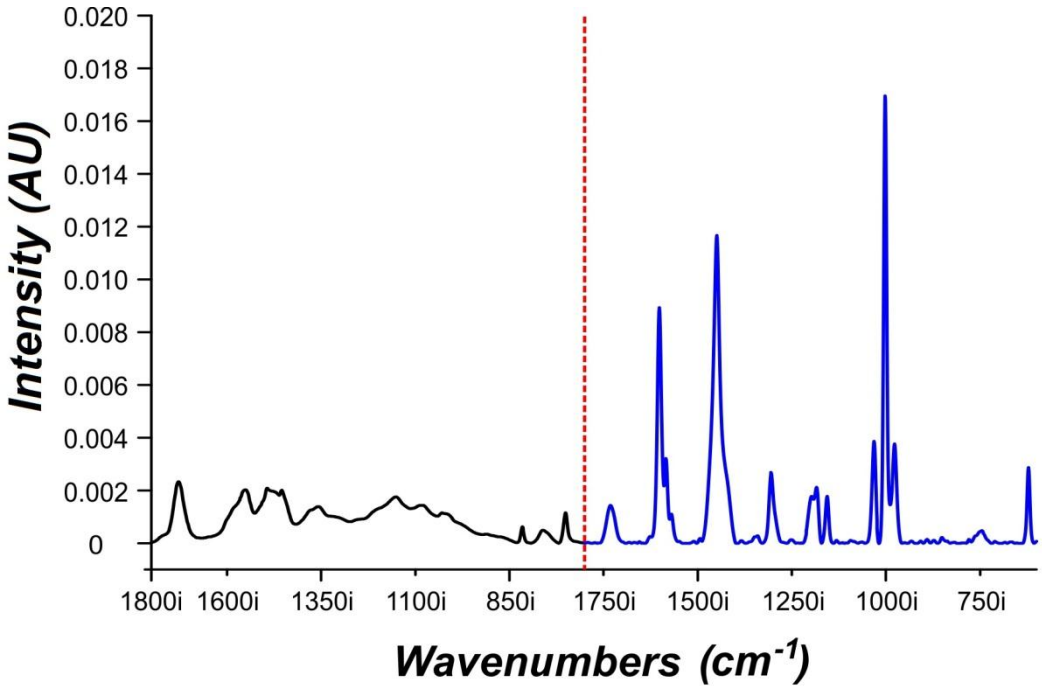

Figure 7.2: Combined area normalised IR (black) and Raman (blue) spectrum obtained from the clear coat of a Holden VZ commodore showing unacceptable bias.

As a result, range normalisation was applied to both the IR and Raman spectra prior to combination. Furthermore, as the Raman spectra were normalised to the aliphatic C-H stretches (~ 3000 cm^{-1}) and then truncated (1800-600 cm^{-1}) so as to only contain spectral contributions of the fingerprint region, the truncated spectra were scaled to provide a similar intensity range to the IR spectra. This approach was utilised as it ensured that the spectral information obtained from the two techniques were weighted equally.

7.3.1 Principal component analysis

PCA performed on the combined IR and Raman dataset (695 spectra) revealed that 97.8 % of the variance was accounted for in the first five PCs (Figure 7.3). Similar to the IR and Raman models, as many as five PCs could be utilised to model the combined dataset. 3-dimensional scores plots were generated by using various combinations of the first five PCs.

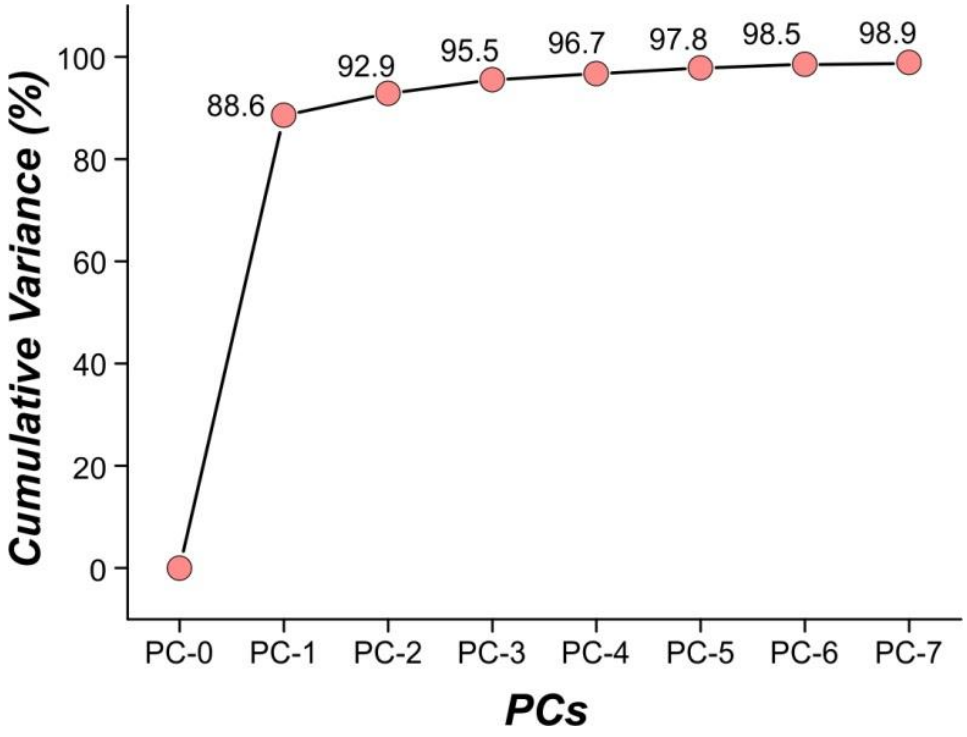

Figure 7.3: Scree plot detailing the variance in each PC generated from the combined dataset.

The PCA scores plot generated from the first three PCs revealed that visually there are 21 groupings present in the combined dataset, which represents an increase in the number of groupings observed relative to the individual IR and Raman models. This indicates that the discriminatory power of the combined model is greater than that of the individual models. Interestingly, whilst the fourth and fifth PC did not divulge additional groupings, these PCs are important in maximising the distinction between the already specified groupings. Figure 7.4 depicts a 3-dimensional scores plot generated by plotting the scores of the projected objects from the first three PCs. Much like the stand-alone IR and Raman models, the samples within the groupings could be correlated to common vehicle descriptors such as the manufacturer, assembly plant, model and year of manufacture.

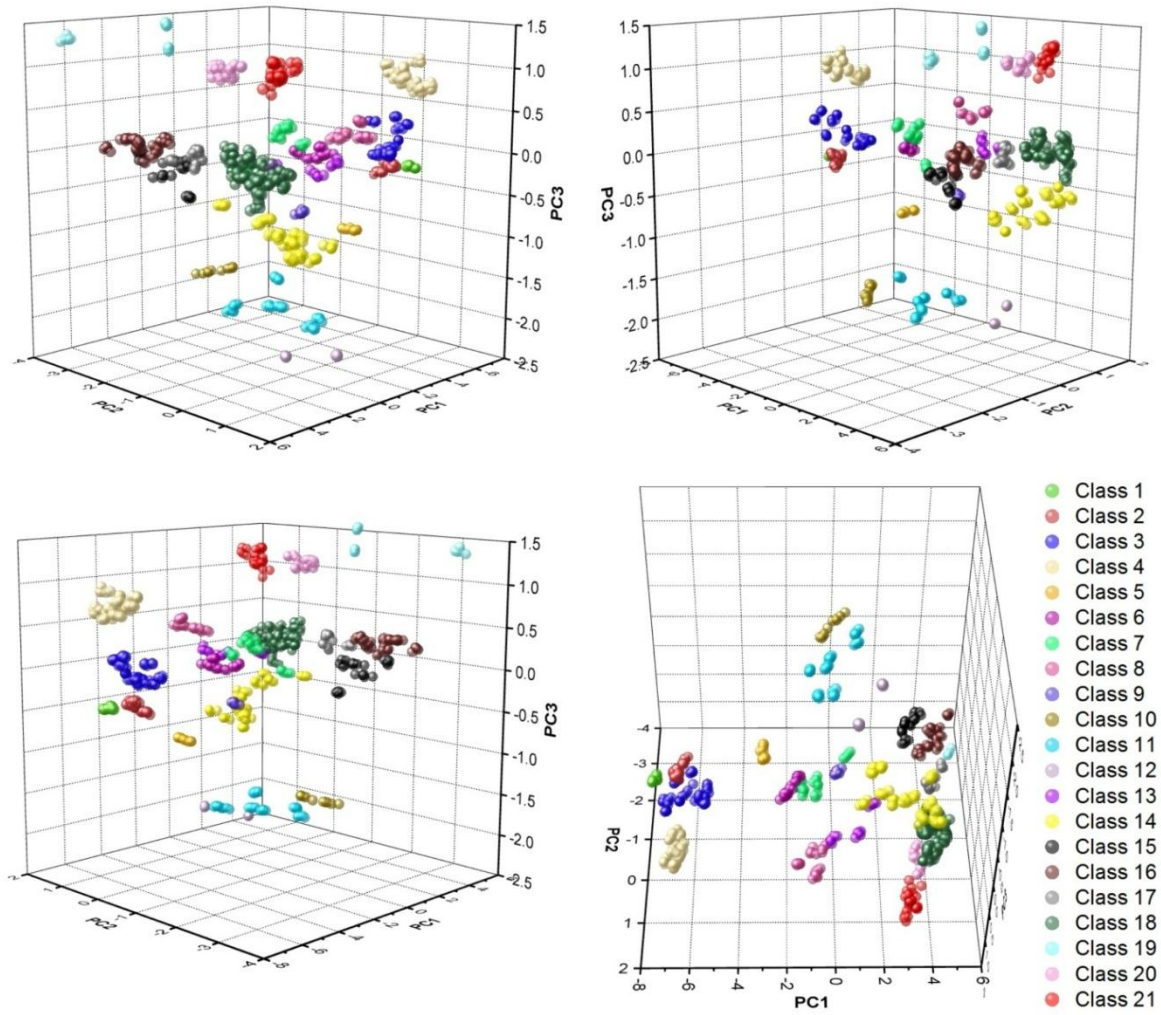

Figure 7.4: Four different perspectives of a 3-dimensional scores plot generated using the first three PCs obtained from PCA of the combined IR-Raman dataset.

An overview of the types of vehicles represented in each grouping is provided below in Table 7.1. For the most part, predictably many of the groupings contained within the previous clear coat models, were also observed in this combined IR-Raman model. Of the 21 groupings present in the combined dataset, 18 of the groupings are common to one of the two clear coat models discussed previously. There are notable exceptions, which includes the samples in classes 4, 17 and 20. Particularly, samples represented in class 4 of this model, were segregated over two groupings in the Raman model; with the Australian-manufactured Toyota vehicles being categorised in class 8, and the Japanese-manufactured Mazda and Toyota vehicles being grouped in class 9. Consequently, in this particular instance, more discriminatory information would be obtained by using the stand-alone Raman model.

Table 7.1: Overview of the samples contained within each PCA grouping of the combined IR-Raman dataset.

Class No.	No. Samples	Vehicles Represented
Class 1	3	BMW
Class 2	8	US (Dodge/Jeep)
Class 3	12	Japan (Mazda/Mitsubishi Lancer/Toyota)
Class 4	13	Japan (Mazda/Toyota); Australia (Toyota)
Class 5	2	Mexico (Dodge)
Class 6	4	Mitsubishi Pajero
Class 7	5	Hyundai
Class 8	6	Germany (Ford Focus)
Class 9	2	SsangYong
Class 10	2	Germany (Ford Mondeo)
Class 11	7	Japan (Subaru/Nissan/Mitsubishi Colt)
Class 12	2	South Korea (Holden)
Class 13	3	Sweden (Saab); UK (Jaguar)
Class 14	13	Thailand (Toyota/Nissan); Honda; Suzuki
Class 15	5	Australia (Holden/HSV) [2001-2003]
Class 16	9	Australia (Holden/HSV) [2004-2007]
Class 17	5	Australia (Holden/HSV) [2008-2009]
Class 18	25	Australia (Holden/HSV) [2009-present]
Class 19	3	Australia (Ford) [2003-2007]
Class 20	4	Australia (Ford) [2008-2009]; Spain (Nissan)
Class 21	6	Australia (Ford) [2009-present]

However, groupings 17 and 20 were only observed in the combined IR/Raman dataset and were not clearly visually discerned in the individual statistical datasets. The samples from group 17 correspond to Australian-made Holden vehicles manufactured from the start of 2008 to mid-2009. The samples represented in this grouping were obtained from a combination of samples in classes 16 and 17 of the IR model, and classes 17 and 18 of the Raman model. Similarly, grouping 20 in the combined dataset consists of samples obtained from Australian-manufactured Ford vehicles made between 2008 and 2009, in addition to Spanish-manufactured Nissan Navara vehicles. These samples were grouped together with the remaining Ford samples in the stand-alone Raman model (i.e. class 19), and the samples contained in class 15 of the IR model. Consequently, based upon the results it can be inferred that the combined dataset may potentially enable more information to be obtained from questioned automotive clear coats, relative to the individual statistical models. Whilst tentative groupings could also be assigned to the samples in classes 17 and 20 of the combined dataset, with the same samples in the stand-alone IR model; the discrimination between the samples is much greater and thus the groupings are more distinct in the augmented dataset. Ultimately, this shows that the Raman data provides a significant contribution to the results obtained from PCA analysis when both datasets are used in combination.

As mentioned above, it was revealed from the PCA scores plot described in Figure 7.4 that there are 21 groupings present in the spectral dataset. The centroid spectra of each grouping were examined, in order to identify spectral features that give rise to the discrimination between the groupings. Figure 7.5 depicts the combined spectra of each centroid, with the red dashed line on the x-axis signifying the demarcation between the IR and Raman spectra.

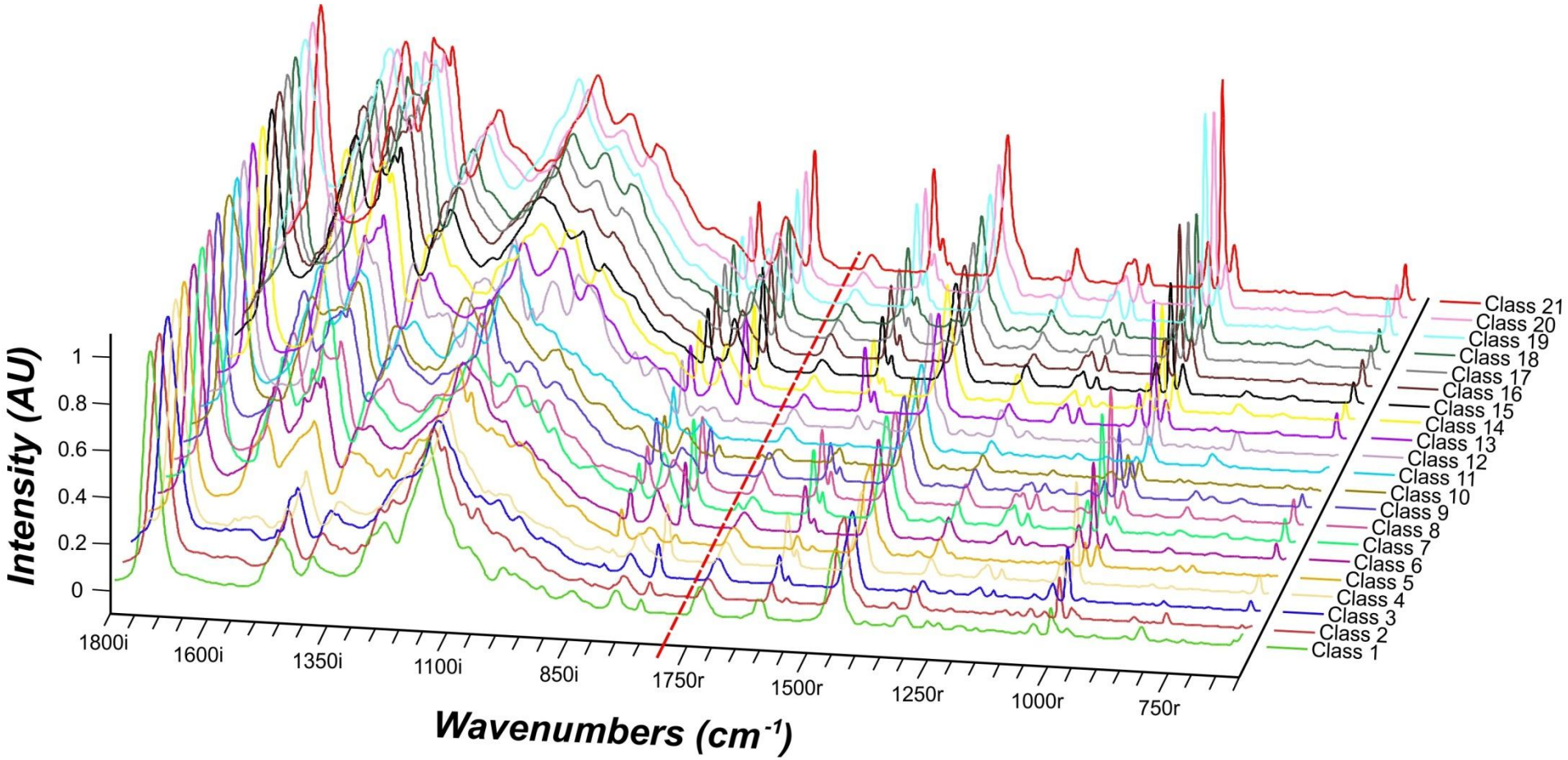

Figure 7.5: Combined IR-Raman spectra obtained from the centroid of each PCA grouping. The red dashed line indicates the point of concatenation between the IR and Raman spectra.

In order to examine the origin of the enhanced discrimination between the PCA groupings in the combined dataset, the loadings plots were examined. The factor loadings for PC1, depicted in Figure 7.6, revealed significant positive correlations at 1549 cm^{-1} and 1493 cm^{-1} in the IR region of the combined spectra. The large loading at 1549 cm^{-1} is indicative of an in-plane triazine ring stretch attributable to melamine, whilst the significant loading at 1493 cm^{-1} could be attributed to both ring and side chain C-N stretches and C=C stretches characteristic for both melamine and styrene respectively. Interestingly, the factor loadings for PC1 (Figure 7.6) closely resembles the loadings plot for PC1 of the IR model. However, although PC1 is weighted significantly more to the IR region of the spectra there is also a slight Raman contribution to PC1; thereby indicating PCA analysis is using both forms of data (i.e. IR and Raman) in combination. The positioning of samples on PC1 of the scores plot can ultimately be attributed to intensity of these two spectral regions. For example, samples with a low intensity of these spectral features attain large negative scores on PC1 (e.g. classes 1-4); whilst samples with a large intensity of these two peaks will have large positive loadings on PC1 (e.g. classes 15-21).

The loadings plot for PC2 revealed strong negative correlations at 1699 cm^{-1} and 1623 cm^{-1} in the IR region of the combined spectra, as shown in Figure 7.7. The large negative loading *ca.* 1699 cm^{-1} can most likely be indicative of a shift in the peak position of the C=O stretch characteristic of the acrylic binder. On the other hand, the negative loading at 1623 cm^{-1} is probably indicative of variation in the shape and slope of a spectral band. Samples which contain large intensities of these spectral features attain negative scores on PC2 (i.e. classes 10, 16 and 19) and vice-versa (i.e. classes 12, 18 and 21). PC2 is responsible for separating the Australian-manufactured Ford (classes 19-21) and Holden (classes 16-18) vehicles. As stated previously, greater separation was observed in these samples in the combined dataset as opposed to the individual IR dataset. This can most likely be rationalised by the fact that although PC2 is weighted more to the IR region of the spectra, there is still a Raman contribution to PC2.

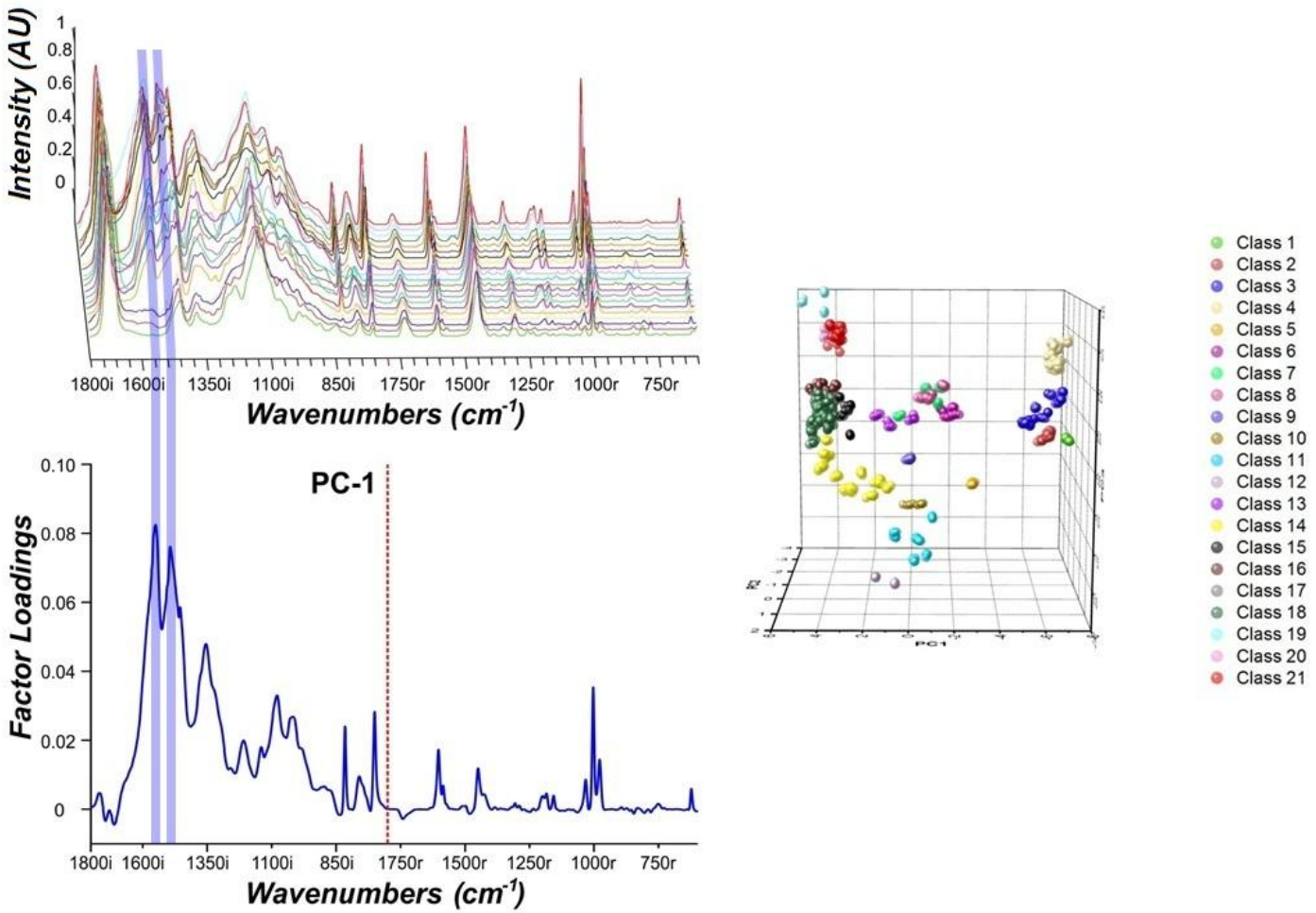

Figure 7.6: Factor loadings plot for PC1. The blue shaded regions overlaid on the representative combined IR-Raman spectra for every class, denote spectral regions that are significantly positively correlated with PC1.

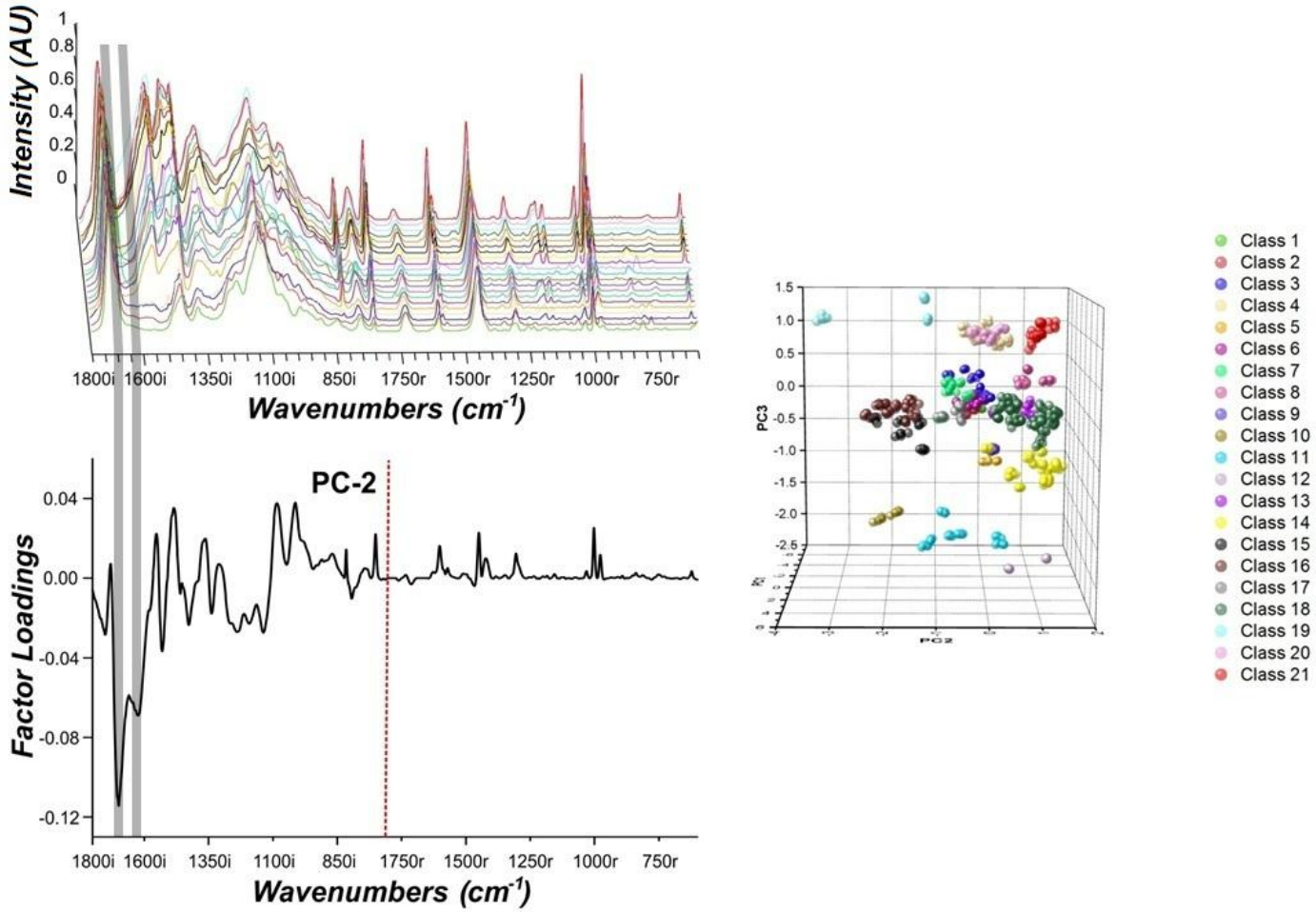

Figure 7.7: Factor loadings plot for PC2. The black regions superimposed on the combined IR-Raman spectra obtained from the class centroid, represent spectral regions significantly negatively correlated with PC2.

Additionally, PC2 of the stand-alone IR model was also responsible for discriminating between the clear coats of Australian-made Ford and Holden vehicles. However, the factor loadings for PC2 obtained from the combined and IR datasets are different. Whilst, the loadings plots for both account for a variation in the shift of the carbonyl peak of the acrylic binder at approximately 1700 cm^{-1}, the combined dataset also contains a significant correlation at 1623 cm^{-1} that deviates from the large correlation observed at 1635 cm^{-1} in the IR dataset. This difference in the factor loadings may also be responsible for the increased discrimination in the samples obtained from Australian-made Ford and Holden vehicles.

The factor loadings for PC3 depicted in Figure 7.8, revealed strong positive correlations at 700 cm^{-1} in the IR region, and 1602 cm^{-1} and 1002 cm^{-1} in the Raman region of the combined spectra. The positive loading *ca.* 700 cm^{-1} in the IR region is characteristic of a =C-H out of plane bending vibration attributable to styrene. Similarly, the positive loadings *ca.* 1602 cm^{-1} and 1002 cm^{-1} is indicative of ring stretching and trigonal ring breathing for styrene respectively. Consequently, samples are differentiated on PC3 based upon the abundance of styrene in the clear coat. Samples with a relatively large abundance of styrene (i.e. classes 19-21) attain large positive scores on PC3, and conversely samples with a low abundance of styrene have large negative scores on PC3 (i.e. classes 10-12). It is important to note that PC3 correlates variation in the main diagnostic peak of styrene in the IR region (*ca.* 700 cm^{-1}), with variation in peaks attributable to styrene in the Raman region (*ca.* 1602 & 1002 cm^{-1}). This is significant as it reinforces and justifies the approach utilised in generating the combined dataset; as the variance in the styrene peaks from both the IR and Raman spectral regions are correlated in PC3. Additionally, although PC3 has a diminished impact on the statistical model as it individually only accounts for 2.6 % of the variability in the dataset, the third PC illustrates an increase in the spectral contribution for the Raman region in comparison to the first and second PC.

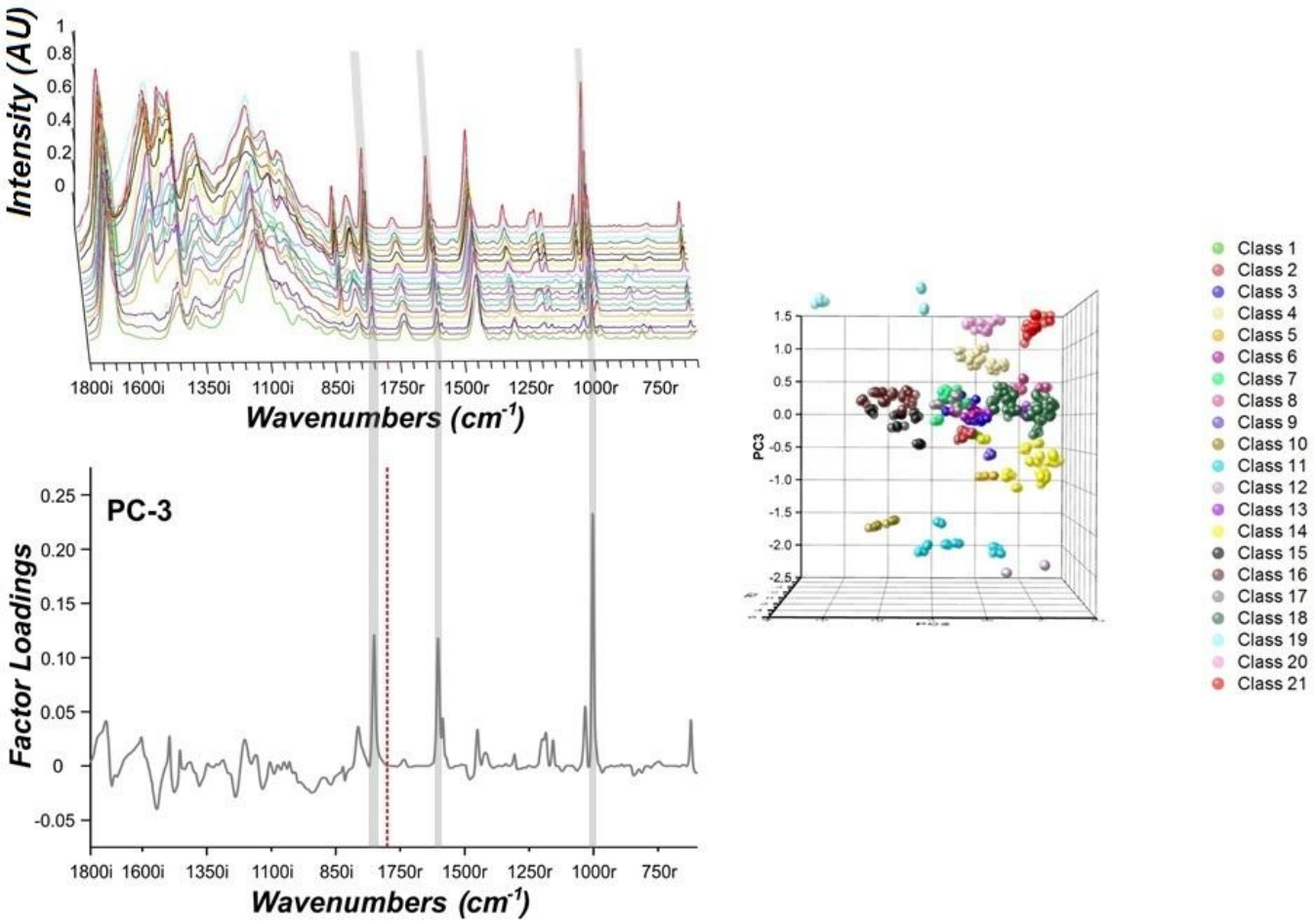

Figure 7.8: Factor loadings plot for PC3. The grey zones superimposed on the combined IR-Raman spectra obtained from each class centroid, signify spectral regions of substantial positive correlation with PC3.

7.3.2 Linear discriminant analysis

LDA was performed on the concatenated dataset in order to ascertain the predictive performance of the model. The LDA calibration model was generated by employing the first five PCs and the classifications obtained from PCA of the calibration data. Whilst only the first three PCs were utilised to visualise the groupings and structure within the dataset, the fourth and fifth PCs were necessary as they enhanced the discrimination between closely projected groupings in the scores plot. It is important to note that PC4 and PC5 did not afford any additional groupings or structure and thus was only utilised to improve discrimination between the already defined groupings. The five PC-score LDA model successfully classified 100 % of the calibration set and 97.6 % of the validation set, as described in the confusion matrices provided in Table 7.2 and Table 7.3 respectively.

Only one sample was incorrectly classified, with a Holden Commodore from class 18 being misclassified with other Holden samples in class 17. In spite of this, the classification accuracy of samples in the combined model is superior to that observed in the statistical model generated from Raman data. In fact, the classification accuracy of the combined model represents a marked improvement in comparison to the previously reported rates of classification for the exclusive Raman model (i.e. 96.9 % and 97.6 % for the training and validation set respectively). Although the predictive performance of the combined model was comparable to that of the individual IR model, the number of groupings present in the combined model is much greater, inferring a greater capacity for discrimination between samples. Consequently, based upon the results obtained from both PCA and LDA of the combined dataset, it can be concluded that the sensitivity and specificity of discrimination between automotive clear coats was improved by combining data obtained from the complementary methods.

Table 7.2: Confusion matrix detailing the results from LDA of the samples in the combined IR-Raman calibration dataset.

Actual

Predicted

Class	1	2	3	4	5	6	7	8	9	10	11	12	13	14	15	16	17	18	19	20	21	Total	% Correct
1	***10***	*0*	*0*	*0*	*0*	*0*	*0*	*0*	*0*	*0*	*0*	*0*	*0*	*0*	*0*	*0*	*0*	*0*	*0*	*0*	*0*	***10***	***100***
2	*0*	***25***	*0*	*0*	*0*	*0*	*0*	*0*	*0*	*0*	*0*	*0*	*0*	*0*	*0*	*0*	*0*	*0*	*0*	*0*	*0*	***25***	***100***
3	*0*	*0*	***40***	*0*	*0*	*0*	*0*	*0*	*0*	*0*	*0*	*0*	*0*	*0*	*0*	*0*	*0*	*0*	*0*	*0*	*0*	***40***	***100***
4	*0*	*0*	*0*	***45***	*0*	*0*	*0*	*0*	*0*	*0*	*0*	*0*	*0*	*0*	*0*	*0*	*0*	*0*	*0*	*0*	*0*	***45***	***100***
5	*0*	*0*	*0*	*0*	***10***	*0*	*0*	*0*	*0*	*0*	*0*	*0*	*0*	*0*	*0*	*0*	*0*	*0*	*0*	*0*	*0*	***10***	***100***
6	*0*	*0*	*0*	*0*	*0*	***15***	*0*	*0*	*0*	*0*	*0*	*0*	*0*	*0*	*0*	*0*	*0*	*0*	*0*	*0*	*0*	***15***	***100***
7	*0*	*0*	*0*	*0*	*0*	*0*	***15***	*0*	*0*	*0*	*0*	*0*	*0*	*0*	*0*	*0*	*0*	*0*	*0*	*0*	*0*	***15***	***100***
8	*0*	*0*	*0*	*0*	*0*	*0*	*0*	***20***	*0*	*0*	*0*	*0*	*0*	*0*	*0*	*0*	*0*	*0*	*0*	*0*	*0*	***20***	***100***
9	*0*	*0*	*0*	*0*	*0*	*0*	*0*	*0*	***10***	*0*	*0*	*0*	*0*	*0*	*0*	*0*	*0*	*0*	*0*	*0*	*0*	***10***	***100***
10	*0*	*0*	*0*	*0*	*0*	*0*	*0*	*0*	*0*	***10***	*0*	*0*	*0*	*0*	*0*	*0*	*0*	*0*	*0*	*0*	*0*	***10***	***100***
11	*0*	*0*	*0*	*0*	*0*	*0*	*0*	*0*	*0*	*0*	***20***	*0*	*0*	*0*	*0*	*0*	*0*	*0*	*0*	*0*	*0*	***20***	***100***
12	*0*	*0*	*0*	*0*	*0*	*0*	*0*	*0*	*0*	*0*	*0*	***10***	*0*	*0*	*0*	*0*	*0*	*0*	*0*	*0*	*0*	***10***	***100***
13	*0*	*0*	*0*	*0*	*0*	*0*	*0*	*0*	*0*	*0*	*0*	*0*	***10***	*0*	*0*	*0*	*0*	*0*	*0*	*0*	*0*	***10***	***100***
14	*0*	*0*	*0*	*0*	*0*	*0*	*0*	*0*	*0*	*0*	*0*	*0*	*0*	***45***	*0*	*0*	*0*	*0*	*0*	*0*	*0*	***45***	***100***
15	*0*	*0*	*0*	*0*	*0*	*0*	*0*	*0*	*0*	*0*	*0*	*0*	*0*	*0*	***15***	*0*	*0*	*0*	*0*	*0*	*0*	***15***	***100***
16	*0*	*0*	*0*	*0*	*0*	*0*	*0*	*0*	*0*	*0*	*0*	*0*	*0*	*0*	*0*	***30***	*0*	*0*	*0*	*0*	*0*	***30***	***100***
17	*0*	*0*	*0*	*0*	*0*	*0*	*0*	*0*	*0*	*0*	*0*	*0*	*0*	*0*	*0*	*0*	***20***	*0*	*0*	*0*	*0*	***20***	***100***
18	*0*	*0*	*0*	*0*	*0*	*0*	*0*	*0*	*0*	*0*	*0*	*0*	*0*	*0*	*0*	*0*	*0*	***90***	*0*	*0*	*0*	***90***	***100***
19	*0*	*0*	*0*	*0*	*0*	*0*	*0*	*0*	*0*	*0*	*0*	*0*	*0*	*0*	*0*	*0*	*0*	*0*	***15***	*0*	*0*	***15***	***100***
20	*0*	*0*	*0*	*0*	*0*	*0*	*0*	*0*	*0*	*0*	*0*	*0*	*0*	*0*	*0*	*0*	*0*	*0*	*0*	***15***	*0*	***15***	***100***
21	*0*	*0*	*0*	*0*	*0*	*0*	*0*	*0*	*0*	*0*	*0*	*0*	*0*	*0*	*0*	*0*	*0*	*0*	*0*	*0*	***20***	***20***	***100***
Total	***10***	***25***	***40***	***45***	***10***	***15***	***15***	***20***	***10***	***10***	***20***	***10***	***10***	***45***	***15***	***30***	***20***	***90***	***15***	***15***	***20***	***490***	***100***

Table 7.3: Confusion matrix showing predicted vs. actual classifications for the samples within the validation set.

Actual

Predicted: Class	1	2	3	4	5	6	7	8	9	10	11	12	13	14	15	16	17	18	19	20	21	Total	% Correct
1	5	0	0	0	0	0	0	0	0	0	0	0	0	0	0	0	0	0	0	0	0	5	100
2	0	15	0	0	0	0	0	0	0	0	0	0	0	0	0	0	0	0	0	0	0	15	100
3	0	0	20	0	0	0	0	0	0	0	0	0	0	0	0	0	0	0	0	0	0	20	100
4	0	0	0	20	0	0	0	0	0	0	0	0	0	0	0	0	0	0	0	0	0	20	100
5	0	0	0	0	0	0	0	0	0	0	0	0	0	0	0	0	0	0	0	0	0	0	-
6	0	0	0	0	0	5	0	0	0	0	0	0	0	0	0	0	0	0	0	0	0	5	100
7	0	0	0	0	0	0	10	0	0	0	0	0	0	0	0	0	0	0	0	0	0	10	100
8	0	0	0	0	0	0	0	10	0	0	0	0	0	0	0	0	0	0	0	0	0	10	100
9	0	0	0	0	0	0	0	0	0	0	0	0	0	0	0	0	0	0	0	0	0	0	-
10	0	0	0	0	0	0	0	0	0	0	0	0	0	0	0	0	0	0	0	0	0	0	-
11	0	0	0	0	0	0	0	0	0	0	15	0	0	0	0	0	0	0	0	0	0	15	100
12	0	0	0	0	0	0	0	0	0	0	0	0	0	0	0	0	0	0	0	0	0	0	-
13	0	0	0	0	0	0	0	0	0	0	0	0	5	0	0	0	0	0	0	0	0	5	100
14	0	0	0	0	0	0	0	0	0	0	0	0	0	20	0	0	0	0	0	0	0	20	100
15	0	0	0	0	0	0	0	0	0	0	0	0	0	0	10	0	0	0	0	0	0	10	100
16	0	0	0	0	0	0	0	0	0	0	0	0	0	0	0	15	0	0	0	0	0	15	100
17	0	0	0	0	0	0	0	0	0	0	0	0	0	0	0	0	5	5	0	0	0	10	50
18	0	0	0	0	0	0	0	0	0	0	0	0	0	0	0	0	0	30	0	0	0	30	100
19	0	0	0	0	0	0	0	0	0	0	0	0	0	0	0	0	0	0	0	0	0	0	-
20	0	0	0	0	0	0	0	0	0	0	0	0	0	0	0	0	0	0	0	5	0	5	100
21	0	0	0	0	0	0	0	0	0	0	0	0	0	0	0	0	0	0	0	0	10	10	100
Total	5	15	20	20	0	5	10	10	0	0	15	0	5	20	10	15	5	35	0	5	10	205	97.6

7.4 Conclusions

It has been demonstrated that a combined statistical model generated by using spectra from two different, complementary analytical techniques (i.e. IR and Raman spectroscopy), can improve the statistical discrimination between automotive clear coats. The LDA results of the combined model depict an improvement in the classification accuracy over the individual Raman model and an increase in the overall discriminating capability over both individual spectroscopic models. An increase in the sensitivity and specificity of the combined approach was observed in comparison to the previously reported individual methods, suggesting that this approach could potentially afford more information concerning a suspect vehicle to forensic investigators.

Chapter 8: Conclusions and suggestions for future work

This dissertation details a series of investigations that were undertaken in order to facilitate the development of analytical and interpretational protocols for automotive paint evidence. A number of instrumental spectroscopic techniques were utilised in conjunction with multivariate statistics, with the aim of characterising specific automotive paint coatings and interpreting the resulting data. The statistical models generated from these studies may potentially be used to procure investigative leads from questioned paint samples.

Chapter 3 investigated the potential of employing ATR FT-IR spectroscopy in combination with chemometrics to characterise and classify a large population of original automotive clear coats. A statistical model was developed with 17 discernible groupings, which could be correlated to common vehicle descriptors; such as country of manufacture and manufacturer, model, assembly plant and year of assembly. The model developed could potentially be utilised in an Australian context to elucidate information about a suspect vehicle from its corresponding paint specimen. However, a couple of significant issues needed to be addressed, before this model can be used in a forensic setting (Chapter 4). Specifically, the effect of chemical component migration amidst automotive paint layers and the potential impact this would have on the classification of automotive clear coats was investigated. Synchrotron FTIR microspectroscopy revealed that migration of the cross-linking agent melamine can and does occur from the underlying layers into the clear coat. This is potentially significant if transmission IR spectra were obtained from a region of the clear coat affected by melamine migration and incorporated into the ATR-based statistical model. This may result in misclassification of the sample and lead to incorrect information being conveyed to law enforcement. However, this issue could be mitigated, by characterising the original clear coats of automotive paint systems with ATR FT-IR spectroscopy. Another issue that was investigated involved the effect of weathering and the environment on original manufacturer clear coats. Automotive paint samples were subjected to the environmental conditions over the course of 18 months and periodically analysed by ATR FT-IR spectroscopy. The resultant IR data was projected onto the statistical model described in Chapter 3, and

it was determined that moderate weathering of the automotive clear coats over an 18 month period, did not affect sample classification. With that being said, further research is still required to investigate the effects of long-term weathering, as the average age of registered vehicles on Australian roads is 10 years. Furthermore, the effect of uneven weathering across different portions of the vehicle also warrants additional investigation.

Whilst the ATR-based clear coat model (Chapter 3) has demonstrated potential in procuring vehicle information from questioned paint specimens, there are situations in which this model cannot be employed. In particular, there are some instances where chemical analysis of the original clear coat is inconclusive, or this coating is not present in the paint system. Consequently, the variability in the chemical composition of the underlying coatings was also investigated, with a view to identifying if the underlying layers of the paint system may aid in vehicle discrimination. Synchrotron FT-IR microspectroscopy was used to characterise the basecoat, primer surfacer and electrocoat primers of a statistically relevant number of automotive paint samples. Synchrotron IR data obtained from the primer surfacer was used to generate a statistical model, and a correlation was made between the PCA groupings as a function of vehicle manufacturer. The benefits of the primer surfacer model are that it can afford specific information pertaining to the vehicle manufacturer and is less likely to be influenced by long-term environmental degradation. It is important to note that no significant variation in the chemical composition of the basecoat apart from colour/pigments, and electrocoat primer was discerned. As only the clear coat and primer surfacer layers were determined to have a highly variable chemical composition that is often characteristic of descriptors of the vehicle, it would be beneficial to utilise chemical information from both coatings to enhance sample discrimination. Whilst, the synergistic effect of the ATR clear coat model (Chapter 3) and the synchrotron IR surfacer model was briefly discussed; it is recommended that further work be undertaken to concatenate synchrotron IR data from the clear coat and primer surfacer layers, in order to generate a statistical model that will have enhanced sample discrimination.

As discovered in Chapter 3, the original clear coat of automotive paint systems is highly variable and this chemical variability can typically be attributed to specific vehicle descriptors. Chapter 6 explored the potential of near-IR FT-Raman spectroscopy in conjunction with chemometrics to characterise and classify the sample population of automotive clear coats. Interestingly, the statistical model generated from Raman data (19 groupings) was deemed to be more discriminating than the equivalent IR model (Chapter 3). This infers that FT-Raman spectroscopy may be better suited to the analysis of automotive clear coats than IR spectroscopy. Furthermore, Chapter 7 also examined the possibility of concatenating IR and Raman data from the automotive clear coats to develop an all-encompassing statistical model. This combined statistical approach was demonstrated to provide better levels of discrimination than the single spectroscopic approaches. Thus, the combined statistical approach has the potential to afford more information to the forensic examiner than the corresponding individual models. Furthermore, this approach is universal and is not solely limited to the analysis and interpretation of automotive paint evidence.

Multivariate statistical analyses of datasets that contain small sample sizes are relatively common in analytical chemistry. The main issue with developing chemometric models from limited numbers of samples can be attributed to the instability and poor predictive quality of the resultant model. Consequently, sample size is of great importance in multivariate statistical analysis. Although the sample population is typically constrained by the economics and logistics of the experiment being conducted, a larger sample size is able to better define the data structure and add confidence to the results obtained. Therefore, the significance of the statistical models generated in this dissertation can primarily be credited to the large sample populations utilised. The statistical models described in Chapters 3 and 6 are defined by 139 independent samples, which represent a substantial increase on the sample sizes of previously reported statistical models generated from automotive paint data. Furthermore, aside from employing sample datasets limited in size, these previous studies also failed to utilise a sufficiently varied sample set, which would ultimately

reduce the predictive performance of the resultant model. Consequently, the statistical models generated in this dissertation provide a significant improvement over the previously reported chemometric models. With that being said, regular expansion of the dataset is constantly required, as with any forensic database, to better define the model with the latest paint formulations and ensure it does not become obsolete.

Due predominantly to increasing environmental regulations and economic convenience, automotive paint technology is in a constant state of flux with automobile manufacturer's regularly changing and revising paint formulations. Similarly, new vehicle types and models are continually being imported into Australia, resulting in an ever-increasing diverse range of vehicles on Australian roads. Consequently, these issues also necessitate the consistent addition of samples to the statistical models, in order to ensure that the model is adequately defined and is therefore adept at classifying unknown, questioned paint specimens. This is of particular importance as all three of the major Australian vehicle manufacturers (Holden, Ford and Toyota) will cease production of vehicles in Australia, by the end of 2017. This is significant because Australian-made vehicles represent roughly 44 % of the samples present in the current statistical models. It is believed that after 2017, these manufacturers will begin to import internationally assembled vehicles into Australia. This will undoubtedly have a significant impact on the current statistical models, and further work will need to be undertaken in the future to reflect the changing landscape of vehicles on the Australian roads.

As previously mentioned, all automotive paint exemplars used in this dissertation were obtained from the roof of the vehicle during the process of sunroof installation. This is important due to manufacturing variation, which may result in detectable differences in the paint composition between, for example, the rear quarter panel and the hood of the vehicle. Furthermore, it is also possible that the manufacturer uses

different formulations to finish different parts of the automobile body, such as the plastic bumper and the steel frame. Although this issue was avoided in the development of the statistical models, due primarily to the fact that automotive paint samples were obtained from the same part of the vehicles, it is anticipated that this may be problematic when applying the model to classify unknown questioned paint samples. This is because it would be impossible in a case situation for the forensic examiner to determine whether a questioned paint sample was from a plastic or metallic portion of the vehicle. Thus, further work is warranted to investigate the *intra*-vehicle paint variability and the implications this might have on the developed statistical models.

In this dissertation, automotive paint evidence was characterised by a variety of vibrational spectroscopic techniques. Whilst these techniques are frequently utilised in this context, mass spectroscopic techniques provide unrivalled chemical specificity and sensitivity. A portion of this dissertation was initially intended to use desorption electrospray ionisation (DESI) mass spectroscopy (MS) to characterise automotive paint coatings and interpret the resultant mass spectroscopic data with multivariate statistics. The rationale behind this line of thinking is that DESI-MS is inherently more sensitive than the previously used vibrational spectroscopic techniques, which will enable the identification of additives and other minor constituents that would not otherwise be observed in the corresponding IR and Raman spectra. Furthermore, DESI-MS is significantly more chemical specific than the vibrational spectroscopic techniques used in these studies, and as such affords improved chemical component identification. Consequently, statistical models generated from mass spectroscopic data are the gold standard, as they will enable unparalleled discrimination between samples. Unfortunately, logistical issues with the instrumentation prevented this work from being undertaken during my PhD tenure, but it is the subject of current studies.

References

1. Toobin, J., *The CSI effect: Annals of law*, in *The New Yorker*. 2007, Conde Nast Publications, Inc.: New York. p. 30-35.

2. Harvey, E. and L. Derksen, *Producing justice, science, and television drama*, in *The CSI Effect: Television, Crime, and Governance*, M. Byers and V.M. Johnson, Editors. 2009, Lexington Books: Plymouth.

3. Holmgren, J.A. and J. Fordham, *The CSI effect and the Canadian and the Australian jury*. Journal of Forensic Sciences, 2011. **56**: p. S63-S71.

4. Science and Technology Committee, *The Forensic Science Service*, 2011: London.

5. National Academy of Sciences, *Strengthening forensic science in the United States: A path forward*, 2009, National Research Council: Washington D.C.

6. Houck, M.M. and J.A. Siegel, *Fundamentals of Forensic Science*. 2nd ed. 2010, Massachusetts: Academic Press.

7. Saferstein, R., *Criminalistics: An Introduction to Forensic Science*. 2001, New Jersey: Prentice Hall.

8. Genge, N., *The Forensic Casebook: The Science of Crime Scene Investigation*. 2002, New York: Ballantine Books.

9. Jackson, A.R.W. and J.M. Jackson, *Forensic Science*. 2004, Essex: Pearson Education Ltd.

10. Shaler, R.C., *Crime Scene Forensics: A Scientific Method Approach*. 2012, Florida: CRC Press

11. Locard, E., *The analysis of dust traces. Part I*. The American Journal of Police Science, 1930. **1**(3): p. 276-298.

12. Bayliss, D.A. and K.A. Chandler, *Paints and paint coatings*, in *Steelwork Corrosion Control*. 2002, Elsevier Science Publishers, Ltd.: Essex. p. 35-61.

13. Bentley, J., *Composition, manufacture and use of paint*, in *Forensic Examination of Glass and Paint: Analysis and Interpretation*, B. Caddy, Editor. 2001, Taylor and Francis: London.

14. Ryland, S.G. and E.M. Suzuki, *Analysis of paint evidence*, in *Forensic Chemistry Handbook*, L. Kobilinsky, Editor. 2011, John Wiley & Sons, Inc.: New Jersey. p. 131-224.

15. Bender, L., *Chemistry/Trace/Paint and Coating: Overview*, in *Encyclopedia of Forensic Sciences*, J.A. Siegel and P.J. Saukko, Editors. 2013, Academic Press: London. p. 245-249.

16. *Coating materials (paints)*, in *Paint and Coatings: Applications and Corrosion Resistance*, P.A. Schweitzer, Editor. 2006, Taylor and Francis Group: Florida. p. 97-152.

17. Holmberg, K., *Paints and printing inks*, in *Handbook of Detergents, Part D: Formulation*, M.S. Showell, Editor. 2006, Taylor and Francis Group: Florida. p. 369-386.

18. Wicks, Z.W. and F.N. Jones, *Coatings*, in *Kirk-Othmer Encyclopedia of Chemical Technology*, J.I. Kroschwitz and M. Howe-Grant, Editors. 2000, John Wiley & Sons, Inc.: New Jersey.

19. Bell, S., *Forensic Chemistry*. 2006, New Jersey: Pearson Prentice Hall.

20. *Composition of paint*, in *Paint and Coatings: Applications and Corrosion Resistance*, P.A. Schweitzer, Editor. 2006, Taylor and Francis Group: Florida. p. 89-95.

21. Talbert, R., *Paint components*, in *Paint Technology Handbook*. 2007, Taylor and Francis Group: Florida. p. 55-73.

22. Farrokhpay, S., *New developments in paint and coatings technology*, in *Paints: Types, Components and Applications*, S.M. Sarrica, Editor. 2011, Nova Science Publishers, Inc.: New York. p. 141-149.

23. Turner, G.P.A., *Introduction to Paint Chemistry and Principles of Paint Technology*. 3rd ed. 1988, London: Chapman and Hall Ltd.

24. Bender, L., *Chemistry/Trace/Paint and Coating: Automotive Paint*, in *Encyclopedia of Forensic Sciences*, J.A. Siegel and P.J. Saukko, Editors. 2013, Academic Press: London. p. 257-264.

25. Petraco, N. and T. Kubic, *Paint Examination*, in *Color Atlas and Manual of Microscopy for Criminalists, Chemists, and Conservators*. 2003, CRC Press LLC: Florida. p. 123-134.

26. *Paint and surface coatings: Theory and practice*. 2nd ed, ed. R. Lambourne and T.A. Strivens. 1999, New York: William Andrew.

27. Streitberger, H., et al., *Paints and coatings, 3. Paint Systems*, in *Ullmann's Encyclopedia of Industrial Chemistry*. 2014, John Wiley & Sons, Inc. p. 1-29.

28. Bradley, M.J., et al., *Paint and glass*, in *Interpol's Forensic Science Review*, N. Nic Daeid and M.M. Houck, Editors. 2010, Taylor & Francis Group. p. 89-151.

29. Muehlethaler, C., L. Gueissaz, and G. Massonnet, *Chemistry/Trace/Paint and Coating: Forensic Paint Analysis*, in *Encyclopedia of Forensic Sciences*, J.A. Siegel and P.J. Saukko, Editors. 2013, Academic Press: London. p. 265-272.

30. Siegel, J.A., *Forensic Science: The Basics*. 1st ed. 2007, Florida: Taylor & Francis Group.

31. *Handbook of Forensic Science*, ed. J. Fraser and R. Williams. 2013, New York: Routledge.

32. *Automotive Paints and Coatings*. 2nd ed, ed. H. Streitberger and K. Dossel. 2008, Weinheim: Wiley-VCH Verlag GmbH & Co. KGaA.

33. Kirkbride, K.P. and V. Otieno-Alego, *Paint examinations*, in *Expert Evidence*, H. Selby and I. Freckelton, Editors. 2010, Thomson Reuters: London.

34. Ryland, S.G., T.A. Jergovich, and K.P. Kirkbride, *Current trends in forensic paint examination*. Forensic Science Review, 2006. **18**(2): p. 97-117.

35. Kirk, P.L., *Crime Investigation*. Second ed. 1953, New York: John Wiley & Sons, Inc.

36. Scientific Working Group for Materials Analysis (SWGMAT), *Forensic paint analysis and comparison*. Forensic Science Communications, 1999. **1**(2).

37. ASTM E-1610-02, *Standard guide for forensic paint examination*, 2002, ASTM International: Pennsylvania.

38. Buzzini, P. and W. Stoecklein, *Forensic sciences/paints, varnishes, and lacquers*, in *Encyclopedia of Analytical Science*, P. Worsfield, A. Townshend, and C.F. Poole, Editors. 2005, Elsevier: Amsterdam. p. 453-464.

39. McCullough, J., *Paint*, in *Wiley Encyclopedia of Forensic Science*, A. Jamieson and A. Moenssens, Editors. 2009, John Wiley & Sons, Inc.: West Sussex. p. 1931-1943.

40. Allen, T.J., *The examination of thin sections of coloured paints by light microscopy*. Forensic Science International, 1992. **57**(1): p. 5-16.

41. Allen, T.J., *Modifications to sample mounting procedures and microtome equipment for paint sectioning*. Forensic Science International, 1991. **52**(1): p. 93-100.

42. Kilbourn, J.H. and R.B. Marx, *Polarized light microscopy of extenders in structural paints: Forensic applications*. The Microscope, 1994. **42**(4): p. 167-175.

43. Cousins, D.R., *The use of microspectrophotometry in the examination of paints*. Forensic Science Review, 1989. **1**: p. 141-161.

44. Cousins, D.R., C.R. Platoni, and L.W. Russell, *The use of microspectrophotometry for the identification of pigments in small paint samples*. Forensic Science International, 1984. **24**(3): p. 183-196.

45. Trzcińska, B., J. Zięba-Palus, and P. Kościelniak, *Application of microspectrometry in the visible range to differentiation of car paints for forensic purposes*. Journal of Molecular Structure, 2009. **924–926**: p. 393-399.

46. Trzcińska, B., J. Zięba-Palus, and P. Kościelniak, *Examination of car paint samples using visible microspectrometry for forensic purposes*. Analytical Letters, 2013. **46**(8): p. 1267-1277.

47. Wilkinson, J.M., J. Locke, and D.K. Laing, *The examination of paints as thin sections using visible microspectrophotometry and Fourier transform infrared microscopy*. Forensic Science International, 1988. **38**(1–2): p. 43-52.

48. Laing, D.K., et al., *The discrimination of small fragments of household gloss paint by microspectrophotometry*. Forensic Science International, 1982. **20**(2): p. 191-200.

49. Laing, D.K., R.J. Dudley, and M.D.J. Isaacs, *Colorimetric measurements on small paint fragments using microspectrophotometry*. Forensic Science International, 1980. **16**(2): p. 159-171.

50. Kopchick, K.A. and C.R. Bommarito, *Color analysis of apparently achromatic automotive paints by visible microspectrophotometry*. Journal of Forensic Sciences, 2006. **51**(2): p. 340-343.

51. Stoecklein, W. and H. Fujiwara, *The examination of UV-absorbers in 2-coat metallic and non-metallic automotive paints*. Science & Justice, 1999. **39**(3): p. 188-195.

52. Collaborative Testing Services Inc., *Paint analysis test No. 04-545 summary report*, 2004, Collaborative Testing Services, Inc.: Virginia.

53. Liszewski, E.A., et al., *Characterization of automotive paint clear coats by ultraviolet absorption microspectrophotometry with subsequent chemometric analysis*. Applied Spectroscopy, 2010. **64**(10): p. 1122-1125.

54. Ryland, S.G., *Infrared microspectroscopy of forensic paint evidence*, in *Practical Guide to Infrared Microspectroscopy*, H.J. Humecki, Editor. 1995, Marcel Dekker, Inc.: New York. p. 163-243.

55. Pavia, D.L., G.M. Lampman, and G.S. Kriz, *Introduction to Spectroscopy*. Third ed. 2001: Thomson Learning, Inc.

56. Beveridge, A., T. Fung, and D. MacDougall, *Use of infrared spectroscopy for the characterisation of paint fragments*, in *Forensic Examination of Glass and Paint: Analysis and Interpretation*, B. Caddy, Editor. 2001, Taylor & Francis: New York.

57. Allen, T.J., *Paint sample presentation for Fourier transform infrared microscopy*. Vibrational Spectroscopy, 1992. **3**(3): p. 217-237.

58. Beauchaine, J.P., J.W. Peterman, and R.J. Rosenthal, *Applications of FT-IR/microscopy in forensic analysis*. Microchimica Acta, 1988. **94**(1-6): p. 133-138.

59. Percy, R.F.E. and R.J. Audette, *Automotive repaints: Just a new look?* Journal of Forensic Sciences, 1980. **25**(1): p. 189-239.

60. Zięba-Palus, J., A. Michalska, and A. Wesełucha-Birczyńska, *Characterisation of paint samples by infrared and Raman spectroscopy for criminalistic purposes*. Journal of Molecular Structure, 2011. **993**(1–3): p. 134-141.

61. Suzuki, E.M., *Forensic science applications of diffuse reflectance infrared Fourier transform spectroscopy (DRIFTS): IV. Direct analysis of metallic paints - sampling considerations*. Journal of Forensic Sciences, 1989. **34**(1): p. 164-179.

62. Suzuki, E.M. and W.R. Gresham, *Forensic science applications of diffuse reflectance infrared Fourier transform spectroscopy (DRIFTS): I. Principles, sampling methods, and advantages*. Journal of Forensic Sciences, 1986. **31**(3): p. 931-952.

63. Giang, Y.S., et al., *Identification of tiny and thin smears of automotive paint following a traffic accident*. Journal of Forensic Sciences, 2002. **47**(3): p. 625-629.

64. Szafarska, M., et al., *Computer analysis of ATR-FTIR spectra of paint samples for forensic purposes*. Journal of Molecular Structure, 2009. **924–926**: p. 504-513.

65. Suzuki, E.M., *Infrared spectra of U.S. automobile original topcoats (1974-1989): II. Identification of some topcoat inorganic pigments using an extended range (4000-220 cm-1) fourier transform spectrometer*. Journal of Forensic Sciences, 1996. **41**(3): p. 393-406.

66. Suzuki, E.M., *Infrared spectra of U.S. automobile original topcoats (1974-1989): VI. Identification and analysis of yellow organic automotive paint pigments-isoindolinone yellow 3R, isoindoline yellow, anthrapyrimidine yellow, and miscellaneous yellows*. Journal of Forensic Sciences, 1999. **44**(6): p. 1151-1175.

67. Suzuki, E.M., *Infrared spectra of U.S. automobile original topcoats (1974-1989): V. Identification of organic pigments used in red nonmetallic and brown nonmetallic and metallic monocoats - DPP red BO and thioindigo Bordeaux*. Journal of Forensic Sciences, 1999. **44**(2): p. 297-313.

68. Suzuki, E.M. and W.P. Marshall, *Infrared spectra of U.S. automobile original topcoats (1974-1989): III. In situ identification of some organic pigments used in yellow, orange, red, and brown nonmetallic and brown*

metallic finishes - benzimidazolones. Journal of Forensic Sciences, 1997. **42**(4): p. 619-648.

69. Suzuki, E.M. and W.P. Marshall, *Infrared spectra of U.S. automobile original topcoats (1974-1989): IV. Identification of some organic pigments used in red and brown nonmetallic and metallic monocoats - quinacridones*. Journal of Forensic Sciences, 1998. **43**(3): p. 514-542.

70. Suzuki, E.M. and M.X. McDermot, *Infrared spectra of U.S. automobile original finishes. VII. Extended range FT-IR and XRF analyses of inorganic pigments in situ - nickel titanate and chrome titanate*. Journal of Forensic Sciences, 2006. **51**(3): p. 532-547.

71. Lavine, B.K., et al., *Simulation of attenuated total reflection Infrared absorbance spectra: Applications to automotive clear coat forensic analysis*. Applied Spectroscopy, 2014. **68**(5): p. 608-615.

72. Griffiths, P.R. and J.A. De Haseth, *Fourier Transform Infrared Spectrometry*. 2nd ed. 2007, New Jersey: John Wiley & Sons, Inc.

73. Edmondstone, G., et al., *An assessment of the evidential value of automotive paint comparisons*. Canadian Society of Forensic Science Journal, 2004. **37**(3): p. 147-153.

74. Eyring, M., M. Lovelace, and D. Sy. *A study of the discrimination of some automotive paint films having identical color codes*. in *NIJ Trace Evidence Symposium*. 2007. Florida.

75. Flynn, K., et al., *Forensic applications of infrared chemical imaging: Multi-layered paint chips*. Journal of Forensic Sciences, 2005. **50**(4): p. 832-841.

76. Edelman, G.J., et al., *Hyperspectral imaging for non-contact analysis of forensic traces*. Forensic Science International, 2012. **223**(1-3): p. 28-39.

77. Australian Synchrotron. *The synchrotron light source*. 2008; Available from: www.synchrotron.org.au/images/SynchrotronScience/machine-fact-sheet_23oct08_final.pdf.

78. Australian Synchrotron. *How is synchrotron light created?* 2009; Available from: www.synchrotron.org.au/index.php/synchrotron-science/how-is-synchrotron-light-created.

79. Marinkovic, N.S., et al., *Synchrotron radiation in biosciences*. Nuclear Instruments and Methods in Physics Research Section B: Beam Interactions with Materials and Atoms, 2005. **241**(1–4): p. 242-246.

80. Chance, B., *Synchrotron radiation in the biosciences*, ed. B. Chance. 1994, Oxford: Clarendon Press.

81. Sun, Z., *The promise of synchrotron radiation in medical science*. Australasian Medical Journal, 2009. **1**(5): p. 1-5.

82. Arfelli, F., *Synchrotron light and imaging systems for medical radiology*. Nuclear Instruments and Methods in Physics Research Section A: Accelerators, Spectrometers, Detectors and Associated Equipment, 2000. **454**: p. 11-25.

83. Brown, G.E. and N.C. Sturchio, *An overview of synchrotron radiation applications to low temperature geochemistry and environmental science*. Reviews in Mineralogy and Geochemistry, 2002. **49**(1): p. 1-115.

84. Iino, K. and N. Umesaki, *Advanced materials analysis using synchrotron radiation and its application in engineering science*. Journal of Physics: Condensed Matter, 2004. **16**(33): p. S3537-S3548.

85. Lengeler, B., *Applications of synchrotron radiation in materials analysis*. Microchimica Acta, 1987. **91**(1-6): p. 455-475.

86. Beckmann, F., *Neutron and synchrotron-radiation-based imaging for applications in materials science – From macro- to nanotomography, in Neutrons and Synchrotron Radiation in Engineering Materials Science: From Fundamentals to Material and Component Characterization*, W. Reimers, et al., Editors. 2008, Wiley-VCH Verlag GmbH & Co. KGaA. p. 287-307.

87. Kempson, I.M., et al., *Applications of synchrotron radiation in forensic trace evidence analysis*. Talanta, 2005. **67**(2): p. 286-303.

88. Australian Synchrotron. *Technical Information (IR)*. Available from: www.synchrotron.org.au/index.php/aussyncbeamlines/infrared-micro/technical-information2.

89. McKellar, A.R.W., *High-resolution infrared spectroscopy with synchrotron sources*. Journal of Molecular Spectroscopy, 2010. **262**(1): p. 1-10.

90. Roy, P., et al., *Infrared synchrotron radiation: From the production to the spectroscopic and microscopic applications*. Nuclear Instruments and Methods in Physics Research Section A: Accelerators, Spectrometers, Detectors and Associated Equipment, 2001. **467–468**(Part 1): p. 426-436.

91. Sloggett, R., et al., *Microanalysis of artworks: IR microspectroscopy of paint cross-sections*. Vibrational Spectroscopy, 2010. **53**(1): p. 77-82.

92. Chalmers, J.M., H.G.M. Edwards, and M.D. Hargreaves, *Vibrational spectroscopy techniques: Basics and instrumentation*, in *Infrared and Raman Spectroscopy in Forensic Science*, J.M. Chalmers, H.G.M. Edwards, and M.D. Hargreaves, Editors. 2012, John Wiley & Sons, Ltd: West Sussex. p. 9-44.

93. Das, R.S. and Y.K. Agrawal, *Raman spectroscopy: Recent advancements, techniques and applications*. Vibrational Spectroscopy, 2011. **57**(2): p. 163-176.

94. Koçak, A., *The role of vibrational spectroscopy in forensic chemistry*, in *Forensic Chemistry Handbook*, L. Kobilinsky, Editor. 2012, John Wiley & Sons, Inc.: New Jersey. p. 251-267.

95. Larkin, P., *Chapter 1 - Introduction: Infrared and Raman spectroscopy*, in *Infrared and Raman Spectroscopy*, P. Larkin, Editor. 2011, Elsevier: Oxford. p. 1-5.

96. Izake, E.L., *Forensic and homeland security applications of modern portable Raman spectroscopy*. Forensic Science International, 2010. **202**(1-3): p. 1-8.

97. Larkin, P., *Chapter 2 - Basic principles*, in *Infrared and Raman Spectroscopy*, P. Larkin, Editor. 2011, Elsevier: Oxford. p. 7-25.

98. Buzzini, P. and G. Massonnet, *A market study of green spray paints by Fourier transform infrared (FTIR) and Raman spectroscopy*. Science & Justice, 2004. **44**(3): p. 123-131.

99. Bell, S.E., et al., *Rapid forensic analysis and identification of "lilac" architectural finishes using Raman spectroscopy*. Applied Spectroscopy, 2005. **59**(1): p. 100-108.

100. Bell, S.E., et al., *Forensic analysis of architectural finishes using fourier transform infrared and Raman spectroscopy, part I: The resin bases*. Applied spectroscopy, 2005. **59**(11): p. 1333-1339.

101. Bell, S.E.J., S.P. Stewart, and W.J. Armstrong, *Raman spectroscopy for forensic analysis of household and automotive paints*, in *Infrared and Raman Spectroscopy in Forensic Science*, J.M. Chalmers, H.G.M. Edwards, and M.D. Hargreaves, Editors. 2012, John Wiley & Sons, Ltd: West Sussex. p. 121-135.

102. Massonnet, G. and W. Stoecklein, *Identification of organic pigments in coatings: Applications to red automotive topcoats: Part III: Raman spectroscopy (NIR FT-Raman)*. Science & Justice, 1999. **39**(3): p. 181-187.

103. Wampler, T.P., G.A. Bishea, and W.J. Simonsick, *Recent changes in automotive paint formulation using pyrolysis-gas chromatography/mass spectrometry for identification*. Journal of Analytical and Applied Pyrolysis, 1997. **40–41**: p. 79-89.

104. Burns, D.T. and K.P. Doolan, *The automation of the acquisition and evaluation of pyrolysis-gas chromatography–mass spectrometry data for paint samples*. Analytica Chimica Acta, 2006. **571**(1): p. 25-29.

105. Challinor, J.M., *Forensic application of pyrolysis capillary gas chromatography*. Forensic Science International, 1983. **21**(3): p. 269-285.

106. Burke, P., et al., *A comparison of pyrolysis mass spectrometry, pyrolysis gas chromatography and infra-red spectroscopy for the analysis of paint resins*. Forensic Science International, 1985. **28**(3–4): p. 201-219.

107. Sobeih, K.L., M. Baron, and J. Gonzalez-Rodriguez, *Recent trends and developments in pyrolysis–gas chromatography*. Journal of Chromatography A, 2008. **1186**(1–2): p. 51-66.

108. Plage, B., A. Berg, and S. Luhn, *The discrimination of automotive clear coats by pyrolysis-gas chromatography/mass spectrometry and comparison of samples by a chromatogram library software*. Forensic Science International, 2008. **177**(2–3): p. 146-152.

109. Zięba-Palus, J., et al., *Pyrolysis-gas chromatography/mass spectrometry analysis as a useful tool in forensic examination of automotive paint traces*. Journal of Chromatography A, 2008. **1179**(1): p. 41-46.

110. Zięba-Palus, J., G. Zadora, and J.M. Milczarek, *Differentiation and evaluation of evidence value of styrene acrylic urethane topcoat car paints analysed by pyrolysis-gas chromatography*. Journal of Chromatography A, 2008. **1179**(1): p. 47-58.

111. Burns, D.T. and K.P. Doolan, *A comparison of pyrolysis–gas chromatography–mass spectrometry and fourier transform infrared spectroscopy for the characterisation of automative paint samples*. Analytica Chimica Acta, 2005. **539**(1–2): p. 145-155.

112. Burns, D.T. and K.P. Doolan, *The discrimination of automotive clear coat paints indistinguishable by Fourier transform infrared spectroscopy via pyrolysis–gas chromatography–mass spectrometry*. Analytica Chimica Acta, 2005. **539**(1–2): p. 157-164.

113. Beam, T.L. and W.V. Willis, *Analysis protocol for discrimination of automotive paints by SEM-EDXA using beam alignment by current centering*. Journal of Forensic Sciences, 1990. **35**(5): p. 1055-1063.

114. Henson, M.L. and T.A. Jergovich, *Scanning electron microscopy and energy dispersive X-ray spectrometry (SEM/EDS) for the forensic examination of paints and coatings*, in *Forensic Examination of Glass and Paint Analysis and Interpretation*, B. Caddy, Editor. 2001, Taylor & Francis: London.

115. De Nolf, W. and K. Janssens, *Micro X-ray diffraction and fluorescence tomography for the study of multilayered automotive paints*. Surface and Interface Analysis, 2010. **42**(5): p. 411-418.

116. Nishiwaki, Y., et al., *Trace elemental analysis of titanium dioxide pigments and automotive white paint fragments for forensic examination using high-energy synchrotron radiation X-ray fluorescence spectrometry*. Journal of Forensic Sciences, 2009. **54**(3): p. 564-570.

117. Haag, L.C., *Element profiles of automotive paint chips by X-ray fluorescence spectrometry*. Journal of the Forensic Science Society, 1976. **16**(3): p. 255-263.

118. Ninomiya, T., *X-ray study of forensic samples at the SPring-8*. Journal of X-Ray Science and Technology, 2005. **13**: p. 109-116.

119. Hobbs, A.L. and J.R. Almirall, *Trace elemental analysis of automotive paints by laser ablation–inductively coupled plasma–mass spectrometry (LA–ICP–MS)*. Analytical and Bioanalytical Chemistry, 2003. **376**(8): p. 1265-1271.

120. Almirall, J.R., et al. *Statistical significance of trace evidence matches using independent physicochemical measurements*. in *Proc. SPIE 2941, Forensic Evidence Analysis and Crime Scene Investigation*. 1997.

121. Bowen, R. and J. Schneider, *Forensic databases paint, shoe prints, and beyond*. National Institute of Justice Journal, 2007(258): p. 34-38.

122. National Law Enforcement and Corrections Technology Center, *PDQ: Tracking down a vehicle*. 2000, Maryland.

123. Royal Canadian Mounted Police. *Paint Data Query (PDQ)*. 2004; Available from: http://www.rcmp-grc.gc.ca/fs-fd/pdfs/pdq-eng.pdf.

124. Lavine, B.K., et al., *Wavelets and genetic algorithms applied to search prefilters for spectral library matching in forensics*. Talanta, 2011. **87**: p. 46-52.

125. Lavine, B.K., et al., *Development of search prefilters for infrared library searching of clear coat paint smears*. Talanta, 2014. **119**: p. 331-340.

126. Goodpaster, J.V. and E.A. Liszewski, *Forensic analysis of dyed textile fibers*. Analytical and Bioanalytical Chemistry, 2009. **394**(8): p. 2009-2018.

127. Wold, S., *Chemometrics; what do we mean with it, and what do we want from it?* Chemometrics and Intelligent Laboratory Systems, 1995. **30**(1): p. 109-115.

128. Lavine, B.K. and J. Workman, *Chemometrics*. Analytical Chemistry, 2013. **85**(2): p. 705-714.

129. Zadora, G., *Chemometrics and statistical considerations in forensic science*, in *Encyclopedia of Analytical Chemistry*, R.A. Meyers, Editor. 2006, John Wiley & Sons, Ltd: West Sussex.

130. Zadora, G., et al., *Statistical Analysis in Forensic Science: Evidential Value of Multivariate Physicochemical Data*. 2014, West Sussex: John Wiley & Sons, Ltd.

131. Morgan, S.L. and E.G. Bartick, *Discrimination of forensic analytical chemical data using multivariate statistics*, in *Forensic Analysis on the Cutting Edge*. 2007, John Wiley & Sons, Inc. p. 333-374.

132. Brereton, R.G., *Chemometrics for Pattern Recognition*. 2009, West Sussex: John Wiley & Sons, Ltd.

133. Miller, J.N. and J.C. Miller, *Statistics and Chemometrics for Analytical Chemistry*. 5th ed. 2005, Essex: Pearson Education Limited.

134. Otto, M., *Chemometrics: Statistics and Computer Application in Analytical Chemistry*. 1999, New York: Wiley-VCH.

135. Elmore, D.L., et al., *Mid-infrared imaging applications in agricultural and food sciences*, in *Spectrochemical Analysis Using Infrared MultiChannel Detectors*, R. Bhargava and I.W. Levin, Editors. 2005, Blackwell Publishing Ltd.: Oxford. p. 261-282.

136. Gemperline, P.J., *Introduction to chemometrics*, in *Practical Guide to Chemometrics*, P.J. Gemperline, Editor. 2006, Taylor & Francis Group, LLC.: Florida. p. 1-6.

137. Varmuza, K. and P. Filzmoser, *Introduction to Multivariate Statistical Analysis in Chemometrics*. 2009, Florida: Taylor & Francis.

138. Gemperline, P.J., *Principal component analysis*, in *Practical Guide To Chemometrics*, P.J. Gemperline, Editor. 2006, Taylor & Francis: Florida. p. 69-104.

139. Adams, M.J., *Chemometrics in Analytical Spectroscopy*. 2nd ed. 2004, Cambridge: The Royal Society of Chemistry.

140. Rencher, A.C., *Methods of Multivariate Analysis*. 2nd ed. 2002, New York: John Wiley & Sons, Inc.

141. Fujikoshi, Y., V.V. Ulyanov, and R. Shimizu, *Multivariate Statistics: High-Dimensional and Large-Sample Approximations*. 2010, New Jersey: John Wiley & Sons, Inc.

142. Reichard, E.J. and J.V. Goodpaster, *Chemometrics applied to the discrimination of synthetic fibres by microspectrophotometry*, 2013, Purdue University: Indiana.

143. Morgan, S.L., et al. *Forensic discrimination of dyed textile fibers using UV-VIS and fluorescence microspectrophotometry*. in *Proceedings of the European Fibres Group*. 2004. Prague.

144. Enlow, E.M., et al., *Discrimination of nylon polymers using attenuated total reflection mid-infrared spectra and multivariate statistical techniques*. Applied Spectroscopy, 2005. **59**(8): p. 986-992.

145. May, C.D. and R.J. Watling, *A comparison of the use of refractive index (RI) and laser ablation inductively coupled plasma mass spectrometry (LA-ICP-MS) for the provenance establishment of glass bottles*. Forensic Science, Medicine, and Pathology, 2009. **5**(2): p. 66-76.

146. Grainger, M.N.C., M. Manley-Harris, and S. Coulson, *Classification and discrimination of automotive glass using LA-ICP-MS*. Journal of Analytical Atomic Spectrometry, 2012. **27**(9): p. 1413-1422.

147. Thanasoulias, N.C., N.A. Parisis, and N.P. Evmiridis, *Multivariate chemometrics for the forensic discrimination of blue ball-point pen inks based on their Vis spectra*. Forensic Science International, 2003. **138**(1–3): p. 75-84.

148. Kher, A., et al., *Forensic classification of ballpoint pen inks using high performance liquid chromatography and infrared spectroscopy with principal components analysis and linear discriminant analysis*. Vibrational Spectroscopy, 2006. **40**(2): p. 270-277.

149. Thanasoulias, N.C., et al., *Application of multivariate chemometrics in forensic soil discrimination based on the UV-Vis spectrum of the acid fraction of humus*. Forensic Science International, 2002. **130**(2–3): p. 73-82.

150. Lee, C.S., et al., *Classification of forensic soil evidences by application of THM-PyGC/MS and multivariate analysis*. Journal of Analytical and Applied Pyrolysis, 2012. **96**: p. 33-42.

151. Barrett, J.A., J.A. Siegel, and J.V. Goodpaster, *Forensic discrimination of dyed hair color: II. Multivariate statistical analysis*. Journal of Forensic Sciences, 2011. **56**(1): p. 95-101.

152. Monfreda, M. and A. Gregori, *Differentiation of unevaporated gasoline samples according to their brands, by SPME–GC–MS and multivariate statistical analysis*. Journal of Forensic Sciences, 2011. **56**(2): p. 372-380.

153. Sandercock, P.M. and E. Du Pasquier, *Chemical fingerprinting of unevaporated automotive gasoline samples*. Forensic Science International, 2003. **134**(1): p. 1-10.

154. Sandercock, P.M.L. and E. Du Pasquier, *Chemical fingerprinting of gasoline: 2. Comparison of unevaporated and evaporated automotive gasoline samples*. Forensic Science International, 2004. **140**(1): p. 43-59.

155. Egan, W.J., et al., *Forensic discrimination of photocopy and printer toners. III. Multivariate statistics applied to scanning electron microscopy and*

pyrolysis gas chromatography/mass spectrometry. Analytical and Bioanalytical Chemistry, 2003. **376**(8): p. 1286-1297.

156. Egan, W.J., et al., *Forensic discrimination of photocopy and printer toners II. Discriminant analysis applied to infrared reflection-absorption spectroscopy*. Analytical and Bioanalytical Chemistry, 2003. **376**(8): p. 1279-1285.

157. Udriştioiu, E.G., et al., *Infrared spectrometry in discriminant analysis of laser printer and photocopy toner on questioned documents*. Instrumentation Science & Technology, 2009. **37**(2): p. 230-240.

158. Feldmann, J.M. and J.V. Goodpaster, *Discrimination of color copier/laser printer toners by Raman spectroscopy and subsequent chemometric analysis*, 2013, Purdue University: Indiana.

159. Kher, A., et al., *Classification of document papers by infrared spectroscopy and multivariate statistical techniques*. Applied Spectroscopy, 2001. **55**(9): p. 1192-1198.

160. Goodpaster, J.V., et al., *Identification and comparison of electrical tapes using instrumental and statistical techniques: II. Organic composition of the tape backing and adhesive*. Journal of Forensic Sciences, 2009. **54**(2): p. 328-338.

161. Goodpaster, J.V., et al., *Identification and comparison of electrical tapes using instrumental and statistical Techniques: I. Microscopic surface texture and elemental composition*. Journal of Forensic Sciences, 2007. **52**(3): p. 610-629.

162. Kochanowski, B.K. and S.L. Morgan, *Forensic discrimination of automotive paint samples using pyrolysis-gas chromatography-mass spectrometry with*

multivariate statistics. Journal of Chromatographic Science, 2000. **38**(3): p. 100-108.

163. Muehlethaler, C., et al., *Survey on batch-to-batch variation in spray paints: A collaborative study*. Forensic Science International, 2013. **229**(1–3): p. 80-91.

164. Muehlethaler, C., G. Massonnet, and P. Esseiva, *The application of chemometrics on Infrared and Raman spectra as a tool for the forensic analysis of paints*. Forensic Science International, 2011. **209**(1–3): p. 173-182.

165. Wilcken, H. and H. Schulten, *Quality control of paints: Pyrolysis-mass spectrometry and chemometrics*. Analytica Chimica Acta, 1996. **336**(1–3): p. 201-208.

166. Mendlein, A.N., J.A. Siegel, and J.V. Goodpaster, *Instrumental and chemometric analysis of automotive clear coat paints by micro laser Raman and UV microspectrophotometry*, 2011, Purdue University: Indiana.

167. Federal Chamber of Automotive Industries. *2013 New vehicle market*. 2013; Available from: http://www.fcai.com.au/sales/-2013-new-vehicle-market.

168. Chattopadhyay, T., U. Bhattacharya, and B.B. Chaudhuri. *On the enhancement and binarization of mobile captured Vehicle Identification Number for an embedded solution*. in *2012 10th IAPR International Workshop on Document Analysis Systems*. 2012.

169. National Highway Traffic Safety Administration, *Vehicle identification number requirements*, in *Code of Federal Regulations*. 2004. p. 157-162.

170. Smylie, W.T., *Vehicle identification*, in *Forensic Investigation of Stolen-Rcovered and Other Crime-Related Vehicles*, E. Stauffer and M. Bonfant, Editors. 2006, Elsevier: Massachusetts.

171. Chang, W., et al., *Comparison of embedding methods used in examining cross-sections of automotive paints with micro-Fourier transform infrared spectroscopy*. Forensic Science Journal, 2002. **1**: p. 55-60.

172. Creagh, D., J. McKinlay, and P. Dumas, *The design of the Infrared beamline at the Australian synchrotron*. Vibrational Spectroscopy, 2006. **41**(2): p. 213-220.

173. Clark, F.R.S. and D.J. Moffatt, *The elimination of interference fringes from Infrared spectra*. Applied Spectroscopy, 1978. **32**(6): p. 547-549.

174. Farrington, P.J., et al., *Suppression of interference fringes in the Infrared spectra of thin polymer films*. Applied Spectroscopy, 1990. **44**(5): p. 901-903.

175. Jeszenszky, É., L. Kocsányi, and P. Richter, *Eliminating the interference pattern in near-Infrared spectra used for identification of thin plastic foils*. Applied Spectroscopy, 2004. **58**(6): p. 693-697.

176. Parkhutik, V., M.S. Martínez, and E.G. Senent, *Processing of Infrared spectroscopy data on thin porous films using software "Prospect"*. Journal of Porous Materials, 2000. **7**(1-3): p. 239-242.

177. Johnson, R.A. and D.W. Wichern, *Applied Multivariate Statistical Analysis*. 2002, New Jersey: Prentice Hall.

178. Jackson, J.E., *A User's Guide to Principal Components*. 1991, New York: John Wiley & Sons, Inc.

179. Socrates, G., *Infrared and Raman Characteristic Group Frequencies*. 3rd ed. 2001, West Sussex: John Wiley & Sons, Ltd.

180. Geffen, C.A. and S. Rothenberg, *Suppliers and environmental innovation: The automotive paint process*. International Journal of Operations & Production Management, 2000. **20**(2): p. 166-186.

181. Kelly, C., *Automotive Paint Technology into the 21st century*, 2009: Victoria.

182. CAMO Process AS, *The Unscrambler Tutorials*, 2006, CAMO.

183. Zhang, C., O. Selinus, and J. Schedin, *Statistical analyses for heavy metal contents in till and root samples in an area of southeastern Sweden*. Science of The Total Environment, 1998. **212**(2–3): p. 217-232.

184. Barthus, R.C. and R.J. Poppi, *Determination of the total unsaturation in vegetable oils by Fourier transform Raman spectroscopy and multivariate calibration*. Vibrational Spectroscopy, 2001. **26**(1): p. 99-105.

185. Bauer, D.R. and L.M. Briggs, *IR spectroscopic studies of degradation in cross-linked networks: Photoenhanced hydrolysis of acrylic-melamine coatings*, in *Characterization of highly cross-linked polymers*. 1984, American Chemical Society. p. 271-284.

186. Nguyen, T., et al., *Relating laboratory and outdoor exposure of coatings III. Effect of relative humidity on moisture-enhanced photolysis of acrylic-melamine coatings*. Polymer Degradation and Stability, 2002. **77**(1): p. 1-16.

187. Mohseni, M., B. Ramezanzadeh, and H. Yari, *Effects of environmental conditions on degradation of automotive coatings*, in *New trends and developments in automotive industry*, M. Chiaberge, Editor. 2011, InTech.

188. Osterhold, M. and P. Glöckner, *Influence of weathering on physical properties of clearcoats*. Progress in Organic Coatings, 2001. **41**(1–3): p. 177-182.

189. Chang, W., et al., *A critical evaluation of spectral library searching for the application of automotive paint database*. Forensic Science Journal, 2003. **2**(1): p. 47-58.

190. Massonnet, G. and W. Stoecklein, *Identification of organic pigments in coatings: Applications to red automotive topcoats: Part II: Infrared spectroscopy*. Science & Justice, 1999. **39**(2): p. 135-140.

191. *The first coating technology in the world that simultaneously reduces VOC and CO_2 emissions*, in *Social & Environmental Report*, 2006. p. 29-30.

192. Bureau of Meteorology. *Climate Classification*. Available from: www.bom.gov.au/iwk/climate_zones/index.shtml.

193. Bureau of Meteorology. *Climate Data Online*. Available from: www.bom.gov.au/climate/data/index.shtml.

194. Australian Radiation Protection and Nuclear Saftey Agency. *Monthly UV index summaries for Perth*. Available from: www.arpansa.gov.au/uvindex/monthly/permonthlysumm.htm.

195. Larché, J.F., P.O. Bussière, and J.L. Gardette, *How to reveal latent degradation of coatings provoked by UV-light*. Polymer Degradation and Stability, 2010. **95**(9): p. 1810-1817.

196. Ramezanzadeh, B., M. Mohseni, and H. Yari, *The role of basecoat pigmentation on the biological resistance of an automotive clearcoat*. Journal of Coatings Technology and Research, 2010. **7**(6): p. 677-689.

197. Ramezanzadeh, B., et al., *An evaluation of an automotive clear coat performance exposed to bird droppings under different testing approaches*. Progress in Organic Coatings, 2009. **66**(2): p. 149-160.

198. Yari, H., et al., *Use of analytical techniques to reveal the influence of chemical structure of clearcoat on its biological degradation caused by bird-droppings*. Progress in Organic Coatings, 2009. **66**(3): p. 281-290.

199. Australian Bureau of Statistics. *Motor Vehicle Census*. 2014; Available from: www.abs.gov.au/ausstats/abs@.nsf/mf/9309.0.

200. Nanetti, P., *Coatings from A to Z*. 2006, Hannover: Vincentz Network.

201. Poth, U., *Automotive coatings formulation: European coatings tech files*. 2008, Hannover: Vincentz Network.

202. Parks, D.W. and D.H. Jacobs, *How to Paint Your Car*. 2013: Motorbooks Int.

203. Leona, M., et al., *Identification of the pre-Columbian pigment Maya blue on works of art by noninvasive UV-Vis and Raman spectroscopic techniques*. Journal of the American Institute for Conservation, 2004. **43**(1): p. 39-54.

204. Hayez, V., et al., *Identification of pigments on a 16th century Persian manuscript by micro-Raman spectroscopy*. Journal of Raman Spectroscopy, 2004. **35**: p. 781-785.

205. Nielsen, S.E., J.P. Scaffidi, and E.J. Yezierski, *Detecting art forgeries: A problem-based Raman spectroscopy lab*. Journal of Chemical Education, 2014. **91**(3): p. 446-450.

206. Chaplin, T.D., R.J.H. Clark, and D.R. Beech, *Comparison of genuine (1851-1852 AD) and forged or reproduction Hawaiian Missionary stamps using Raman microscopy*. Journal of Raman Spectroscopy, 2002. **33**: p. 424-428.

207. Castro, K., et al., *Scientific examination of classic Spanish stamps with colour error, a non-invasive micro-Raman and micro-XRF approach: The King Alfonso XIII (1889–1901 "Pelón") 15 cents definitive issue*. Journal of Cultural Heritage, 2008. **9**(2): p. 189-195.

208. Burgio, L. and R.J.H. Clark, *Comparative pigment analysis of six modern Egyptian papyri and an authentic one of the 13th century BC by Raman microscopy and other techniques*. Journal of Raman Spectroscopy, 2000. **31**(5): p. 395-401.

209. Colomban, P., *Lapis lazuli as unexpected blue pigment in Iranian Lâjvardina ceramics*. Journal of Raman Spectroscopy, 2003. **34**(6): p. 420-423.

210. Colomban, P., et al., *Raman identification of materials used for jewellery and mosaics in Ifriqiya*. Journal of Raman Spectroscopy, 2003. **34**(3): p. 205-213.

211. Bell, S.E., et al., *Forensic analysis of architectural finishes using fourier transform infrared and Raman Spectroscopy, part II: White paint*. Applied Spectroscopy, 2005. **59**(11): p. 1340-1346.

212. Stewart, S.P., et al., *Forensic examination of multilayer white paint by lateral scanning Raman spectroscopy*. Journal of Raman Spectroscopy, 2012. **43**(1): p. 131-137.

213. Buzzini, P., G. Massonnet, and F.M. Sermier, *The micro Raman analysis of paint evidence in criminalistics: Case studies*. Journal of Raman Spectroscopy, 2006. **37**(9): p. 922-931.

214. De Gelder, J., et al., *Forensic analysis of automotive paints by Raman spectroscopy*. Journal of Raman Spectroscopy, 2005. **36**(11): p. 1059-1067.

215. Suzuki, E.M. and M. Carrabba, *In situ identification and analysis of automotive paint pigments using line segment excitation Raman spectroscopy: I. Inorganic topcoat pigments*. Journal of Forensic Sciences, 2001. **46**(5): p. 1053-69.

216. Suzuki, E.M., *Infrared spectra of U.S. automobile original finishes (post – 1989). VIII: In situ identification of bismuth vanadate using extended range FT-IR spectroscopy, Raman spectroscopy, and X-ray fluorescence spectrometry*. Journal of Forensic Sciences, 2014. **59**(2): p. 344-363.

217. Zięba-Palus, J. and J. Wąs-Gubała, *An investigation into the use of micro-Raman spectroscopy for the analysis of car paints and single textile fibres*. Journal of Molecular Structure, 2011. **993**(1–3): p. 127-133.

218. Lambert, D., et al., *Raman analysis of multilayer automotive paints in forensic science: measurement variability and depth profile*. Journal of Raman Spectroscopy, 2014.

219. Skenderovska, M., B. Minceva-Sukarova, and L. Andreeva, *Application of micro-Raman and FT-IR spectroscopy in forensic analysis of automotive topcoats in the Republic of Macedonia*. Macedonian Journal of Chemistry and Chemical Engineering, 2008. **27**(1): p. 9-17.

220. Hans-Ulrich, G., *Infrared and Raman spectroscopy*, in *Analytical Techniques in Combinatorial Chemistry*, M.E. Swartz, Editor. 2000, Marcel Dekker, Inc.: New York.

221. Ellis, G., M. Claybourn, and S.E. Richards, *The application of fourier transform Raman spectroscopy to the study of paint systems*. Spectrochimica Acta Part A: Molecular Spectroscopy, 1990. **46**(2): p. 227-241.

222. Kuptsov, A.H., *Applications of fourier transform Raman spectroscopy in forensic science*. Journal of Forensic Sciences, 1994. **39**(2): p. 305-318.

223. Nakamoto, K., *Theory of normal vibrations*, in *Infrared and Raman Spectra of Inorganic and Coordination Compounds: Part A: Theory and Applications in Inorganic Chemistry*. 2008, John Wiley & Sons, Inc.: New Jersey.

224. GE Security, *Raman spectroscopy: The science behind the technology*, 2006.

225. AZoM. *Analyzing polymers and their formulation using Raman spectroscopy*. 2013; Available from: http://www.azom.com/article.aspx?ArticleID=8428.

226. Lin-Vien, D., et al., *The Handbook of Infrared and Raman Characteristic Frequencies of Organic Molecules*. 1991, London: Academic Press.

227. Pallipurath, A., et al., *Multivariate analysis of combined Raman and fibre-optic reflectance spectra for the identification of binder materials in simulated medieval paints*. Journal of Raman Spectroscopy, 2013. **44**(6): p. 866-874.

228. Bueno, J. and I.K. Lednev, *Advanced statistical analysis and discrimination of gunshot residue implementing combined Raman and FT-IR data*. Analytical Methods, 2013. **5**(22): p. 6292-6296.

Appendices

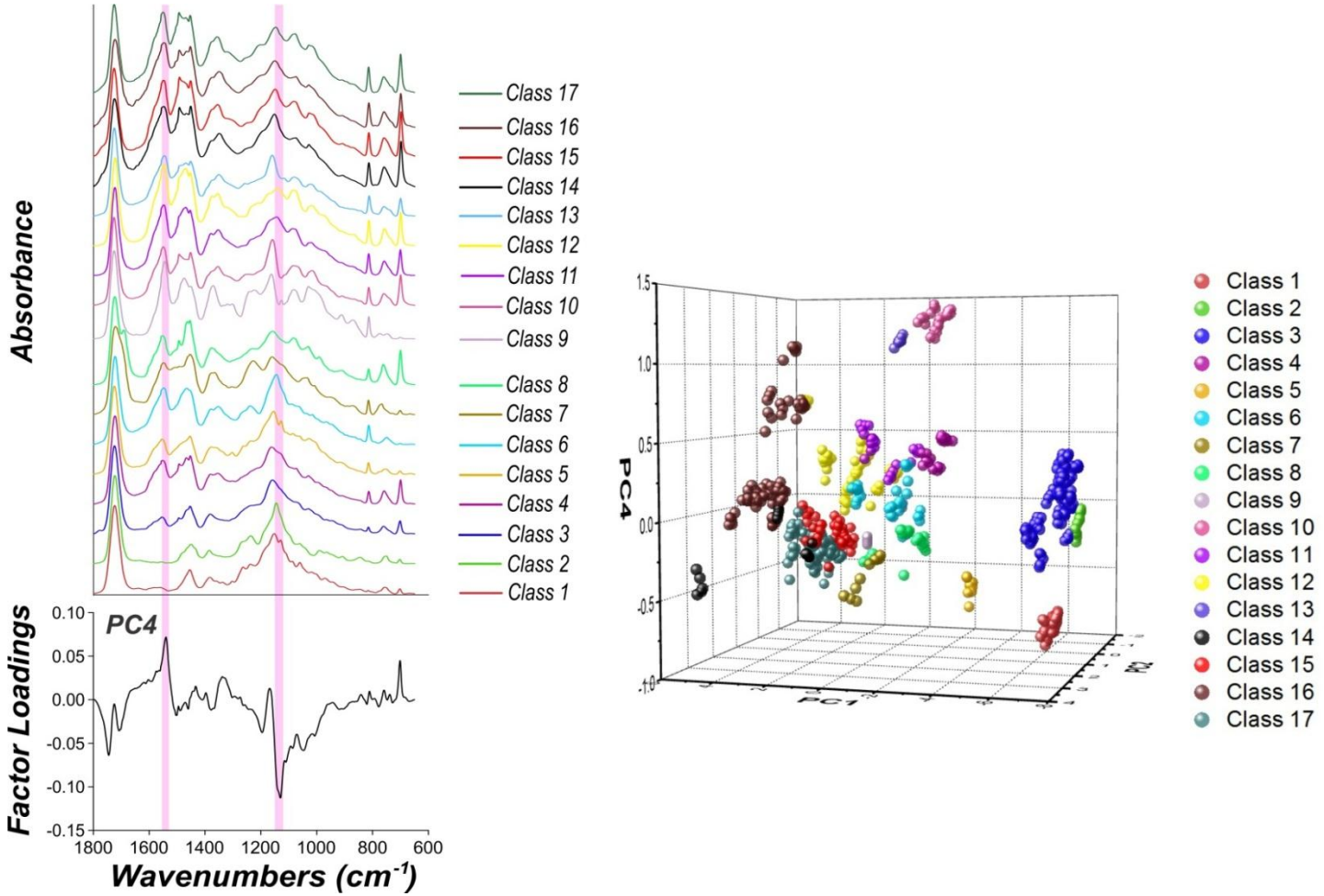

Figure A.1: Factor loadings plot for PC4. The purple zones superimposed on the representative Raman spectra for each grouping, denote spectral regions significantly correlated with PC4.

Table A.1: Discriminant values for a true class 11, class 12, and the misclassified sample.

Discriminant Values

	Cl. 1	Cl. 2	Cl. 3	Cl. 4	Cl. 5	Cl. 6	Cl. 7	Cl. 8	Cl. 9	Cl. 10	Cl. 11	Cl. 12	Cl. 13	Cl. 14	Cl. 15	Cl. 16	Cl. 17
Cl. 12-1	-420.4	-415.0	-323.8	-98.8	-168.0	-80.2	-207.4	-156.5	-172.6	-64.1	-19.1	**-5.1**	-35.8	-115.1	-76.1	-45.2	-38.6
Cl. 12-2	-425.1	-422.8	-328.9	-104.4	-170.8	-84.5	-199.7	-151.5	-162.8	-70.2	-21.4	**-5.6**	-41.2	-121.3	-80.5	-49.5	-41.2
Cl. 12-3	-428.5	-426.2	-330.7	-104.8	-173.1	-85.3	-198.0	-149.9	-161.8	-69.3	-21.0	**-5.2**	-40.1	-119.7	-80.9	-47.6	-41.3
Cl. 12-4	-412.2	-412.4	-319.1	-99.0	-162.7	-82.4	-199.9	-147.7	-168.8	-70.5	-19.9	**-5.9**	-42.7	-112.9	-73.3	-46.3	-36.0
Cl. 12 -5	-428.2	-418.1	-328.7	-99.5	-173.3	-79.2	-214.6	-164.9	-176.8	-59.6	-19.2	**-5.4**	-31.0	-117.7	-79.4	-45.2	-41.6
Cl. 11-1	-313.6	-322.4	-207.2	-51.1	-113.9	-101.5	-207.2	-99.2	-216.7	-30.3	**-7.7**	-26.2	-35.4	-88.4	-48.3	-51.2	-36.1
Cl. 11-2	-312.7	-324.6	-207.9	-52.7	-113.4	-103.9	-205.0	-96.1	-216.4	-34.7	**-8.9**	-26.8	-39.8	-86.1	-46.6	-51.0	-34.4
Cl. 11-3	-311.6	-323.0	-207.0	-51.8	-112.2	-100.0	-196.7	-92.5	-208.8	-34.5	**-8.0**	-25.9	-37.8	-88.4	-49.8	-50.3	-36.2
Cl. 11-4	-312.3	-322.7	-207.0	-51.5	-112.8	-100.6	-200.8	-95.1	-211.8	-32.8	**-7.8**	-26.0	-36.8	-88.4	-49.1	-50.6	-36.1
Cl. 11-5	-310.9	-323.5	-207.1	-52.3	-111.6	-99.5	-191.8	-89.5	-205.2	-36.6	**-8.2**	-25.9	-39.1	-88.6	-50.6	-50.1	-36.5
Misclassified-1	-335.3	-330.6	-244.5	-64.1	-117.8	-60.2	-177.2	-122.1	-165.1	-47.7	**-10.3**	**-14.0**	-27.7	-123.0	-77.6	-56.1	-47.2
Misclassified-2	-324.2	-319.7	-236.1	-61.7	-111.3	-58.2	-177.2	-121.7	-166.2	-48.9	**-11.2**	**-16.5**	-29.6	-126.7	-78.6	-60.5	-48.9
Misclassified-3	-316.7	-312.4	-229.4	-58.7	-107.1	-56.9	-175.9	-119.5	-167.8	-48.1	**-10.9**	**-17.9**	-29.6	-126.2	-78.1	-61.1	-49.3
Misclassified-4	-322.7	-319.7	-235.2	-61.7	-110.2	-59.4	-176.3	-119.5	-166.2	-50.1	**-11.1**	**-16.4**	-31.2	-125.1	-76.8	-60.3	-47.4
Misclassified-5	-323.5	-319.7	-235.6	-61.6	-110.8	-58.5	-176.7	-120.6	-166.2	-49.4	**-11.1**	**-16.4**	-30.4	-125.9	-77.7	-60.4	-48.2

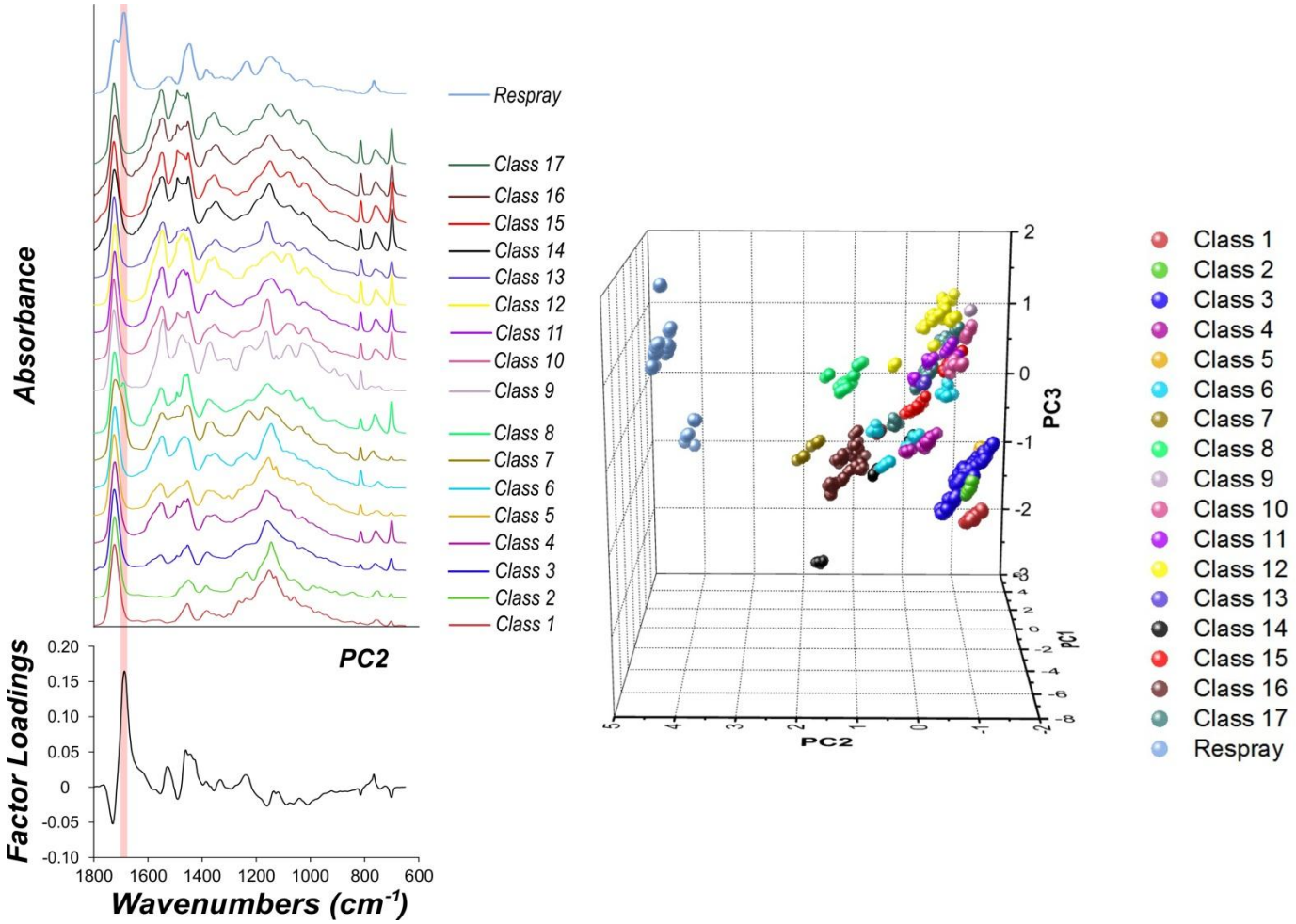

Figure A.2: Factor loadings plot for PC2. The significant positive correlation at ca. 1690 cm^{-1} (red zone) is characteristic of polyurethane, and is principally responsible for the discrimination of the respray clear coats from their OEM counterparts on PC2.

Table A.2: Discriminant values for the Mazda 3 (class 3) vehicle over the 18 month exposure period.

Discriminant Values

	Cl. 1	Cl. 2	Cl. 3	Cl. 4	Cl. 5	Cl. 6	Cl. 7	Cl. 8	Cl. 9	Cl. 10	Cl. 11	Cl. 12	Cl. 13	Cl. 14	Cl. 15	Cl. 16	Cl. 17
Initial-1	-45.4	-60.3	**-5.5**	-88.3	-57.2	-206.2	-330.0	-198.3	-509.8	-215.1	-217.0	-338.2	-254.0	-316.0	-267.7	-326.1	-303.6
Initial-2	-42.2	-57.3	**-4.9**	-89.8	-57.0	-208.9	-339.6	-205.3	-521.6	-219.9	-221.5	-343.7	-259.5	-316.9	-268.2	-330.2	-305.5
Initial-3	-41.8	-57.5	**-4.9**	-92.2	-58.1	-212.2	-341.5	-206.7	-524.4	-223.4	-224.8	-347.7	-263.5	-320.9	-271.6	-334.5	-309.2
Initial-4	-44.5	-56.8	**-5.1**	-88.1	-57.9	-206.4	-341.1	-207.5	-520.8	-214.7	-219.3	-341.7	-254.3	-317.5	-268.7	-328.7	-305.8
Initial-5	-43.3	-59.6	**-5.4**	-91.8	-58.5	-211.4	-335.4	-202.1	-518.4	-222.1	-223.0	-345.5	-261.7	-320.0	-271.7	-332.4	-308.5
2Months-1	-41.7	-62.7	**-6.1**	-99.0	-60.4	-220.5	-332.1	-198.8	-518.3	-234.3	-231.1	-354.1	-274.5	-329.0	-279.4	-342.6	-316.2
2Months-2	-43.9	-58.7	**-5.4**	-91.4	-59.1	-210.8	-337.9	-204.7	-520.6	-220.7	-223.2	-346.1	-260.4	-320.6	-272.5	-332.6	-309.5
2Months-3	-43.9	-57.6	**-5.3**	-90.9	-59.4	-210.5	-342.0	-208.0	-524.5	-219.6	-223.4	-346.7	-259.6	-320.5	-272.2	-332.7	-309.8
2Months-4	-44.3	-59.6	**-5.6**	-90.5	-58.9	-210.3	-337.0	-203.3	-520.1	-219.7	-221.9	-344.6	-259.4	-317.6	-270.4	-330.1	-307.5
2Months-5	-41.2	-57.6	**-5.1**	-96.1	-60.0	-216.3	-341.2	-207.7	-525.7	-229.1	-230.1	-353.9	-269.4	-328.9	-279.0	-341.8	-316.5
4Months-1	-42.0	-62.2	**-6.1**	-98.7	-60.9	-220.1	-333.0	-200.1	-519.9	-233.8	-231.4	-354.9	-273.9	-329.1	-280.2	-342.4	-317.2
4Months-2	-42.9	-62.5	**-6.2**	-100.1	-62.0	-221.1	-331.4	-199.8	-517.1	-234.2	-232.5	-356.2	-274.3	-334.3	-284.2	-345.7	-320.6
4Months-3	-42.3	-61.2	**-5.8**	-98.0	-60.9	-219.1	-334.5	-201.6	-520.2	-232.0	-230.8	-354.4	-272.1	-329.9	-280.5	-342.5	-317.4
4Months-4	-41.0	-63.4	**-6.6**	-98.0	-59.8	-220.2	-333.2	-198.6	-522.9	-235.6	-230.8	-353.8	-275.5	-321.9	-275.1	-338.2	-312.6
4Months-5	-44.1	-61.6	**-5.9**	-94.5	-60.2	-214.6	-331.7	-199.6	-516.1	-225.7	-225.8	-348.7	-265.3	-324.5	-276.4	-336.0	-312.9
6Months-1	-38.8	-61.8	**-6.2**	-103.1	-61.0	-226.8	-340.4	-204.1	-529.2	-242.8	-237.8	-361.7	-284.1	-332.6	-281.8	-349.7	-319.9
6Months-2	-42.0	-59.6	**-5.4**	-96.9	-60.4	-218.0	-338.6	-204.6	-522.6	-229.7	-229.9	-353.4	-270.3	-329.4	-279.0	-342.3	-316.3
6Months-3	-44.6	-63.2	**-5.9**	-91.6	-56.7	-209.1	-319.8	-190.3	-499.7	-220.8	-218.6	-338.8	-259.2	-320.8	-271.0	-329.8	-305.6
6Months-4	-45.1	-61.6	**-5.9**	-94.5	-60.0	-213.2	-328.0	-197.8	-509.0	-223.5	-224.3	-346.6	-262.9	-328.6	-278.4	-337.4	-313.9
6Months-5	-41.9	-62.4	**-5.7**	-95.1	-57.7	-215.5	-329.3	-195.9	-512.8	-228.5	-225.1	-346.6	-268.2	-322.5	-272.6	-335.7	-308.9
8Months-1	-42.6	-64.0	**-6.6**	-100.7	-62.5	-224.0	-334.7	-200.2	-523.0	-236.5	-233.9	-357.9	-277.4	-330.3	-281.7	-344.8	-319.2
8Months-2	-46.8	-65.4	**-6.8**	-97.1	-62.5	-218.1	-325.9	-194.8	-509.5	-227.0	-266.9	-349.8	-267.0	-329.7	-280.8	-339.2	-316.5
8Months-3	-44.8	-62.9	**-6.2**	-97.7	-62.2	-219.2	-332.7	-200.0	-516.8	-228.9	-229.3	-352.8	-269.4	-331.0	-281.3	-342.0	-317.9
8Months-4	-46.1	-65.0	**-6.6**	-94.6	-60.8	-216.0	-327.6	-194.8	-511.5	-224.6	-224.1	-346.5	-264.6	-322.6	-274.9	-334.1	-311.1
8Months-5	-48.0	-65.5	**-6.7**	-90.8	-59.3	-210.3	-321.9	-190.9	-503.0	-217.6	-217.9	-339.0	-256.7	-318.0	-270.6	-327.3	-305.7
18Months-1	-39.7	-81.3	**-19.6**	-147.7	-82.4	-283.0	-359.0	-216.8	-565.6	-312.3	-292.0	-421.1	-358.1	-384.8	-328.5	-412.3	-369.6
18Months-2	-45.9	-96.1	**-30.3**	-170.8	-95.6	-311.7	-369.9	-224.1	-581.6	-344.6	-317.2	-447.6	-392.7	-410.0	-350.1	-442.0	-392.2
18Months-3	-42.8	-90.4	**-27.7**	-168.8	-94.8	-310.3	-378.5	-231.3	-591.7	-342.9	-318.5	-450.5	-391.6	-409.7	-350.2	-442.9	-393.7
18Months-4	-41.6	-85.1	**-22.0**	-154.8	-86.8	-293.2	-365.4	-220.6	-572.4	-320.9	-300.0	-429.9	-368.3	-394.2	-335.6	-423.2	-377.5
18Months-5	-41.8	-84.8	**-21.3**	-152.2	-85.5	-290.0	-362.0	-217.8	-568.0	-316.9	-296.3	-425.8	-364.0	-390.8	-332.7	-419.0	-374.2

Table A.3: Discriminant values for the Holden VE SV6 (class 17) vehicle over the 18 month exposure period.

Discriminant Values

	Cl. 1	Cl. 2	Cl. 3	Cl. 4	Cl. 5	Cl. 6	Cl. 7	Cl. 8	Cl. 9	Cl. 10	Cl. 11	Cl. 12	Cl. 13	Cl. 14	Cl. 15	Cl. 16	Cl. 17
Initial-1	-368.6	-375.5	-281.7	-73.0	-147.8	-103.5	-297.9	-183.4	-313.3	-64.4	-26.5	-30.9	-56.5	-30.6	-13.6	-19.3	**-4.1**
Initial-2	-363.7	-370.6	-277.7	-71.2	-144.8	-102.0	-296.8	-182.2	-313.2	-63.9	-26.1	-31.2	-56.3	-31.0	-13.3	-19.9	**-4.1**
Initial-3	-365.9	-372.6	-280.0	-72.5	-146.1	-103.1	-300.4	-185.0	-315.1	-64.7	-26.8	-31.3	-57.1	-31.4	-13.0	-20.7	**-3.8**
Initial-4	-360.3	-368.1	-275.8	-71.3	-142.8	-102.7	-298.2	-182.5	-314.9	-66.0	-27.1	-32.4	-58.8	-31.5	-12.7	-21.7	**-3.9**
Initial-5	-361.9	-369.2	-275.4	-70.3	-143.3	-101.6	-293.0	-178.7	-309.3	-63.0	-25.1	-30.4	-55.6	-31.9	-13.7	-20.1	**-4.3**
2Months-1	-381.7	-386.3	-291.7	-75.3	-156.9	-103.1	-297.7	-187.0	-316.2	-63.6	-27.4	-31.5	-53.2	-26.3	-16.6	-13.0	**-6.1**
2Months-2	-387.6	-390.8	-296.5	-76.7	-160.4	-103.1	-299.9	-190.3	-317.0	-62.9	-27.6	-31.0	-51.8	-26.4	-17.5	-11.9	**-6.6**
2Months-3	-375.6	-380.2	-286.0	-72.5	-152.9	-101.3	-295.6	-184.5	-314.8	-61.8	-26.1	-31.2	-52.1	-26.9	-16.0	-13.6	**-6.0**
2Months-4	-378.8	-383.4	-288.5	-73.6	-154.7	-101.7	-294.0	-183.9	-312.8	-62.1	-26.1	-30.7	-51.8	-27.0	-16.9	-12.9	**-6.3**
2Months-5	-376.2	-381.6	-288.4	-74.5	-153.5	-103.0	-300.2	-188.0	-319.5	-65.6	-28.3	-32.8	-55.8	-26.3	-15.1	-14.8	**-5.3**
4Months-1	-377.3	-385.3	-288.4	-75.7	-155.0	-106.3	-294.1	-181.7	-316.6	-67.5	-29.0	-33.9	-58.0	-25.0	-16.0	-14.1	**-6.3**
4Months-2	-371.5	-378.3	-283.5	-72.7	-150.9	-102.9	-294.0	-181.8	-316.1	-65.2	-27.6	-33.2	-55.8	-25.8	-15.4	-14.5	**-5.9**
4Months-3	-391.5	-398.2	-298.3	-79.1	-162.0	-105.4	-282.9	-176.7	-299.6	-64.4	-26.0	-28.1	-52.6	-29.1	-20.7	-11.5	**-7.6**
4Months-4	-373.0	-380.1	-285.4	-73.8	-151.7	-103.2	-294.1	-182.4	-315.4	-66.4	-28.0	-33.0	-56.7	-26.3	-15.6	-14.8	**-5.7**
4Months-5	-381.4	-388.1	-291.2	-76.0	-157.4	-105.7	-294.2	-183.0	-316.0	-65.9	-28.5	-33.1	-55.8	-24.9	-17.0	-12.6	**-6.8**
6Months-1	-374.3	-383.3	-286.2	-75.3	-152.9	-106.3	-291.7	-179.1	-314.3	-68.3	-28.8	-33.8	-59.0	-25.8	-15.8	-15.1	**-6.1**
6Months-2	-386.9	-393.9	-296.5	-79.1	-159.9	-107.3	-295.1	-184.1	-311.9	-67.0	-28.4	-30.9	-56.7	-27.4	-17.0	-14.0	**-5.7**
6Months-3	-366.9	-377.5	-280.6	-73.5	-148.1	-104.1	-283.7	-173.0	-308.8	-69.9	-28.4	-34.1	-60.2	-26.9	-16.6	-15.9	**-6.5**
6Months-4	-384.6	-393.7	-295.1	-79.4	-158.3	-106.9	-286.5	-177.8	-305.6	-69.7	-28.5	-31.0	-58.4	-28.0	-18.4	-14.0	**-6.4**
6Months-5	-369.2	-377.5	-282.2	-73.1	-149.7	-104.3	-293.5	-180.4	-316.6	-67.4	-28.4	-34.2	-58.4	-25.8	-14.9	-15.7	**-5.7**
8Months-1	-379.8	-386.6	-290.2	-75.6	-156.0	-104.3	-292.2	-182.0	-313.7	-66.2	-28.1	-32.6	-55.7	-25.6	-17.2	-12.9	**-6.6**
8Months-2	-378.5	-385.5	-288.7	-74.8	-155.1	-103.3	-288.1	-179.1	-310.5	-65.7	-27.4	-32.2	-54.9	-25.9	-18.0	-12.4	**-7.1**
8Months-3	-375.3	-383.8	-286.6	-74.7	-153.2	-103.8	-285.5	-176.3	-309.0	-67.6	-27.8	-32.8	-56.9	-26.2	-17.8	-13.3	**-7.0**
8Months-4	-378.2	-385.2	-288.0	-74.4	-154.7	-102.7	-285.4	-177.0	-307.5	-64.8	-26.6	-31.4	-54.0	-26.6	-18.4	-12.2	**-7.3**
8Months-5	-370.7	-379.7	-282.8	-73.4	-150.4	-103.7	-286.1	-175.4	-310.2	-67.4	-27.7	-33.3	-57.6	-26.2	-16.8	-14.4	**-6.6**
18Months-1	-364.2	-387.6	-282.3	-83.8	-149.7	-117.4	-261.8	-153.6	-299.1	-92.4	-38.4	-44.2	-81.6	-30.6	-24.4	-22.9	**-13.1**
18Months-2	-364.3	-387.9	-282.0	-83.7	-150.0	-117.8	-261.3	-152.9	-298.9	-92.1	-38.3	-44.3	-81.4	-30.4	-24.5	-22.7	**-13.4**
18Months-3	-383.2	-405.3	-299.1	-91.0	-161.8	-123.3	-275.2	-165.2	-307.5	-94.3	-41.0	-43.7	-82.9	-28.2	-23.4	-21.1	**-11.8**
18Months-4	-359.0	-384.8	-279.0	-84.6	-146.7	-119.5	-260.3	-150.9	-297.5	-95.9	-39.7	-45.5	-85.9	-33.4	-24.5	-26.9	**-13.5**
18Months-5	-362.9	-386.3	-280.8	-83.1	-148.7	-116.7	-260.1	-152.1	-297.1	-91.6	-37.7	-43.6	-80.9	-31.1	-24.4	-23.0	**-13.1**

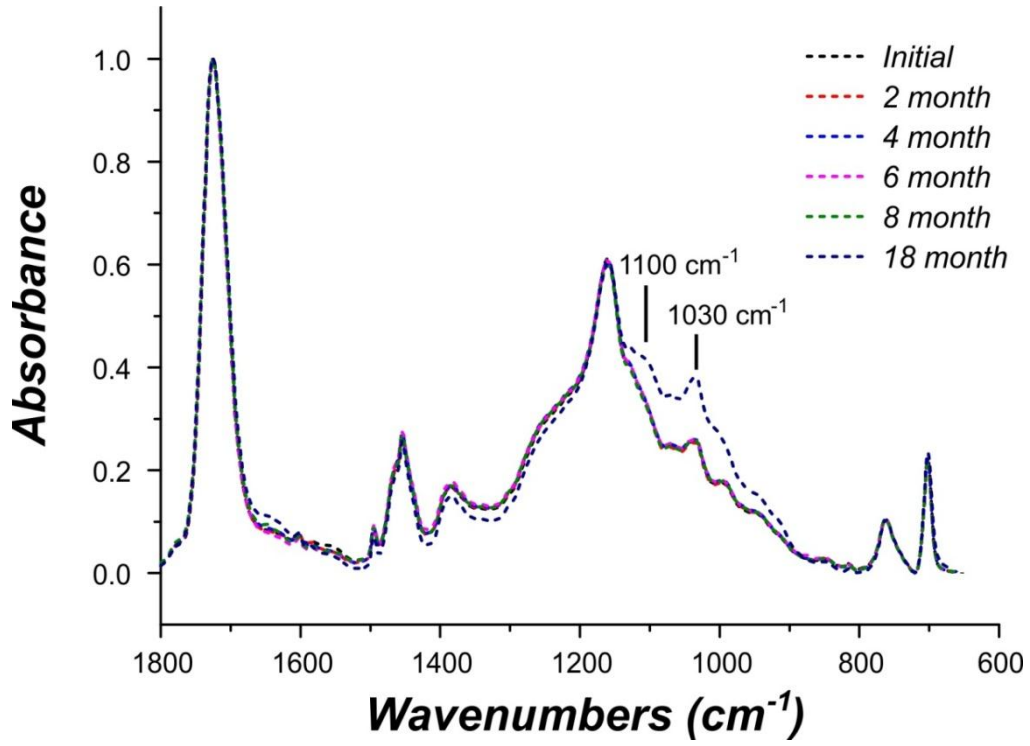

Figure A.3: Averaged ATR FT-IR spectra obtained from the clear coat of the Mazda 3 vehicle after every sampling interval.

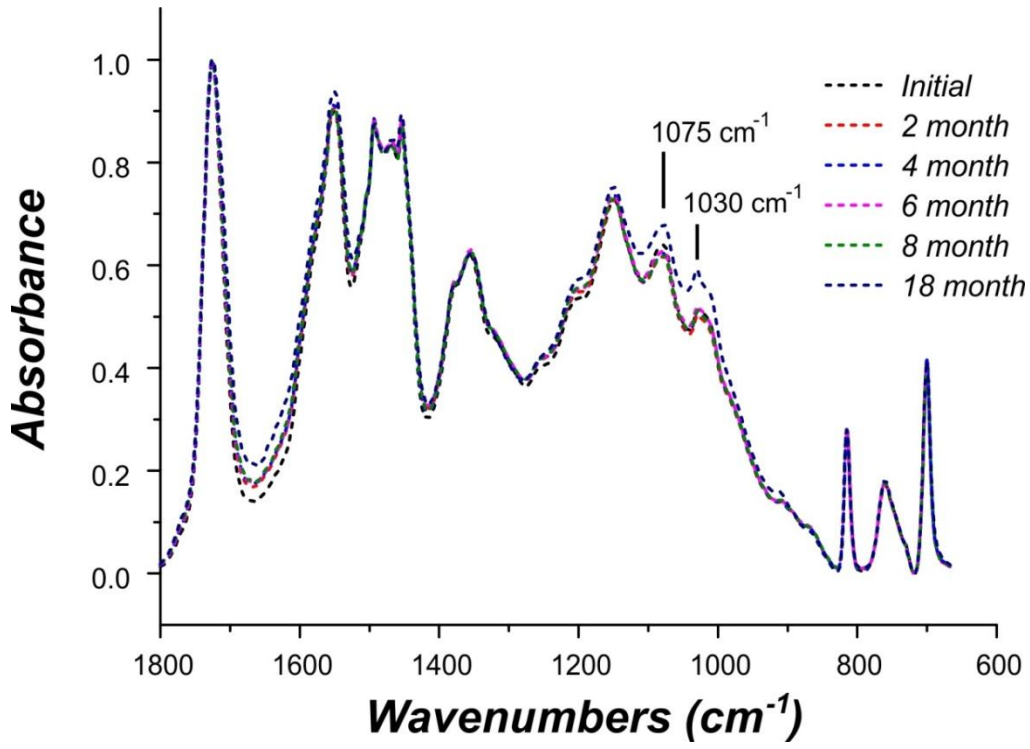

Figure A.4: Averaged ATR FT-IR spectra obtained from the clear coat of the Holden VE SV6 vehicle after every sampling interval.

Table A.4: Discriminant values for the misclassified samples in the Raman statistical model.

Discriminant Values

Calibration	Cl. 1	Cl. 2	Cl. 3	Cl. 4	Cl. 5	Cl. 6	Cl. 7	Cl. 8	Cl. 9	Cl. 10	Cl. 11	Cl. 12	Cl. 13	Cl. 14	Cl. 15	Cl. 16	Cl. 17	Cl. 18	Cl. 19
Suzuki Vitara-1	-299.8	-208.3	-130.5	-93.5	-176.3	-182.7	-184.9	-211.1	-203.7	-73.2	-30.6	**-7.1**	-92.1	-28.9	**-6.8**	-44.2	-83.7	-56.8	-104.1
Suzuki Vitara-2	-297.8	-207.1	-129.3	-91.8	-176.4	-180.2	-181.5	-207.2	-199.7	-71.3	-30.1	**-6.8**	-91.0	-28.1	**-6.2**	-42.4	-84.7	-57.5	-105.7
Suzuki Vitara-3	-299.0	-208.1	-132.0	-93.1	-177.1	-179.5	-182.6	-207.6	-200.2	-72.2	-30.6	**-7.2**	-90.6	-27.8	**-6.6**	-42.5	-81.1	-54.7	-102.0
Suzuki Vitara-4	-304.0	-209.8	-129.8	-94.9	-173.6	-186.5	-190.6	-211.8	-209.5	-72.0	-30.4	**-7.4**	-96.5	-31.1	**-7.0**	-46.2	-82.6	-56.1	-104.9
Suzuki Vitara-5	-306.5	-212.1	-130.7	-94.0	-175.7	-184.1	-191.2	-217.2	-210.3	-77.1	-29.8	**-7.4**	-96.8	-31.5	**-7.0**	-46.3	-82.0	-56.3	-104.9
Honda Civic-1	-223.3	-156.7	-143.5	-86.9	-160.9	-139.6	-130.0	-152.5	-151.5	-46.0	-47.3	**-17.9**	-49.6	**-15.9**	-25.1	-46.9	-68.7	-49.6	-80.5
Honda Civic-2	-225.3	-158.5	-144.8	-88.5	-162.3	-142.0	-131.8	-153.9	-152.8	-46.7	-47.8	**-17.8**	-49.9	**-16.0**	-24.9	-47.0	-68.7	-49.5	-79.3
Honda Civic-3	-224.3	-157.9	-144.5	-87.7	-162.4	-140.4	-129.9	-151.5	-150.5	-45.6	-47.6	**-17.8**	-49.3	**-15.6**	-24.7	-46.0	-68.9	-49.7	-79.7
Honda Civic-4	-226.1	-160.0	-143.4	-85.4	-158.2	-141.3	-143.3	-154.2	-152.9	-46.6	-47.9	**-17.9**	-50.2	**-16.1**	-24.5	-47.5	-69.0	-49.8	-80.5
Honda Civic-5	-226.0	-159.8	-143.1	-85.0	-158.4	-141.5	-135.8	-154.5	-153.1	-46.8	-47.8	**-18.0**	-50.4	**-16.2**	-24.5	-47.5	-69.1	-50.0	-81.1
Holden VE-1	-406.1	-294.9	-256.9	-160.6	-253.2	-141.6	-256.8	-281.5	-246.6	-177.6	-83.8	-95.5	-164.7	-89.5	-85.6	-101.3	**-6.6**	**-8.3**	-95.9
Holden VE -2	-411.3	-298.8	-261.8	-163.0	-255.5	-140.1	-261.2	-284.5	-268.5	-182.6	-86.9	-100.3	-170.2	-94.5	-90.6	-105.6	**-6.1**	**-9.9**	-99.0
Holden VE -3	-425.6	-306.8	-258.4	-162.0	-253.5	-144.5	-273.3	-295.3	-280.4	-188.2	-82.8	-98.0	-179.7	-98.5	-88.5	-107.0	**-5.4**	**-10.7**	-102.2
Holden VE -4	-425.7	-307.7	-259.2	-162.0	-254.7	-145.5	-271.9	-290.0	-276.1	-184.9	-82.6	-95.9	-177.4	-96.6	-86.3	-103.6	**-5.3**	**-11.2**	-98.9
Holden VE -5	-415.6	-299.7	-255.3	-158.6	-250.3	-140.6	-264.9	-286.7	-272.1	-181.8	-81.6	-95.6	-173.0	-94.4	-86.5	-103.7	**-5.5**	**-10.3**	-99.9

Validation	Cl. 1	Cl. 2	Cl. 3	Cl. 4	Cl. 5	Cl. 6	Cl. 7	Cl. 8	Cl. 9	Cl. 10	Cl. 11	Cl. 12	Cl. 13	Cl. 14	Cl. 15	Cl. 16	Cl. 17	Cl. 18	Cl. 19
Toyota Hilux-1	-360.2	-278.3	-188.9	-144.1	-250.2	-250.4	-211.5	-187.8	-186.5	-72.5	-67.5	**-14.7**	-99.8	-37.3	**-8.5**	-28.9	-119.9	-94.1	-89.4
Toyota Hilux -2	-355.1	-274.7	-186.4	-143.5	-248.4	-252.4	-209.2	-186.9	-185.8	-70.5	-68.2	**-14.3**	-97.9	-36.8	**-8.7**	-29.8	-124.2	-97.2	-91.5
Toyota Hilux -3	-359.1	-277.6	-187.7	-143.9	-249.9	-251.7	-211.0	-187.5	-186.4	-71.9	-67.9	**-14.7**	-99.9	-37.7	**-8.7**	-29.3	-122.9	-96.5	-91.6
Toyota Hilux -4	-360.2	-278.8	-189.1	-144.5	-251.4	-251.2	-210.8	-186.7	-185.3	-72.0	-68.2	**-15.0**	-99.9	-37.5	**-8.6**	-28.5	-122.0	-95.8	-90.8
Toyota Hilux -5	-365.5	-281.9	-189.9	-144.8	-251.5	-250.8	-214.8	-190.3	-189.1	-74.8	-67.2	**-15.1**	-103.0	-38.8	**-8.7**	-29.1	-119.1	-93.9	-90.3